AN INVESTIGATION OF THE EFFECT OF HYDRODYNAMIC STRESS ON THE GROWTH, MORPHOLOGY AND METABOLISM OF MICROORGANISMS

Suzanne Illing

Thesis Presented for the Degree of
DOCTOR OF PHILOSOPHY
in the Department of Chemical Engineering
UNIVERSITY OF CAPE TOWN
September 1996

Bioprocess Research Group
Department of Chemical Engineering
University of Cape Town
Rondebosch
Cape Town
South Africa

AN INVESTIGATION OF THE EFFECT OF HYDRODYNAMIC STRESS ON THE GROWTH, METABOLISM AND MORPHOLOGY OF MICROORGANISMS

Suzanne Illing

Chemical Engineering Department, University of Cape Town, Private Bag, Rondebosch, Cape Town, 7700, South Africa.

September 1996

The cultivation of bacteria requires high levels of agitation and aeration to satisfy the mass transfer requirements of the cells. Associated with these conditions are turbulent forces which may act on the surfaces of the cells and be detrimental to their growth, metabolism and morphology. Reactor design and operation may require a compromise between the stress sensitivity and the mass transfer requirements of the microbial system. In this project, the development of general predictive techniques to optimise the design and operation for stress sensitive microorganisms was sought.

The effect of hydrodynamic stress on the growth, metabolism and morphology of *Corynebacterium glutamicum* (ATCC 13032) and *Brevibacterium flavum* (NRRL 11475) was investigated in a stirred tank bioreactor in the absence of mass transfer limiting conditions. The results showed that hydrodynamic trauma had no effect on the growth and metabolism of the bacteria. Breakup of bacterial aggregates was however observed, the extent of which depended on the intensity of the hydrodynamic conditions. The extent of aggregate breakup was greater for *Corynebacterium glutamicum*. It was postulated that the bacteria were held together by a growth associated biomolecular adhesive.

The kinetics and mechanism for *Corynebacterium glutamicum* aggregate breakup in the absence of a gaseous phase, were studied in a stirred tank reactor and capillary flowloop system. A model was developed to describe the rate of aggregate breakup caused by aggregate-turbulent eddy interactions in the impeller zone of the stirred tank reactor and in the wall region of the capillary, in the absence of air bubbles. It assumes that aggregate

disruption is caused by the interaction with similarly sized eddies. The extent of aggregate breakup was a function of the magnitude of the turbulent force as well as the total duration of the force event. A similar model was developed to describe the rate of microbial cell death. The forces associated with turbulent eddies in the impeller zone of the stirred tank reactor were compared with those of collapsing air bubbles at the air medium interface. The results showed that both contributed to the total force acting on the cells.

SYNOPSIS

Cultivation of microbial cells requires high levels of agitation and aeration to ensure adequate mass transfer, homogeneous suspension and minimal circulation time. Associated with these conditions are turbulent forces which may act on the surfaces of the cells and result in sub-optimal microbial productivity. Reactor design and operation may therefore require a compromise between the stress sensitivity and the mass transfer requirements of the microbial system. In this project, the nature and extent of biological response in unicellular microbial systems was studied. The development of general predictive techniques to optimise the design and operation of bioreactors for stress sensitive microorganisms was sought.

Hydrodynamic forces resulting from increased agitation were reported to cause decreased microbial productivity (Toma *at al.*, 1991), change in the metabolic pathways of bacteria (Fowler and Robertson, 1991; Toma *et al.*, 1991) and changes in the size and shape of microorganisms (Wase and Patel, 1985). For plant cells the stress levels required to inhibit growth were 4 orders of magnitude lower than those required to disrupt the cells (Dunlop *et al.*, 1993). Furthermore the biological and physical characteristics of microorganisms were proposed to dictate the extent to which cells were influenced by hydrodynamic forces (Mersmann *et al.*, 1990).

Literature findings regarding the cause of hydrodynamic trauma were divided into two groups. The first attributed metabolic inhibition to the interaction of cells with turbulent eddies of a similar size in regions of high shear stress found near the impeller (Kunas and Papoutsakis, 1990; Toma *et al.*, 1991). The interaction of cells with collapsing air bubbles at the free surface fell in the second category (Handa-Corrigan *et al.*, 1989; Oh *et al.*, 1989).

Studies reported in the literature have concentrated mainly on the more sensitive animal cells and filamentous fungi. In this study the biological response of more resistant bacteria cells to hydrodynamic conditions is investigated.

The effect of hydrodynamic stress on the growth, metabolism and morphology of *Corynebacterium glutamicum* (ATCC 13032) and *Brevibacterium flavum* (NRRL 11475) was investigated in a stirred tank bioreactor in the absence of mass transfer limiting conditions. The results showed that the local energy dissipation rates in the laboratory stirred tank reactor experiments (e_{AVE} = 47.5 m^2/s^3) were insufficient to influence the growth, metabolism or integrity of the bacteria. Breakup of bacterial aggregates was however observed, the extent of which depended on the intensity of the hydrodynamic conditions. The extent of aggregate breakup was greater for *Corynebacterium glutamicum* than *Brevibacterium flavum*. In a capillary flowloop, operated at an average energy dissipation rate of 9650 m^2/s^3, the biological response observed for *Corynebacterium glutamicum* was also limited to breakup of the cell aggregates. Hydrodynamic characterisation of the flow systems showed that the distribution of turbulence was highly inhomogeneous, with maximum local energy dissipation rates occurring in the impeller zone of the stirred tank reactor (e_{imp} = 11875 m^2/s^3) and in the wall region of the capillary (e_{wall} = 144810 m^2/s^3). The ratio of maximum and average energy dissipation rates of 25 and 15 were determined for the respective flow systems.

The kinetics and mechanism for *Corynebacterium glutamicum* aggregate breakup in the absence of a gaseous phase, was studied in a stirred tank reactor and capillary flowloop system. The extent of aggregate breakup was a function of the magnitude of the turbulent force as well as the total duration of the force event. A model was developed to describe the rate of aggregate breakup caused by interactions betweeen aggregates and turbulent eddies in the impeller zone of the stirred tank reactor and in the wall region of the capillary, in the absence of air bubbles. The model assumed that aggregate disruption was caused by the interaction of aggregates with similarly sized turbulent eddies; hence aggregate breakup was caused by eddies in the viscous dissipation subrange. The rate of *Corynebacterium glutamicum* aggregate breakup gave a first order dependence with respect to the maximum energy dissipation rate, in accordance with the aggregate breakup model.

A similar model was developed to describe the rate of microbial cell death. The cell death model was successfully applied to data for mammalian TB/C3 hybridoma cells and the plant cells *Morinda citrifolia* reported in the literature (Zhang *et al.*, 1993 ; Zhang *et al.*, 1995;

Kieran *et al.*, 1995). Where hybridoma cells were exposed to extreme energy dissipation rates over few circulations, a first order dependence on maximum energy dissipation rate was found. When the cells were exposed frequently to the force events, the correlations showed that the cell envelope strength of the hybridomas in the stirred tank reactor increased with total exposure time due to preferential destruction of the more susceptible cells. Hybridoma cell death was caused by eddies in the viscous dissipation subrange. The cell envelope strength of the plant cells increased with total exposure time in the turbulent capillary flow. Plant cell death was caused by eddies in the inertial convection subrange. No fatigue effects owing to continued exposure to hydrodynamic trauma were observed.

The forces associated with turbulent eddies in the impeller zone were compared to those caused by collapsing air bubbles at the air medium interface in a stirred tank and airlift reactor. Both the interaction of microbial cells with turbulent eddies in the impeller discharge zone, as well as with collapsing air bubbles at the air medium interface contributed to the total force acting on the cells.

It was suggested that the model describing the interaction of cells and aggregates with turbulent eddies, could be used to predict the biological response in process flow situations where the gaseous phase is absent *eg* in pump circuits, separation devices and disruption equipment. It was recommended that in future work, rigorous experiments be carried out to determine the effect of bubble size distribution, bubble frequency, surface active agents and circulation time on the extent of aggregate breakup or cell death associated with collapsing bubbles.

ACKNOWLEDGEMENTS

This study could not have been achieved without the support of the staff in the Chemical Engineering Department, family and friends.

Firstly I would like to express my sincere thanks to my supervisor, Dr Sue Harrison, for her guidance, training and encouragement over the past five years. I am most grateful for the opportunity to present my work at an international conference in Switzerland.

Dr Jim Petrie contributed many useful suggestions based on his comprehensive knowledge of fluid flow. He has been extremely accommodating of my many requests for information. Professor Hansford, who is part of the bioprocess engineering group, has always given me good advise. I would like to thank Bill Randall for his willingness to assist in tasks relating to electronic and computer matters. He was responsible for the design of the circulation time conductivity probe, the fermenter load cell and the bubble sizer. Dave Deglon, who designed and developed the conductivity probe for measuring velocity profiles, gave much of his time to characterise the hydrodynamic conditions in the stirred tank reactor.

Tony Barker, Peter Tobias and Joachim Macke, were responsible for designing and repairing the experimental apparatus. I would like to thank Linda Harrower and Jenny Löwenadler for their assistance in the laboratory. I would also like to acknowledge the services of Granville de la Cruz, James Daniels, Maria Josias, Martin Wiiliams and Jackie Mshudulu. I would especially like to thank all the postgraduates for their comradeship. My stay in the chemical engineering department has been a most enjoyable one.

I am most grateful to the Foundation for Research and Development, who gave the financial support for the project.

Special thanks are due to my parents, who have always given me unconditional support and encouragement. Finally, I would like to thank my friends.

NOMENCLATURE

a	fluctuating velocity under isotropic conditions, m s^{-1}
A_1	first order rate constant in Equation 1
A_2	constant in Equation 13
A_3	constant in Equation 21
A_4	constant in Equation 21
A_5	constant in Equation 29
A_6	constant in Equation 29
A_7	constant in Equation 30
A_8	constant in Equation 60
A_9	constant in Equation 61
B_1	constant in Equation 83
B_2	constant in Equation 95
B_3	constant in Equation 100
B_4	constant in Equation 103
B_5	constant in Equation 106
B_6	constant in Equation 108
B_7	constant in Equation 109
B_8	constant in Equation 113
B_9	constant in Equation 116
C_o	oxygen concentration, mg/l^{-1} or ppm
C_o^*	saturation concentration of oxygen in bulk liquid, mg l^{-1} or ppm
C_p	concentration of primary amino acid produced, g l^{-1}
C_s	concentration of glucose, g l^{-1}
C_x	viable concentration of cells, m^{-3}
C_{xo}	initial concentration of viable cells, m^{-3}
C_V	volume concentration of flocs/aggregates or volume concentration of intact microbial cells
d	diameter of eddy or particle, m
d_{AVE}	average diameter, m

d_b	baffle diameter, m
d_{ch}	plant cell chain diameter, m
d_C	cell diameter, m
d_{eq}	equivalent spherical diameter, m
d_F	mean aggregate/floc diameter, m
$(d_F)_{MAX}$	maximum aggregate diameter, m
d_{MAX}	maximum diameter, m
d_p	primary particle diameter, m
d_{SM}	bubble sauter mean diameter, m
d_t	stable floc diameter, m
D	capillary/impeller diameter, m or dilution rate, hr^{-1}.
D_{MC}	maximum eddy diameter, m
D_{MIN}	minimum eddy diameter, m
e	turbulent energy dissipation rate per unit mass, $m^2\ s^{-3}$
$\bar{e}$	energy dissipation rate per unit mass due to mean velocity fluctuations, $m^2\ s^{-3}$
e_{AVE}	average turbulent energy dissipation rate per unit mass, $m^2\ s^{-3}$
e_b	turbulent energy dissipation rate per unit mass in the bulk, $m^2\ s^{-3}$
e_i	turbulent energy dissipation rate per unit mass in the impeller zone, $m^2\ s^{-3}$
e_{MAX}	maximum turbulent energy dissipation rate per unit mass, $m^2\ s^{-3}$
e_w	wall turbulent energy dissipation rate per unit mass, $m^2\ s^{-3}$
$E_1(n)$	one dimensional energy spectrum function in frequency space
E_k	kinetic energy, kg $m^2\ s^{-2}$
E_s	surface energy, kg $m^2\ s^{-2}$
E_{sb}	bursting surface energy, kg $m^2\ s^{-2}$
f	frequency of eddy formation, s^{-1}
f_{app}	apparent friction factor
F_1	viscous force, kg m s^{-2}
F_2	inertial force, kg m s^{-2}
F	force, kg m s^{-2}
g	gravitational acceleration, m s^{-2}
h_D	dispersion height, m

H	liquid height, m
H_c	clearance of impeller off bottom, m
k	total kinetic energy per unit mass, $m^2\ s^{-2}$
k_f	turbulent friction factor
k_La	volumetric mass transfer coefficient, s^{-1}
K	compressibility modulus
K_B	frictional loss coefficient in Equation 77
KE	kinetic energy, $kg\ m^2\ s^{-2}$
l	impeller blade length, axis length of ellipsoid, m
l_C	length of cell, m
L	Eulerian macroscale/capillary length, m
L_d	length of downcomer in airlift, m
L_r	length of riser in airlift, m
L_{RES}	resultant turbulent macroscale
m	impeller blade frequency, s^{-1}
n	eddy frequency, Hz
n_F	number concentration of parent flocs/aggregates
n_p	number of primary particles eroded per disruption
N	number of passes, number of measurements
N_{crit}	critical agitation rate, s^{-1}
N_p	power number
N_{rpm}	agitation rate, s^{-1}
P	pressure, $kg\ m^{-1}\ s^{-2}$
P_g	gassed power input, $kg\ m^2\ s^{-3}$
P_o	ungassed power input, $kg\ m^2\ s^{-3}$
q	root mean square turbulent velocity, $m\ s^{-1}$
Q	liquid flow rate, $m^3\ s^{-1}$
Q_g	gas flow rate, $m^3\ s^{-1}$
r	correlation coefficient
r_o	critical distance (9λ), m
R	impeller radius, m
R_D	rate of disruption of aggregates, $m^{-3}\ s^{-1}$

R_e	Reynold's number
R_E	Eulerian auto-correlation coefficient
R_p	particle Reynold's number
$(R_p)_c$	critical Reynold's number
R_δ	Reynold's number
S	spacing between impellers, m
t	time
t_c	circulation time, s
t_{exp}	exposure time, s
T	tank diameter, m
T_b	bursting membrane tension, kg s^{-2}
T'	integral time scale of turbulence, s
u	fluctuating velocity, m s^{-1}
u_r	radial fluctuating velocity, m s^{-1}
u_z	axial fluctuating velocity, m s^{-1}
u_Θ	tangential fluctuating velocity, m s^{-1}
$\overline{u}(d)$	root mean square velocity difference between two points a distance d apart, m s^{-1}
$\overline{u}_1(d)$	root mean square velocity difference for eddies of size d in the viscous dissipation subrange, m s^{-1}
$\overline{u}_2(d)$	root mean square velocity difference for eddies of size d in the inertial convection subrange, m s^{-1}
u^*	friction velocity, m s^{-1}
U	instantaneous velocity, m s^{-1}
$\overline{U}$	average velocity, m s^{-1}
U_r	average radial velocity, m s^{-1}
U_z	average radial velocity, m s^{-1}
U_Θ	average radial velocity, m s^{-1}
U_c	average circulation velocity, m s^{-1}
U_{gr}	superficial gas velocity in the riser, m s^{-1}
U_{ld}	superficial liquid velocity in the downcomer, m s^{-1}
U_{lr}	superficial liquid velocity in the riser, m s^{-1}

U_{sg}	superficial gas velocity, m s^{-1}
U_{tip}	impeller tip speed, m s^{-1}
v_{imp}	impeller speed, m s^{-1}
V	liquid volume, m^3
V_D	dispersion volume, m^3
V'_L	liquid volume in riser of airlift, m^3
x	average number of primary cells/aggregate
y	fatigue exponent in Equation 101
y^+	dimensionless distance from capillary wall, m
Y_{sx}	growth yield, g glucose (g cell)$^{-1}$
Y_{px}	primary amino acid yield, g amino acid (g cell)$^{-1}$

Greek letters

γ	mean deformation rate, s^{-1}
δ	cell envelope thickness/ length of side of cubic fluid element, m
Δ_{ij}	rate of strain, s^{-1}
ϵ_g	overall gas holdup
ϵ_{gd}	gas holdup in the downcomer
ϵ_{gr}	gas holdup in the riser
λ	Kolmogorov microscale, m
λ_f	Eulerian micro time scale, m
λ_{MIN}	minimum local Kolmogorov microscale, m
λ_{IMP}	Kolmogorov microscale in the impeller zone, m
λ_w	Kolmogorov microscale at the wall in the capillary, m
μ	dynamic viscosity, kg m^{-1} s^{-1}
μ_{app}	apparent viscosity, kg m^{-1} s^{-1}
μ_G	viscosity of gas, kg m^{-1} s^{-1}
μ_L	viscosity of liquid, kg m^{-1} s^{-1}
ν	kinematic viscosity, m^2 s^{-1}

$\varkappa$	cell envelope composition
ρ	fluid density, kg m^{-3}
ρ	liquid density, kg m^{-3}
ρ_p	particle density, kg m^{-3}
$\sigma_{AGGREGATE}$	specific strength of aggregate, kg s^{-2}
σ_{CELL}	specific cell strength, kg s^{-2}
σ	liquid surface tension, kg s^{-2}
τ	time delay in auto-correlation function
τ_E	Eulerian micro time scale, s
τ_{ij}	shear stress, kg m^{-1} s^{-2}
τ_o	wall shear stress, kg m^{-1} s^{-2}
τ_y	floc yield strength, kg m^{-1} s^{-2}

TABLE OF CONTENTS

LIST OF FIGURES

LIST OF TABLES

1 INTRODUCTION

Agitation and aeration ensure the effective distribution of oxygen and nutrients essential for optimal growth of microorganisms in fermenters. It has been shown that hydrodynamic forces, associated with agitation and collapsing bubbles, are exerted on the cell wall structure and may result in sub-optimal bacterial productivity (Toma *et al.*, 1991). For stress sensitive microorganisms the bioreactor design and operating conditions may therefore require a compromise between the mass transfer requirements and the stress sensitivity of the particular biological system. The latter may also dictate the design and operating parameters of pump circuits, separation devices and disruption equipment. Correlations are available to predict the mass transfer potential of a system (Joshi *et al.*, 1982). Equivalent prediction of the stress sensitivity based on the hydrodynamic conditions in stirred tank reactors and other flow systems is not available. To achieve such prediction, the predominant fluid force governing the biological response must be identified. To predict or determine the critical conditions in bioreactors, it is necessary to identify the biological response, to characterise the hydrodynamic conditions in the system, and then to evaluate the critical conditions at which the biological response is observed.

Based on the literature, three hypotheses have been formulated for investigation in this thesis. It has been hypothesised that *Corynebacterium glutamicum* and *Brevibacterium flavum* are sensitive to hydrodynamic trauma. Stress induced changes in the lysis, rate of growth, metabolic activity, metabolic pathway and morphology may be observed. The second hypothesis was that the mechanism of hydrodynamic trauma was due to the interaction of microorganisms with turbulent eddies in the impeller discharge zone as well as with collapsing air bubbles at the air medium interface. Finally it was hypothesised that the biological response of microorganisms could be correlated with hydrodynamic parameters based on a fundamental hydrodynamic trauma model.

In this thesis the cultivation of the Gram positive bacteria, *Corynebacterium glutamicum* and *Brevibacterium flavum* in a stirred tank bioreactor has been studied. *Brevibacterium flavum*

was chosen for the investigation based on previous findings (Toma *et al.*, 1991) that its growth was inhibited at high agitation rates in a stirred tank reactor. As *Corynebacterium glutamicum* has important industrial significance in South Africa as a lysine producer it was selected for this study. The bacteria have a similar morphology and physiology, and are both lysine producers. Hydrodynamic stress experiments were carried out in a stirred tank reactor in the absence of mass transfer limiting conditions. It was necessary to choose suitable analytical techniques to measure the five possible responses mentioned previously. The hydrodynamic conditions in the flow systems were characterised. The kinetics and mechanism of the biological response of *Corynebacterium glutamicum* has been investigated in a stirred tank reactor and capillary flowloop system. A model has been developed to describe the interaction of microorganisms with turbulent eddies in the absence of a gaseous phase. The purpose of the model is to provide a predictive technique to optimise the design and operation of flow systems where the gaseous phase is absent, to minimise the detrimental effects associated with hydrodynamic trauma. The contribution of collapsing air bubbles to the total hydrodynamic force acting on the cells has been investigated.

In the second chapter of the thesis, the literature covering hydrodynamic stress in all microbial and single cell systems is reviewed and further analysed. Models developed to describe the interaction of cells with fluid forces are discussed. Correlation of experimental data of the biological response with hydrodynamic parameters is reviewed. Characterisation of hydrodynamic conditions in stirred tank reactors is discussed and suitable correlations identified. Using these, the hydrodynamic conditions have been calculated for the stirred tank reactor at specified operating conditions at which biological responses have been observed.

The experimental procedures concerning the growth of the microorganisms, reactor configurations and the analytical techniques for characterising hydrodynamic parameters and measuring biological responses are described in Chapter 3. The experimental programme is discussed.

In Chapter 4 the results concerning the hydrodynamic characterisation of the stirred tank reactor, flowloop system and airlift reactor in terms of local and average energy dissipation rates, circulation times and bubble sizes are presented and discussed.

The results of the response of *Brevibacterium flavum* and *Coryenbacterium glutamicum* to various levels of agitation and aeration in a stirred tank reactor measured in terms of lysis, viability, rate of metabolism and shift in metabolic pathway, and morphology changes are discussed in Chapter 5. The mass transfer potential of the stirred tank reactor is also elucidated to ensure that the growth experiments are carried out in the absence of mass transfer limiting conditions.

In Chapter 6 the kinetics and mechanism of *Corynebacterium glutamicum* aggregate breakup in a stirred tank reactor and flowloop system are investigated. A model is developed to describe the rate of breakup caused by interactions between the aggregates and the turbulent eddies in the absence of a gaseous phase. The applicability of the model to other microbial systems is investigated.

The forces associated with turbulent eddies in the impeller discharge zone are compared with those of collapsing air bubbles at the air medium interface in a stirred tank reactor and an airlift reactor in Chapter 7.

Finally in Chapter 8, conclusions are drawn based on pertinent experimental results in the thesis. Recommendations for further research in the field are made.

2. REVIEW OF THE LITERATURE

2.1 INTRODUCTION

To understand how microorganisms respond to hydrodynamic stress, it is necessary to consider the structure and functioning of microbial cells, the reported response to hydrodynamic conditions and the hydrodynamic conditions prevailing in a typical plant with which microbes are associated. The cell architecture of microorganisms and metabolic functioning within the cell are discussed in the first section of the literature review (Sections 2.2 and 2.3 respectively). In this study the effect of hydrodynamic stress on the growth, metabolism and morphology of bacteria has been investigated. To gain insight in this little researched area, literature findings on hydrodynamic stress in all microbial and single cell systems have been reviewed. Reported effects of hydrodynamic stress on unicellular microorganisms, filamentous fungi, animal cells, plant cells and non-living particles are discussed in Section 2.4.

In order to identify and predict the predominant fluid force acting on cell surfaces, it is necessary to characterise fluid flow in bioreactors and associated plants in terms of flow patterns, local fluid mean and turbulent fluctuating velocities, average energy dissipation rates and local energy dissipation rates. In the next section of the literature review (Section 2.5) hydrodynamic characterisation of stirred tank reactors is addressed. These findings are used to calculate local energy dissipation rates in the stirred tank reactors in which the response, of different microorganisms or cell types, to hydrodynamic forces have been reported.

Finally the predominant cause of biological responses to hydrodynamic forces, presented in the literature, are discussed in Section 2.6. Models developed to describe the interaction of cells with fluid forces are presented. Correlations of experimental biological response data with hydrodynamic parameters are reviewed.

2.2 THE ARCHITECTURE OF MICROORGANISMS

Some understanding of how microorganisms respond to hydrodynamic stress can be gleamed from four aspects of the cell anatomy (Prokop and Bajpai, 1992):

[1] the cell membrane and/or cell wall which forms the physical barrier against the hydrodynamic forces,

[2] the cell cytoskeleton which absorbs the energy generated by turbulence,

[3] the cell size which determines the magnitude of kinetic energy adsorbed by the cell,

[4] the presence of a mechanism to receive fluid mechanical stimuli.

All microorganisms are surrounded by a lipid bilayer membrane, through which the cell communicates with the environment. Bacteria, yeasts and plant cells have an additional protective cell wall surrounding the cell membrane. In bacteria the cell wall consists of a thick homogeneous peptidoglycan or murein layer. Peptidoglycan is an enormous polymer consisting of many identical subunits made up of sugar derivatives and amino acids. This forms a rigid barrier between the cell and the extracellular environment. Cells which lack a cell wall will generally be more susceptible to damage by hydrodynamic forces. Bacteria may either be Gram positive or Gram negative, depending on the construction of the cell envelope. While the envelope in Gram positive bacteria has a single cell membrane, there are two membranes in Gram negative cells. The outer and inner cell membranes enclose a region called the periplasmic space. The peptidoglycan layer lies between the outer membrane and the periplasmic space. Gram positive bacteria are generally considered to be mechanically stronger as they have a thicker peptidoglycan layer.

The cytoskeleton is a complex network of protein filaments that extend throughout the cytoplasm of the cell. There are three types of cytoplasmic fibres that make up the cell cytoskeleton: the microtubules, actin filaments and the intermediate filaments. In eucaryotes the cytoskeleton is involved in conducting intracellular transport and enabling cellular movement in an organised fashion. The cytoskeleton is attached to the cell membrane via specialized proteins. In cells which are only surrounded by a cell membrane, the cytoskeleton plays an important role in providing structural support and determining cell shape (Lloyd,

1982; Watt, 1986).

Some organisms possess protein receptors in the cell wall or cell membrane, which are sensitive to mechanical stress. Evidence for these receptors has been found in yeasts (Gustin *et al.*, 1986), plant cells (Falke *et al.*, 1986) and animal cells (Stockbridge and French, 1988). These cells therefore have evolved a specific regulatory response to mechanical stimuli. The receptors permit rapid adjustments to changing environmental conditions. These receptors are believed to be ion channels which pass specific ions when mechanically stimulated. The signal is rapidly transmitted throughout the cell by ion channel networking via cytoskeletal elements and the cell may respond accordingly. Ando *et al.* (1991) have shown that hydrodynamic stress induced changes in the Ca^{2+} content of vascular epithelial cells.

2.3 THE BIOCHEMISTRY OF GRAM POSITIVE BACTERIA

It is necessary to have a thorough understanding of the biochemistry of microorganisms in studying the metabolic effects of hydrodynamic stress.

A living cell is a complex chemical reactor in which enzyme catalysed reactions occur. The total of all reactions occurring in the cell is termed the metabolism. The energy that the cell obtains from the environment is used for the chemical synthesis of complex molecules for growth, for the transport of ionic and neutral substances into and out of the cell and for mechanical work required in cell division. Not all cells possess the same internal chemistry. Reactions in the cell may be divided into three groups: break down of nutrients, biosynthesis of small molecules and biosynthesis of large molecules.

ATP plays an important role as an energy shuttle in the cell. The hydrolysis of ATP releases a substantial amount of energy, -7.3 kcal/mol. By reversing the reaction, free energy can be stored for later use. ATP reactions occur simultaneously with other biochemical reactions in the cell, either supplying energy or storing energy.

Nucleotide derivatives, especially nicotinamide adenine dinucleotide (NAD) and its phosphorylated form (NADP) are important electron carrying agents in oxidation-reduction reactions in the cell. Besides being electron shuttles, they play an important role in the synthesis of ATP in aerobic metabolism.

The breakdown of nutrients to obtain energy is called catabolism. *Corynebacterium glutamicum* and *Brevibacterium flavum* utilise the Embden-Meyerhof-Parnas pathway (glycolysis) to break glucose down to pyruvate. Stored energy and reducing power in the form of 2 moles of ATP and 2 moles of NADH result from the overall EMP pathway. The pathway also provides carbon skeletons as starting materials in cellular biosynthetic reactions. Respiration is the energy-producing process in which pyruvate is oxidised by oxygen (Figure 1). The reactions peculiar to respiration start with pyruvate. Additional reducing power is generated from pyruvate by converting it to acetyl co-enzymeA. The first phase of the oxidation is carried out in the tricarboxylic acid (TCA) cycle. Acetyl CoA is oxidised to CO_2. In each pass around the TCA cycle, four pairs of hydrogen atoms are liberated. Three pairs are transferred to NAD and the fourth pair to flavin adenine dinucleotide. The TCA cycle serves an important function in providing a pool of precursors for biosynthetic reactions.

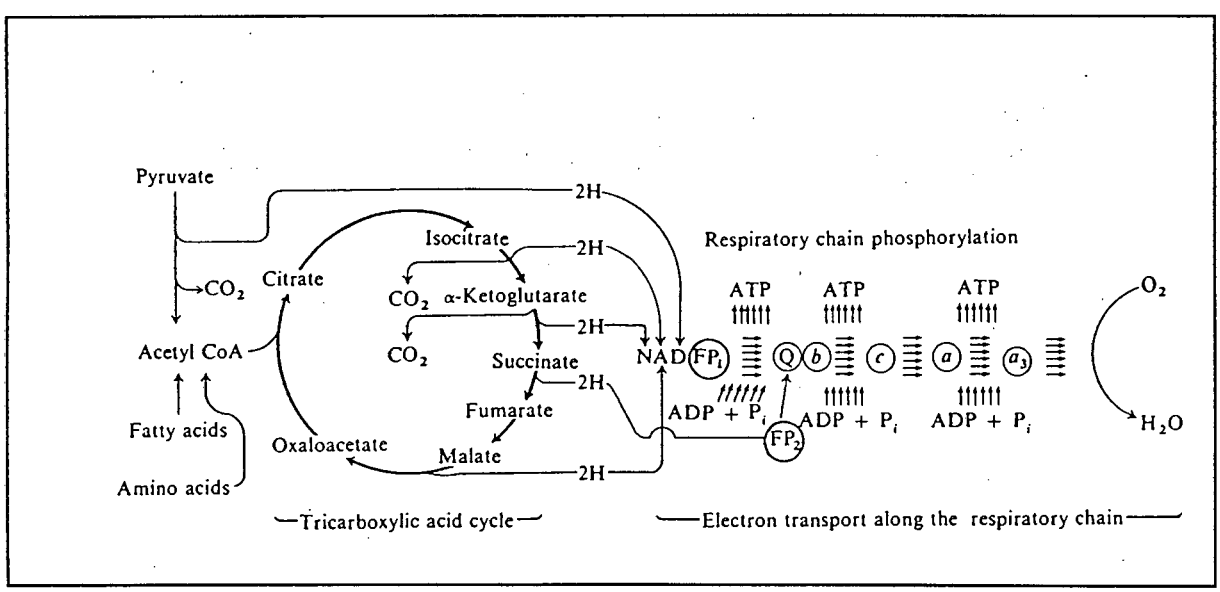

Figure 1 Generation of ATP through respiration (Bailey and Ollis, 1986).

In the second phase of respiration, the hydrogen atoms are passed through a sequence of reactions in the respiratory chain, during which ATP is regenerated from ADP. Electrons

from NADH are transferred to coenzyme Q via FAD in FP1. In this transfer 1 mole of ATP is regenerated for each pair of electrons passing. The electrons from the succinate dehydrogenation are passed directly to coenzyme Q via FAD in FP2. The electrons are then passed through a sequence of cytochromes b, c, a and a3 during which ATP is generated twice for each electron pair. At the end the hydrogen atoms combine with O_2 to give H_2O. Respiration potentially makes available to the cell 30 moles of ATP, compared to 8 moles of ATP made available during glycolysis.

The EMP and TCA cycles are amphibolic. Some intermediates are constantly being drawn off in biosynthetic side streams. The complete oxidation of glucose to H_2O and CO_2 represents an upper limit to the ATP yield in a respiring cell.

The stored energy and reducing power acquired by the cell during catabolism is invested in the biosynthesis of small and large molecules. Generally the reactions are thermodynamically unfavourable and require ATP hydrolysis. Because nutrient elements are often more oxidised than their cellular forms, reducing power is also required. The small molecules include amino acids, nucleotides, fatty acids and lipids.

The amino acids can be grouped into four families which are distinguished by their chemical properties and common precursors (Figure 2). The synthesis of all the amino acids begins with carbon metabolism intermediates. For fatty acid and lipid biosynthesis, acetyl CoA and glycerol serve as the starting materials.

Macromolecules such as polysaccharides, porphyrins, cellulose, proteins, RNA, DNA and glycogen are formed from their monomeric precursors.

Cell membranes regulate transport processes to maintain the internal cell pH and composition at a favourable level, to regulate cell volume, to admit and concentrate nutrients and to secrete toxic compounds. There are three main means of transport: passive diffusion, facilitated diffusion and active transport. Passive diffusion is spontaneous as material moves from a region of high concentration to a region of low concentration. In facilitated diffusion the material still moves across a positive concentration gradient except that the diffusion is

accelerated by carrier proteins, called permeases, which combine with the substrate and carry it across the membrane. With active transport, the substrate is carried across the membrane by carrier molecules against the concentration gradient. This process requires metabolic energy. The membrane contains numerous proteins which are able to recognise specific compounds in the cell environment and connect with cellular control systems in response to changing environmental conditions.

The cell must be able to control its array of chemical reactions so that energy, materials and electrons are used efficiently.

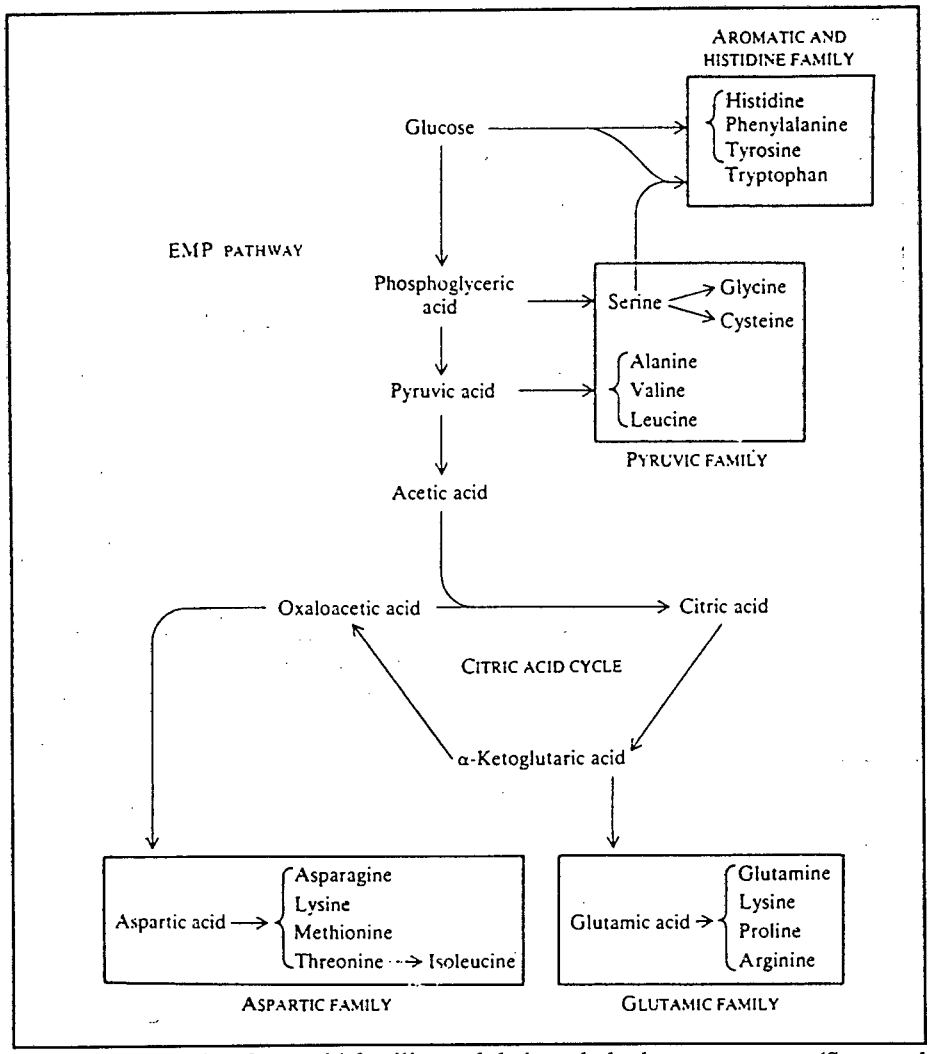

Figure 2 The amino fatty acid families and their carbohydrate precursors (Stent and Calendar, 1978).

2.4 SHEAR EFFECTS

2.4.1 Introduction

The relative differences in the stress sensitivity of different cell types is dictated by the biological and physical properties of the cells. Mersmann *et al.* (1990) compared the susceptibility of a range of microorganisms to rupture in disruption devices. The results are presented in Table 1.

Table 1 Susceptibility of microorganisms to rupture in disruption devices (Mersmann *et al.*, 1990).

ORGANISM	AVERAGE SIZE μm	MAXIMUM SHEAR STRESS N/m^2	DISRUPTION DEVICE	REFERENCE
Bacteria	d_C: <1 l_C: <5			
Micrococcus luteus		$< 10^8$	high pressure homogeniser	Büschelberger *et al.*, 1989
Synecoccus nidulans		$< 10^7$	stirred tank reactor/ free jet apparatus	Markl *et al.*, 1985
Yeast	d_C: 5 l_C: 5			
Saccharomyces cerevisiae		$< 8\times10^7$	high pressure homogeniser	Büschelberger *et al.*, 1989
Plant cells	d_C: 4-10 l_C: <100			
Chlamydomonas reinhardii		$< 2\times10^6$	stirred tank reactor/ free jet apparatus	Markl *et al.*, 1985
Animal cells	d_C: 10-20 l_C: 10-20			
Hela S3		< 500	turbulent capillary	Augenstein *et al.*, 1971
Tetrahymena				
Hybridoma		< 4	Couette viscometer	Midler and Finn, 1966
		< 0.005	stirred tank reactor	Fazekas *et al.*, 1983

Dunlop *et al.* (1994) have shown that hydrodynamic trauma may result in morphological changes, metabolic changes or, in the extreme case, cell rupture. The energy required to induce metabolic changes was several orders of magnitude lower than that required to disrupt cells.

Table 2 Values of the total viscous energy dissipation per unit volume at which 90 and 50% of the original biological activity of carrot cells are maintained under turbulent conditions in a Haake viscometer (Dunlop *et al.*, 1994).

BIOLOGICAL ACTIVITY	$E_{C,90}$ (J/m^3)	$E_{C,50}$ (J/m^3)
Mitochondrial activity	4×10^1	1×10^4
Aggregate breakup	9×10^4	2×10^6
Lysis	3×10^5	1×10^9

2.4.2 Unicellular microorganisms

Bacteria are tough due to their small size (0.5 to 3 μm) and strong peptidoglycan cell wall. It is generally thought that bacteria are immune to the effects of turbulent eddies, because of their small size. There is however some evidence to the contrary.

Toma *et al.* (1991) showed that the growth of the Gram positive *Brevibacterium flavum* (22LD) was inhibited at high agitation rates in a 3 liter stirred tank equipped with two turbine impellers. The sucrose uptake rate, oxygen utilisation rate and specific growth rate peaked at an optimum impeller tip speed of 3.11 m/s and aeration rate of 3.2 l/min. In the calculation of the average energy dissipation rate, the power input due to sparging is insignificant compared to the impeller power input. This corresponds to an average energy dissipation rate in the range 8.7 to 11.4 m^2/s^3. The ATP level declined sharply at higher impeller tip speeds, indicating a shift in the metabolism from the oxidative TCA cycle to the glycolytic pathway. High stirring intensities increased the production of histadine decarboxylase, and hence histamine, a stress indicator. The inhibition of bacterial growth was attributed to the interaction of cells with turbulent flow in the impeller discharge zone of the stirred tank. A critical zone was considered where the kinetic energy of the medium flow was greater than that required to produce a mechanical effect on the cell.

Ruklisha *et al.* (1989) using the same strain of *Brevibacterium flavum* and the same apparatus, showed that at a high impeller tip speed of 3.46 m/s, increased sucrose

concentration induced a Crabtree effect. The appearance of this effect was characterised by an incomplete TCA cycle, increased glutamate dehydrogenase and glycolysis enzyme activities, increased RNA and protein content per cell, a high value of total reducing activity in the cell and increased lactate dehydrogenase activity. The Crabtree effect was not observed at a low impeller tip speed of 1.04 m/s. Analogous changes of metabolic enzyme activity in *Brevibacterium flavum* were observed upon an intensive aeration in the fermenter. It was suggested that hydrodynamic stress caused changes in the properties of the cell membrane and damage to the oxidative phosphorylation chain and its functions. The Crabtree effect has been explained by a repression of the phosphorylation site *1* of the electron transport chain, namely $NADH_2$ dehydrogenase and a repression of succinate dehydrogenase (Doelle *et al.*, 1983).

Yeasts are generally larger than bacteria (5 μm) and they have thick cell walls. Further experiments by Toma *et al.* (1991) showed that the growth of *Saccharomyces cerevisiae* peaked at an impeller tip speed of 2.76 m/s and an aeration rate of 3.2 l/min. This corresponds to an average energy dissipation rate between 6 and 8 m^2/s^3. Vrana *et al.* (1982) observed the mechanical disruption of mother *Saccharomyces cerevisiae* cells in an airlift reactor fitted with a high-speed motor axle with rotating knives at an impeller tip speed of 12.3 m/s. It was suggested that the multi-budscarred mother cells were less resistant to mechanical strain than the daughter cells as their rigid polysaccharide cell wall is interrupted.

Fowler and Robertson (1991) showed that the catabolic activity of Gram negative *Escherichia coli* increased reversibly with increased hydrodynamic stress in a parallel plate flow chamber. The total acid yield and glucose consumption increased, and the spectrum of organic acids produced changed. It was postulated that the change was due to an osmoregulatory response induced by stressed bacteria to restore cell turgor.

Wase and Patel (1985) showed that the mean cell volumes of *Bacillus cereus*, *Staphylcoccus epidermis*, *Saccharomyces cervisiae* and *Escherichia coli* were directly proportional to the agitation rate of the fermenter. Agitation speed had no effect on cell growth or dry biomass concentration, hence the increased cell volume was due to an increase in the water content of the cells. The impeller speed was varied in the range 1.6 to 5.3 m/s. Edwards *et al.*

(1989) observed that *Escherichia coli* cells were twice as long when grown in a combined type coaxial cylinder and cone and plate viscometer bioreactor at a shear stress level of 14.5 Nm^{-2} than when grown in a shake flask. Neseratnam *et al.* (1982) showed that *Klebsiella pneumonia* cells grown at intense agitation conditions were more susceptible to ultrasonic disintegration than cells grown at milder conditions. This change in stress sensitivity may have been attributed directly to a change in cell volume. Larger cells are more susceptible to rupture. Bronnenmeier and Markl (1982) observed a decrease in the trichome lengths of *Spirulina platensis* at increased levels of hydrodynamic stress. *Spirulina platensis* bacteria, approximately 15 μm in diameter, link together by plasmatic filaments to form a helical structure called a trichome. The maximum growth rate occurred at an impeller tip speed of 2.35 m/s which corresponds to an average energy dissipation rate of 3.89 m^2/s^3.

Logan and Wilkinson (1991) showed that the fractal nature of microbial aggregates was a function of the type of microorganism and the mixing conditions used to develop aggregates. With increasing shear forces, an increase in the fractal number was observed. Experiments were conducted with *Zoogloea ramigera* and *Saccharomyces cerevisiae*. The former is a Gram negative rod shaped bacterium that flocculates during the late exponential phase. The cells attach via cellulose fibrils. *Saccharomyces cerevisiae* attach by Ca^{2+} bridging between surface carboxyl groups or by a longer bridge involving intermediate polypeptides.

2.4.3 Filamentous fungi

Fungi may grow in a pelleted or mycelial form. They are susceptible to hydrodynamic stress due to their filamentous type structure. The pellet form can vary from being loose and fluffy to being compact and smooth at stressed conditions. Blanch and Bhavaraju (1976) described two mechanisms of pellet disruption in stirred tanks: the chipping of pellicles from the surface and the direct splitting of the pellets. The mycelial form dominates in stirred tank reactors at higher agitation speeds as it is a mechanically more resistant morphological structure (Mitard and Riba, 1988; Dabee and Harrison, 1996). Van Suijdam and Metz (1981) showed that at high agitation speeds the hyphae are shorter, thicker and more branched. The decrease in hyphal length is a direct result of breakage of the hyphae.

Toma *et al.* (1991) observed that the growth rate of *Trichoderma reesei* decreased beyond an impeller tip speed of 0.52 m/s and an aeration rate of 3.2 l/min. This corresponded to an average energy dissipation rate of between 0.03 and 0.05 m^2/s^3.

Ujcovo *et al.* (1980) showed that citric acid production of *Aspergillus niger* peaked at an impeller speed of 600 rpm and an aeration rate of 1 l/min in a 1 liter single turbine stirred tank. The initial drop in citric acid production was not due to cell damage but to an induced shift in metabolism. Smith *et al.* (1990) showed that an impeller tip speed of 3.33 m/s and an aeration rate of 5.4 l/min was optimum for penicillin production of *Penicillium chrysogenum* in a 10 liter reactor (average energy dissipation rate of 3.3 m^2/s^3). Higher agitation and aeration rates inhibited production of the metabolite. The specific penicillin production rate was correlated with the power input per unit volume and the inverse of the circulation time, $P_g/D_i^3 t_C$. The greater the frequency of the circulation through the impeller discharge zone, the greater the mycelial damage and the lower the rate of penicillin synthesis by the culture. Özbas and Kutsal (1991) found optimum riboflavin yields and *Ashbya gossypii* concentrations in a 0.42 l fermenter fitted with Rushton turbine impellers at an impeller tip speed of 0.42 m/s and an aeration rate 0.1 l/min (average energy dissipation rate of 0.0135 m^2/s^3). Disintegration of cells occurred at more extreme conditions. An empirical equation was developed to correlate the riboflavin production rate to gassed power input per unit volume, the gas superficial velocity and the maximum microorganism concentration. Gusek *et al.* (1991) showed that *Thermomonospora fusca* biomass production was comparable in a shake flask and a 10 l fermenter fitted with two marine impellers, agitated at an impeller speed of 1.6 m/s and aerated at 3 l/min. However, the shake flask culture yielded 30 μg protease/ml compared to 4.6 μg/ml in the fermenter. The use of Rushton impellers at an impeller tip speed of 1.18 m/s produced a 5-fold decrease in biomass.

Dabee and Harrison (1996) showed that an impeller speed of 5.8 m/s in a 5 liter stirred tank reactor, growth and productivity of *Mucor rouxii* was inhibited. After a period of adaption, the growth and productivity levels recovered. Morphology changes were also observed. At a low impeller speed (2.1 m/s), the morphology of exponentially growing cells was yeast-like (arthrodpores). At an impeller speed of 5.9 m/s, the mycelial form predominated. The hyphae were thick, short and branched.

The leakage of intracellular nucleotides from fungi at high stirrer speeds was reported by Tanaka *et al.* (1975). The release was not due to cell disruption. Ujcovo *et al.* (1980) found no correlation between nucleotide release and stirrer speed.

2.4.4 Animal cells

Animal cells are particularly susceptible to hydrodynamic trauma, because they are large (10-100 μm) and they lack a protective cell wall.

Moreira *et al.* (1995a) investigated the kinetics and mechanism of the disruption of Baby Hamster Kidney cell aggregates in spinner flasks. Disruption of aggregates occurred by two mechanisms: fragmentation and surface erosion of cells from large aggregates. It was also observed that fluid forces compact the aggregates (Moreira *et al.*, 1995b). The empirical relationship between the aggregate diameter and the power dissipation per unit volume was close to -1/4, suggesting a correlation with a critical turbulence microscale. Al-Rubeai *et al.* (1990) achieved a lower maximum cell number and growth rate of TB/C3 murine hybridomas at high agitation in shaker bottles. The synthesis of DNA was also inhibited. The mitochondrial activity increased as a response to stress, possibly in order to supply energy to repair damage. Nollert *et al.* (1991) showed that endothelial cells respond within minutes of exposure to laminar shear stress by increasing their metabolism and increasing the level of secondary messengers inositol triphosphate and calcium ion concentration.

Zhang *et al.* (1995) observed the total disruption of TB/C3 hybridoma cells in a standard 2 liter stirred tank reactor fitted with a Rushton turbine impeller at an impeller tip speed of 6.02 m/s in the absence of sparging. This corresponded to an average energy dissipation rate of 58 m^2/s^3. Peterson *et al.* (1990) showed that hybridoma cells (CRL-8018) taken from the lag or stationary phase were more sensitive to shear than those from the exponential phase. Zhang *et al.* (1992a) found that the mechanical strength of TB/C3 hybridomas rose significantly in the exponential phase and fell in the death phase. Lee *et al.* (1988) showed that hybridoma cells (S3H5/γ2bA2) in the stationary and death phase were more sensitive to cell death caused by shear forces, associated with mechanical agitation, than cells in the exponential phase.

Abu-Reesh and Kargi (1989) showed that turbulent shear was more damaging to hybridoma membrane integrity, respiration activity and cell lysis than laminar shear. Tan *et al.* (1992) observed more cell damage of hybridomas cells when the agitation speed, in a 1.3 l bioreactor equipped with a cell-lift impeller, was increased abruptly by a large step change (60 to 160 rpm) than when agitation speeds were changed gradually by small steps. This indicated that cells are able to acclimatise to hydrodynamic forces that are increased gradually.

Losses of hybridoma viability over long periods has been observed by Abu-Reesh and Kargi (1989) and Smith *et al.* (1987). Milder and Finn (1966) sheared osmotically shocked protozoa in a coaxial cylindrical viscometer and reported damage in two phases. A rapid initial loss of cell integrity was followed by secondary damage to the cell membrane at a lower rate. The latter may result from fatigue effects on repeatedly stressed cells. Al-Rubeai *et al* (1995b), based on their experimental findings, hypothesised that there are two mechanisms of hybridoma cell destruction by hydrodynamic forces, and that their relative expression is dependent on the energy dissipation rate. A cell will die passively from necrosis as a result of mechanical damage at sufficiently high levels of stress intensity. Active cell suicide, apoptosis, occurs with milder mechanical forces. The cell may initially invoke repair mechanisms, but the ongoing stress may eventually cause the induction of the apoptotic pathway. The cytoskeleton collapses, causing a rapid decrease in the physical strength of the cell. Exposure to forces to which it was previously resistant, now results in its complete destruction.

Because the hydrodynamics in stirred tanks are poorly understood, better characterised capillary systems have been used to study shear effects on animal cells. The energy dissipation rates in capillary flow are several orders of magnitude higher than those found in stirred tank reactors. Al-Rubeai *et al.* (1995a) showed that the exposure of TB/C3 hybridoma cells to turbulent capillary flow, resulted in the preferential destruction of older cells. McQueen *et al.* (1987) showed that the probability of mouse myeloma cell lysis per pass through a capillary tube increased with wall shear stress level and increased with residence time per pass in the tube. Lysis was observed at a wall shear stress level of 180 N/m^2. Augenstein *et al.* (1971) found that cell damage of mammalian cells in turbulent

capillary flow could be characterised by a rate constant which was first order with respect to cell number and dependent on the wall shear stress in the capillary section.

Zhang *et al.* (1993) modelled the disruption of TB/C3 hybridoma cells in turbulent capillary flow. It was assumed that cells were deformed by similarly sized eddies. The surface deformations were postulated to increase membrane tension and then to disrupt the cell when the surface energy was exceeded. The animal cell was considered to be an incompressible fluid surrounded by an elastic membrane. This is a gross simplification of the complex structure of a typical animal cell. The mechanical cell properties, cell bursting tension, elastic area compressibility modulus and cell size, were measured using the micromanipulation method (Zhang *et al.*, 1992b). The model was tested in turbulent capillary flow up to an average energy dissipation rate of 2×10^4 m^2/s^3 and found to underestimate cell damage by 15%. The model gave a poor estimate of cell damage in a stirred tank reactor (Zhang *et al.*, 1995). Born *et al.* (1992) developed a model to predict disruption of animal cells by laminar shear stress. It was proposed that cells deformed into prolate ellipsoids when exposed to laminar shear stress and disrupted when the bursting membrane tension, as predicted by the micromanipulation technique, was overcome.

Cell damage has been attributed to the interaction of cells with similarly sized turbulent eddies in the impeller discharge zone as well as with collapsing air bubbles at the air medium interface. Kunas and Papoutsakis (1990) found that two phenomena participate in cell damage: bulk-liquid turbulence and vortex formation with associated bubble entrainment and bubble breakup. In the absence of vortex formation, hybridoma cells flourished at impeller tip speeds up to 2.6 m/s. At higher speeds, the local impeller zone Kolmogorov microscale (< 13 μm) approached the cell diameter (12 μm), and cell damage ensued. With a vortex, growth was inhibited at a lower impeller tip speed of 0.7 m/s. In this case the impeller zone Kolmogorov microscale was larger than the cell diameter. Hydrodynamic forces that accompany gas bubbles collapsing at the air liquid interface were implicated as the source of the cell damage. Oh *et al.* (1989) grew three murine hybridomas in surface-aerated 1.4 l reactors agitated by propellers or Rushton turbines. Cell growth and viability, monoclonal antibody production, glucose and lactate consumption and metabolic activity were unaffected at impeller tip speeds of 0.26 to 1.18 m/s provided no air was entrained at the surface. If air

was sparged or entrained, cell growth rates declined with increasing impeller tip speeds. Handa-Corrigan *et al.* (1989) ascribed the damaging effect to mammalian cells in a bubble column to the bubble disengagement zone and not to the bubble riser or bubble distributor zone. They found that cell viability depended on the cell type, the bubble size and the bubble frequency. Small bubbles at high frequencies resulted in decreased viability.

Protective agents are commonly used to improve the survival of animal cells exposed to hydrodynamic stress. Non-ionic surfactants, such as Pluriol PE6800 and Pluronic F68, have a concentration dependent protective effect, as does foetal calf serum. Pluronic F68 has been shown to increase the strength of cells (Zhang *et al.*, 1992d). Lee *et al.* (1989) have suggested that serum can decrease the shear sensitivity of hybridomas by changing the physiological properties of the cells. Since the surfaces of bubbles and cells are hydrophobic, cells tend to adhere to bubbles as they rise to the surface. Cells in the vicinity of collapsing air bubbles are subjected to rapid accelerations which may be detrimental to their viability. Pluronic F68 coats the bubble and cell surface preventing their adhesion thereby protecting the cells. Antifoam on the other hand increases the degree of cell damage by increasing the hydrophobicity of the cell and bubble surfaces (Zhang *et al.*, 1992c).

2.4.5 Plant Cells

Single plant cells in suspension can range from 20 to 100 μm in diameter. Plant cells in suspension cultures have a tendency to aggregate primarily due to incomplete cell separation after mitosis. Plant cells are surrounded by a thick rigid cellulose-based cell wall. The cytoplasm is highly dense and structured. Plant cells also possess large vacuole compartments, in some cases 80% of the cell volume.

Leckie *et al.* (1991) showed that impeller speed affected the growth and alkaloid accumulation of *Catharanthus roseus* cells. Using two standard 12 cm diameter turbine impellers in a 7.5 liter stirred tank reactor, the growth and alkaloid production decreased with increasing impeller tip speed in the range 1.88 m/s to 4.4 m/s.

Nicotiana tabacum cells were subjected to shear stresses in a Couette-type shearing device

and changes in cell viability, cell lysis and the accumulation of secondary metabolites (phenolics) monitored (Hooker *et al.*, 1989). Increasing shear stress caused an increase in cell death, lysis and secretion of phenolics. Cultures in the late exponential and early stationary phases were more susceptible to damage than cultures in the lag, early exponential and late stationary phases.

The shear susceptibility of *Morinda citrifolia* cultures was investigated in turbulent capillary flow by Kieran *et al.* (1995). Shear stresses were varied from 25 to 350 N/m^2. The relative viability loss was found to conform to a first order model in which the rate constant was observed to increase with the imposed shear stress:

$$\frac{C_X}{C_{X_o}} = e^{-A_1 t_{exp}} \qquad (1)$$

where C_{Xo} is the viability of the sample before shearing, C_X is the viability after an exposure time of t_{exp} seconds, and A_1 is the first order rate constant. A linear relationship was identified between the specific death rate constant and the imposed shear stress. Morphological measurements showed that over the course of the shear tests, there was a reduction in the mean chain length and in the spread of the data.

Experiments conducted in a Couette cylindrical viscometer showed that carrot cells (*Daucus carota*) exhibit a wide variety of biological responses depending on the magnitude of the applied force (Dunlop *et al.*, 1994). In the range 0.5 to 100 N/m^2, carrot cells lost the ability to grow and divide. Intracellular enzyme activity was not seriously affected until a shear stress level of 750 N/m^2 was applied. At 3000 N/m^2 intracellular enzyme activity was severely compromised. Membrane integrity was damaged at shear stress levels in the 3000 to 10000 N/m^2 range. Cell lysis only occurred at stresses in excess of 10000 N/m^2 applied over an hour period. In each case the loss of the biological response could be characterised by a first order rate constant.

Since cell viability was lost at stress levels 2 to 3 orders of magnitude below that required to compromise membrane integrity, it has been presumed that plant cells have a mechanism for sensing the applied force and responding to it. Lintelhac and Vasecky (1984) and Pickard

(1984) postulated that plant cells possess receptors in the cell membrane or the cell wall, which communicate the magnitude of the applied stress to the control centres in the cell via secondary messengers. At shear stresses greater than 10 N/m^2, control pathways are activated which selectively inhibit mitosis without affecting membrane integrity or the electron transport chain activity. Dunlop *et al.* (1994) showed that the intracellular enzyme activity and cell lysis are affected by turbulent stresses lower in magnitude than those required to generate the same degree of damage in laminar flows.

2.4.6 Non-living Particles

The breakup of flocs by turbulent shear stresses has been studied extensively. The breakup of flocs is influenced critically by two opposing factors, namely the mechanical strength of the flocs and the breaking forces. Two floc breakup mechanisms have been suggested: surface erosion of primary particles and floc splitting (Parker *et al.*, 1972; Glasgow, 1989; Ayazi Shamlou *et al.*, 1990; Moreira *et al.*, 1995a). Parker *et al.* (1972) correlated the rate of surface erosion with the number of flocs (n_F), the disruption frequency ($f(d_l)$, equal to the frequency of similarly sized turbulent eddies) and the number of primary particles released per erosion (n_p).

Poncelet and Neufeld (1989) studied the breakage of nylon capsules in a turbine reactor. The microcapsules simulated animal cells. The breakage kinetics were first order with respect to microcapsule concentration. The empirical study showed that the breakage constant was dependent on temperature and particle size, and proportional to the average shear rate and the third power of the impeller angular velocity.

2.4.7 Conclusions

Hydrodynamic forces, associated with agitation and collapsing bubbles in bioreactors are exerted on the cell wall structure and may result in sub-optimal microbial activity. The relative differences in sensitivity of different cell types is dictated by biological and physical properties of the cells. Bacteria and lower eukaryotes are much less sensitive to hydrodynamic stress than higher eukaryotes due to their small size and the presence of a cell

wall. When microorganisms form aggregates through flocculation or hyphal growth they are more susceptible as they experience a larger fraction of the fluid kinetic energy. Cells interact with similarly sized turbulent eddies; larger eddies contain more energy. Animal and plant cells are more sensitive to shear forces. Animal cells are large in size and lack a protective cell wall. Plant cells are even larger than animal cells and form large aggregates, however they possess a rigid cellulolytic cell wall.

Animal cells from the stationary and death phases are more sensitive to damage due to hydrodynamic stress than cells in the exponential phase. This is contrary to results obtained for bacteria and yeasts, where the stationary phase cells are mechanically more resistant than exponentially growing cells .

Five categories of biological response have been identified: change in integrity, viability, metabolic rate, metabolic pathway and morphology. Loss of cell integrity implies complete rupture of the cell envelope. Viability is defined as the ability of a cell to divide or its ability to exclude viability stains. Metabolic rate changes have been observed as decreased growth rate, substrate utilisation rate, oxygen utilisation rate and metabolite production rate. A shift in the product spectrum, a change in the metabolism from the TCA cycle to the glycolytic pathway and the release of stress indicators (histamine) have been reported as metabolic pathway changes. Morphological changes with regard to size and shape have been described. In the study of the biological response to hydrodynamic stress, it is important that suitable analytical techniques be chosen to enable the detection of changes in each of these categories.

Modelling of cell breakage, loss of viability and productivity changes in animal cells, plant cells and fungi has shown that the biological response to hydrodynamic stress is a function of the magnitude of the hydrodynamic force and the exposure time.

2.5 HYDRODYNAMIC CHARACTERISATION OF BIOREACTORS

2.5.1 Description of flow patterns

The overall flow pattern in a stirred tank generated by a disk turbine is shown in Figure 3. The rotating disk turbine causes radial flow outward. This radial jet entrains the surrounding fluid and slows down as it approaches the wall. At the wall the stream is split into an upward and a downward portion which circulate through the bulk of the tank and return to the impeller region.

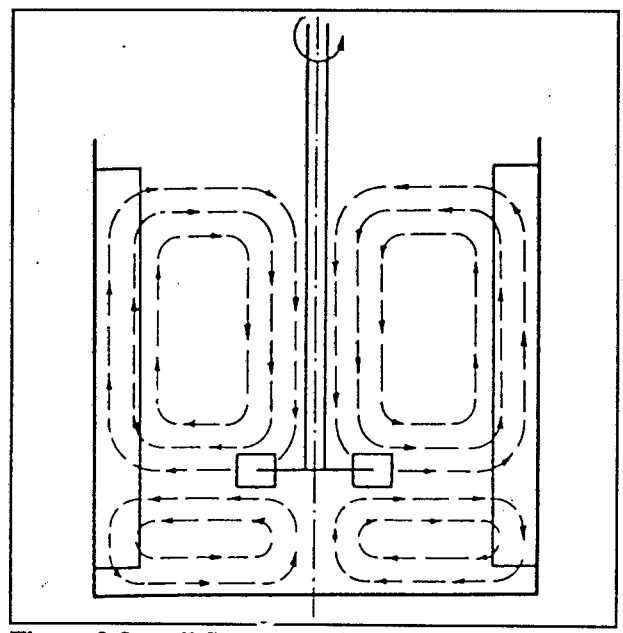

Figure 3 Overall flow pattern in a stirred tank generated by a disk turbine (Joshi *et al.*, 1982).

As the blade moves forward, fluid is accelerated over and under the blades, and forced inward by centrifugal and pressure forces toward the back of the blade. A stable vortex is formed which is convected outward from the blade. For a disk impeller, a pair of counter rotating vortices are formed, one along the top edge and the other along the bottom edge of the blade (Figure 4 and 5).

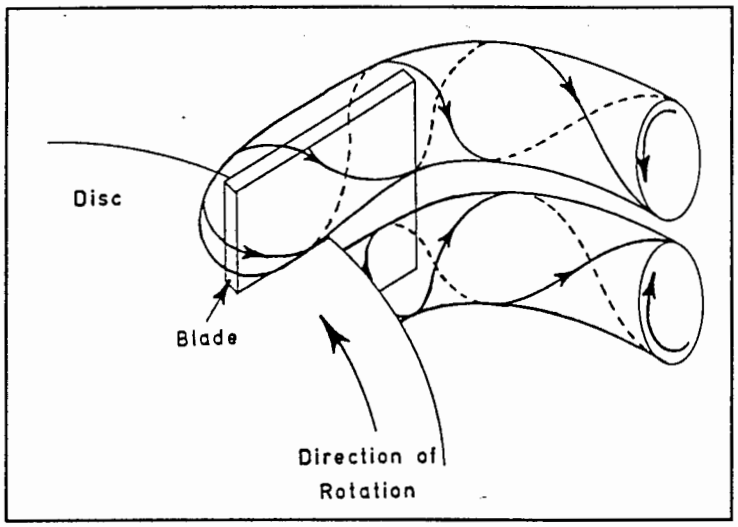

Figure 4 Trailing vortices behind a Rushton turbine blade (Stoots and Calabrese, 1989).

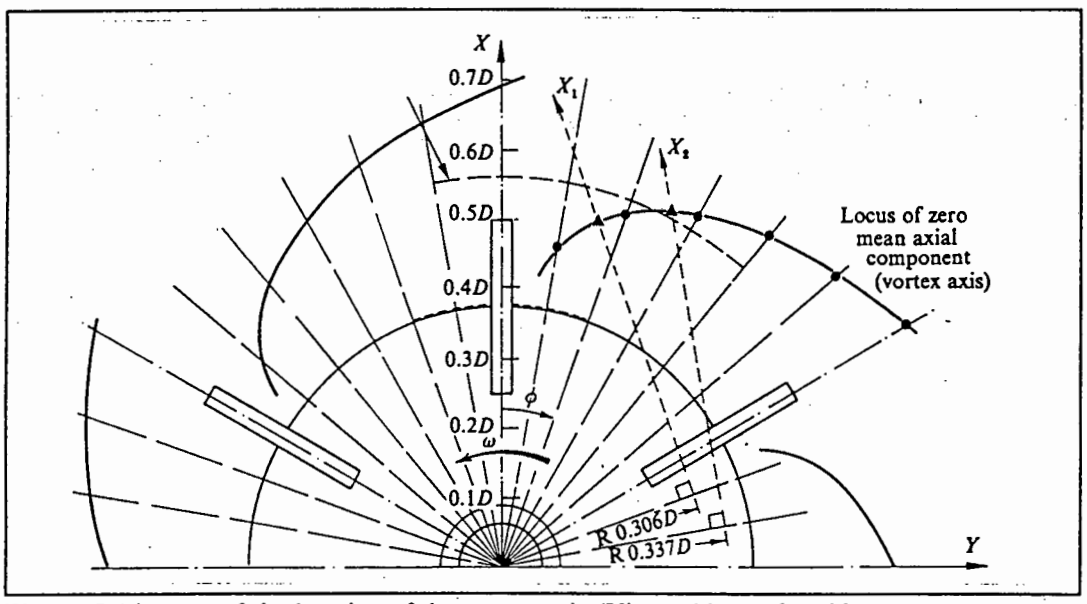

Figure 5 Diagram of the location of the vortex axis (Yianneskis *et al.*, 1987).

Flow in a stirred tank is highly inhomogeneous with most of the energy from the impeller being dissipated in the impeller region. Flow at the tip of the blade and in the trailing vortex is characterised by steep mean velocity gradients and high pseudo-turbulence. This is the only part in the reactor where the contribution to energy dissipation by mean velocity gradients

is significant. It is as high as 10% of the total energy dissipation at the blade tip and decreases to 1% for the remainder of the vortex system (Calabrese and Stoots, 1989). As the vortex moves away from the blade, it breaks down into a region of very strong turbulence just over one blade width from the edge of the impeller (Calabrese and Stoots, 1989). Due to fluid friction, this is a region of highest energy dissipation.

2.5.2 Basic Principles of fluid mechanics

As a guide to understanding the theory of turbulent flow in stirred tank reactors, some of the basic principles and terminologies used in fluid mechanics have been described (Calabrese and Stoots, 1989).

The instantaneous velocity at a point (U_i) is the sum of the average velocity ($\bar{U}_i$), and the fluctuation velocity (u_i):

$$U_i = \bar{U}_i + u_i \tag{2}$$

For N measurements of the ith component, the average velocity is:

$$\bar{U}_i = \frac{1}{N} \sum_{k=1}^{N} U_{ik} \tag{3}$$

The mean square turbulent velocity is the variance of the distribution of the instantaneous velocity:

$$\overline{u_i^2} = \frac{1}{N} \sum_{k=1}^{N} (U_{ik} - \bar{U}_i)^2 \tag{4}$$

The magnitude of the mean velocity ($\bar{U}$) and the magnitude of the root mean square (RMS) turbulent velocity (q) is the vector sum of their three individual components:

$$\bar{U} = [\bar{U}_x^{\,2} + \bar{U}_y^{\,2} + \bar{U}_z^{\,2}]^{\frac{1}{2}} \tag{5}$$

$$q = [\overline{u_x^2} + \overline{u_y^2} + \overline{u_z^2}]^{\frac{1}{2}} \quad (6)$$

The total kinetic energy per unit mass (k) is a measure of the strength of turbulence in a velocity field:

$$k = \frac{1}{2}q^2 \quad (7)$$

To assess the hydrodynamic forces that exist in a flow field, one needs to evaluate the stress caused by the mean velocity gradients as well as the Reynold's stress due to the velocity fluctuations. The stress due to mean velocity gradients is given by Newton's law of viscosity. Each of the three components of velocity can vary in the three coordinate directions. There are therefore nine components of stress tensor τ_{ij}:

$$\tau_{ij} = \mu \Delta_{ij} \quad (8)$$

where Δ are the components of the mean rate of deformation tensor for incompressible flows:

$$\Delta_{ij} = \frac{\partial \overline{U}_i}{\partial x_j} + \frac{\partial \overline{U}_j}{\partial x_i} \quad (9)$$

The mean deformation rate γ due to normal and shear stresses is given by:

$$\dot{\gamma} = \sqrt{\frac{1}{2} \Delta : \Delta} \quad (10)$$

The rate of energy dissipation ($\bar{e}$) due to mean velocity gradients is a function of the kinematic viscosity and the mean deformation rate,

$$\bar{e} = \nu \dot{\gamma}^2 \quad (11)$$

Since Reynold's stress (τ^t) accounts for simultaneous velocity fluctuations in two directions, measurement of this quantity is difficult.

$$\tau^t = \rho \overline{u_i u_j} \quad (12)$$

It is therefore necessary to relate it to a quantity that is more readily measured. Turbulent

kinetic energy (k) is a measure of the Reynold's stress (Calabrese and Stoots, 1989). To obtain an estimate of the turbulent energy dissipation rate per unit mass (e), the rate of energy dissipation at a point may be assumed equal to the rate of turbulent energy production. The production rate can be related to the RMS turbulent velocity and the resultant length scale of the large energy producing eddies, L_{RES}, which is of the order of the blade width in stirred tanks.

$$e = \frac{A_2 \, k^{\frac{3}{2}}}{L_{RES}} \tag{13}$$

where

$$L_{RES} = \sqrt{L^2_r + L^2_z + L^2_\theta} \tag{14}$$

and A_2 is 0.85 (Wu and Patterson, 1989).

The large energy containing eddies decay into smaller eddies. The energy flows continuously from the large macroscale eddies to the smallest microscale eddies, where viscous losses convert the kinetic energy into heat. Kolmogorov (1941) suggested that, in fully turbulent, a range of eddy sizes exist in which the turbulence can be considered to be isotropic. This is called the universal equilibrium subrange and is totally independent of external conditions. The properties of the eddies are determined solely by the energy input and the viscous dissipation. At the high wave number end of the universal equilibrium subrange, where viscous energy is dominant there is an eddy size, the Kolmogorov microscale (λ) which is uniquely determined by the kinematic viscosity and the viscous energy dissipation (Kolmogorov ,1941):

$$\lambda = \left(\frac{\nu^3}{e}\right)^{\frac{1}{4}} \tag{15}$$

Local isotropic conditions can usually be assumed in the impeller region of a stirred tank (Kawase and Moo Young, 1990). In typical biochemical engineering literature (Cherry and Papoutsakis, 1986; Ayazi Shamlou *et al.*, 1995), the eddies in the universal equilibrium subrange are subdivided according to whether their size is smaller or larger than the

Kolmogorov microscale. Eddies in the viscous dissipation subrange are smaller than the λ. Eddies with sizes greater than λ fall in the inertial convection subrange.

According to the isotropic theory of turbulence (Kolmogorov, 1941), the root-mean square velocity difference for eddies of diameter d in the viscous dissipation subrange (u_1) is given by:

$$\overline{u_1}(d) = \sqrt{\left(\frac{2}{15}\right)} \left(\frac{e}{\nu}\right)^{\frac{1}{2}} d \qquad \textbf{(16)}$$

The root-mean square velocity difference for eddies of diameter d in the inertial convection subrange (u_2) is given by:

$$\overline{u_2}(d) = 1.57\, e^{\frac{1}{3}}\, d^{\frac{1}{3}} \qquad \textbf{(17)}$$

2.5.3 Measurement of hydrodynamics in stirred tank reactors

Flow visualisation and flow measurement studies have been used by a number of researchers to characterise flow in the impeller region (Cutter, 1966; Placek and Tavlarides, 1985; Yianneskis *et al.*, 1987; Costes and Couderc, 1988; Wu and Patterson, 1989; Calabrese and Stoots, 1989; Ranade and Joshi, 1990). Fluid velocity has been measured by means of a hot-wire anemometer (Rao and Brodkey, 1972), a conductivity probe (Ranz, 1958), a laser-Doppler anemometer (Durst et al, 1976), photographic techniques (Cutter, 1966) and a Pitot tube (Rao and Brodkey, 1972).

The one dimensional energy spectra (E_1) can be obtained from the Fourier transform of the Eulerian autocorrelation coefficient (R_E) of the velocity fluctuations at a fixed point, *viz.*

$$\tilde{E}_1(n) = 2\overline{u^2} \int_{-\infty}^{\infty} R_E(\tau) e^{i2\pi n\tau} d\tau \qquad (18)$$

where n is the frequency and τ is the time delay in the auto-correlation function. The autocorrelation coefficient is given by,

$$R_E(\tau) = \frac{\overline{u(t)u(t+\tau)}}{\overline{u^2}} \qquad (19)$$

where t is time (Hinze, 1959). As the autocorrelation coefficient is a symmetric function, its Fourier transform is a real function and only the cosine part of the integral need be evaluated in determining the one dimensional energy spectrum. In a like manner, the autocorrelation coefficient can be obtained from the inverse Fourier transform of the energy spectrum function. The auto-correlation coefficient is commonly used for determining the macro and micro time scales of turbulence and for identifying large scale periodic fluctuations in the flow.

The vortices which periodically sweep the impeller region introduce a periodic non-random element to the random turbulent motion. This element of turbulence, termed pseudo-turbulence needs to be accounted for when determining experimental velocity fluctuations in stirred tanks. One of the reasons for variation in the turbulent flow characteristics reported from experimental results, is failure to account for this periodic component. This would result in an over-estimation of turbulence in the vortex region near the blade. Wu and Patterson (1989) corrected the total observed fluctuating velocity using the auto-correlation method. It was assumed that the periodic component of the turbulent velocity fluctuation could be represented by the first two terms of a Fourier series as a function of time or frequency. The contribution of the periodic component was then determined explicitly by calculating its contribution to the auto-correlation function:

$$\overline{u(t)u(t-\tau)_{tot}} = \overline{u(t)u(t-\tau)_{rand}} + \overline{u(t)u(t-\tau)_{per}} \quad (20)$$

$$\overline{u(t)u(t-\tau)_{per}} = \frac{A_3^2}{2}\cos 2m\pi\tau + \frac{A_4^2}{2}\cos 4m\pi\tau \quad (21)$$

where A_3 and A_4 are constants and m is the impeller blade frequency.

A feature of the energy spectrum is that the integral over all the frequencies gives the mean square turbulent velocity:

$$\int_0^\infty E_1(n)dn = \overline{u^2} \quad (22)$$

The Eulerian macro (T_E) and micro (τ_E) time scales can be obtained from the energy spectrum function (E_1):

$$T_E = \frac{E_1(0)}{4\overline{u^2}} \quad (23)$$

$$\tau_E^2 = \frac{\overline{u^2}}{2\pi^2\int_0^\infty n^2 E_1(n)dn} \quad (24)$$

The time scales can be converted to length scales on multiplying by the convection velocities, U_C (Wu and Patterson, 1989). These can be approximated with the local mean velocities if Taylor's frozen field hypothesis applies (Sato *et al.*, 1967; Majumdar *et al.*, 1970, Rao and Brodkey, 1972, Komasawa *et al.*, 1974; Barthole *et al.*, 1983). In this hypothesis it is assumed that in a turbulent system, the mean fluid velocity in the direction of the fluctuating velocity is large in comparison with the magnitude of the fluctuations. Taylor's hypothesis is regarded as valid if $u/U < 0.1$. The macro and micro length scales (L_f and λ_f) give an approximation of the large energy containing eddies and the smallest most frequent eddies.

The energy dissipation rate can be obtained from the turbulence microscale according to (Rao and Brodkey, 1972; Komasawa *et al*, 1974, Okamoto *et al*, 1981):

$$e = \frac{30\nu\overline{u^2}}{\lambda_f^2} \tag{25}$$

The resultant turbulent macroscale and the turbulent kinetic energy can also be used to determine the local energy dissipation rate (Batchelor, 1953) as described in Equation 13.

Turbulence is always three dimensional and a complete characterisation of the system requires the elucidation of the energy spectrum in three dimensional wave number space. If turbulence is isotropic, the energy spectrum in all directions is isotropic and a one dimensional spectrum is sufficient to describe the system.

A number of researchers have determined turbulence flow parameters in stirred tanks driven by Rushton turbine impellers. The geometric parameters and operating conditions used in their measurements are listed in Table 3. All flow studies have been performed in cylindrical stirred tanks fitted with 6-bladed standard Rushton turbine impellers (w = D/5, l = D/4) and four equally spaced baffles of diameter T/10, where w is the blade width, l is the blade length, D is the impeller diameter, T is the tank diameter, H is the liquid height and H_c is the clearance of the impeller off the bottom. A number of conclusions may be drawn from these flow studies.

Table 3 Geometric parameters and operating conditions used in flow studies.

REFERENCE	H/T	D/T	H_c/T	AGITATION RATE rpm
Cutter(1966)	1	1/3	1/3	200-700
Yianneskis *et al*, 1987	1	1/3	1/4, 1/3, 1/2	300
Costes and Couderc, 1988	1	1/3	1/2	75,115, 165
Wu and Patterson, 1989	1	1/3	1/3	100, 200, 300
Calabrese and Stoots, 1989	1	1/3	1/2	180
Ranade and Joshi, 1990	1	1/3	1/2	300

2.5.3.1 Mean flow velocities in stirred tank reactors

The maximum average radial and tangential mean velocities (averaged over an impeller revolution of 360°) exist near the tip of the centreline of the impeller and are 0.7 to 0.8 times the impeller tip speed, U_{tip} (Figures 6 and 7). The plane containing the maximum radial and tangential velocities bends upward slightly away from the impeller, the extent of which is a function of impeller geometry and position (Yianneskis *et al.*, 1987). The mean radial and tangential velocity gradients decrease with radial distance from the impeller. The tangential velocity component decreases more sharply than the radial velocity component. The vertical profiles of radial and tangential velocity components become more and more flat as one moves away from the impeller, due to the entrainment of surrounding fluid. The fluid approaching the impeller from above and below has an almost flat profile and an axial velocity of about 0.15 U_{tip}. The axial velocity is much smaller than the other two components of velocity and decreases with increasing radial distance until the point where the impeller stream splits into two streams, one moving upward the other downward.

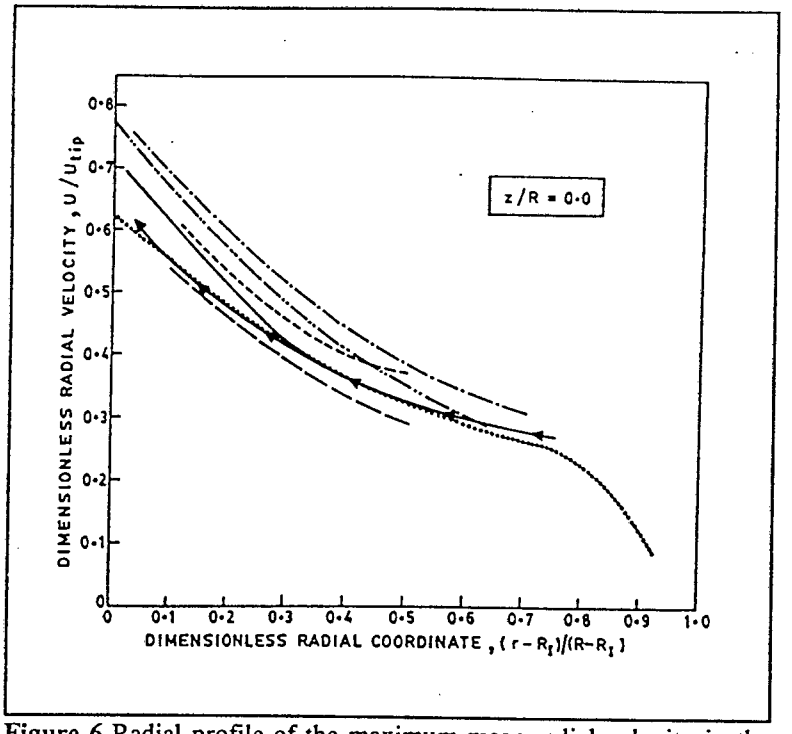

Figure 6 Radial profile of the maximum mean radial velocity in the centre of the impeller stream (Renade and Joshi, 1990).

Cutter (1966) .....
Cooper and Wolf (1968) — — — — — — — —
Van der Molen and Van Maanen (1978) —..—..—..—
Drblohlav *et al.* (1978) -
Chen *et al.* (1988) —.—.—.—.—.—.—.—.—.—
Wu and Patterson (1989) ◄——◄——◄——◄——◄
Ranade and Joshi (1990) ————————————

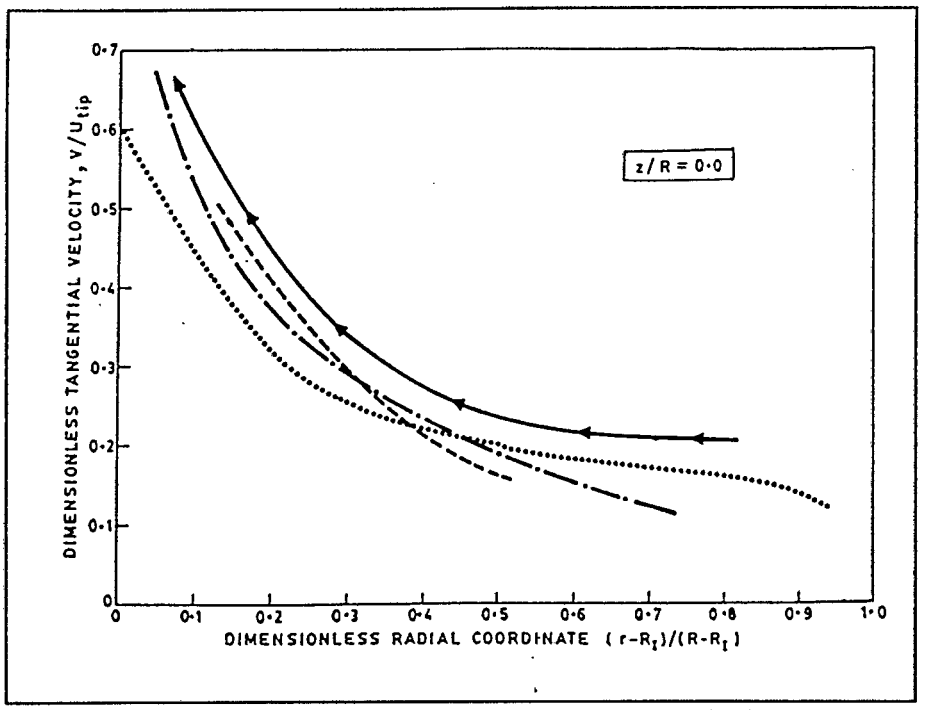

Figure 7 Radial profile of the maximum mean tangential velocity in the centre of the impeller stream (Renade and Joshi, 1990). Legend as in Figure 6.

2.5.3.2 Mean square fluctuating velocity

As mentioned previously, the value of the total mean square turbulent fluctuating velocity can be separated into a periodic component due to the vortex motion and a random component due to fluid turbulence (Wu and Patterson, 1989). A comparison of the radial profiles of the total and random mean square turbulent fluctuating velocities (averaged over 360°) in Figure 8 show that the periodic component dominates near the impeller and decreases with radial distance from the impeller. Its contribution to the total fluctuating velocity decreased from 80% near the impeller to a negligible portion impeller diameter away from the impeller. The random turbulence is still developing near the impeller, but becomes dominant about two impeller blade widths away in the region of high turbulence where the vortices break down. The average random mean square turbulence fluctuating velocity increases to the maximum value of 0.4 U_{tip} and then decreases with increasing radial distance in the centreline of the impeller stream.

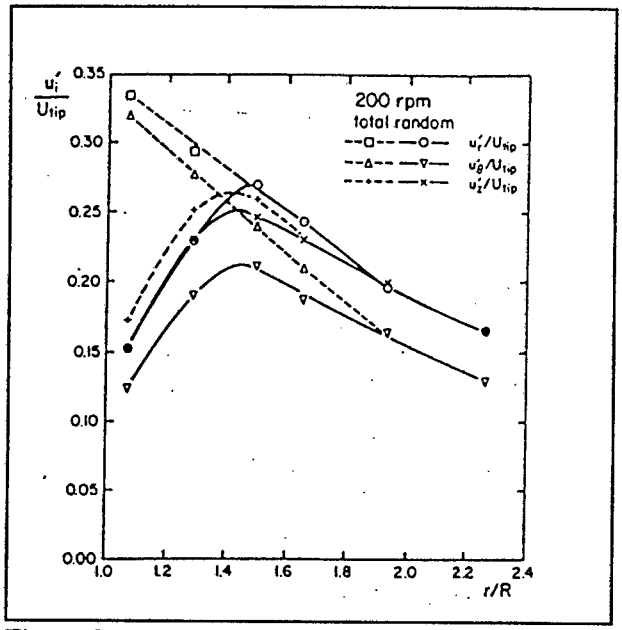

Figure 8 Radial distribution of the mean square fluctuating velocity at the centre of the impeller stream where R is the impeller radius and r is the distance from the impeller shaft in the radial direction (Wu and Patterson, 1989).

The mean square fluctuating turbulence velocities were averaged over an impeller revolution. Yianneskis *et al.* (1987) showed that the total local fluctuating velocity varied with angle between the blades. A maximum was reached approximately 20° beyond the blade, the position at which the periodic component of turbulence peaked *i.e.* where the mean velocity peaked. The mean square fluctuating velocity is in itself an average of squared fluctuating velocities as a function of time.

Costes and Couderc (1988) showed that, in non-dimensional form, the mean and fluctuating velocity profiles were independent of the system size and the rotational speed of the turbine. The experimental results can therefore be used as general boundary conditions for geometrically similar systems.

2.5.3.3 Overall energy balances

Attempts at overall energy balances over various regions of a stirred tank have been reported. The vessel may be divided into three regions: the impeller swept volume, the impeller stream and the circulation region. The impeller swept volume is the cylindrical region containing the impeller with r varying from zero to 1.08 R (where R is the impeller radius) and z from -

2w to 2w. The impeller region is the annulus region from r = 1.08 R to 2.26 R with the same range of z as the impeller swept volume.

In the impeller stream and the impeller swept volume, turbulent intensity is high. The turbulent energy dissipation is the difference between the inflow and the outflow of kinetic energy through the boundaries, plus the power input from the impeller if it is contained in the control volume. The contribution of potential energy, pressure work and viscous dissipation energy can be assumed negligible. The radial kinetic energy flow rate through the surface at r is:

$$KE_r = \frac{\rho}{2}\int_{z_1}^{z_2}\int_{0}^{2\pi} \overline{[(\bar{U}_r + u_r)^2 + (\bar{U}_\theta + u_\theta)^2 + (\bar{U}_z + u_z)^2](\bar{U}_r + u_r)}\, r\, d\theta dz \qquad (26)$$

The axial kinetic energy flow rate through the surface at z is,

$$KE_z = \rho\pi\int_{r_1}^{r_2}\int_{0}^{2\pi} \overline{[(\bar{U}_r + u_r)^2 + (\bar{U}_\theta + u_\theta)^2 + (\bar{U}_z + u_z)^2)](\bar{U}_z + u_z)}\, r\, d\theta dr \qquad (27)$$

In the calculation of the kinetic energy flow rates, the periodic element fluctuation velocities should be included as they contribute to the total kinetic energy.

The power input through the impeller can be calculated from the power number correlation:

$$P_o = N_p\, \rho\, v_{imp}^{\ 3}\, D^5 \qquad (28)$$

where P_o is the ungassed power drawn, N_p is the power number, v_{imp} is the impeller speed and D is the impeller diameter.

Wu and Patterson (1989) concluded that 30% of the total energy was dissipated in the impeller swept volume, 30% in the impeller region and 40% in the circulation region. Cutter (1966), who ignored the axial contribution of kinetic energy flow rate, showed that the distribution of kinetic energy to the three regions was 20, 50 and 30% respectively. In an impeller swept region bounded by $0 < r < 1.5R$ and by $-2w < z < 2w$, Ranade and Joshi (1990) calculated the energy dissipation rate to be 35 to 40% of the total input rate. This

report agrees well with the results of Wu and Patterson (1989). The fluid in the impeller region represents only about 9% of the total. The energy dissipation rate per unit mass in the impeller stream is therefore 15 fold that in the rest of the vessel.

2.5.3.4 Power consumption

The total energy dissipated in a stirred tank is related to the power consumption of the impeller. The latter has been measured and correlated (Rushton *et al.*, 1950; Bates *et al.*, 1963; Bates *et al.*, 1966; Nienow and Miles, 1971) and is given by Equation 28. The power number, N_p, in the relationship is a function of Reynold's number and vessel geometry (Figure 9).

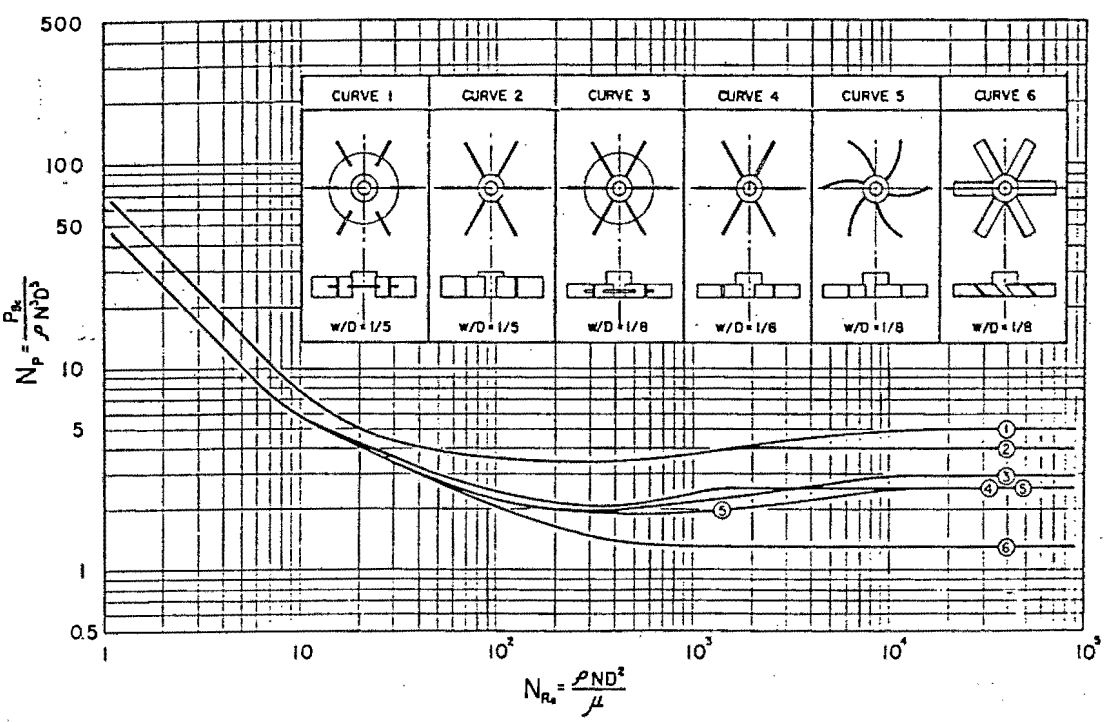

Figure 9 Power number Reynold's number correlation in Newtonian fluids for various turbine impeller designs in baffled tanks with d_b = T/10 (Bates *et al.* 1963).

The dependent effect of blade width and blade number on the agitated power drawn has been investigated by O'Connell and Mack (1950) who observed that:

$$\frac{P_1}{P_2} = \frac{A_5(w_1/D_1)^{A_6}}{23.7(w_2/D_2)^{1.09}} \quad (29)$$

where P_2 is the reference power drawn by a 6-bladed turbine. For a 2-bladed turbine A_5 = 13.8 and A_6 = 1.23, for a 4-bladed turbine A_5 = 19.4 and A_6 = 1.15 and for a 6-bladed turbine A_5 = 23.7 and A_6 = 1.09.

The clearance beneath the impeller affects the agitated power drawn. The power number of a standard Rushton 6-bladed impeller was found to increase from 0.42 to 5 as the impeller clearance ratio C/D was increased from 0.25 to 1 (Bates *et al.*, 1963). No effect on the power drawn was observed above a clearance ratio of 1.

The introduction of air into a stirred tank reduces the medium density and therefore reduces the power consumed by the impeller. Michel and Miller (1962) correlated the gassed power drawn by the impeller:

$$P_g = A_7 \left[\frac{P_o^2 \, v_{imp} \, D^3}{Q_g^{0.56}}\right]^{0.45} \quad (30)$$

where A_7 is a function of impeller geometry and Q_g is the air flow rate. Yung *et al.* (1979) found that A_7 = 0.812 for a 6-bladed Rushton turbine and 0.829 for a four-bladed paddle for a range of D/T values from 0.225 to 0.45. Loiseau *et al.* (1977) obtained a value of A_7 of 0.83 for a standard 6-bladed turbine with D/T of 1/3 located at a distance T/3 from the bottom of the vessel. Loiseau *et al.* (1977) obtained a good fit of their experimental data with Equation 30 for,

$$1 < \frac{P_o^2 \, v_{imp} \, D^3}{Q_g^{0.56}} < 10^7 \quad (31)$$

The effect of multiple impellers on the agitated power drawn has been investigated. For ungassed systems, Bates *et al.* (1963) observed that the power drawn by 2 standard Rushton turbine impellers was double that for a single turbine impeller if the impeller spacing ratio, S/D was greater than 1.5 (Figure 10).

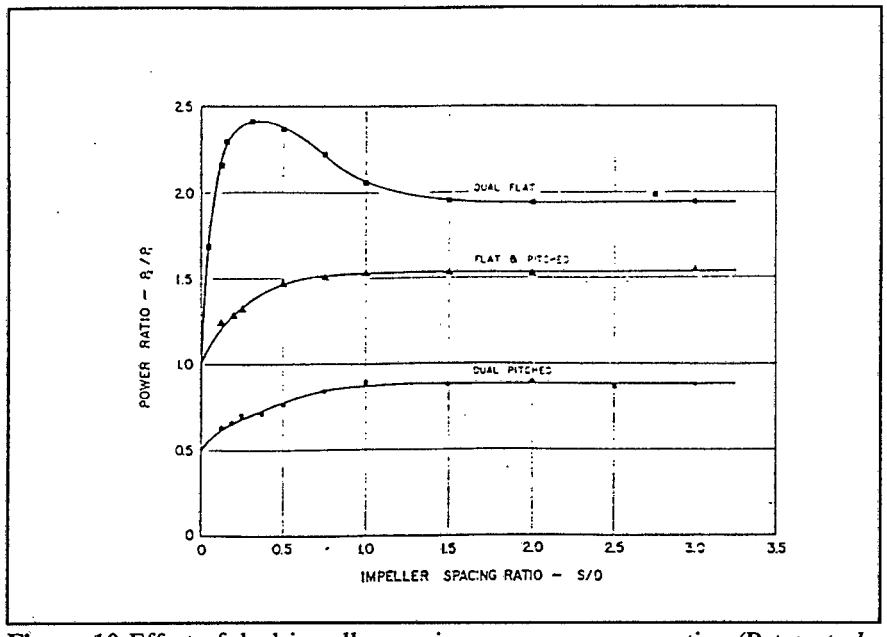

Figure 10 Effect of dual impeller spacing on power consumption (Bates *et al.*, 1963).

Since all the gas passes through the lower impeller the power drawn by the lower impeller can be estimated by gassed power correlations. Since less gas passes through the upper impeller (Chiampo and Marotto, 1995), the gassed power drawn by the upper impeller is always greater than that drawn by the lower impeller and always less than the ungassed power of the upper impeller.

$$(P_g/P_o)_1 < (P_g/P_o)_2 < 1 \tag{32}$$

The overall average energy dissipation rate per unit mass (e_{AVE}) can be determined from the power drawn,

$$e_{AVE} = \frac{P_g}{V\rho} \tag{33}$$

where V is the liquid volume.

2.5.3.5 Local energy dissipation rates

Reported values of turbulent energy dissipation rates vary widely (Table 4). The observed discrepancies stem from differences in the choice of the eddy length and the use of the random or total turbulent kinetic energy.

Table 4 Energy dissipation rates in a stirred tank ($e = A_2 k^{3/2}/L_{RES}$).

REFERENCE	e DATA	L_{RES}	k	A_2
Cutter(1966)		Based on space correlation measurements	total	1.44
	e_{MAX}/e_{AVE} = 70 at blade tip	0.3w		
	e_i/e_{AVE} = 20 e_b/e_{AVE} = 0.26	0.3 to 0.5w 0.7w		
Okamoto *et al*(1981)	e_i/e_{AVE}=15.6 e_b/e_{AVE} = 0.27	Used Eulerian microscale (Equation 25) to calculate e	total	
Costes and Couderc(1988)		Order of magnitude estimate	total	4.4
	e_i/e_{AVE}=5 to 10	5w		
Wu and Patterson(1989)		Based on auto-correlation function	random	0.85
	e_{max}/e_{AVE}=23.5 distance 2w from impeller tip in centreplane	0.5w		
	e_i/e_{AVE}=13	0.5 to 0.7w		

Wu and Patterson (1989) evaluated axial, radial and tangential Eulerian length macroscales in the impeller zone. The results are shown in Figure 11. In the region near the blade tip the resultant length macroscale is approximately 0.35 times the blade width. The value decreases to approximately 0.25 times the blade width about two blade widths away from the impeller, the region corresponding to maximum turbulence. The macroscale then increases again with increasing radial distance from the minimum value to about 0.5 at the edge of the impeller stream.

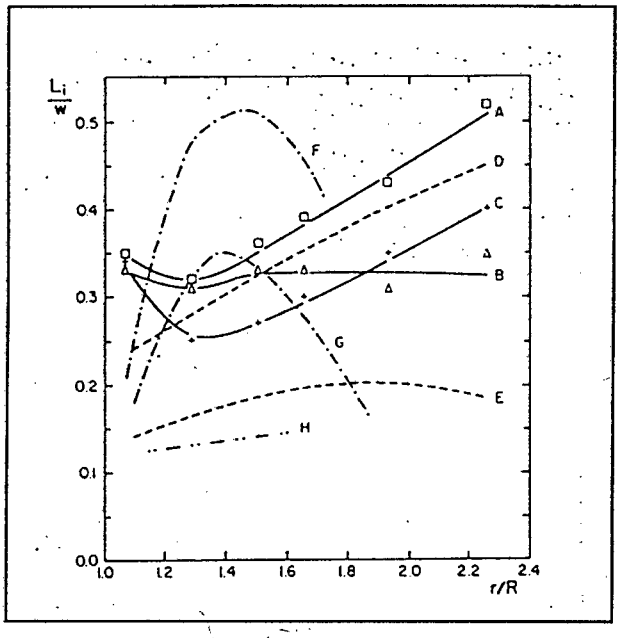

Figure 11 Radial distribution of Eulerian length macroscale at the centre of the impeller stream (Wu and Patterson, 1989):(A),(B) and (C) are the radial, tangential and axial turbulence macroscales respectively at 200 rpm from Wu and Patterson (1989); (D) and (E) are the axial and radial turbulence macroscales from Cutter (1966); (F) and (G) are the radial turbulence macroscales for a 6" and 5" impeller respectively from Majumdar (1970); (H) radial turbulence macroscale from Komasawa *et al.* (1974).

Wu and Patterson (1989) are unique in basing the turbulent energy dissipation on the random fluctuating velocity component. All the other energy dissipation rates are over-estimates of the actual values. This is particularly relevant at the tip of the impeller where the periodic fluctuating velocity dominates (Figure 8). Local values of energy dissipation rate in the impeller region, reported by several research groups, have been compared by Wu and Patterson as a function of radial distance (Figure 12).

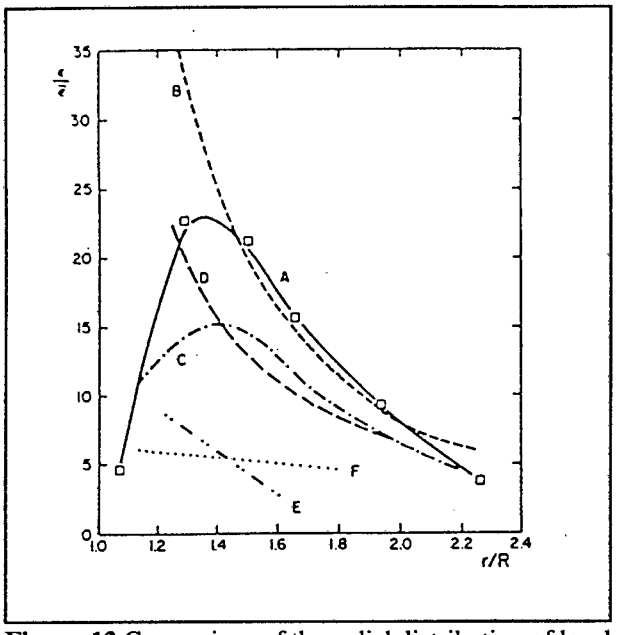

Figure 12 Comparison of the radial distribution of local energy dissipation rates at the centre of the impeller stream (Wu and Patterson, 1989).

(A) 200 rpm Wu and Patterson (1989),
(B) Cutter (1966)
(C) Laufhutte and Mersmann (1985),
(D) Rao and Brodkey (1972),
(E) Komosawa *et al.* (1974),
(F) Okamoto *et al.* (1981).

The ratio e/e_{AVE} should be independent of impeller speed and impeller diameter for geometrically similar systems as (Placek and Tavlarides, 1985),

$$\frac{e}{e_{AVE}} \sim \frac{(N^2D^2)^{\frac{3}{2}}/D}{(N^3D^5)/(T^2H)} = \frac{T^2H}{D^3} \qquad (34)$$

2.5.3.6 Evaluation of hydrodynamic stress parameters in biological systems

Using the correlations for impeller power consumption (Equations 28, 29, 30, 32), the average and local maximum energy dissipation rates have been estimated for various stirred tank configurations at the operating conditions at which a biological response of various organisms have been reported in the literature (Table 5). This is limited to instances where sufficient specification of hydrodynamic conditions was given. The maximum energy dissipation rate in the impeller region of the stirred tank reactors was assumed to be 25 times the average energy dissipation rate (Wu and Patterson, 1989).

Table 5 Calculated levels of local and average energy dissipation rates at which different kinds of organisms are traumatised.

REFERENCE	SYSTEM	ORGANISM AND SIZE	N_{crit} rpm	RESPONSE	e_{AVE} m^2/s^3	e_{MAX} m^2/s^3
Toma *et al.* (1991)	2* 6-bladed Rushton impellers in 3 litre tank D = 0.066 $^{-2}$ m, T = 0.15 $^{-1}$ m Q = 1 vvm H/T = 2 S/D = 2 d_b = 0.022 $^{-2\ m}$ 3 baffles	*Brevibacterium flavum* d: 0.8 μm l: 1.3 μm *Saccharomyces cerevisiae* d_{ave} = 5μm	900 800	partial inhibition of microbial growth - decrease O_2 uptake rate - decrease sucrose uptake rate - decreased growth rate - shift in ATP pathway	8.7 < e < 11.4 6 < e < 8	±250 ±175
Dunlop and Ye (1994)	1* 6-bladed Rushton impeller in 1.45 litre tank D = 0.09 $^{-2}$ m Q = 0.16 vvm 4 baffles	carrot cells d_{ave} = 194 μm	300	Complete inhibition of mitochondrial activity and growth Cells still intact	e = 2.54	± 63.5
Zhang *et al.* (1995)	1* 6-bladed Rushton impeller in 2 litre tank T = 0.115 $^{-1}$ m D = 0.0575 $^{-2}$ m H/T = 2 Q = zero 4 baffles	hybridoma cells d_{ave} = 12 μm	1500 2000	45% disruption of cells 85% disruption of cells	e = 25 e = 58	± 625 ±1450

2.5.4 Conclusions

Studies on the hydrodynamic characterisation of stirred tank reactors have shown that turbulence is highly inhomogeneous with maximum fluid velocities occurring in the impeller zone. The reported ratio of local energy dissipation rate in the impeller zone to the average energy dissipation rate vary from 13 to 25. A value of 0.26 was reported in the bulk of the tank. It is therefore reasonable to assume that the most hostile cell hydrodynamic force interactions will occur in the impeller zone, characterised by high energy dissipation rates.

The three components of turbulence intensity have been found to be similar in the impeller region of stirred tanks. Hence turbulence may be considered to be isotropic in this region. It has been shown that vortices periodically sweep the impeller region, and introduce a periodic non-random element to the random turbulent motion. This periodic component of the total apparent turbulence is termed pseudo-turbulence. Failure to account for this periodic component would produce an over-estimation of turbulence in the impeller region.

The theory has been developed to allow the calculation of average energy dissipation rates in stirred tank reactors in terms of impeller speeds, tank geometry, and gas flow rates. The application of these equations to literature systems discussing biological responses, allow the comparison of energy dissipation rates across the systems. In the literature the importance of the Kolmogorov microscale of turbulence in evaluating critical forces in bioreactors has been implicated. The calculation of the average energy dissipation rate allows the evaluation of the critical Kolmogorov microscale of turbulence.

2.6 THE CAUSES OF HYDRODYNAMIC TRAUMA

In the literature, two mechanisms causing hydrodynamic trauma are dominant. The first attributes metabolic inhibition to the interaction of cells with turbulent eddies of a similar size in regions of high shear stress found near the impeller (Kunas and Papoutsakis, 1990; Smith and Lilly, 1990; Vanags *et al.*, 1990; Toma *et al.*, 1991). The interaction of cells with collapsing air bubbles at the air medium interface fall in the second category (Handa-

Corrigan *et al.*, 1989; Oh *et al.*, 1989; Boulton-Stone and Blake, 1993; Garcia-Briones and Chalmers, 1994)

2.6.1 The interaction of cells with turbulent eddies in the impeller stream

The interaction of cells with turbulent eddies in the impeller discharge zone of a stirred tank reactor has been described as a sufficiently hostile event to cause harm to the cells. Eddies which are much larger than the cell will tend to entrain it. Where the density of the cell and the surrounding media are similar, there will be little relative motion. Eddies which are much smaller than the cell have insufficient energy to cause significant harm. Eddies whose size approaches that of the cell diameter impart the maximum hydrodynamic force (van Suijdam and Metz, 1981). If the turbulent eddy is smaller than the cell, it will not have sufficient energy to cause harm.

The turbulence in stirred tanks is highly inhomogeneous with maximum fluid velocities occurring in the impeller zone. Wu and Patterson reported a ratio of impeller zone and average energy dissipation rate of 23.5. It is therefore reasonable to assume that the most hostile cell-eddy interaction will occur in the impeller zone, characterised by high energy dissipation rates.

Vanags *et al.* (1990) showed that with similar overall power introduction, the criterion of uneven energy distribution was notably less in a counterflow double impeller system compared to a cocurrent flow double impeller system. The counterflow system was more efficient in terms of biomass yield of *Trichoderma viride* obtained.

Van Suijdam and Metz (1981) and Smith *et al.* (1990) both support the concept of a dispersion zone in the impeller region where the turbulent forces are greater than those required to break the cell wall of microorganisms. The probability of rupture would be proportional to the number of times the microorganism encounters the impeller region and the size of the volume in the impeller region where the turbulent forces are greater than the tensile strength of the cell walls.

Studies on particle breakage in turbulent flow fields (Parker *et al.*, 1972; Cherry and Papoutsakis, 1986; Ayazi Shamlou and Titchener-Hooker, 1993; Ayazi Shamlou *et al.*, 1995) suggest that the key parameter that needs to be considered is the ratio of the size of the cells to the size of the smallest eddies, the Kolmogorov microscale λ. For particle diameters less than λ, breakage is caused by eddies in the viscous dissipation subrange. Shear stresses due to fluctuating velocity differences acting on opposite sides of the particle predominate. When the particle size is greater than λ, breakage is due to the interaction with eddies in the inertial convection subrange and the resultant Reynold's stress.

Typical values of the Kolmogorov microscale in the impeller zone of a 2 liter stirred tank reactor (Zhang *et al.* 1995) and 100 m^3 (Einsele, 1978) stirred tank are 9μm and 16 μm respectively (Equation 15). Hence for bacteria and unicellular yeasts (< 5 μm), stresses due to shear forces are significant. In these calculations it was assumed that the ratio of the local energy dissipation rate in the impeller zone and the average energy dissipation rate was 23.5 (Wu and Patterson, 1989). The impeller tip speed in the two systems were 3 m/s and 5m/s respectively.

Matsuo and Unno (1981) considered the particle Reynold's number, R_p, rather than the scale of the eddy or the particle size to be the controlling parameter. R_p is given by,

$$R_p = \frac{\rho \bar{u}(d) d}{\mu} \tag{35}$$

where $\bar{u}(d)$ is the difference in velocity between two points a distance d apart, and d is the diameter of the particle.

In isotropic and homogenous turbulence, if the scale of the particle is small compared with the macroscale of mean motion, a force balance on a fluid particle equal in size to the particle, using the Navier Stokes equation of motion with Eulerian coordinates gives,

$$\begin{aligned} \rho \frac{\partial u_x}{\partial t} \delta x \delta y \delta z = {} & (\rho g - \frac{\partial P}{\partial x}) \delta x \delta y \delta z - \rho (u_x \frac{\partial u_x}{\partial x} + u_y \frac{\partial u_x}{\partial y} + u_z \frac{\partial u_x}{\partial z}) \delta x \delta \delta y \delta z \\ & + \mu [2 \frac{\partial}{\partial x} (\frac{\partial u_x}{\partial x}) + \frac{\partial}{\partial y} (\frac{\partial u_x}{\partial y} + \frac{\partial u_y}{\partial x}) + \frac{\partial}{\partial z} (\frac{\partial u_x}{\partial z} + \frac{\partial u_z}{\partial x})] \delta x \delta y \delta z \end{aligned} \tag{36}$$

The term on the left hand side represents the change in velocity with respect to time and is only important when a density difference between the particle and the fluid exists. The first term on the right side of the equation represents the gravity force and the hydrostatic pressure and becomes important when differences in compressibility between the particle and the fluid exist. The second and third terms on the right hand side of the equation are the inertial (Reynold's stress) and viscous force terms which are significant when differences in deformability between the particle and the fluid occur. For a neutrally buoyant particle, such as a microorganism, only the viscous and inertial forces need to be considered.

When the magnitude of u_x,u_y and u_z are similar and equal to a and the magnitude of δx, δy, and δz are similar and equal to δ, the inertial and viscous terms can be written as,

$$\rho u_x(\frac{\partial u_x}{\partial x})\delta x\delta y\delta z \cong \rho a^2\delta^2 \tag{37}$$

$$\mu\frac{\partial}{\partial x}(\frac{\partial u_x}{\partial x})\delta x\delta y\delta z \cong \mu a\delta \tag{38}$$

respectively. The ratio of these two terms gives a type of Reynold's number, $R_\delta = \rho a\delta/\mu$. If one assumes that the diameter of the particle is equal to δ and that the difference in velocity between two points a distance d apart, $\bar{u}(d)$, is comparable to a, then the predominant force acting on a particle is determined by the particle Reynold's number, $R_p = \rho\bar{u}(d)d/\mu$. When R_p is smaller than a critical value, $(R_p)_c$, the viscous term in the force balance predominates and when R_p is larger than $(R_p)_c$ the Reynold's stress becomes important.

Matsuo and Unno (1981) assumed that the difference in velocity between two points a distance r apart can be evaluated using the Kolmogorov theory of turbulence structure (Kolmogorov, 1941). For the range of eddies in the viscous dissipation subrange where r is near zero, $\bar{u}_1(r)$ is given by:

$$\bar{u}(r) = \sqrt{\frac{2}{15}} \left(\frac{e}{\nu}\right)^{\frac{1}{2}} r \tag{39}$$

For the inertial convection subrange, $\bar{u}_2(r)$ is given by:

$$\bar{u}(r) = 1.57\, e^{\frac{1}{3}}\, r^{\frac{1}{3}} \tag{40}$$

The change-over point between using Equations 39 and 40, is obtained by setting $\bar{u}_1(r_0)=\bar{u}_2(r_0)$ and solving for r_0.

$$r_0 = 9\left(\frac{\nu^3}{e}\right)^{\frac{1}{4}} = 9\lambda \tag{41}$$

Hence if the particle diameter is less than 9λ, viscous forces predominate and the maximum surface force acting on the particle is given by:

$$\begin{aligned} F_1 &= \mu \frac{\partial}{\partial y}\left(\frac{\partial u_x}{\partial y} + \frac{\partial u_y}{\partial x}\right)\delta x \delta y \delta z \approx 2\mu a \delta \approx 2\mu\left(\frac{\partial \bar{u}(r)}{\partial r}\right)d^2 \\ &\approx 2\mu\left(\frac{\delta u(r)}{\delta r}\right)_{r=0} d^2 = 2\mu\sqrt{\frac{2}{15}}\left(\frac{e}{\nu}\right)^{\frac{1}{2}} d^2 \end{aligned} \tag{42}$$

If the particle diameter is greater than 9λ, the inertial force predominates and,

$$\begin{aligned} F_2 &= \rho u_y \frac{\partial u_x}{\partial y} \partial x \partial y \partial z \approx \rho a^2 \delta^2 \\ &\approx \rho \overline{v^2}(d) d^2 = \rho\ 1.57^2\, e^{\frac{2}{3}}\, d^{\frac{8}{3}} \end{aligned} \tag{43}$$

In the approach of Matsuo and Unno (1981), r_0 rather than the Kolmogorov microscale, λ, splits the universal equilibrium subrange.

Smith and Reilly (1992) suggested that there were three fundamental scalings to consider in the scale up of fermenters for stress sensitive organisms. The first concerned the magnitude of the force, the second the frequency with which the organism experienced that force in its

passage through the impeller stream, and finally the frequency of the passage through the impeller region. The straining component of turbulence was considered to be responsible for inducing mechanical stress on microorganisms provided that the organism is 10% or more of the Kolmogorov microscale. If the small scale motions are isotropic, the tensile force acting across the central plane of a spherical organism of diameter d is given by:

$$F = \frac{37}{8}\pi\mu\left(\frac{e}{\nu}\right)^{\frac{1}{2}}d^2 \tag{44}$$

In terms of scale up variables this can be approximated as:

$$F = \frac{37}{8}\ \pi\mu d^2\ \left(\frac{N_p Re}{2\pi}\right)^{\frac{1}{2}}\ N_{rpm} \tag{45}$$

where N_{rpm} is the agitation rate in revolutions per second and N_p is the power number.

The frequency, f, with which an organisms is subjected to a force greater than F is given by:

$$f \sim \left(\frac{\lambda}{L}\right)T' \sim \frac{D\left(\frac{2\pi}{N_P\ Re^3}\right)^{\frac{1}{4}}}{\frac{D}{15}}\ \frac{1}{30N_{rpm}}\ \left(\frac{2^{\frac{3}{2}}5}{N_p}\right)^{\frac{1}{3}}\ \left(\frac{T}{D}\right) \tag{46}$$

where λ is the Kolmogorov microscale, L is the integral length scale, T' is the integral time scale of turbulence, N_p is the power number, D is the impeller diameter and T is the tank diameter. The frequency of passage through the impeller zone is given by the inverse of the circulation time. This was estimated as:

$$t_C = \frac{H+T}{U_c} = \frac{H+T}{\frac{1}{2}\left(\frac{D}{w}\right)\left(\frac{D}{T}\right)^{\frac{7}{6}}\ N_{rpm}D} \tag{47}$$

where H is the liquid height, w is the blade width and U_c is the circulation velocity.

The rate of disruption of aggregates (R_D) in a turbulent flow field has been assumed equal to the product of the number concentration of the parent flocs (n_F), the frequency of

disruption by similarly sized eddies, f, and the number of primary particles eroded per disruption, n_p (Parker *et al.*, 1972; Brown and Glatz, 1987; Ayazi Shamlou *et al*, 1990). Assuming a mean size for the parent flocs, d_F, the number of parent flocs was given by:

$$n_F \propto \frac{C_V}{d_F^3} \qquad (48)$$

where C_V is the volume concentration of flocs.

The number of primary particles generated per disruption was assumed proportional to the number of particles in the outside layer of the floc:

$$n_p \propto \left(\frac{d_F}{d_p}\right)^2 \qquad (49)$$

where d_p is the diameter of the primary particles. For erosion induced by eddies in the inertial convection subrange of the turbulent energy spectrum:

$$f(d_t) \propto \frac{e^{1/3}}{d_t^{2/3}} \qquad (50)$$

where d_t is the stable floc diameter. This was determined from a force balance between the shear yield strength of the floc surface (τ_y) and the surface fluid-induced stresses:

$$\tau_y = k_f \rho \bar{u}_{MAX}^2 \qquad (51)$$

where k_f is the turbulent friction factor and $\bar{u}_{MAX}$ is the maximum peak velocity of the fluid relative to the particle of size d_t. The latter was given by the following expression:

$$\bar{u}_{MAX} = \frac{\sqrt{\beta}}{(3)^{1/6}} \left(\frac{\rho_p - \rho}{\rho_p - \rho/2}\right)^{1/3} (1/k_f)^{1/3} \left(\frac{2d_t}{3}\right)^{1/3} e^{1/3} \qquad (52)$$

where ρ is the density of the fluid, ρ_p is the density of the particle and β is a constant. For similar particle and fluid densities, the maximum stable diameter d_t was therefore,

$$d_t \propto \left(\frac{e}{\nu}\right)^{-1} \tag{53}$$

The size of the parent flocs (d_F) was equated to the maximum stable floc size (d_t) and the rate of surface erosion was therefore given by:

$$\frac{dn_p}{dt} = n_F \times f(d_t) \times n_p \propto C_V \left(\frac{e}{\nu}\right)^2 \tag{54}$$

For fluid-induced attrition by eddies in the viscous dissipation subrange, the frequency of the eddies was given by:

$$f(d_t) \propto \left(\frac{e}{\nu}\right)^{1/2} \tag{55}$$

The maximum stable floc size was obtained from a force balance between the strength of the floc and the viscous force given by:

$$\tau_y \frac{\pi d_t^2}{4} = 3\pi\, d_t\, \mu\, \bar{u}(d_t) \tag{56}$$

where $\bar{u}(d_t)$ is the velocity of the fluid relative to that of the particle. This was correlated by the following expression:

$$\bar{u}(d_t) \propto \frac{1}{3\pi\mu} (\rho_p - \rho) \frac{1}{6}\pi d_t^3 \frac{e}{\nu} \tag{57}$$

The rate of surface erosion was therefore,

$$\frac{dn_p}{dt} \propto C_V \left(\frac{e}{\nu}\right) \tag{58}$$

As already mentioned it is proposed that drops and microorganisms accept energy from similarly sized eddies in the surrounding liquid (Zhang *et al.*, 1993; Tsouris and Tavlarides, 1994). In preliminary work, Zhang *et al.* (1993) assumed that mammalian cells adsorbed the kinetic energy of eddies in the inertial convection subrange since the cells were larger than the Kolmogorov microscale.

$$E_k = 0.086\ \pi\ e^{\frac{2}{3}}\ d^{\frac{11}{3}} \tag{59}$$

It was suggested that this kinetic energy manifested itself as surface energy (E_s).

In subsequent work, Zhang and Thomas (1996) modified the mammalian cell death model (Equation 59). It was assumed that cells were distorted by all eddies of the same size or smaller than the cell. An energy number distribution was derived by manipulating formulae used for describing isotropic turbulence. The energy transfer between eddies and cells in turbulent flow was modelled and the energy carried by the cells estimated. The eddy number distribution was given by:

$$f(d) = A_8\ d^{-4} \tag{60}$$

where d is the diameter of the eddies and A_8 is a constant.

The mean value of the cell surface energy E_s was determined as:

$$E_s = \frac{1.7\ A_9\ \rho\ e^{\frac{2}{3}}\ d_C^{\,2} \int_{D_{MIN}}^{D_{MC}} \frac{e^{-2.55\ \nu e^{-\frac{1}{3}} d^{-\frac{4}{3}}}}{d^{\frac{1}{3}}} d(d)}{\left(\frac{1}{D_{MIN}} - \frac{1}{D_{MC}}\right)} \tag{61}$$

where A_9 is a constant, D_{MIN} and D_{MC} are the minimum and maximum eddy sizes that the cell can interact with, and d_C is the cell diameter. The cell disrupted when the bursting surface energy E_{sb} was exceeded. The latter was estimated by the cell intrinsic mechanical properties,

$$E_{sb} = \pi\ d_C^{\,2}\ T_b\ \left(1 + \frac{T_b}{K}\right) \tag{62}$$

where T_b is the bursting membrane tension and K is the elastic area compressibility modulus.

Using the theory of the interaction of microorganisms with similarly sized turbulent eddies, the hydrodynamic forces acting on stress sensitive microorganisms in stirred tanks have been calculated using Equations 42 and 43. A critical particle diameter of 9λ (Matsuo and Unno,

1981), determined from Equation 41, has been used as the controlling parameter in determining the mechanism of trauma (Table 6). The local impeller zone energy dissipation rate was assumed to be 25 times the average energy dissipation rate. The results show that for the bacteria, yeast and animal cell studies, viscous effects predominate. For the plant cells, the inertial forces were significant.

Table 6 Calculated levels of local and average energy dissipation rates at which different kinds of organisms are traumatised.

REFERENCE	SYSTEM	ORGANISM AND SIZE	N_{crit} rpm	RESPONSE	e_{AVE} m^2/s^3	e_{MAX} m^2/s^3	λ_{imp} μm	HYDRO-DYNAMIC STRESS N/m^2
Toma *et al.* (1991)	2* 6-bladed Rushton impellers 3 l tank D = 0.066 m T = 0.15 m Q = 1 vvm H/T = 2 S/D = 2 d_b = 0.022 m 3 baffles	*Brevibacterium flavum* d: 0.8 μm l: 1.3 μm	900	partial inhibition of microbial growth	8.7 < e < 11.4	±250	8	viscous shear stress = 11.2
		Saccharomyces cerevisiae d_{ave} = 5μm	800	- decrease O_2 uptake rate - decrease sucrose uptake rate - decreased growth rate - shift in ATP pathway	6 < e < 8	±175	8.7	viscous shear stress = 9.7
Dunlop and Ye (1994)	1* 6-bladed Rushton impeller 1.45 l tank D = 0.09 m Q = 0.16 vvm 4 baffles	carrot cells d_{ave} = 194 μm	300	Complete inhibition of mitochondrial activity and growth Cells still intact	e = 2.54	±63.5	11	inertial stress = 66.6
Zhang *et al.* (1995)	1* 6-bladed Rushton impeller 2 l tank T = 0.115 m D = 0.058 m H/T = 2 Q = zero 4 baffles	hybridoma cells d_{ave} = 12 μm	1500	45% disruption of cells	e = 25	±625	6.3	viscous shear stress = 17.7
			2000	85% disruption of cells	e = 58	±1450	5.1	viscous shear stress = 27

2.6.2 The interaction of cells with collapsing air bubbles

Several researchers report the damaging effects of bubbles when they break at the air medium interface. Oh *et al.* (1989) and Gardner *et al.* (1989) showed that only the combination of agitation and sparging (not agitation alone) was sufficient to retard the growth and cause damage to murine hybridoma cells. These results are described in detail in Section 2.4.4. Kunas and Papoutsakis (1990) found that two phenomena participate in cell damage: bulk-liquid turbulence, and vortex formation with associated bubble entrainment and bubble breakup.

Handa-Corrigan *et al.* (1989) showed that smaller bubbles and higher bubble frequencies were more detrimental to hybridoma cells. Trinh *et al.* (1994) showed that *Spodoptera frugiperda* insect cells were killed when attached to 3.5mm bubbles rupturing at the surface. The surfaces of cells and bubbles are naturally hydrophobic and hence cells tend to adhere to a bubble as it rises to the air medium interface. Dahlback *et al.*(1981) have shown that the accumulation of bacteria on the air liquid interface is directly proportional to the hydrophobicity of the bacterial cell surface. Electrostatic interactions have also been reported to contribute to cell gas adhesion (Kjelleberg, 1985).

There are extensive reports in the literature regarding the protective effects of Pluronic F-68, and serum against cell damage (Gardner *et al.*, 1989; Lee *et al.*, 1989; Michaels *et al.*, 1990; Tan *et al.*, 1993; Zhang *et al.*, 1992c; Trinh *et al.*, 1994). It has been shown that the protective effect of an additive may be attributed to an altered ability of a cell to resist hydrodynamic forces (Zhang *et al.*, 1992d; Ramirez and Mutharasan, 1990), changes in the degree of bubble-cell attachment (Handa-Corrigan *et al.*,1989 ; Zhang *et al.*, 1992c) and changes in the hydrodynamic forces associated with bubble rupture.

Zhang *et al.* (1992d) have shown through micro-manipulation experiments that Pluronic F-68 increases the cell wall strength of hybridomas. The observed protective effect of serum is partly due to its ability to stimulate growth and to increase the cell wall strength. The improved resilience of microorganisms grown in complex media over those organisms grown in minimal media is well accepted (Gray *et al.*, 1972). A Pluronic F-68 molecule consists

of a hydrophobic moiety flanked by two hydrophillic moieties. It has been proposed that the hydrophobic portion of the molecule attaches to the bubble and cell surfaces and that the hydrophillic ends extend into the culture medium as hydrated coils. The stable hydrated layer formed around both the bubbles and the cells prevent their direct interaction. Antifoam on the other hand increases the degree of cell damage by increasing the hydrophobicity of cells and bubbles (Zhang *et al.*, 1992). Cells are therefore carried more effectively to the bubble bursting region. Additives may also affect the magnitude of the hydrodynamic forces associated with bubble rupture. Kolmogorov (1941) and Hinze (1955) have shown that the mean bubble size is proportional to the surface tension raised to the power of 0.6. Antifoam reduces the surface tension of the medium (Atkinson and Mavituna, 1983). This causes the bubble size to decrease, resulting in more lethal bubbles. Pluronic F-68 on the other hand increases the surface tension of the medium with a resultant increase in bubble size and a reduction in the number of lethal bubbles.

Microscopic visualisation of bubble-cell adsorption and the bubble rupture event by Chalmers and Bavarian (1991) has elucidated the mechanism of cell damage by rupturing bubbles. Cells adsorbed onto the bubble are carried to the air medium interface with the rising bubble. As the bubble approaches the interface, the high pressure field generated in front of the rising bubble drains the liquid between the bubble and the interface until only the bubble film, and the cells contained therein, separate the bubble from the interface. Once a disturbance ruptures the film, the hole created expands rapidly. The material from the expanding hole forms a toroidal ring which advances to the edge of the bubble cavity. Liquid from this ring as well as liquid on the bubble cavity interface flows down the side of the cavity wall. At the bottom of the cavity, the boundary layer flow forms an upward and a downward jet. The upward jet breaks up into droplets which are ejected upward into the air. The rupture of a bubble releases a large amount of energy into a small volume of fluid over the short time span of the event. Chalmers and Bavarian (1991) proposed that two mechanisms were responsible for damage to cells attached to the bubbles:

a) release of potential energy as the film breaks (cells may be struck by the rapidly advancing toroidal rim as they sit on a stationary part of the bursting lamella),

b) high velocity and shear stresses in the boundary layer flow.

Trinh *et al.* (1994) showed that insect cells attached to the bubble film as well as those in the near vicinity of the film were killed when the film retracted. It was suggested that the cells near the film were caught up in the boundary layer flow. Tramper *et al.* (1986) proposed that associated with each bubble is a "specific hypothetical killing volume". This killing volume is likely to consist of cells and medium making up the bubble film and the thin layer surrounding the bubble cavity in which the boundary layer flows occur.

Garcia-Briones *et al.* (1991) evaluated the velocity field of the flow occurring as a bubble ruptures. As the hydrodynamics of collapsing films could not be accounted for, only the hydrodynamics of the collapsing bubble cavity were modelled numerically. High rates of strain and local energy dissipation rates were calculated in the regions close to the collapsing bubble cavity and in the upward and downward jets. The maximum value of stress occurred where the flow converged at the axis of symmetry (4797 N/m^2 for 4.3×10^{-4} s for a 0.7mm bubble and 1998 N/m^2 for 1.4×10^{-3} s for a 1.7mm bubble). The flow was always extensional and not a simple shear flow in the maximum stress regions. It was found that the rate of energy dissipation increased rapidly as the size of the bubble decreased.

Boulton-Stone and Blake (1993) numerically modelled the free surface motion resulting when a bubble bursts. Pressure fields and energy dissipation rates were calculated as a function of position and time. The maximum energy dissipation occurred beneath the bubble just before jet formation and was seen to increase with decreasing bubble size. At this point, fluid is rapidly accelerated into one of the jets. Cells are likely to be stretched and ruptured by the high strain rates. The contribution of viscous forces made only a small contribution to the stresses in the downward jet region. Figure 13 shows the calculated maximum energy dissipation rates as a function of bubble radius. Typical reported bubble sizes in stirred tanks for marine impellers (Kunas and Papoutsakis, 1990) vary from 1 to 3 mm at 220 rpm (entrained bubbles) and 0.3 to 0.05 mm at 700 rpm (entrained bubbles). The corresponding energy dissipation rates for these two size ranges are 10 to 5×10^4 m^2/s^3 and 1×10^7 to 1×10^8 m^2/s^3 respectively according to the data of Boulton-Stone and Blake (1993).

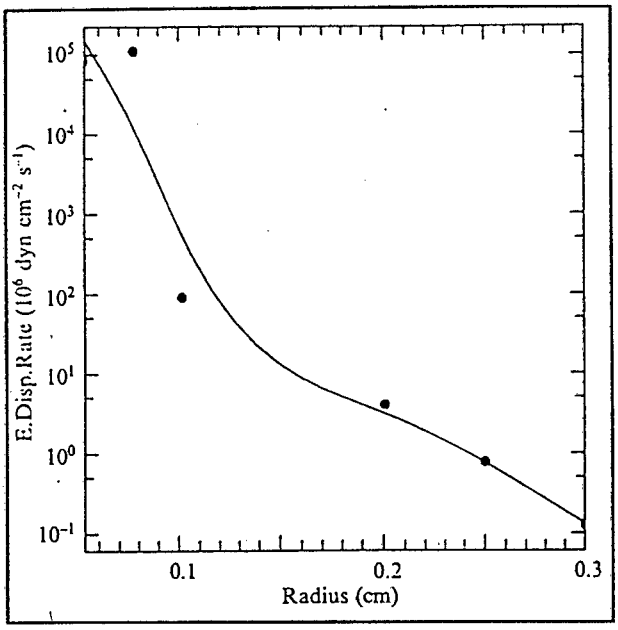

Figure 13 Maximum energy dissipation rates as a function of bubble radius (Boulton-Stone and Blake, 1993).

2.6.3 Conclusions

Literature reports regarding the causes of hydrodynamic trauma were divided into two groups. The first attributes metabolic inhibition to the interaction of cells with similarly sized turbulent eddies. The extent of cell damage is a function of the magnitude of the kinetic energy of the eddies as well as the cumulative time of exposure to the forces. The interaction of cells with collapsing air bubbles at the air medium interface fall in the second category. It has been shown that the smallest bubbles at the highest frequencies inflict the most damage.

Studies suggest that the ratio of the cell diameter to the Kolmogorov microscale of turbulence is a key parameter in determining the mechanism of cell breakage. Where d/λ is less than 9, breakage of cells is caused by eddies in the viscous dissipation subrange. When the particle size is greater than 9λ, breakage is commonly due to the interaction of particles with eddies in the inertial convection subrange. Application of this hypothesis to microbial cell systems in which biological responses have been reported, showed that viscous forces predominated for the bacteria, yeast and animal cells. Inertial forces were dominant in the

plant cell system.

Hydrophobic interactions are responsible for the adhesion of cells to bubbles. Cells are carried to the air liquid interface and are subjected to the release of a large amount of energy when the bubble bursts. Maximum values of energy dissipation rate occurred beneath the bubble just before jet formation and were seen to increase with decreasing bubble size.

3. EXPERIMENTAL PROCEDURE

3.1 GROWTH OF MICROORGANISMS

3.1.1 Organisms

Corynebacterium glutamicum (ATCC 13032) and *Brevibacterium flavum* (NRRL 11475) were used in the trauma experiments. The Gram positive bacteria consist of ellipsoidal cells, with dimensions of 0.7 μm by 1.4 μm. These may occur singly, in pairs or in irregular masses. In South Africa the bacteria play an important role in animal nutrition as lysine producers. The non-auxotrophic *Corynebacterium glutamicum* and auxotrophic *Brevibacterium flavum* strain were obtained from AECI (Modderfontein).

3.1.2 Media

A complex medium was used for pre-inoculum cultures. This contained (per liter): 10g tryptone, 10g yeast extract, 5g NaCl. The pH was adjusted to 7.

The composition of the inoculum, batch and continuous media for the *Corynebacterium glutamicum* bacteria consisted of (per liter): 20g glucose, 0.4g $MgSO_4.7H_2O$, 75mg $Na_2EDTA.2H_2O$, 25 mg $FeSO_4.7H_2O$, 0.1g NaCl, 50 mg $CaCl_2$, 7g $(NH_4)_2SO_4$, 3g K_2HPO_4, 1g KH_2PO_4, 1 mg biotin, 10 ml trace salts. The $(NH_4)_2SO_4$, K_2HPO_4, KH_2PO_4 and biotin were autoclaved together separately from the other salts and the two portions mixed after cooling. The trace salt solution consisted of (per liter): 200mg $MnSO_4$, 20mg $Na_2B_4O_7.4H_2O$, 10mg $(NH_4)_6MoO_{24}.4H_2O$, 200mg $FeCl_3.6H_2O$, 50mg $ZnSO_4.7H_2O$, 20mg $CuCl_2.2H_2O$ (Kiss and Stephanopoulos, 1991).

The *Brevibacterium flavum* inoculum, batch and continuous media consisted of (per liter): 70g glucose, 0.5 g $MgSO_4.7H_2O$, 0.008g $MnSO_4.H_2O$, 0.01g $FeSO_4$, 15g $(NH_4)_2SO_4$, 1g KH_2PO_4, 0.002g biotin, 0.05g thiamine-hydrochloride, 1.5g niacin, 0.5g DL-methionine,

0.25g L-threonine, 0.2g L-alanine, 10g yeast extract. The glucose, $MgSO_4.7H_2O$, $MnSO_4.H_2O$ and $FeSO_4$ were autoclaved together separately from the other components and the two portions mixed after cooling. The pH of both portions was adjusted to pH 7 before autoclaving (AECI Ltd, Modderfontein).

The glucose-containing portion of the two media components for the *Corynebacterium glutamicum* and *Brevibacterium flavum* batch and continuous experiments was sterilized *in situ*. The sterilisation procedure is described in Appendix B.

Sigma antifoam 289 (0.5g/l) was added to the glucose solution before the sterilisation step for the batch and continuous media for both bacterial species. The antifoam mixture contained silicone and organic defoamers.

3.1.3 Inoculum preparation and growth conditions

The 250ml shake flasks containing 30ml of complex media were inoculated from the agar stock plates. The *Corynebacterium glutamicum* and *Brevibacterium flavum* pre-inoculum cultures were grown at 30°C for 18 hours and 23 hours respectively. The inoculum cultures for the bioreactors were prepared by transferring the pre-inoculum cultures into the 1 liter shake flasks containing 300ml simple media and incubating at 30°C for 12 and 23 hours respectively. The shake flasks were agitated at 95 rpm.

The cultures were grown at 30°C and a pH of 7 in a 7.3 liter Chemap stirred tank reactor. Two molar NaOH and NH_4OH were used to maintain the neutral pH in the *Corynebacterium glutamicum* and *Brevibacterium flavum* bioreactors respectively. The reactors were fitted with sterilizable Ingold pH (model 764-31) and Phoenix dissolved oxygen (model 025P2532007) electrodes. The pH was controlled by a UCT pH controller driving a UCT peristaltic dosing pump. The base reservoir was positioned on a scale pan interfaced to a data logger for continuous monitoring of base consumption. The dissolved oxygen probe was linked to a UCT amplifier and the dissolved oxygen concentration was recorded continuously. The air supply to the culture vessel was passed through a pressure regulating unit, an oil filter, a rotameter and a sterile carbon filter before entering the reactor. The exhaust gasses passed

through a sterile carbon filter and a condenser cooled with tap water. The temperature of the vessel was maintained to within 0.5 °C by heating a water stream that passed through two stainless steel coils situated near the baffle cage. Bacterial samples were taken aseptically using a steam sterilizable sample port at the base of the culture vessel. For the continuous culture, the reactor feed was added at a constant flow rate using two UCT peristaltic pumps in parallel. The feed bottle was placed on a 60kg load cell to facilitate measurement of flow rate. The bioreactor rested on a sensitive load cell. The output from the load cell was linked to the output pump flow controller. The controller switched the output pump on when the mass of the fermenter overshot the setpoint mass. A schematical diagram of the batch culture apparatus is shown in Figure 14.

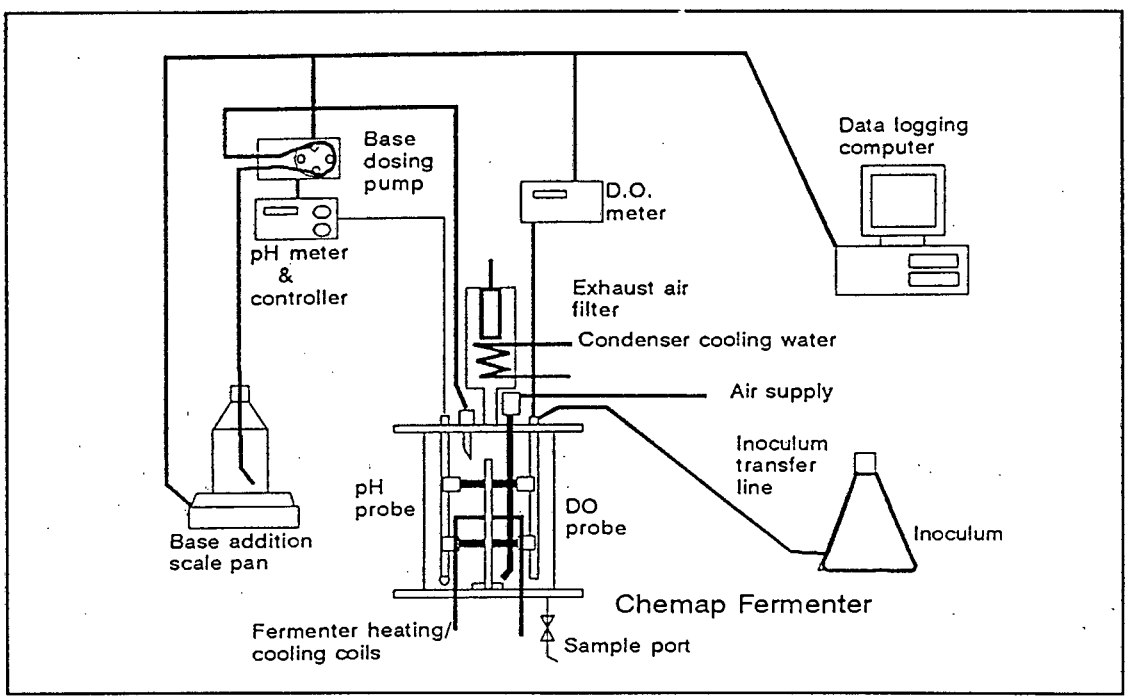

Figure 14 Schematical diagram of the batch culture apparatus.

3.2 REACTOR CONFIGURATIONS

3.2.1 Chemap stirred tank reactor

Corynebacterium glutamicum was cultivated in a 7.3 liter Chemap stirred tank reactor fitted with Rushton turbine impellers of the following dimensions: diameter 0.08m, width 0.02 m and length 0.02 m. The diameter of the tank was 0.2m. The reactor was fitted with four

baffles of 0.03 m width. In continuous culture, a 3.5 liter working volume was used with a single impeller set at an impeller clearance one third of the liquid height. The bubble and bubble-free batch reactor experiments were carried out in 5 and 7.3 liter working volumes respectively using two impellers with an impeller clearance of 0.04 m, and an impeller spacing of 0.12 m.

3.2.2 Airlift reactor

The perspex cylindrical airlift reactor had the following geometry: tank diameter of 0.063m, a riser diameter of 0.035 m, a riser length of 0.315 m, a riser clearance of 0.015 m and a unaerated liquid height of 0.305 m. A perforated pipe sparger was fitted at the base of the riser. The 16 holes of the sparger had diameters of 0.0007 m. A superficial gas velocity (based on the riser cross sectional area) of 0.2 m/s was maintained.

3.2.3 Flowloop

The flow loop system consisted of a 1 liter conical flask for sampling and gaseous exchange, a variable speed peristaltic pump (Masterflex I/P H-07549-40 drive, H-07019-43 pumphead) and a narrow 304 stainless steel capillary 0.14 m long with an internal diameter of 0.8 mm in which the cells were exposed to extreme hydrodynamic conditions. The capillary had converging/diverging ends to minimise the pressure drop associated with sudden contractions and expansions in the flow. All the components were linked with 6mm ID thick-walled Nalgene tubing.

3.3 HYDRODYNAMIC CHARACTERISATION OF REACTORS

3.3.1 Mass transfer

The volumetric liquid side mass transfer coefficient, k_La, was measured using the well known gassing-in technique (Van't Riet, 1979). The liquid in the stirred tank reactor was deaerated to a low oxygen concentration by bubbling with nitrogen. Air flow to the reactor was started

and the change in dissolved oxygen concentration monitored with time from the instant the air flow began. When actively respiring cells were present in the reactor, the method of measuring k_La was modified. The air supply to the reactor was turned off and the dissolved oxygen concentration decreased at a rate equal to the oxygen consumption by the cells. When the dissolved oxygen reached 2 ppm, the air supply was restored and the dissolved oxygen concentration increased back to the initial level. A plot of the difference between the rate of increase in dissolved oxygen concentration and the average oxygen consumption rate as a function of dissolved oxygen concentration gave a straight line with a slope of k_La (Equation 63).

$$\frac{dC_O}{dt} = k_L\, a\, (C_O^* - C_O) + OUR \qquad (63)$$

where C_O is the dissolved oxygen concentration, C_O^* is the saturation concentration in the bulk liquid and OUR is the oxygen utilisation rate.

3.3.2 Velocity profile

The velocity profile was measured in the stirred tank by a conductivity probe based on the electrochemical reaction involving the oxidation and reduction of the ferro and ferri-cyanide ions (Ranz, 1958). The response of the electrochemical probe has been reported as being equivalent to or better than the hot wire anemometer (Ranz, 1958). Measurements were carried out in cell free media supplemented with 0.5g/l antifoam.

The probe consisted of a 50 μm diameter platinum wire cathode set into the tip of a 4 mm diameter perspex rod, tapered at 30 degrees to a sharp point. A large platinum anode was formed by winding several lengths of wire around the untapered section of the perspex rod 5mm from the tip. The diffusion rate of ferric ions to the cathode limited the flow of current when a 300 mV potential was applied to the cathode in a solution of 0.2 M KCl, 0.003 M potassium ferric cyanide and 0.003 M potassium ferrous cyanide. The reactions involved in the system are:

$$Fe\,[CN]_6^{3-} + é \rightarrow Fe\,[CN]_6^{4-} \qquad \text{at cathode}$$

$$Fe\,[CN]_6^{4-} \rightarrow Fe\,[CN]_6^{3-} + é \qquad \text{at anode}$$

The probe was calibrated by pumping electrolyte through a 5 mm diameter perspex pipe perpendicular to the probe tip at a known flow rate. To ensure consistency, the probe was washed with HCl and re-calibrated every 15 minutes during the velocity measurement programme.

Current from the electrochemical probe was amplified and converted to voltage. A schematical diagram of the amplifier circuit is shown in Figure 15. Because the diffusion current was of the order of 1 microampere, low frequency electrical noise had to be carefully eliminated. High frequency noise, greater than 10 kHz, was eliminated by a first order analogue low pass filter in the amplifier circuit. The voltage signal was digitised by an analogue to digital computer card and saved as an ASCII text file. For each test, 20 000 data points were sampled at a frequency of 4 kHz, which gave an effective maximum frequency of 2kHz. Data was analysed by a spectral analysis programme. Each data set was divided into 100 records of 2048 data points, giving a resolution of 2 Hz in the calculated energy spectra. The programme performed a Fast Fourier Transform (FFT) on the autovariance for each record and ensemble-averaged results over the 100 records. The mean was removed and the data tapered using a Hanning window and a 50% overlap prior to applying the FFT. The tapering option eliminates the effects of discontinuities at the end of each time series.

The one dimensional energy spectrum in frequency space (E_1) was obtained from the Fourier transform of the Eulerian autocorrelation coefficient (R_E) of the velocity fluctuations at a fixed point, by means of,

$$E_1(n) = 2\overline{u^2}\int_{-\infty}^{\infty} R_E(\tau)e^{i2\pi n\tau}d\tau \qquad \textbf{(64)}$$

where n is the frequency and τ is the time delay in the autocorrelation function.

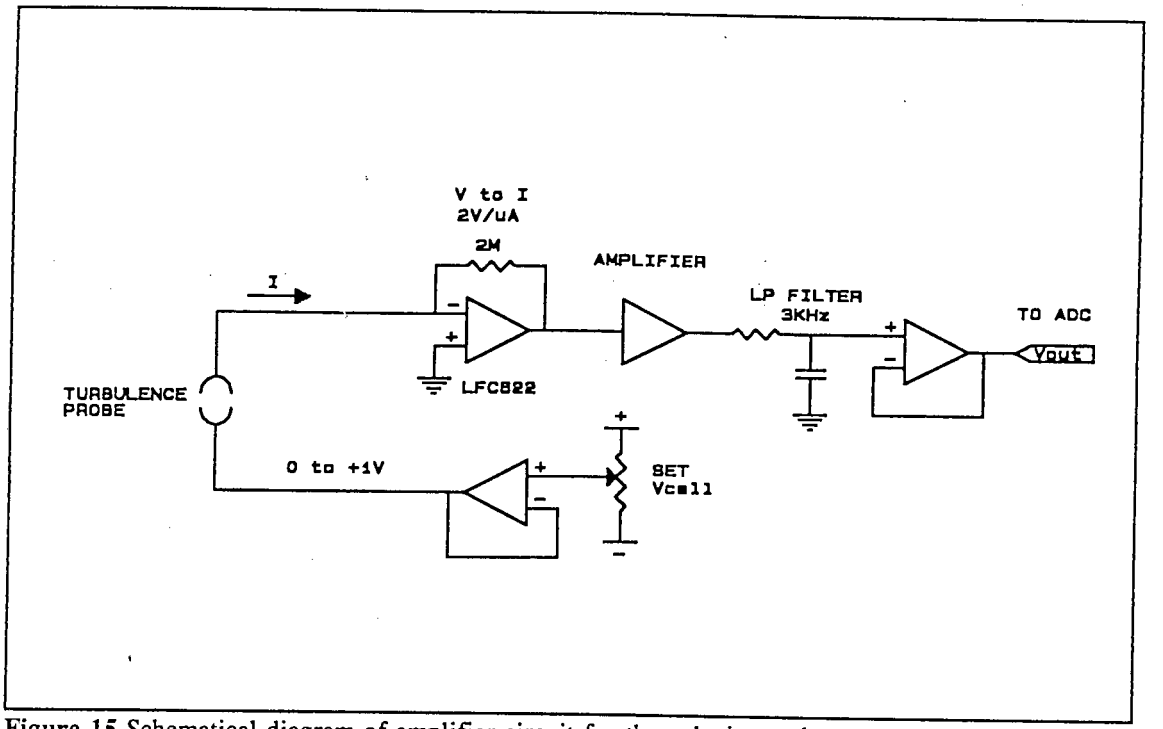

Figure 15 Schematical diagram of amplifier circuit for the velocity probe.

The autocorrelation coefficient is given by:

$$R_E(\tau) = \frac{\overline{u(t)u(t+\tau)}}{\overline{u^2}} \tag{65}$$

where t is time (Hinze, 1959).

The autocorrelation coefficient is used for determining the macro and micro time scales of turbulence and for identifying periodic components in the flow. These periodic velocity fluctuations, so called "pseudo turbulence", which result from the disturbance of impeller vortices were subtracted from the total turbulence in the calculations (Wu and Patterson, 1989).

$$(R_E)_{RANDOM} = (R_E)_{TOTAL} - (R_E)_{PERIODIC} \tag{66}$$

Using the corrected random autocorrelation coefficient, the turbulence energy spectra were calculated and used to determine the mean squared random turbulent velocity (Equation 67) and the energy dissipation rates (Equation 68) in the stirred tank.

$$\int_0^\infty E_1(n)dn = \overline{u^2} \tag{67}$$

The Eulerian microscale was not used to determine the energy dissipation rate as the relationship is limited by the assumption of isotropic turbulence, and the difficulties in determining the turbulent microscale. The short sampling period of 5 secs gave insufficient data points for the low frequency energy spectra to calculate the macroscale of turbulence accurately. The Eulerian macroscale was therefore estimated to be a quarter of the blade width at a distance of r/R = 1.2 from the impeller tip and equal to the blade width in the bulk region of the tank (Majumdar *et al.*, 1970, Rao and Brodkey, 1972, Wu and Patterson, 1989).

The local rate of energy dissipation was determined from the turbulent kinetic energy k and the resultant turbulent macroscale L_{RES} (Wu and Patterson, 1989),

$$e = \frac{0.85\ k^{\frac{3}{2}}}{L_{RES}} \tag{68}$$

$$k = \frac{1}{2}\left(\overline{u_r^2}+\overline{u_z^2}+\overline{u_\theta^2}\right) \tag{69}$$

$$L_{res} = \sqrt{L_r^2 + L_z^2 + L_\theta^2} \tag{70}$$

3.3.3 Bubble size measurement

The bubble sizer consisted of a 0.5 mm glass capillary tube with a belled end, to facilitate bubble capture, passing between two pairs of photo-transistor-LED detectors mounted 5 mm apart. As the bubbles pass the detectors, they are monitored as a change in light intensity. This change is a result of the difference in refractive indices of light and air. About 3000 bubbles are sized for an accurate bubble size distribution. The bubbles are collected in a gas

burette so that the total bubble volume can be determined. The length and velocity pulses generated by the passage of bubbles past the detectors were processed to give the distribution of the bubble diameters (O'Connor *et al.*, 1990).

3.3.4 Circulation time

The circulation time in the stirred tank reactor was measured using a pulse injection technique (Holmes *et al.*, 1964). 0.05 ml of 98 wt % H_2SO_4 was rapidly injected into the turbine centre. The conductivity cell, consisting of three concentric 0.09m diameter copper wires situated around the upper impeller detected the acid as it was dispersed. The change in conductivity was recorded as function of time. The circulation time was estimated as the average distance between successive peaks in the conductivity versus time plots. A schematical diagram of the amplifier circuit for the conductivity probe is shown in Figure 16. In the capillary flow system, circulation time was calculated by dividing the total flow volume by the volumetric flow rate. The volumetric flowrate was determined by measuring the volume of the fluid pumped into a 100 ml measuring cylinder in a 10 second interval. The measurments were carried out in triplicate.

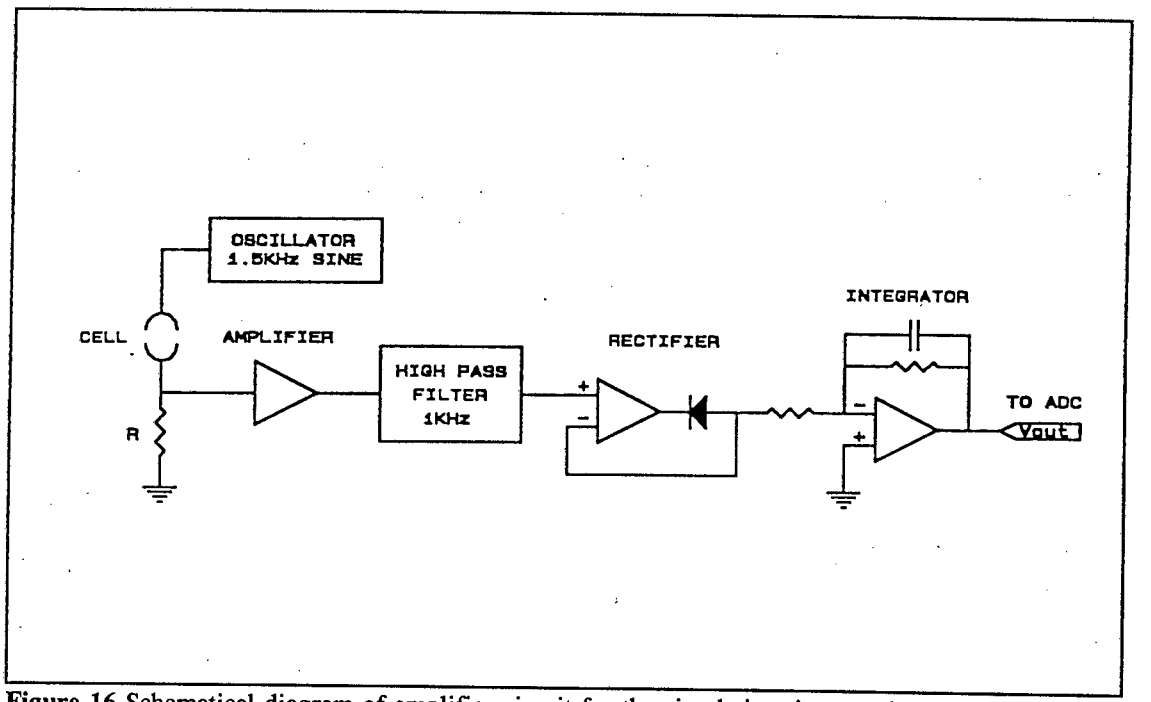

Figure 16 Schematical diagram of amplifier circuit for the circulation time conductivity probe.

3.4 ANALYSIS OF BIOLOGICAL RESPONSE

A microorganism uses its available resources, such as glucose and O_2, to produce various products, maintain intracellular functioning and for repair mechanisms. Hydrodynamic trauma may result in changes in the mass flux of these metabolic pathways or in morphological changes. It is therefore important that these changes be measured using suitable analytical techniques. Cell viability (ability to reproduce), rate of metabolism, shift in metabolic pathway, lysis and morphological changes were measured. The principle of measurement in each category is described below. Details of the methods are given in Appendix A.

3.4.1 Viability

Plate counts were performed as a measure of cell viability. The latter was defined as the ability of a single cell or aggregate to reproduce. The agar media contained (per liter): 10g tryptone, 10g yeast extract, 5g NaCl and 15g bacteriological agar.

3.4.2 Rate of metabolism and shift in metabolic pathway

The rate of metabolism and possible shift metabolic pathway were measured in terms of biomass formation (dry biomass concentration and absorbance at 660 nm), substrate utilisation (residual glucose concentration), oxygen utilisation rate and product formation (amino acid production and base consumption).

Residual glucose was measured colorimetrically based on the oxidation of glucose to gluconic acid and H_2O_2 (Boehringer Mannheim Cat. 124036). Specific amino acid production was determined by high pressure liquid chromatograph (HPLC) analyses using a cation exchange column. Lysine was measured by its enzymatic conversion to saccharopine with concomitant conversion of NADH to NAD^+ (Nakatani *et al.*, 1972, Kiss and Stephanopoulos, 1991), which was measured. Base consumption was measured gravimetrically to provide an estimate of the acidic metabolites produced.

Oxygen utilisation rate measurements were done off-line, following dilution of the sample into fresh sterile medium at 30°C. The medium contained (per liter): 5g glucose, 0.8g NaCl, 0.2g KI, 2.254g Na_2HPO_4 and 0.2g KH_2PO_4. This method ensured reproducibility and minimised error due to slow probe response time and high oxygen consumption rates. The off-line measurement also eliminated the need to vary hydrodynamic conditions in the reactor, required in on-line measurements. The reduced hydrodynamic stress during the measurement phase of the on-line procedure may have affected the overall metabolic response.

3.4.3 Lysis

Lysis was measured as the amount of intracellular protein in the extracellular environment. Supernatant samples were assayed for protein using the Biorad and Lowry protein assays.

3.4.4 Morphology

Morphological changes were observed through a phase contrast light microscope (Nikon 80094) at 1000 fold magnification. Bacterial aggregate counts were performed using a Superior counting chamber. The chamber was divided up into 0.0025 mm^2 squares, 0.1 mm in depth. Samples were stained with methyl violet for easier identification.

Particle size analysis by laser light diffraction of bacterial samples, suspended in sodium phosphate buffer was carried out in a Malvern 3600Ec particle sizer fitted with a 63mm lens. The principle of operation of the particle sizer is based on conventional Fourier optics. The beam of light from a low power Helium-Neon laser is scattered by particles in its path. The scattered light incident on a Fourier transform lens forms a diffraction pattern on a detector. The scattering angle is related to the particle diameter. Large particles have peak energies at low angles of scatter and *vice versa*. The zeta potential of bacteria at different pH was determined using a Malvern Electrophoresis Analyser ZET5004. An electric field was applied between two platinised platinum electrodes across the length of a 4mm quartz capillary cell and the resultant velocity of particles measured by laser light scattering. Cells were suspended in 0.05 M phosphate buffer for the pH range between pH 6 and 8 and 0.05 M

citrate-phospate buffer for the pH range between pH 3 to 7. A 1/10 dilution ratio was used.

3.5 EXPERIMENTAL PROCEDURE

Using the equipment and methods outlined in the previous section, the following experimental procedure was followed.

3.5.1 Evaluation of the hydrodynamics in the flow systems

The hydrodynamics in the stirred tank reactor, flowloop and airlift reactor were characterised in terms of local energy dissipation rates, circulation times and bubble sizes. All hydrodynamic measurements were carried out in cell free media supplemented with 0.5 g/l antifoam. The radial and tangential mean and fluctuating velocities were measured at the impeller tips in the bubble free and sparged stirred tank reactors at impeller speeds of 1.68 and 3.35 m/s. The random turbulent energy spectra, the random fluctuating velocities and the turbulent energy dissipation rates were also determined. Higher impeller speeds could not be investigated due to high frequency noise from the electrical circuit of the speed control fitted to the motor. The bulk random tangential velocities and turbulent energy dissipation rates were evaluated at the top, middle and bottom of the reactor for the two impeller system and at the middle for the single impeller system. Energy dissipation rates were calculated for the flowloop and airlift reactor.

Bubble sizes were measured in the sparged 5 liter stirred tank reactor at impeller speeds of 1.68, 3.35, 4.6 and 6.7 m/s and a superficial gas velocity of 0.005 m/s, and in the airlift reactor at a riser superficial gas velocity of 0.2 m/s.

Using both the conductivity technique and the correlations of Bryant *et al.* (1979), Chisti and Moo Young (1988) and Reub *et al.* (1988), the circulation times were determined in the 5 liter sparged stirred tank reactor, 7 liter bubble free stirred tank reactor, flowloop system and airlift reactor at various operating conditions.

3.5.2 The biological response of hydrodynamic stress

Batch cultures of *Corynebacterium glutamicum* and *Brevibacterium flavum* were carried out to characterise the growth, media requirements and operating conditions for the continuous cultivations. For *Corynebacterium glutamicum*, three batch cultivations were carried out. The first two were identical and were grown at stressed conditions (impeller tip speed 6.7 m/s and superficial air velocity of 0.013 m/s). The third batch cultivation was grown at milder hydrodynamic conditions. Agitation and aeration conditions were chosen such that the dissolved oxygen level in the vessel never dropped below 2 mg/l and that bacterial growth was therefore not limited by mass transfer. This limit was chosen to be slightly higher than the critical dissolved oxygen concentration determined by Kargi and Moo Young (1985) in a yeast culture , $C_{O(CRIT)} = 0.1\ C_O^*$. Samples from the cultivations were characterised in terms of growth rate through turbidity and dry mass, viability through plate counts, metabolic activity through oxygen and glucose utilisation rate and cell lysis through bacterial protein release.

For *Brevibacterium flavum* a single batch cultivation was carried out at mild agitation conditions in the absence of mass transfer limitations. After 28 hours the impeller speed was increased from 2.51 m/s to 3.35 m/s. The aeration rate remained unchanged at 0.005 m/s. Bacterial samples were analysed in terms of turbidity, oxygen utilisation rate, plate counts, protein concentration, lysine production, base consumption and glucose concentration.

The oxygen transfer potential of the stirred tank reactor with a working volume of 3.5 liters fitted with a single impeller was determined experimentally using the gassing-in technique. Measurements were carried out in the following media: *Corynebacterium glutamicum* fresh simple media, *Brevibacterium flavum* fresh simple media and *Corynebacterium glutamicum* stationary phase culture. The stationary phase *Corynebacterium glutamicum* culture medium contained non-respiring cells which had been heat shocked by heating to 60°C. The following agitation and aeration conditions were used.

Table 7 Agitation and aeration conditions for k_La measurement in the 3.5 liter stirred tank reactor using fresh and stationary phase medium of a 40 g/l and 200 g/l glucose *Corynebacterium glutamicum* cultivation.

MEDIUM	HYDRODYNAMIC CONDITIONS	
	IMPELLER TIP SPEED m/s	SUPERFICIAL GAS VELOCITY m/s
Corynebacterium glutamicum stationary phase culture medium (40 g/l glucose), dry mass: 17 g/l	1.26 1.68 2.51 3.35 4.19 4.71 5.86 6.7 8.38	0.004 0.005 0.006 0.006 0.007 0.005 0.01 0.013 0.013
Corynebacterium glutamicum stationary phase culture medium (200 g/l glucose), dry mass: 88.6 g/l	6.7	0.013
Corynebacterium glutamicum fresh simple media	1.68 3.35 5.03 6.7 6.7	0.005 0.005 0.005 0.005 0.013
Brevibacterium flavum fresh simple media	1.68 3.35 5.03 6.7	0.005 0.005 0.005 0.005

Continuous Chemap stirred tank cultivations of *Corynebacterium glutamicum* were carried out at dilution rates of 0.36 hr^{-1} and 0.1 hr^{-1} in the absence of mass transfer limiting conditions. *Brevibacterium flavum* was grown at a dilution rate of 0.105 hr^{-1}, also in the absence of mass transfer limiting conditions. Steady states at different agitation and aeration conditions were characterised in terms of dry biomass, turbidity, specific glucose utilisation rate, specific oxygen utilisation rate, supernatant protein concentration, amino acid production, plate counts, particle size analysis by laser light scattering and microscopic observation. The following agitation and aeration conditions were used.

Table 8 Agitation and aeration conditions for the *Brevibacterium flavum* and *Corynebacterium glutamicum* continuous cultivations.

CONTINUOUS CULTURE	HYDRODYNAMIC CONDITIONS	
	IMPELLER TIP SPEED m/s	SUPERFICIAL GAS VELOCITY m/s
Brevibacterium flavum $D = 0.105\ hr^{-1}$	3.35 5.03 6.7	0.005 0.005 0.005
Corynebacterium glutamicum $D = 0.36\ hr^{-1}$	1.68 3.35 5.03 6.7	0.005 0.005 0.005 0.005
Corynebacterium glutamicum $D = 0.1\ hr^{-1}$	4.7 6.8 8.38	0.005 0.01 0.013

The nature of the intra-cellular forces in *Corynebacterium glutamicum* cell aggregates was investigated. The zeta potential and particle size of *Corynebacterium glutamicum* aggregates were determined over the pH range from pH 2.5 to 8. The aggregates were broken up by subjecting cells grown up in a shake flask to the hydrodynamic forces in the flow loop apparatus. The cells were pumped at a flow rate of 3.93×10^{-6} m^3/s through a 0.8mm capillary for 35 minutes. The effect of the addition of EDTA and Ca^{2+} ions on the aggregate size distribution of disrupted *Corynebacterium glutamicum* aggregates during a re-agglomeration phase was investigated.

3.5.3 Kinetics and mechanism of hydrodynamic stress effect

The mechanism and kinetics of the biological response and the development of correlations to predict the response were investigated by subjecting *Corynebacterium glutamicum* cells grown in continuous culture at mild agitation conditions (impeller speed 1.68 m/s and 0.005 m/s superficial air velocity) at a dilution rate of 0.36 hr^{-1} to the conditions detailed below for periods up to 150 minutes:

a) Cells were agitated in the Chemap stirred tank reactor with a working volume of 7.3 liters at impeller tip speeds of 3.35, 4.6 and 6.7 m/s in the absence of an air liquid interface. Special care was taken to completely fill the reactor after taking each sample so that no air was entrained during mixing.

b) Cells were agitated in the Chemap stirred tank reactor operated at a working volume of 5 liters at impeller tip speeds of 3.35, 4.6 and 6.7 m/s and a superficial N_2 velocity of 0.005 m/s. N_2 was used to simulate the O_2 limiting environment of the former bubble free system.

c) Cells were pumped through the capillary flow system at flow rates of 3.93×10^{-6} m^3/s and 4.93×10^{-6} m^3/s.

d) Cells were circulated in the 1 liter airlift reactor at a superficial N_2 velocity of 0.21 m/s (based on the cross section of the riser).

Cell samples were analysed in terms of dry biomass, particle size analysis by laser light scattering and microscopic observation.

4. EVALUATION OF THE HYDRODYNAMICS IN THE FLOW SYSTEMS

4.1 INTRODUCTION

In order to identify and predict the predominant fluid force acting on cell surfaces, it is necessary to evaluate the fluid flow conditions in the experimental apparatus. It has been reported that both the interaction of cells with turbulent eddies in the impeller region of a stirred tank and in the wall region of a capillary, and with collapsing air bubbles at the air medium interface may be important. In this chapter, the hydrodynamics in the stirred tank reactor, flowloop and airlift reactor are characterised in terms of local energy dissipation rates, circulations times and bubble sizes. The energy dissipation rates and bubble sizes are critical parameters in determining the magnitude of the hydrodynamic force. The circulation time and bubble frequency provide a measure of the frequency of exposure to the hydrodynamic forces.

4.2 ENERGY DISSIPATION RATES

4.2.1 Stirred tank reactor

The velocity profile was measured in the stirred tank by the conductivity probe (Ranz, 1958). The one dimensional energy spectrum in frequency space (E_1) was obtained from the Fourier transform of the Eulerian autocorrelation coefficient (R_E) of the velocity fluctuations at a fixed point (Equation 64). The spectra (Figure 17) displayed the general form and characteristics of similar spectra obtained by numerous other researchers (Cutter, 1966; Majumdar *et al.*, 1970; Wu and Patterson, 1989). Most of the energy is contained in the low frequency eddies. In the inertial convection subrange, a characteristic slope of -5/3 (discussed by Wu and Patterson, 1989) is evident. In the viscous dissipative region, E(n) varied with n^{-5} compared to n^{-7} obtained by Gunkel and Weber (1975), where n is the frequency.

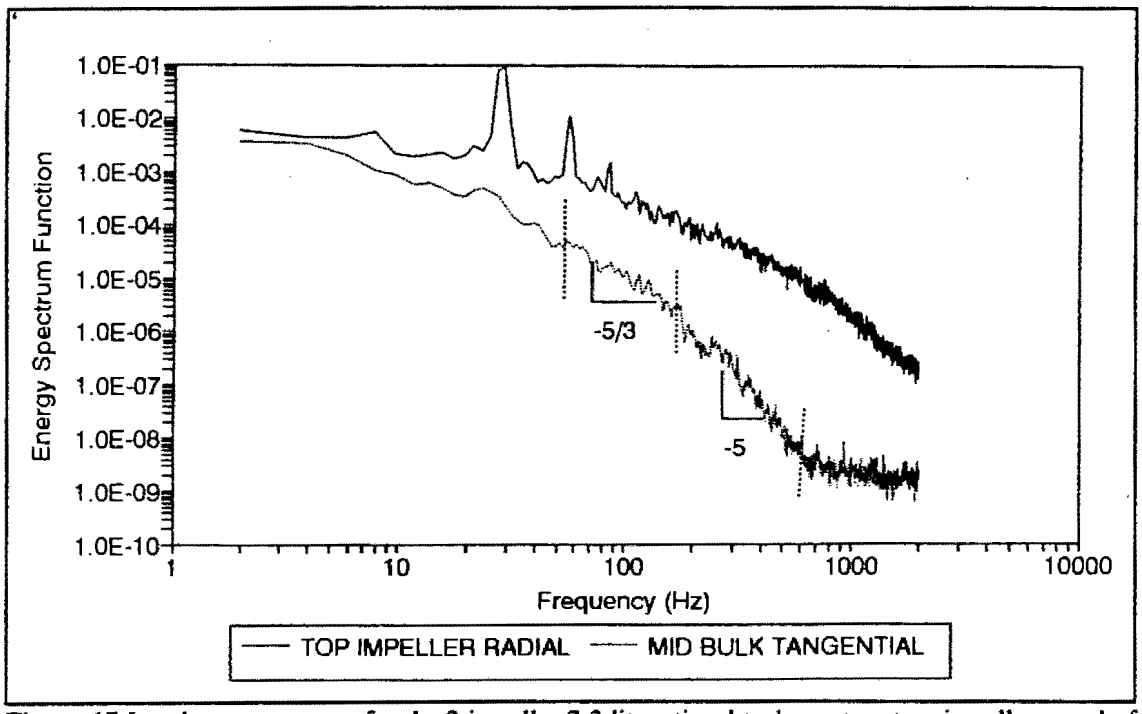

Figure 17 Local energy spectra for the 2 impeller 7.3 liter stirred tank reactor at an impeller speed of 1.68 m/s.

There were significant variations between the spectra in the bulk region of the tank and the impeller zone. The spectra obtained at the impeller tip at an impeller speed of 1.68 m/s in Figure 17 displayed the characteristic periodic component (Wu and Patterson, 1989). The first peak of the impeller tip energy spectra corresponds to the frequency at which the impeller blades pass the measuring point, 27 s^{-1}. The peak is accompanied by smaller peaks at integer multiples of the impeller speed. The periodic component accounted for 66% of the area under the energy spectrum (mean square turbulent velocity). No significant periodic component was observed in the energy spectra for the middle bulk region of the tank. The random energy spectrum was obtained from the corrected random auto-correlation coefficient. The latter was obtained by subtracting the periodic contribution from the total auto-correlation coefficient.

The random energy spectra were used to calculate the mean squared random turbulent velocities and the energy dissipation rates in the stirred tank. In the calculation of the energy dissipation rates, the turbulent kinetic energy did not contain any contribution of periodic fluctuations and a state of isotropic turbulence was assumed. In the impeller zone the axial fluctuating velocity was approximated as the average of the tangential and radial fluctuating

velocities. In the bulk regions, the radial and axial fluctuating velocities were assumed equal to the measured tangential fluctuating velocity. The approximation of local isotropy was supported by the similarity of the tangential and radial fluctuating velocities in the impeller zone as shown in Table 9.

The Eulerian macroscale was estimated to be a quarter of the blade width (0.5 mm) at the point of measurement near the impeller tip and equal to the blade width (2 mm) in the bulk region of the tank (Majumdar *et al.*, 1970; Rao and Brodkey, 1972; Wu and Patterson, 1989). The macroscales at a given point in the tank were assumed to be equal in magnitude in all directions.

Results of the local energy dissipation rates normalised with respect to the mean power input for the stirred tank reactor are presented in Table 10. The mean power input was estimated using correlations developed by O'Connel and Mack (1950), Rushton *et al.* (1950), Michel and Miller (1962) and Bates *et al.* (1963). Sample calculations are presented in Appendix C1. For the aerated systems, the local energy dissipation rate values in the impeller region were 20 to 30 times the overall mean energy dissipation rates. These compare well with the local impeller zone energy dissipation rates obtained by Wu and Patterson (1989) and Okamoto *et al.* (1981), which were 23.5 and 15.6 times the overall mean energy dissipation rates respectively. The values in the bulk varied from 0.02 to 0.4 times the average which agree with the reported results of Cutter (1966) and Okamoto *et al.* (1981), which were 0.27 times the average.

The normalised values of energy dissipation rate were similar for the two impeller speeds investigated (Table 10). Okamoto *et al.* (1981) found that the distribution of the normalised local energy dissipation rate in a stirred tank was independent of Reynold's number for geometrically similar vessels. The same normalised energy dissipation rate distribution was assumed for the two higher agitation speeds.

Table 9 The measured random fluctuating velocities (u) and mean velocities (U) in the stirred tank reactor.

	7 LITER NO SPARGING 2 IMPELLERS m/s				5 LITER SPARGING U_{sg} = 0.005 m/s 2 IMPELLERS m/s				3 LITER SPARGING U_{sg} = 0.005 m/s 2 IMPELLERS m/s			
IMPELLER TIP SPEED	1.68 m/s		3.35 m/s		1.68 m/s		3.35 m/s		1.68 m/s		3.35 m/s	
	u	U	u	U	u	U	u	U	u	U	u	U
TOP IMPELLER												
radial	0.43	1.62	1.01	3.45	0.71	1.25	1.01	2.77				
tangential	0.43	1.18	0.8	2.46	0.51	0.79	1.11	2.27				
BOTTOM IMPELLER												
radial	0.37	1.48	0.77	3.42	0.54	0.84	1.06	2.77	0.52*	0.91*	0.85*	2.43*
tangential	0.34	1.06	0.94	3.09	0.53	0.85	0.94	2.37	0.36*	0.69*	0.77*	2.22*
TOP BULK tangential	0.12	0.193	0.28	0.42	0.16	0.22	0.24	0.36				
MIDDLE BULK tangential	0.19	0.32	0.43	0.63	0.09	0.12	0.22	0.39	0.18*	0.31*	0.21*	0.34*
BOTTOM BULK tangential	0.36	0.63	0.79	1.55	0.09	0.12	0.29	0.58				
MIDDLE INSIDE BULK tangential	0.18	0.24	0.42	0.6	0.18	0.14	0.42	0.33	0.17*	0.4*	0.14*	0.21*

*single impeller used

The ratio of local and average energy dissipation rates for the bubble free system in the impeller region are lower than expected. This may be due to the entrainment of air at the surface as the air liquid interface could not be removed in the measuring system. The local energy dissipation rates for the 5 liter sparged impeller system show that the lower impeller draws less power than the upper impeller. This is expected as less of the gas volume passes through the upper impeller (Hicks and Gates, 1976).

Table 10 Local rates of energy dissipation (normalised with respect to correlated average energy dissipation rate).

IMPELLER SPEED	PROBE LOCATION	7 LITER NO SPARGING 2 IMPELLERS	5 LITER SPARGING U_{sg} 0.005 m/s 2 IMPELLERS	3.5 LITER SPARGING U_{sg} 0.005 m/s 1 IMPELLER
1.68 m/s		e_{AVE} = 1.19 m^2/s^3	0.84 < e_{AVE} < 1.26 m^2/s^3	e_{AVE} = 0.603 m^2/s^3
	Upper impeller	12.1	33.2-49.5	
	Lower impeller	7.2	21.5-32	26.6
	Top bulk	0.07	0.15-0.23	0.43
	Middle outer bulk	0.28	0.02-0.04	0.4
	Middle inner bulk	0.24	0.22-0.33	
	Bottom bulk	1.7	0.02-0.04	
3.35 m/s		e_{AVE} = 9.15 m^2/s^3	7.5 < e_{AVE} < 10.42 m^2/s^3	e_{AVE} = 3.03 m^2/s^3
	Upper impeller	14.2	20.8-28.9	
	Lower impeller	11.9	17.3-24	32
	Top bulk	0.11	0.06-0.08	0.13
	Middle outer bulk	0.38	0.05-0.07	0.04
	Middle inner bulk	0.35	0.11-0.15	
	Bottom bulk	2.3	0.32-0.44	
4.6 m/s		e_{AVE} =23.8 m^2/s^3	20.5 < e_{AVE} < 27.6 m^2/s^3	e_{AVE} = 14.6 m^2/s^3
6.7 m/s		e_{AVE} = 73.2 m^2/s^3	66.6 < e_{AVE} < 86.7 m^2/s^3	e_{AVE} = 47.5 m^2/s^3

4.2.2 Turbulent capillary flow

The extensive studies of Laufer (1954) indicated that, in pipe flow, the local energy dissipation rate per unit mass is at a maximum near $y^+ = 12$, where y^+ is the dimensionless distance from the pipe wall (2y/D). The value of $e_w D/2u^{*3}$ at this location is approximately 230, where e_w is the energy dissipation rate per unit mass in the wall region of the pipe, D is the pipe diameter and u^* is the friction velocity. The average energy dissipation rates, the maximum energy dissipation rates, the minimum Kolmogorov microscales (Equation 15) and the Reynold's numbers, calculated for a 0.8 mm capillary at volumetric flow rates of 3.93×10^{-6} and 4.93×10^{-6} m^3/s are given in Table 11. Detailed calculations of energy dissipation rates are given in the Appendix C2. The flow in the tube is turbulent as the Reynold's numbers are greater than 4000. The applicability of the theory of turbulence to calculate the energy dissipation rates is therefore valid.

Table 11 Energy dissipation rate in a 0.8 mm diameter turbulent capillary

FLOWRATE m^3/s	e_{AVE} m^2/s^3	e_{wall} m^2/s^3	λ_{wall} μm	Re
3.93×10^{-6}	5030	79920	1.88	6255
4.93×10^{-6}	9650	144810	1.62	7846

4.2.3 Airlift reactor

According to Chisti and Moo-Young (1987), the pneumatic power input for an airlift reactor, when the isothermal expansion of gas is the predominant source of power is given by:

$$\frac{P_g}{V_L} = \rho_L \, g \, U_{gr} \frac{A_r}{A_r + A_d} \tag{71}$$

where U_{gr} is the superficial gas velocity in the riser, and A_r and A_d are the cross sectional areas in the riser and downcomer respectively. For a superficial gas velocity in the riser of 0.2 m/s in the airlift reactor, the pneumatic power input per unit volume was calculated to

be 668 W/m^3. This equates to an average energy dissipation rate of 0.668 m^2/s^3.

4.3 BUBBLE SIZE

The measured and correlated Sauter mean bubble sizes in the sparged stirred tank reactor (U_{sg} 0.005 m/s) at different agitation speeds (1.68 to 6.7 m/s) and in the airlift reactor at a superficial gas velocity in the riser of 0.2 m/s are presented in Table 12. Correlations of Calderbank (1958), Bhavaraju *et al.* (1978) and Dussop and Gros (1982) were used as appropriate. Calderbank determined the Sauter mean diameter in a stirred tank reactor using an air water system as:

$$d_{SM} = 2.25 \frac{\sigma^{0.6}}{\rho_L (\frac{P}{V})^{0.4}} \epsilon_g^{0.5} (\frac{\mu_G}{\mu_L})^{0.25} \tag{72}$$

where σ surface tension of the liquid, (P/V) is the power input per unit volume, ϵ_g is the gas holdup and μ_G and μ_L are the gas and liquid velocities. The gas holdup was measured as the difference between the unaerated liquid height and the aerated liquid height, divided by the aerated liquid height. The bubble size correlation developed by Bhavaraju *et al.* (1978) for power law fluids in airlift reactors is given by:

$$d_{SM} = 0.7 \frac{\sigma^{0.6}}{(\frac{P_g}{V'_L})^{0.4} \rho_L^{0.2}} (\frac{\mu_{app}}{\mu_G})^{0.1} \tag{73}$$

where V'_L is the liquid volume in the riser and μ_{app} is the apparent liquid viscosity. Dussop and Gros (1982) proposed that the Sauter mean bubble size in aqueous sodium sulphite in an airlift reactor can be estimated as:

$$d_{SM} = 1.64 \epsilon_g (\frac{P_g}{V_D})^{-0.77} \tag{74}$$

where V_D is the dispersion volume. The correlation was valid for $200 \leq P_g/V_D \leq 1500$.

Visual observation of the bubbles in the two flow systems clearly indicated that the bubbles in the stirred tank were smaller than those in the airlift reactor. The presence of a very fine bubble swarm was apparent in the stirred tank reactor. The bubble sizer developed by O'Connor *et al.* (1990) is not able to measure bubble sizes smaller than 0.5 mm; hence experimental results for the stirred tank reactor are an overestimation of the Sauter mean diameter in the vessel. This is borne out by comparison with the correlation of Calderbank (1958), based on a similarly sized stirred tank at the same flow rates using an air-water system (Table 12). The correlations predicted the bubble size to decrease with increased agitation as expected, whereas experimental results yielded an unexpected increase in bubble size with increased agitation. Use of the bubble sizer of O'Connor *et al.* (1990) is thus inappropriate in the laboratory stirred tank bioreactor.

Comparison of the experimentally determined bubble sizes in the airlift reactor and the Sauter mean bubble sizes determined by correlations of Bhavaraju *et al.* (1978) and Dussop and Gros (1982) indicated good agreement. This corresponds to the claims of O'Connor *et al.* (1990) that bubbles in the range 0.5 to 8 mm can be measured by their bubble sizer.

Table 12 Sauter mean bubble diameters in the airlift and the stirred tank reactor.

FLOW SYSTEM	IMPELLER TIP SPEED	MEASURED d_{SM}	CORRELATED d_{SM}	REFERENCE
5 liter sparged stirred tank reactor: 9.5 l/min	1.68 m/s 3.35 m/s 4.6 m/s 6.7 m/s	1.27 mm 1.25 mm 1.34 mm 1.33 mm	0.006-0.007 $\sigma^{0.6}$ → 0.82-0.95 mm 0.0034-0.0039 $\sigma^{0.6}$ → 0.46-0.53 mm 0.0025-0.0029 $\sigma^{0.6}$ → 0.34-0.39 mm 0.0018-0.002 $\sigma^{0.6}$ → 0.25-0.27 mm	Calderbank, 1958
airlift reactor: U_{gr} 0.2 m/s		1.77 mm	0.013 $\sigma^{0.6}$ → 1.77 mm 1.3 mm	Bhavaraju *et al.*, 1978 Dussop and Gros, 1982

4.4 CIRCULATION TIME

For the stirred tank reactor, circulation times were measured by the conductivity technique and estimated by calculation according to Reuß (1988). The correlation of Reuß (1988) was developed using stirred tank reactors with diameters of 0.2 m, 0.39 m and 0.48 m agitated by two 6-bladed Rushton-turbines. Two impellers with a diameter to length to width ratio of 20:5:4 were used. The mean circulation times were measured using a magneto flow follower technique and were correlated by the following relationship:

$$Nt_C = 0.76 \left(\frac{H}{T}\right)^{0.6} \left(\frac{T}{D}\right)^{2.7} \quad (75)$$

where N is the agitation speed, t_C is the circulation time, H is the liquid height, T is the tank diameter and D is the impeller diameter. The correlation developed by Bryant *et al.* (1979) showed that aeration had a negligible effect on the circulation time in the sparged stirred tank:

$$t_C[aerated\ system] = t_C[unaerated\ system](1 + 0.1Q_g) \quad (76)$$

where Q_g is the volumetric gas flow rate in m^3/s.

In the capillary flow system, the circulation time was calculated by dividing the total flow volume of 1.152 liters by the volumetric flow rate.

In the airlift reactor, the circulation time was estimated as the ratio of the circulation distance and the circulation velocity. According to Chisti and Moo Young (1988), the superficial liquid velocity U_{lr} in the riser of an internal loop airlift reactor can be calculated as follows:

$$U_{lr} = \left[\frac{2gh_D(\epsilon_{gr}-\epsilon_{gd})}{\frac{K_B}{(1-\epsilon_{gd})^2}(\frac{A_r}{A_d})^2}\right]^{0.5} \quad (77)$$

where h_D is the dispersion height, ϵ_{gr} and ϵ_{gd} the gas holdups in the riser and downcomer respectively, and A_r and A_d the cross sectional areas of the riser and downcomer respectively. K_B is the frictional loss coefficient for the bottom of the reactor. For internal loop airlift reactors K_B is given by:

$$K_B = 11.402(\frac{A_d}{A_b})^{0.789} \quad (78)$$

where A_b is the flow area under the baffle (Chisti and Moo-Young, 1993). The superficial liquid velocity in the downcomer, U_{ld}, is derived according to the continuity equation:

$$U_{ld}A_d = U_{lr}A_r \quad (79)$$

From a mass balance, the overall gas holdup ϵ is given by:

$$\epsilon_g = \frac{A_r\epsilon_{gr} + A_d\epsilon_{gd}}{A_r + A_d} \quad (80)$$

The overall gas holdup can be measured experimentally as the difference between the unaerated liquid height and the aerated liquid height, divided by the aerated liquid height. At a riser superficial gas velocity of 0.2 m/s, the gas holdup was 0.112. Bello *et al.* (1984) proposed that:

$$\epsilon_{gd} = 0.89\epsilon_{gr} \quad (81)$$

for concentric draught tube internal loop airlifts. Applying the above set of equations the circulation time in the airlift reactor was calculated as:

$$t_{C(airlift)} = \frac{L_r}{U_{Lr}} + \frac{L_d}{U_{Ld}} \quad (82)$$

Circulation times determined for the stirred tank reactor, capillary flowloop system and airlift reactor using the above correlations are presented in Table 13.

Table 13 Circulation times in the stirred tank reactor, flow loop system and airlift reactor.

SYSTEM	CONDITIONS	MEASURED t_C	CALCULATED t_C	REFERENCE
5 liter sparged stirred tank reactor: U_{sg} = 0.005 m/s	v_{imp} = 0.84 m/s v_{imp} = 1.67 m/s v_{imp} = 3.35 m/s v_{imp} = 4.6 m/s v_{imp} = 6.7 m/s	1.29 s 0.91 s 0.65 s 0.45 s	2.7 s 1.35 s 0.67 s 0.49 s 0.34 s	Reub *et al.*, 1988, Bryant *at al.*, 1979
7.3 liter bubble free stirred tank reactor	v_{imp} = 1.67 m/s v_{imp} = 3.35 m/s v_{imp} = 4.6 m/s v_{imp} = 6.7 m/s	0.98 s 0.71 s	1.71 s 0.85 s 0.62 s 0.43 s	Reub *et al.*,1988
Flowloop	Q = 3.93×10^{-6} m^3/s Q = 4.93×10^{-6} m^3/s	3.9 min 3.13 min		
Airlift	U_{gr} = 0.2 m/s		5.6 s	Chisti and Moo Young (1988).

A typical circulation time response curve, obtained in the experimental determination of circulation time in the stirred tank reactor, is shown in Figure 18. The circulation time is determined from the separation of the peaks. Measured circulation times are included in Table 13. For the sparged and bubble free stirred tank reactors, the correlated and measured circulation times agreed reasonably well at impeller tip speeds above 3.35 m/s. Incompletely developed flow patterns at low impeller tip speeds may account for the discrepancy between the correlated and the measured results. In the measuring system, it was assumed that the upper and lower impeller had similar flow patterns (Mukutaka *et al.*, 1981). The bubble free stirred tank reactor had a larger volume in the upper impeller region and one would therefore

expect the circulation time in this region to be larger than that in the lower impeller region and larger than the circulation time for a symmetrical impeller system as predicted by the correlation. In the bubble free system at impeller speeds greater than 3.35 m/s, electrical interference from the entrainment of slugs of air completely obscured the circulation time signal. The circulation time measuring technique was not sensitive enough to measure the circulation time at an impeller speed of 6.7 m/s in the bubble system. Correlated circulation times have been used in the aggregate breakup model.

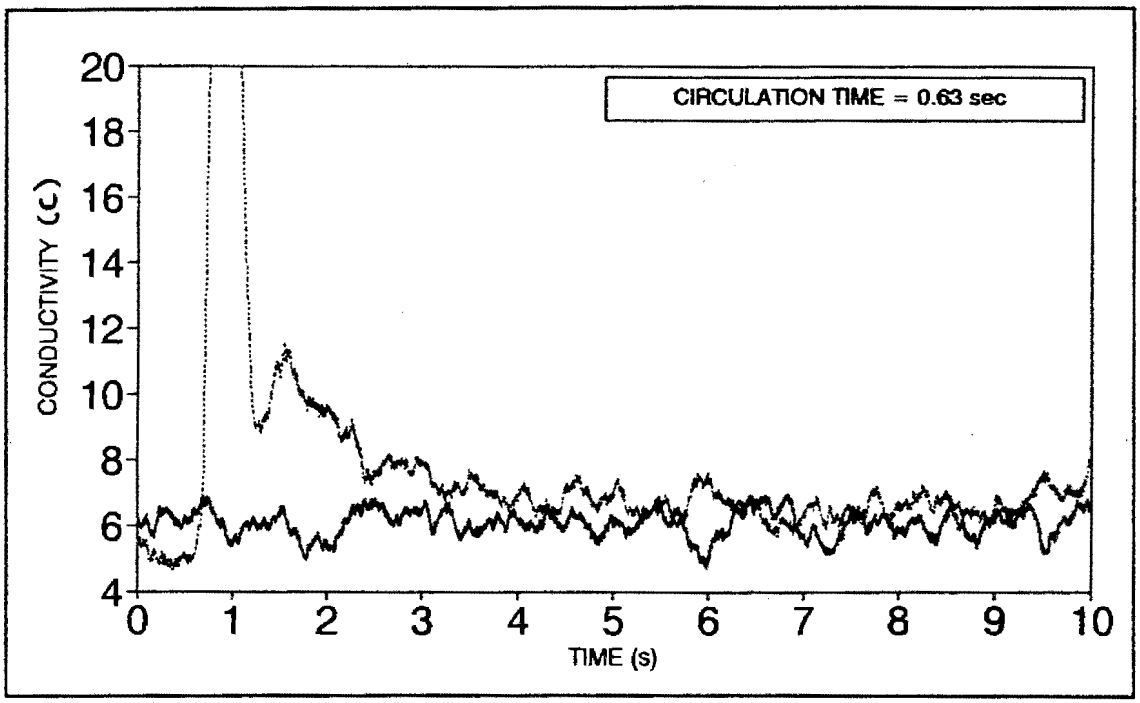

Figure 18 A typical circulation time response curve in the 5 liter sparged stirred tank reactor: impeller speed 3.35m/s, U_{sg} 0.005 m/s (baseline represents background noise).

4.5 CONCLUSIONS

4.5.1 Experimental determination of the energy dissipation rates in the Chemap stirred tank reactor showed that the correlations of O'Connel and Mack (1950), Rushton *et al.* (1950), Michel and Miller (1962) and Bates *et al.* (1963) gave an accurate estimate of the average energy dissipation rate. The assumption of local isotropy in the impeller zone was supported by the similarity of the tangential and radial components and hence the validity of this assumption in calculating the turbulent kinetic energy and the resultant turbulent macroscale was justified. The physical

study showed that the distribution of energy dissipation rates in the flow systems were highly uneven. It is therefore important that biological responses be correlated with the maximum local forces rather than the mean forces.

4.5.2 Microorganisms are exposed to extreme hydrodynamic forces in the wall region of the capillary in the capillary flowloop system where the local energy dissipation rate was approximately 15 times the average energy dissipation rate in the capillary. The overall average energy dissipation rate values were 100 times greater in magnitude than in the stirred tank reactor.

4.5.3 The average energy dissipation rate in the airlift reactor at the conditions investigated was the same order of magnitude as that calculated for the bubble free and sparged stirred tank reactor at an impeller speed of 1.68 m/s.

4.5.4 The bubbles in the stirred tank reactor were smaller than those in the airlift reactor; hence the forces exerted on the surface of microbial cell due to its interaction with collapsing air bubbles would be greater in the sparged stirred tank reactor.

4.5.5 Circulation times in the flowloop system were 2 to 3 orders of magnitude greater than in the stirred tank reactor.

5. THE BIOLOGICAL RESPONSE OF MICROORGANISMS TO HYDRODYNAMIC STRESS

5.1 INTRODUCTION

Literature studies have shown that the effect of hydrodynamic stress on microorganisms can manifest itself as a change in morphology, shift in metabolic pathway, reduction in growth rate, loss in cell viability or in the extreme case a loss in cell integrity. The response of *Brevibacterium flavum* and *Corynebacterium glutamicum* to various levels of agitation and aeration in a stirred tank reactor was measured in terms of lysis, viability, rate of metabolism and shift in metabolic pathway, and morphology changes using suitable analytical techniques. Experiments were carried out in the absence of mass transfer limiting conditions to ensure that observed changes were solely due to the effect of mechanical forces being exerted on the cell wall.

5.2 BATCH GROWTH PROFILES

The basic batch growth profiles of *Corynebacterium glutamicum* and *Brevibacterium flavum* were determined to characterise the growth, media requirements and operating conditions for the continuous cultivations. Samples taken at various times during the batch runs were analysed in terms of turbidity, dry mass, specific plate counts, oxygen utilisation rate, glucose concentration and bacterial protein release.

The specific plate count was calculated as the number of colonies per gram of dry biomass. Microscopic observation of the bacteria (Figure 19) showed that the bacteria have a tendency to agglomerate, hence the specific plate count is a measure of the number of aggregates per gram of biomass. It should be borne in mind that the specific plate counts can also change as a function of the dry weight per cell due to changes in cell size and accumulation of storage products.

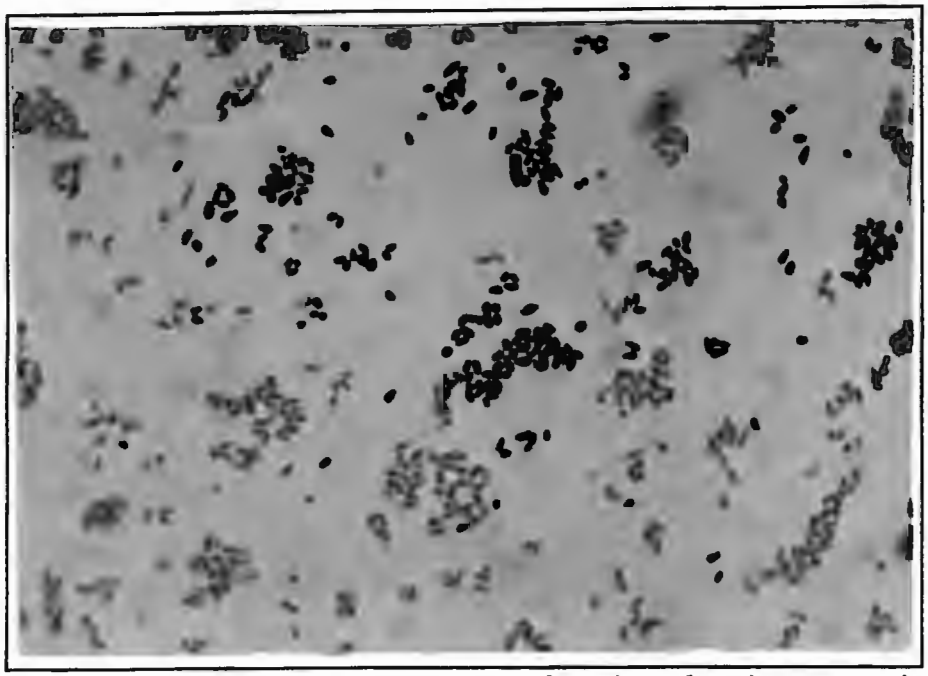

Figure 19 Microscopic observation of *Corynebacterium glutamicum* grown in complex media in shake flask for 12 hours (1mm = 1μm).

For *Brevibacterium flavum*, a single batch cultivation was performed at an impeller speed of 2.51 m/s and a superficial gas velocity of 0.005 m/s. After 28 hrs, the impeller speed was increased to 3.35 m/s to avoid mass transfer limiting conditions. The batch growth profiles are shown in Figures 20 and 21. For *Corynebacterium glutamicum*, two batch experiments were carried out at identical conditions (impeller speed 6.7 m/s and superficial gas velocity 0.013 m/s). The growth profiles are presented in Figures 22, 23 and 24.

The shape of the growth curves indicate that the logistic equation should model the data adequately. The logistic curve (Bailey and Ollis, 1986) given by:

$$C_x = \frac{C_{xo} e^{B_1 t}}{1 - B_2 C_{xo} (1 - e^{B_1 t})} \qquad (83)$$

where C_x is the concentration of cells, C_{xo} is the initial concentration of cells, t is the cultivation time and B_1 and B_2 are constants, was fitted to the dry biomass data. The constants, B_1 and B_2, are equivalent to the inverse of the time taken to reach the stationary phase, and the inverse of the concentration of the stationary phase population respectively. The calculated values for B_1 and B_2 and the correlation coefficient for these batch experiments are presented in Table 14.

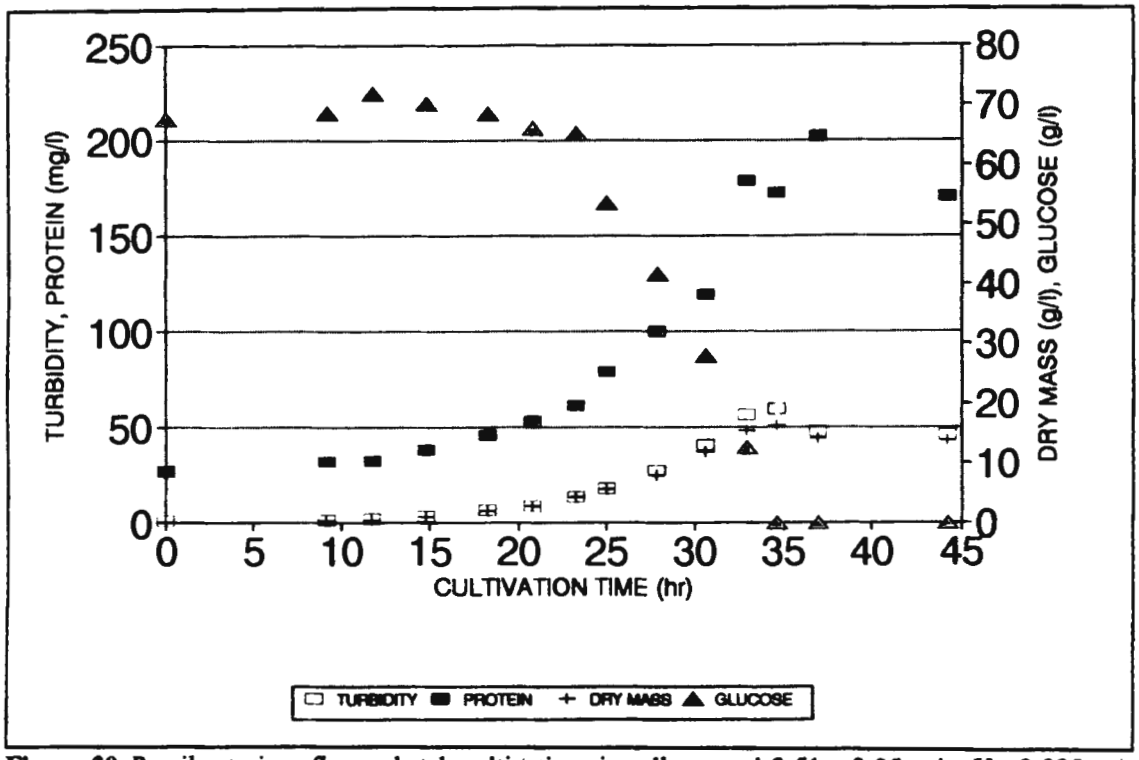

Figure 20 *Brevibacterium flavum* batch cultivation: impeller speed 2.51 - 3.35 m/s, U_{sg} 0.005 m/s (biomass, residual glucose, extracellular protein).

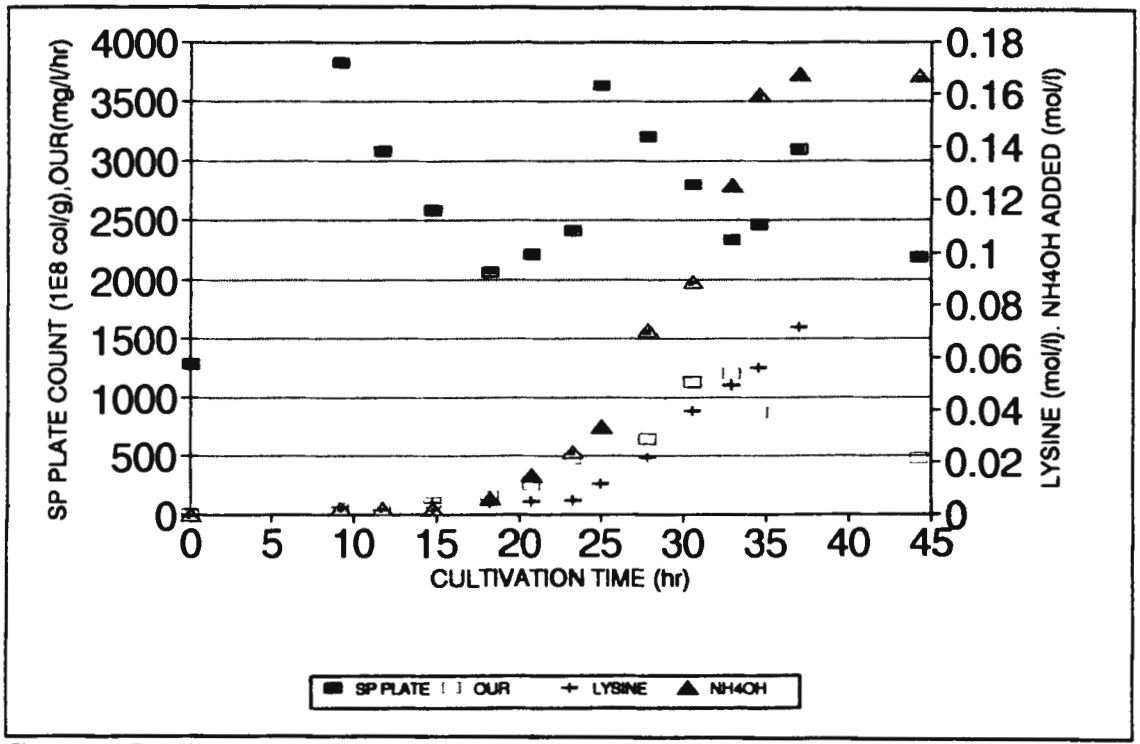

Figure 21 *Brevibacterium flavum* batch cultivation: impeller speed 2.51 - 3.35 m/s, U_{sg} 0.005 m/s (specific plate count, oxygen utilisation rate, lysine, base addition).

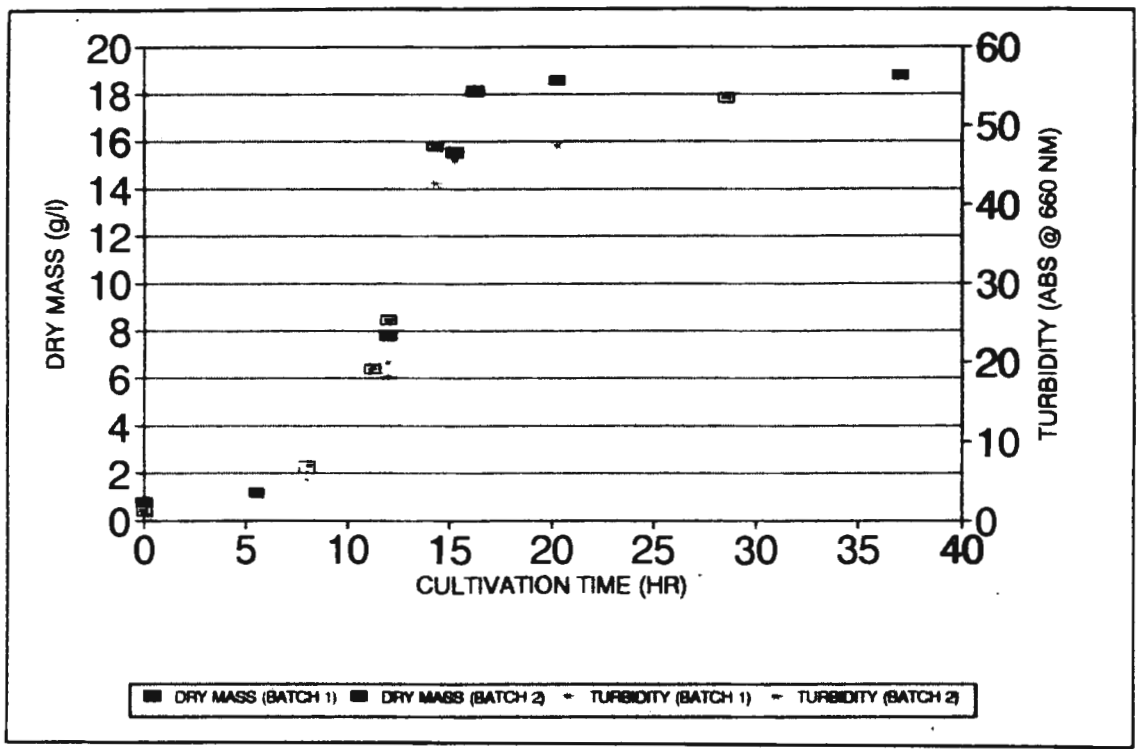

Figure 22 *Corynebacterium glutamicum* batch cultivation: impeller speed 6.7 m/s, U_{sg} 0.013 m/s (biomass concentration).

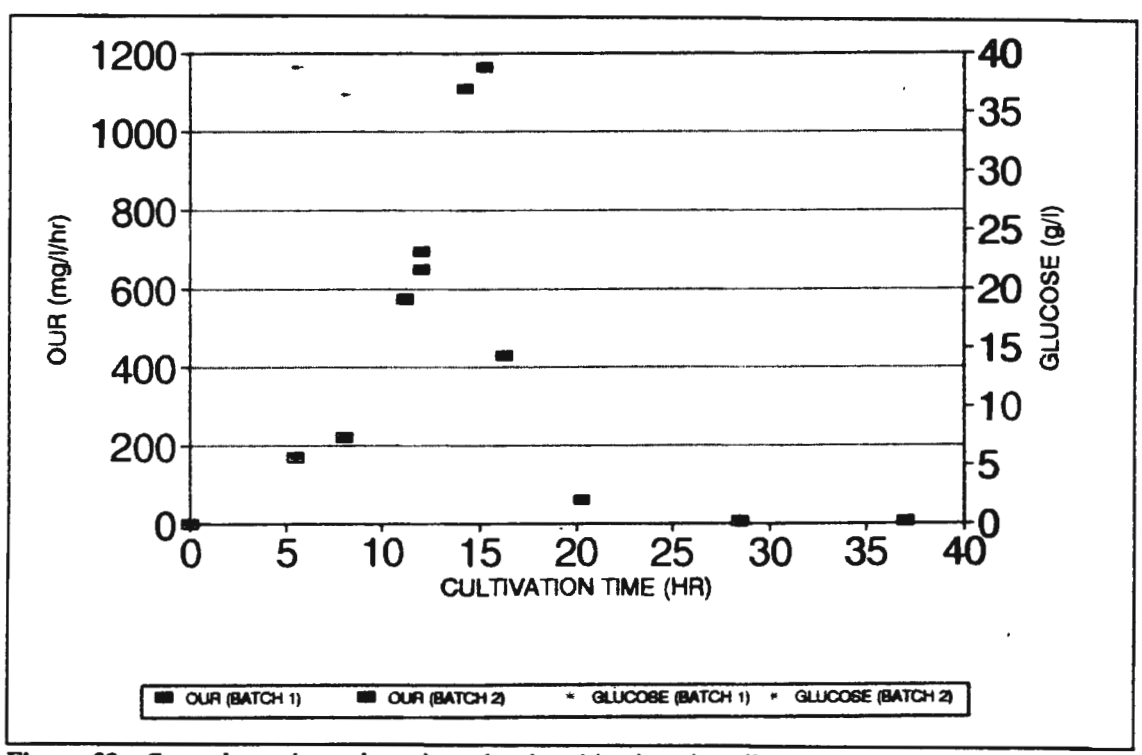

Figure 23 *Corynebacterium glutamicum* batch cultivation: impeller speed 6.7 m/s, U_{sg} 0.013 m/s (oxygen utilisation rate and residual glucose).

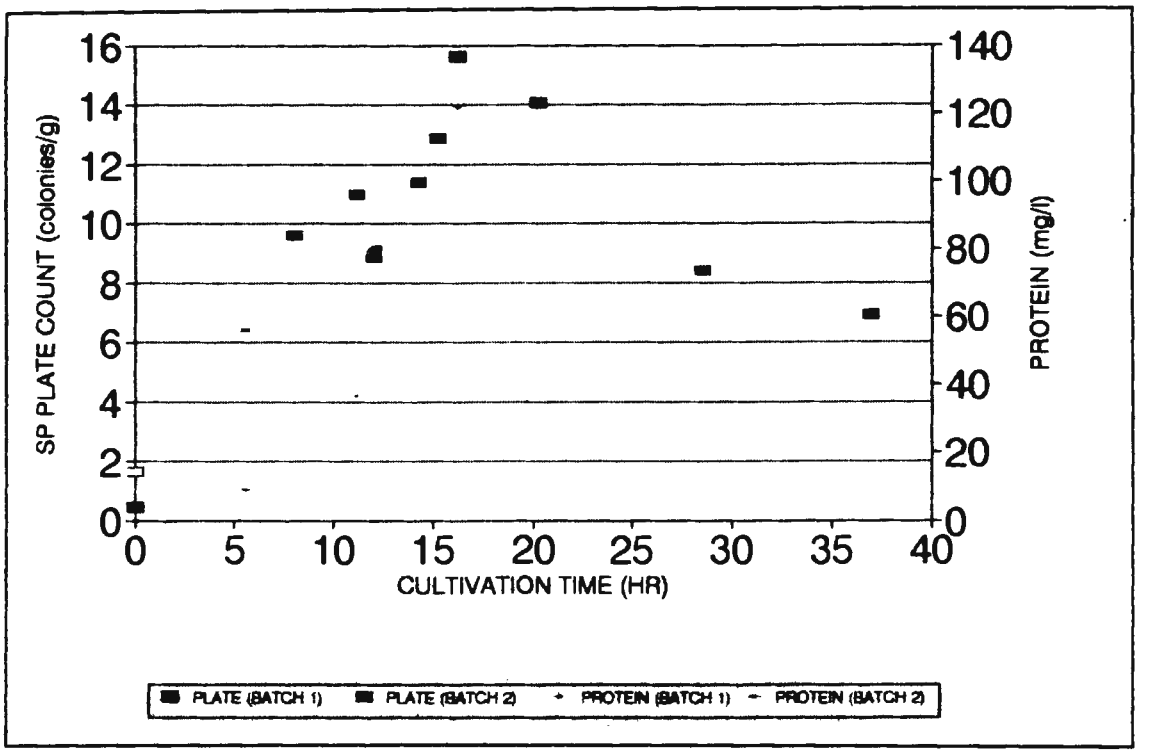

Figure 24 *Corynebacterium glutamicum* batch cultivation: impeller speed 6.7 m/s, U_{sg} 0.013 m/s (specific plate count and extracellular protein).

Table 14 Logistic curve constants for *Corynebacterium glutamicum* and *Brevibacterium flavum* batch growth curves.

BACTERIA	CONDITIONS	B_1 s^{-1}	B_2 l/g	r
Corynebacterium glutamicum	Chemap batch cultivation impeller speed: 6.7 m/s U_{sg}: 0.013 m/s	 0.62 0.62	 0.057 0.053	 0.92 0.94
Brevibacterium flavum	Chemap batch cultivation impeller speed: 3.35 m/s U_{sg}: 0.005 m/s	0.275	0.057	0.92

The similarity of the logistic constants for the *Corynebacterium glutamicum* batch experiments shows that the growth curves are identical and that the experiments are therefore reproducible. Reproducibility of the batch reaction profiles for *Corynebacterium glutamicum* is confirmed in Figures 22-24.

For the *Corynebacterium glutamicum* batch cultivation, the specific oxygen utilisation rate decreased from 120 mg O_2 per hour per gram of dry cell mass at the start of exponential growth to 69 mg per hour per gram dry cell mass in the late exponential phase. This compares reasonably with specific oxygen utilisation rate data from batch experiments for auxotrophic *Corynebacterium glutamicum* (ATCC 21253) obtained by Kiss and Stephanopoulos (1991), which dropped from 133 mg per hour per gram dry cell mass in the early exponential phase to 66 mg per hour per gram dry cell mass in the late exponential phase. An initial glucose concentration of 200 g/l was used in their batch experiment.

The specific plate counts of the *Corynebacterium glutamicum* batch cultivation shown in Figure 24, were observed to increase with cultivation time *i.e* agglomeration behaviour was more pronounced at the start of the cultivation. The specific plate counts decreased during the death phase due to autolysis.

The protein concentrations measured in the supernatants of both the *Corynebacterium glutamicum* and *Brevibacterium flavum* batch cultures were low. Only 1.5% of the total cell protein was released into the supernatant.

Comparison of the *Brevibacterium flavum* growth curve (Figure 20) shows that lysine is a mixed growth associated product, accumulating during the exponential and stationary phases. According to the stoichiometry of lysine production, 1 mole of NH_4OH is consumed for every mole of lysine produced. A comparison of the rates of ammonium hydroxide consumption and lysine production shows the ratio is approximately 2; indicating the presence of other mixed growth associated acidic products.

5.3 MASS TRANSFER POTENTIAL

It is essential that mass transfer limiting conditions are avoided in the study of hydrodynamic stress on the biological response of microorganisms. The oxygen transfer potential of the stirred tank reactor with a working volume of 3.5 liters fitted with a single impeller was determined experimentally using the gassing-in technique. Errors due to the time delay of the

probe were minimal as the probe response time of 8 seconds was less than $1/k_La$ (van't Riet, 1979). Measurements were carried out in both media and bacterial suspensions (17-89 g dry weight/l) over a range of agitation and aeration conditions (impeller speed 1.3 - 8.4 m/s, U_{sg} 0.004 - 0.013 m/s). Since salinity and the presence of antifoam agents effect the volumetric mass transfer coefficient, k_La, the mass transfer potential was measured in the fresh media used for *Corynebacterium glutamicum* and *Brevibacterium flavum* . The effect of viscosity on k_La was investigated by performing mass transfer potential measurements as a function of biomass in the cell suspension. The stationary phase *Corynebacterium glutamicum* culture contained non-respiring cells which had been inactivated by heating to 60°C. The results of the experiments are presented in Table 15.

A decline in the mass transfer coefficient during the bacterial cultivation was observed due to an increase in the viscosity of the suspension. It was found that the liquid side volumetric mass transfer coefficient, k_La, decreased from 0.099 through 0.089 to 0.067 s^{-1} as the concentration of *Corynebacterium glutamicum* increased from zero through 17.0 to 88.6 g/l of dry biomass. The mass transfer potential increased with increasing agitation and aeration conditions. The k_La values for the *Corynebacterium glutamicum* and *Brevibacterium flavum* cell free media were identical at the same hydrodynamic conditions.

The experimentally determined mass transfer coefficients agreed reasonably with empirical correlation of Chandrasekhar and Calderbank (1981). This correlation was based on experiments carried out in an air-water system using a geometrically similar stirred tank reactor. Factors which may account for differences in the results may be the presence of an antifoam agent and the high salinity of the fresh media. The antifoam agent increases the value of the oxygen mass transfer coefficient as the surface tension is reduced (Kawase and Moo-Young, 1990). The value of k_La can be expected to increase with increasing concentration of electrolytes (Robinson and Wilke ,1973).

From the batch experimental data presented in Figure 23, it is seen that the peak oxygen demand of a 20g/l batch *Corynebacterium glutamicum* cultivation was 1600 mg/l/hr. This could be satisfied at an impeller tip speed of 4.71 m/s and a superficial gas velocity (U_{sg}) of 0.005 m/s. For the *Brevibacterium flavum* culture, the peak oxygen demand of 1240 mg/l/hr

for a 70 g/l glucose feed cultivation (Figure 21), could be met at an impeller speed of 3.35 m/s and a superficial gas velocity of 0.005 m/s.

Table 15 K_La measured in 3.5 liter stirred tank reactor using fresh medium and stationary phase culture of a 40 g/l and 200 g/l glucose *Corynebacterium glutamicum* cultivation.

MEDIUM	HYDRODYNAMIC CONDITIONS		Experimental k_La s^{-1}	Correlated k_La s^{-1}
	IMPELLER TIP SPEED m/s	SUPERFICIAL GAS VELOCITY m/s		
Corynebacterium glutamicum stationary phase culture medium, dry mass: 17 g/l (feed glucose: 20 g/l)	1.26 1.68 2.51 3.35 4.19 4.71 5.86 6.7 8.38	0.004 0.005 0.006 0.006 0.007 0.005 0.01 0.013 0.013	0.012 0.028 0.044 0.051 0.065 0.07 0.085 0.089 0.118	
Corynebacterium glutamicum stationary phase culture medium dry mass: 88.6 g/l (feed glucose: 200 g/l)	6.7	0.013	0.067	
Corynebacterium glutamicum fresh simple media (glucose: 20 g/l)	1.68 3.35 5.03 6.7 6.7	0.005 0.005 0.005 0.005 0.013	0.034 0.051 0.062 0.078 0.099	0.011 0.037 0.074 0.122
Brevibacterium flavum fresh simple media (glucose: 70 g/l)	1.68 3.35 5.03 6.7	0.005 0.005 0.005 0.005	0.034 0.051 0.062 0.078	0.011 0.037 0.074 0.122

5.4 BATCH STUDIES OF THE EFFECT OF HYDRODYNAMIC STRESS ON *CORYNEBACTERIUM GLUTAMICUM*

To investigate the effect of hydrodynamic stress on the batch growth of *Corynebacterium glutamicum*, a third batch cultivation was carried out at mild agitation and aeration conditions chosen such that the dissolved oxygen concentration always exceeded 3 mg/l to ensure that bacterial growth was not mass transfer limited. The agitation and aeration conditions are given as a function of time in Table 16. The resultant growth curve was compared with that obtained for the stressed conditions (impeller speed 6.7 m/s and superficial gas velocity 0.005 m/s). Biomass concentration (turbidity and dry mass), growth rate, oxygen utilisation rate, residual glucose concentration and extracellular protein concentration as a function of time are presented in Figures 25, 26 and 27. In Table 17, the specific plate counts are compared.

Table 16 Operation strategy for *Corynebacterium glutamicum* mild batch experiment.

CULTIVATION TIME hr	IMPELLER TIP SPEED m/s	SUPERFICIAL AIR VELOCITY m/s	DO mg/l
0	1.26	0.004	7.52
4	1.26	0.004	5.03
5.5	1.26	0.004	3.36
8	1.68	0.005	3.98
11	2.51	0.006	3.55
12	3.35	0.0062	3.48
13	5.02	0.009	3.87
14.25	5.86	0.01	3.24
26.75	4.19	0.007	7.52

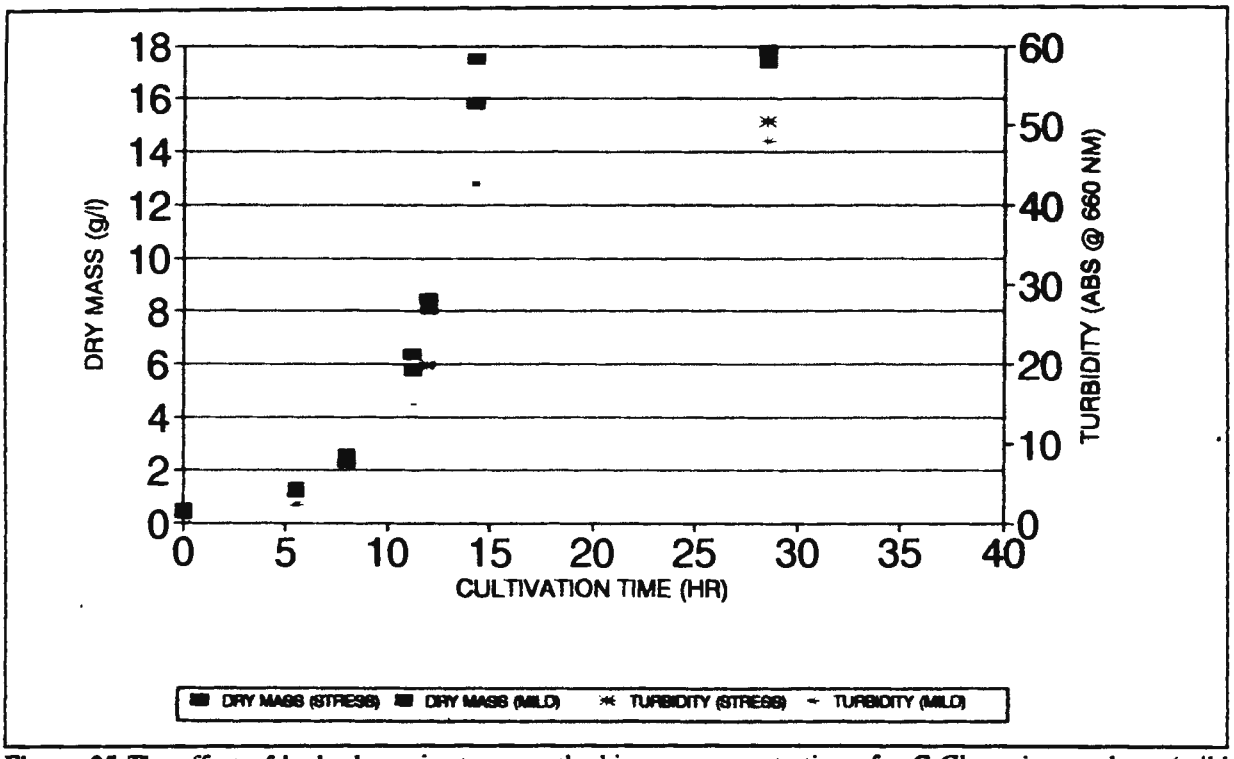

Figure 25 The effect of hydrodynamic stress on the biomass concentration of a *C.Glutamicum* culture (mild conditions in Table 16, stressed conditions at v_{imp} 6.7 m/s and U_{sg} 0.005 m/s).

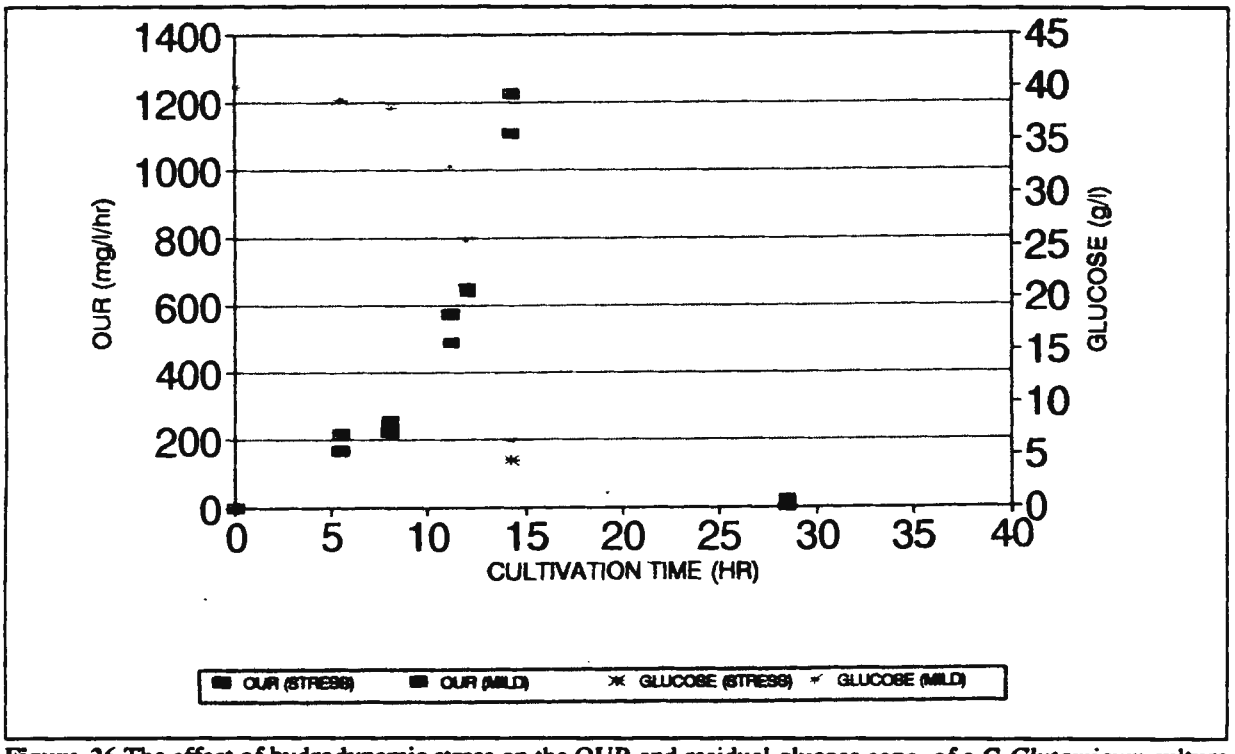

Figure 26 The effect of hydrodynamic stress on the OUR and residual glucose conc. of a *C.Glutamicum* culture (mild conditions in Table 16, stressed conditions at v_{imp} 6.7 m/s and U_{sg} 0.005 m/s).

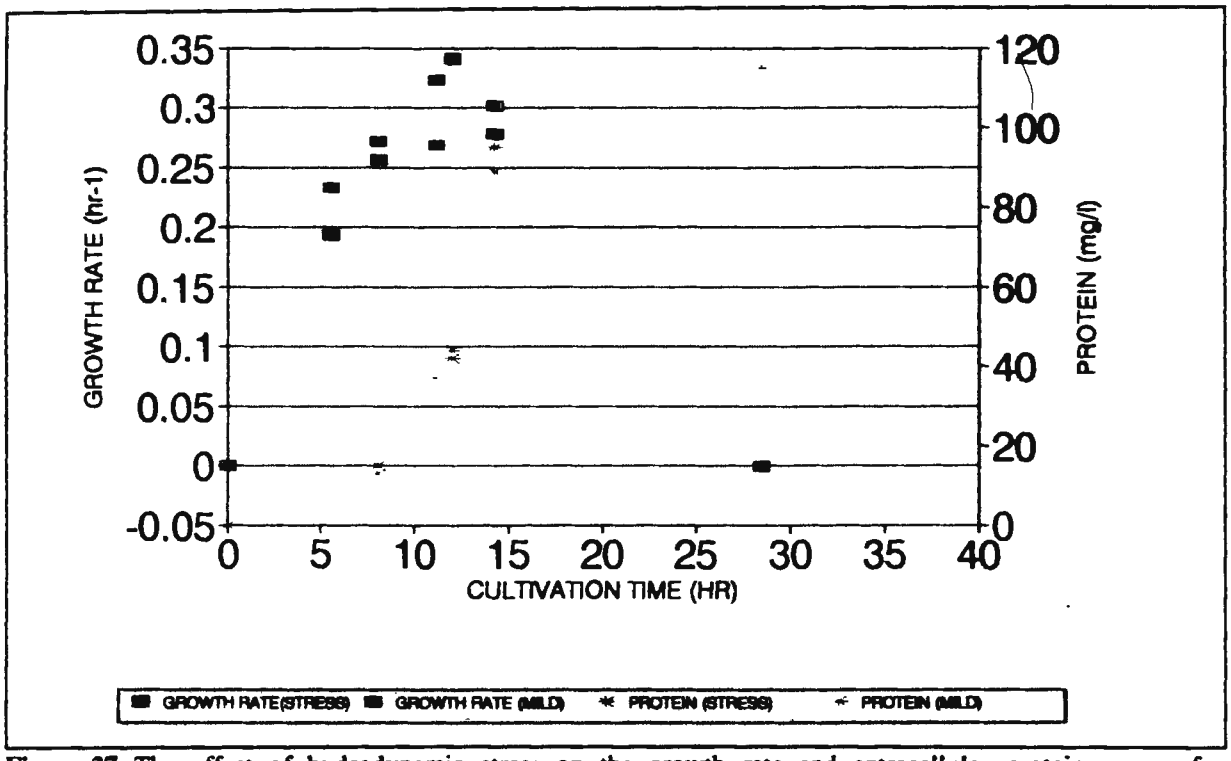

Figure 27 The effect of hydrodynamic stress on the growth rate and extracellular protein conc. of a *C.Glutamicum* culture (mild conditions in Table 16, stressed conditions at v_{tip} 6.7 m/s and U_{sg} 0.005 m/s).

A comparison of the mild and stressed experiments showed no significant differences in the dry biomass concentration, turbidity, extracellular protein concentration, oxygen utilisation rate and residual glucose concentration as a function of time. There was, however, a difference in the specific plate counts. In Table 17, the average specific plate counts of the two stressed batch cultivations are compared with the specific plate counts obtained for the mild batch cultivation. The difference between the specific plate count results was greatest when the difference in hydrodynamic conditions was greatest *i.e.* at the start of the mild cultivation. The variation in the specific plate count results between the mild and stressed conditions was attributed to the breakup of bacterial aggregates. As discussed previously, the degree of bacterial aggregation decreased with cultivation time as shown in Table 17 by the increase in specific plate counts at the stressed conditions.

Table 17 Specific plate counts of *Corynebacterium glutamicum* as a function of hydrodynamic conditions.

	MILD			STRESSED		
CULTIVATION TIME hr	IMPELLER TIP SPEED m/s	U_{sg} m/s	SPECIFIC PLATE COUNT $*10^8$ col/g	IMPELLER TIP SPEED m/s	U_{sg} m/s	AVERAGE SPECIFIC PLATE COUNT $*10^8$ col/g
0	1.26	0.004	0.061	6.7	0.0126	0.165
5.5	1.26	0.004	0.229	"	"	0.647
8	1.68	0.005	0.284	"	"	0.961
12	3.35	0.006	0.780	"	"	0.898
14.25	5.86	0.010	0.800	"	"	1.210

The logistic curve (Equation 83) was fitted to the dry biomass data for the milder agitation and aeration conditions. The results in Table 18, show that there was no significant change in the logistic curve constants under mild and stressed conditions; hence hydrodynamic trauma had no inhibitory effect on the growth of the bacteria.

Table 18 Logistic curve constants for the *Corynebacterium glutamicum* mild and stressed batch growth curves.

BACTERIA	CONDITIONS	B_1 s^{-1}	B_2 l/g	r
Corynebacterium glutamicum	Stressed conditions: impeller speed: 6.7 m/s U_{sg}: 0.013 m/s	0.62 0.62	0.057 0.053	0.92 0.94
	Mild conditions (Table 16)	0.61	0.053	0.87

5.5 THE INVESTIGATION OF HYDRODYNAMIC STRESS IN CONTINUOUS CULTURE

A bacterial cell uses its available resources, such as glucose and oxygen, to divide, produce various products, maintain intracellular functioning and for repair mechanisms. Hydrodynamic trauma may result in changes in the mass flux of these metabolic pathways. At a constant dilution rate in the absence of mass transfer limiting conditions and hydrodynamic trauma effects, changes in the hydrodynamic conditions should have no effect on the growth rate, glucose utilisation rate, oxygen utilisation rate and product formation rate of the cells.

The effect of hydrodynamic trauma on the growth of *Corynebacterium glutamicum* (ATCC 13032) and *Brevibacterium flavum* (NRRL 11475) in continuous culture was investigated. Continuous culture of *Corynebacterium glutamicum* was carried out at dilution rates of 0.360 and 0.100 hr^{-1} in a Chemap stirred tank reactor in the absence of mass transfer limitations. The dilution rates corresponded to cells growing in the early and late exponential phases. *Brevibacterium flavum* were grown at a dilution rate of 0.105 hr^{-1}, also in the absence of mass transfer limitations. Steady states at different agitation and aeration conditions, in the range of impeller speeds from 1.7 - 8.4 m/s and superficial gas velocities of 0.005 to 0.013 m/s, were characterised in terms of dry biomass, turbidity, specific glucose utilisation rate, specific oxygen utilisation rate, supernatant protein concentration, amino acid production, plate counts, particle size analysis by laser light scattering and microscopic observation. The results obtained for *Corynebacterium glutamicum* and *Brevibacterium flavum* are reported in Figures 28-30 and Figures 31-32 respectively. The growth and amino acid yields, Y_{sx} and Y_{px} for the continuous experiments at the various hydrodynamic conditions are presented in Table 19. These indicators of metabolic pathway are given by:

$$Y_{sx} = \frac{dC_s/dt}{dC_x/dt} \tag{84}$$

$$Y_{px} = \frac{dC_p/dt}{dC_x/dt} \tag{85}$$

where C_x is the concentration of cells, C_s is the glucose concentration and C_p is the lysine concentration for *Brevibacterium flavum* culture samples and the glutamic acid concentration for *Corynebacterium glutamicum* culture samples. The HPLC analysis of the amino acid composition of the 0.1 hr^{-1} *Corynebacterium glutamicum* and 0.105 hr^{-1} *Brevibacterium flavum* continuous steady state samples are presented in Table 20.

Microscopic photographs of the steady state (D = 0.36 hr^{-1}) samples of *Corynebacterium glutamicum* aggregates at the different hydrodynamic conditions are presented in Figure 36. The particle size analyses by laser light scattering and specific plate counts of *Corynebacterium glutamicum* and *Brevibacterium flavum* steady state samples at different agitation and aeration conditions are presented in Table 21. The particle size analysis is presented in terms of the average aggregate diameter and the average number of cells per aggregate. The average number of primary cells per aggregate, x, was calculated by assuming that the primary cells making up the aggregate were tightly packed in a cubic structure in the aggregate. The average number of primary cells per aggregate was given by:

$$x = \left(\frac{d_{AGGREGATE}}{d_{eq}}\right)^3 \tag{86}$$

where $d_{AGGREGATE}$ is the diameter of the aggregate and d_{eq} is the equivalent diameter of the primary cells. The elliptical primary cells were approximated as a sphere having an equivalent diameter (d_{eq}) given by:

$$d_{eq} = (l_x \times l_y \times l_z)^{\frac{1}{3}} \tag{87}$$

where l_x, l_y and l_z are the axes of an ellipsoid. The average length of the axes were determined from microscopic analysis as shown in Figures 33 and 34. The dimensions of 100

cells were measured. The averaged results gave dimensions of 1.4, 0.7 and 0.7 μm These dimensions correspond to an equivalent diameter of 0.9 μm. The increase in the number of aggregates at different hydrodynamic conditions relative to the steady state sample at an impeller speed of 1.68 m/s and superficial gas velocity 0.005 m/s was compared in terms of plate counts and laser light scattering for the *Corynebacterium glutamicum* and *Brevibacterium flavum* cultures grown at 0.36 hr^{-1} and 0.105 hr^{-1} respectively in Figure 35.

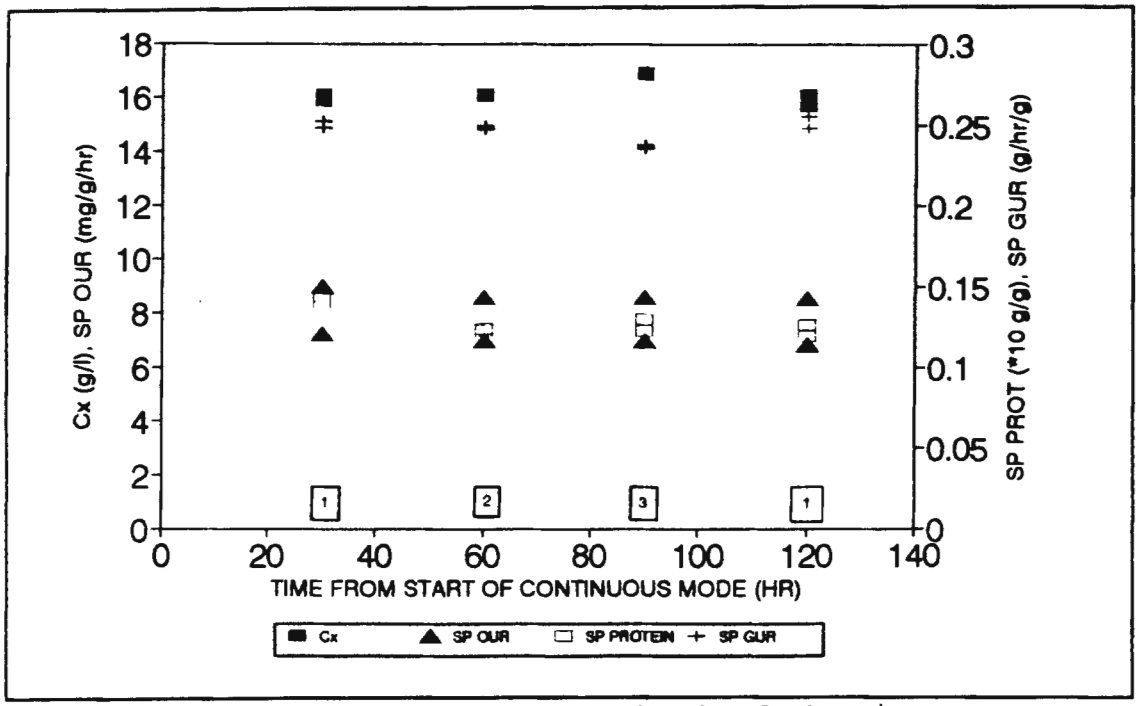

Figure 28 Continuous cultivation of *Corynebacterium glutamicum* D=0.1 hr^{-1}:
[1] v_{imp} 4.7 m/s, U_{sg} 0.005 m/s; [2] v_{imp} 6.81 m/s, U_{sg} 0.01 m/s; [3] v_{imp} 8.4 m/s, U_{sg} 0.013 m/s.

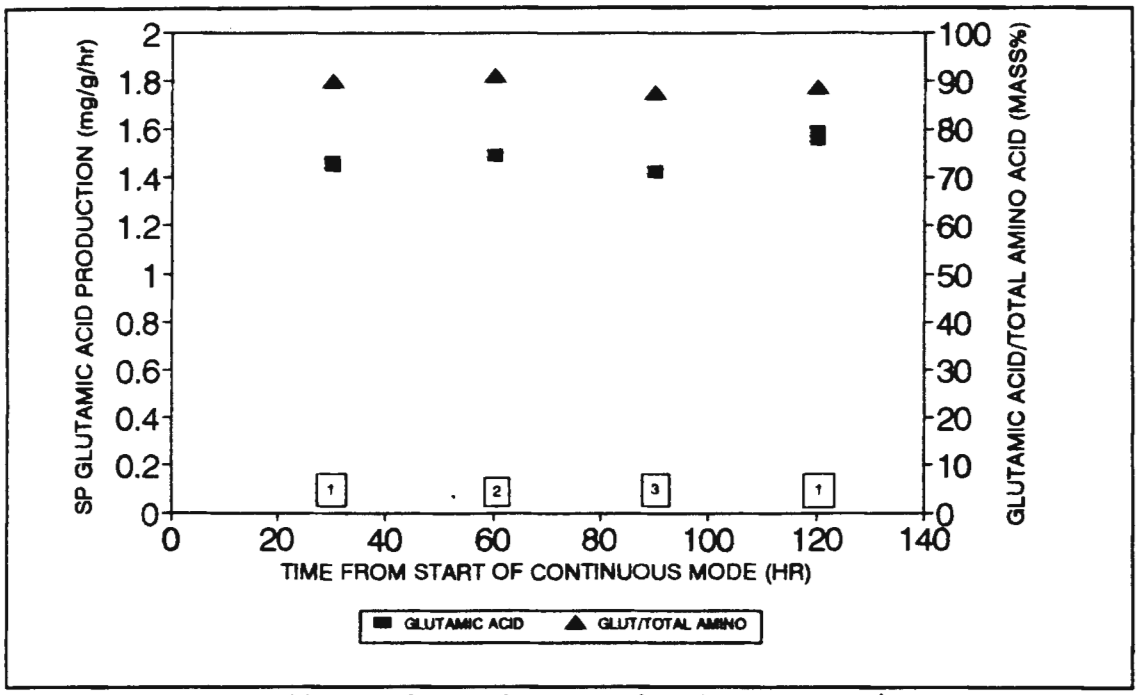

Figure 29 Continuous cultivation of *Corynebacterium glutamicum* D=0.1 hr^{-1}:
[1] v_{imp} 4.7 m/s, U_{sg} 0.005 m/s; [2] v_{imp} 6.81 m/s, U_{sg} 0.01 m/s; [3] v_{imp} 8.4 m/s, U_{sg} 0.013 m/s.

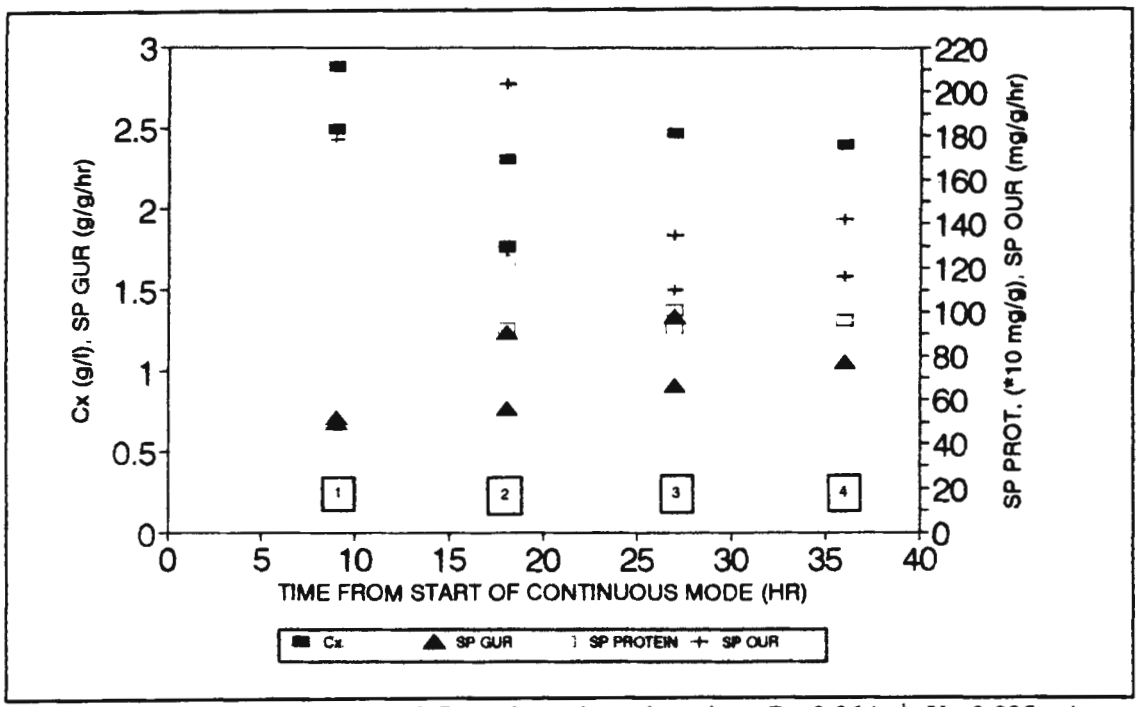

Figure 30 Continuous cultivation of *Corynebacterium glutamicum* D=0.36 hr^{-1}, U_{sg} 0.005 m/s: [1] v_{imp} 5.03 m/s; [2] v_{imp} 6.7 m/s; [3] v_{imp} 1.68 m/s; [4] v_{imp} 3.35 m/s.

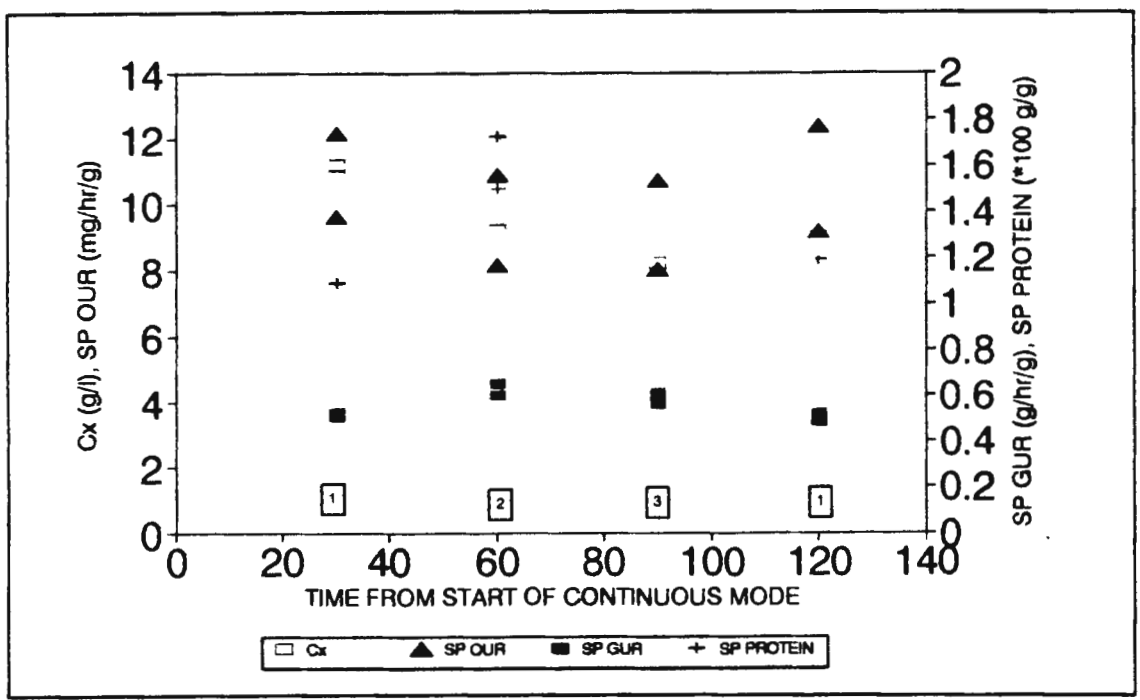

Figure 31 Continuous cultivation of *Brevibacterium flavum* D=0.1 hr^{-1}, U_{sg} 0.005 m/s: [1] v_{imp} 3.35 m/s; [2] v_{imp} 5.03 m/s; [3] v_{imp} 6.7 m/s.

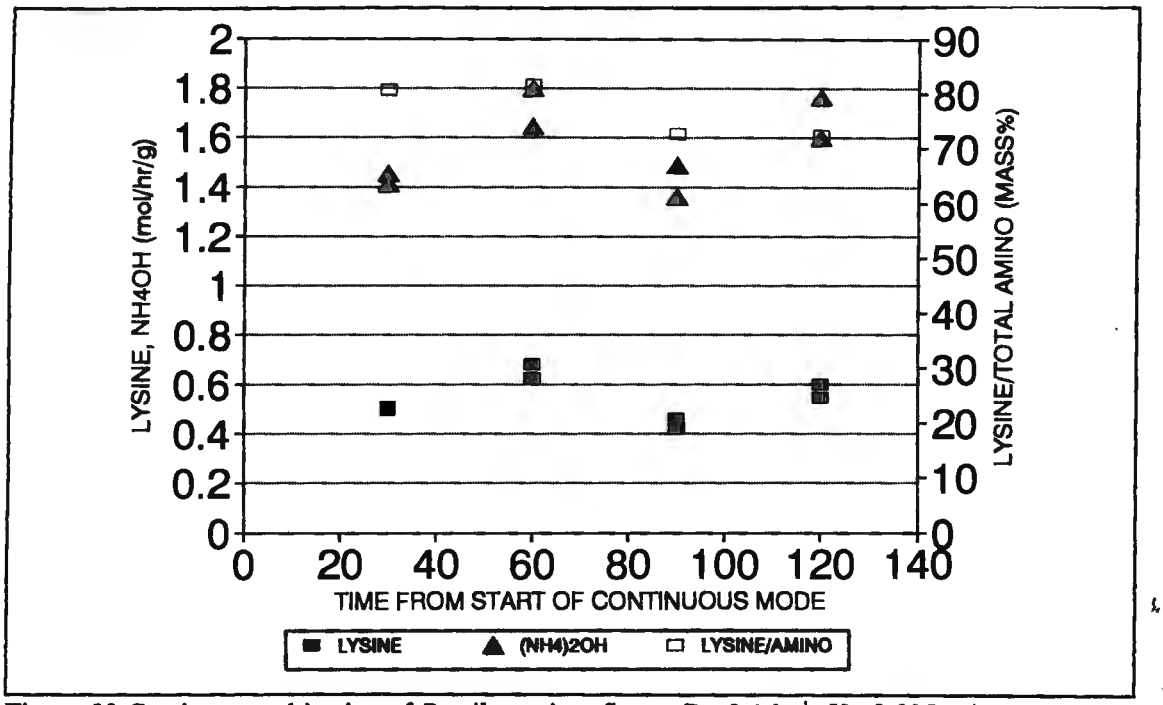

Figure 32 Continuous cultivation of *Brevibacterium flavum* D=0.1 hr^{-1}, U_{sg} 0.005 m/s: [1] v_{imp} 3.35 m/s; [2] v_{imp} 5.03 m/s; [3] v_{imp} 6.7 m/s.

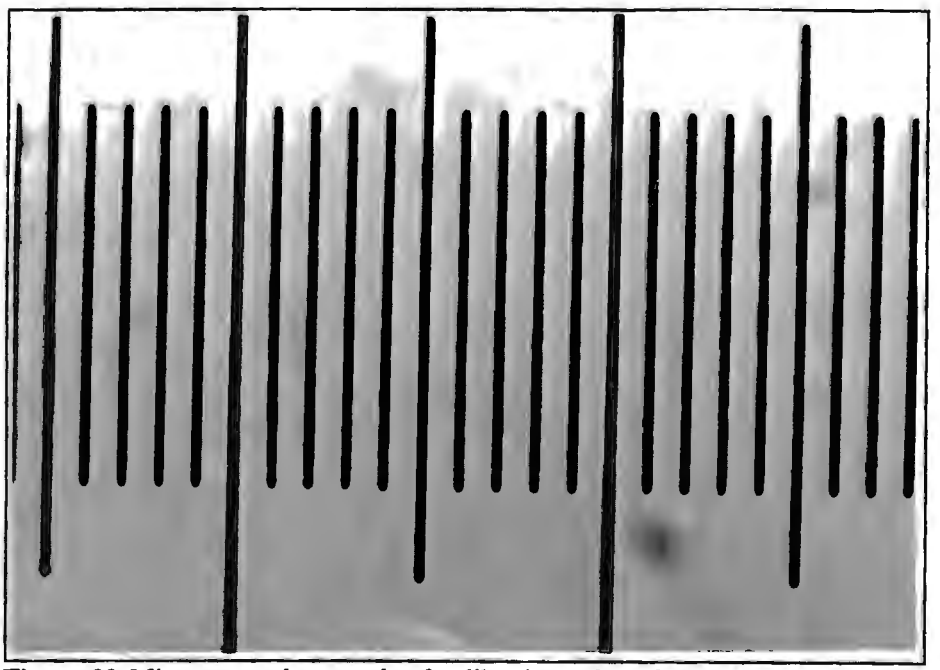

Figure 33 Microscope photograph of calibration ruler where the actual distance between the parallel divisions is 4 μm (100X magnification).

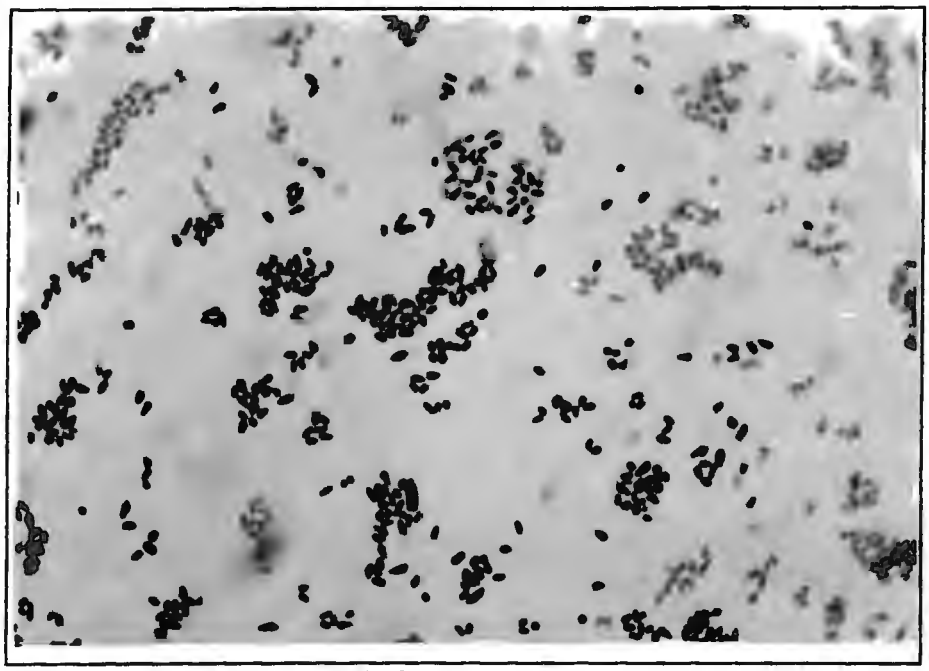

Figure 34 Microscope photograph of *Corynebacterium glutamicum* aggregates grown in complex media in shake flasks for 12 hours (1mm = 1μm).

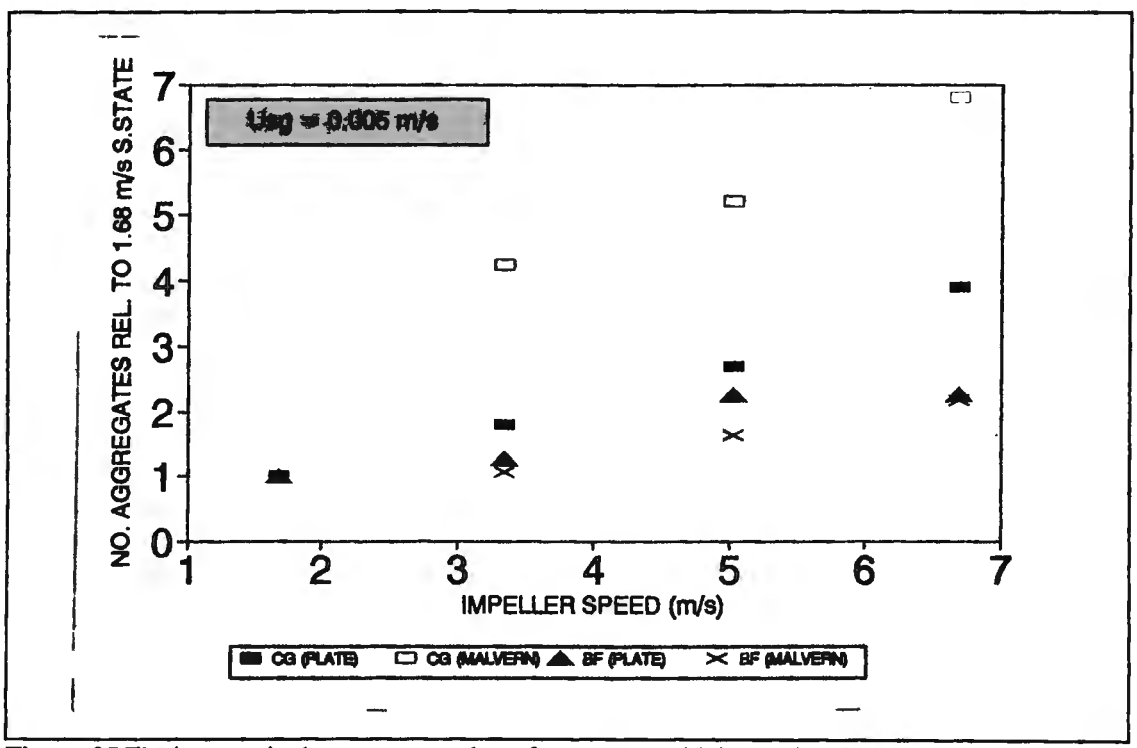

Figure 35 The increase in the average number of aggregates with increasing tip speed relative to culture at a tip speed of 1.68 m/s.
Cultures: *C. glutamicum* at D = 0.36 hr^{-1}, *B. flavum* at D = 0.105 hr^{-1},

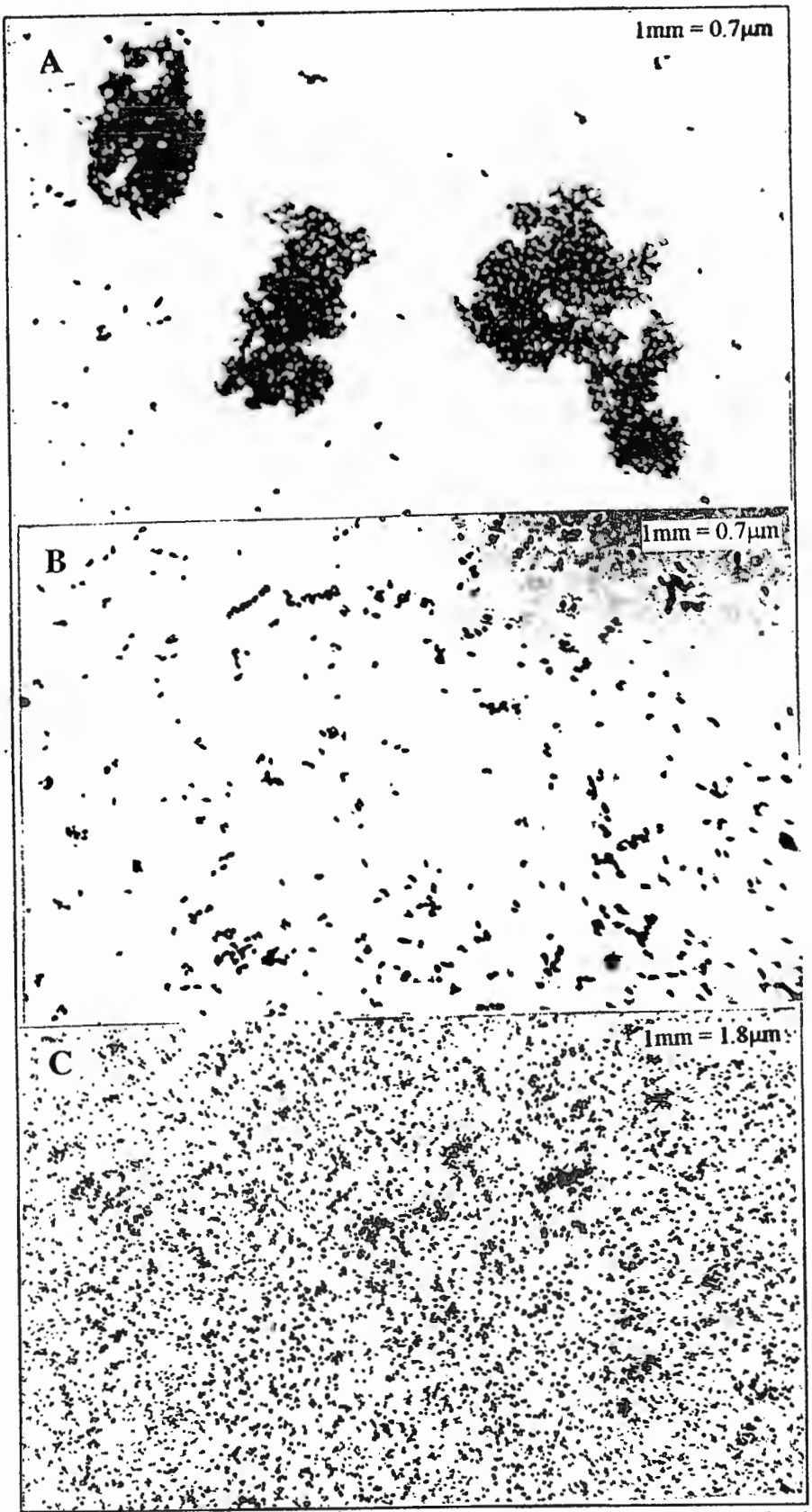

Figure 36 Microscopic photographs of *C. glutamicum* steady states (D = 0.36 hr^{-1}) at U_{sg} 0.005 m/s: [A] v_{imp} 1.68 m/s, [B] v_{imp} 4.6 m/s, [C] v_{imp} 6.7 m/s.

Table 19 Growth and amino acid yields (Y_{xs} and Y_{px}) of *Corynebacterium glutamicum* (glutamic acid) and *Brevibacterium flavum* (lysine) in continuous culture.

BACTERIA	HYDRODYNAMIC CONDITIONS		Y_{xs} g cells per g glucose	Y_{px} g specified amino acid per g cell
	IMPELLER SPEED m/s	U_{sg} m/s		
Corynebacterium glutamicum D = 0.1 hr^{-1}	4.7	0.005	0.40	0.014
	4.7	0.005	0.40	0.016
	6.8	0.01	0.40	0.015
	8.4	0.013	0.42	0.016
Corynebacterium glutamicum D = 0.36 hr^{-1}	1.68	0.005	0.33	
	3.35	0.005	0.34	
	5.03	0.005	0.46	
	6.7	0.005	0.37	
Brevibacterium flavum D = 0.105 hr^{-1}	3.35	0.005	0.20	0.69
	3.35	0.005	0.21	0.8
	5.03	0.005	0.17	0.89
	6.7	0.005	0.18	0.6

Table 20 Specific amino acid composition of *Corynebacterium glutamicum* and *Brevibacterium flavum* steady state samples.

BACTERIA	HYDRODYNAMIC CONDITIONS		DRY MASS g/l	AMINO ACID COMPOSITION (mol %)							
	IMPELLER SPEED m/s	U_{sg} m/s		GLY	ALA	LEU	ILE	VAL	MET	LYS	GLU
Corynebacterium glutamicum D = 0.1 hr^{-1}	4.71	0.005	16.0	15	3						82
	4.71	0.005	15.9	17	3						80
	6.81	0.010	16.1	12	2						86
	8.40	0.013	16.9	18	2						80
Brevibacterium flavum D = 0.105 hr^{-1}	3.35	0.005	11.0	0	13	2	0	7	3	75	
	3.35	0.005	6.6	4	16	3	1	8	5	63	
	5.03	0.005	8.8	1	12	2	0	5	3	77	
	6.70	0.005	8.6	2	16	3	1	8	4	66	

Table 21 Plate count and laser light scattering results for the *Corynebacterium glutamicum* and *Brevibacterium flavum* continuous cultures at different levels of hydrodynamic stress.

BACTERIA AND DILUTION RATE	HYDRODYNAMIC CONDITIONS		SPECIFIC PLATE COUNT colonies/g	MEAN AGGREGATE DIAMETER μm	AVERAGE NUMBER OF PRIMARY CELLS PER AGGREGATE
	IMPELLER TIP SPEED m/s	SUPERFICIAL GAS VELOCITY m/s			
Corynebacterium glutamicum 0.1 hr^{-1}	4.71	0.005	9.5		
	4.71	0.005	9.4		
	5.76	0.007	10.6		
	6.81	0.009	12.8		
	8.38	0.013	13.1		
Corynebacterium glutamicum 0.36 hr^{-1}	1.68	0.005	2.8	3.3	49
	3.35	0.005	5.04	2.26	16
	5.03	0.005	7.43	1.99	11
	6.7	0.005	10.6	1.75	7
Brevibacterium flavum 0.105 hr^{-1}	1.68	0.005	1.6	2.74	
	3.35	0.005	2.04	2.87	
	3.35	0.005	2.3	2.39	
	5.03	0.005	3.61	1.99	
	6.7	0.005	3.63	1.69	

The dry biomass, specific oxygen utilisation rate, specific glucose utilisation rate (Figures 28, 30, 31), specific lysine production for *Brevibacterium flavum* (Figure 32) and specific glutamic acid production for *Corynebacterium glutamicum* (Figure 29) and supernatant protein concentration (Figures 28, 30, 31) were independent of hydrodynamic conditions. This was validated up to an impeller tip speed of 8.38 m/s and a superficial gas velocity of 0.013 m/s (average energy dissipation rate 76 m^2/s^3) for the 0.100 hr^{-1} *Corynebacterium glutamicum* cultivation, and up to impeller tip speeds of 6.7 m/s and a superficial gas velocity of 0.005 m/s (average energy dissipation rate of 47.5 m^2/s^3) for the *Corynebacterium glutamicum* and *Brevibacterium flavum* at dilution rates of 0.360 hr^{-1} and 0.105 hr^{-1} respectively. No trend was observed between the growth and product yields and hydrodynamic conditions in the stirred tank reactor as shown in Table 19. Analysis of the

amino acid composition of culture samples showed that there was no change in the spectra of amino acids produced at increased levels of hydrodynamic stress.

Microscopic observations showed that the breakup of bacterial aggregates increased with increasing hydrodynamic conditions. The breakup of *Corynebacterium glutamicum* aggregates grown at a dilution rate of 0.36 hr^{-1} may be observed in Figure 36. The aggregate diameter decreased with increasing energy dissipation rates.

In Table 21, an increase in the number of colonies per gram dry mass is seen with increasing trauma (specific plate count). This increase was due to the breakup of agglomerates (Figure 36). A comparison of the aggregate number determined by plate count and laser light scattering is given for *Corynebacterium glutamicum* in continuous culture at a dilution rate of 0.36 hr^{-1} . The increase in the number of agglomerates relative to the 1.68 m/s steady state according to the laser light scattering was twice that according to the specific plate counts. It is postulated that the exposure to hydrodynamic stress mediated a loss in the ability of *Corynebacterium glutamicum* to divide on solid media. The ratio of plate counts to total particle counts was however independent of hydrodynamic conditions. However no effect on the viability of the cells in liquid media was observed as shown by the unchanging dry biomass results in Figure 30. For the steady state culture of *Brevibacterium flavum*, the particle count determined by laser light scattering and specific plate counts showed reasonable agreement. The cells therefore did not lose their ability to divide on solid media. The extent of *Corynebacterium glutamicum* aggregate breakup was greater than that of *Brevibacterium flavum*.

5.6 THE NATURE OF INTERCELLULAR FORCES IN *CORYNEBACTERIUM GLUTAMICUM* AGGREGATES

Cells may form aggregates due to a number of phenomena. The adhesive effect of intracellular organic material may cause cells to clump together. If the cells possess an electrostatic charge (usually negative), a chelating agent such as Ca^{2+} may form salt bridges between the charged particles. Agglomeration may also be due to the hydrophobicity of the

cells. The nature of the intra-cellular forces resulting in the formation of *Corynebacterium glutamicum* aggregates was investigated.

Zeta potential measurements and particle size analysis by laser light scattering of *Corynebacterium glutamicum* aggregates as a function of pH over the range pH 2.5 to 8 are reported in Figure 37. The effect of the addition of EDTA and Ca^{2+} ions on the aggregate size distribution of disrupted *Corynebacterium glutamicum* aggregates was investigated (Table 22). If the negatively charged bacteria were held together by metal cations, the addition of EDTA to the disrupted aggregates would result in the chelation of the cations by EDTA. Subsequent addition of excess Ca^{2+} (relative to free EDTA molecules) should result in the chelation of the bacteria. The aggregates were broken up by subjecting cells grown up in a shake flask to the hydrodynamic forces in the flow loop apparatus. The cells were pumped through a 0.8mm capillary at a flow rate of 3.93×10^{-6} m^3/s for 35 minutes. These conditions corresponded to an average energy dissipation rate of 5030 m^2/s^3 (Zhang *et al.*, 1993).

The zeta potential measurements (Figure 37) show that the bacteria have a strong negative charge at the neutral pH of culture conditions. The point of zero charge occurred at pH 3. No change in the aggregate size was observed in the pH range 3 to 8. The hydrophobic aggregation of neutral particles can therefore be discounted as an adhesive mechanism. No change in the aggregate size distribution of the disrupted bacterial aggregates was observed (Table 22) with the addition of EDTA and the subsequent addition of excess Ca^{2+} cations. The addition of Ca^{2+} to the disrupted aggregates did not accelerate the reaggregation of the bacteria in the shake flask. Cell clumping is therefore not a result of the electrostatic interaction of a chelating agent with the negatively charged cells. The disrupted bacterial aggregates did not reaggregate 1 hour after being transferred into shake flasks (Table 22). Reaggregation of the cells occurred after 1 day on growth in shake flasks in complex media. It has therefore been postulated that cells produce a growth-associated biomolecular adhesive which is responsible for the formation of aggregates.

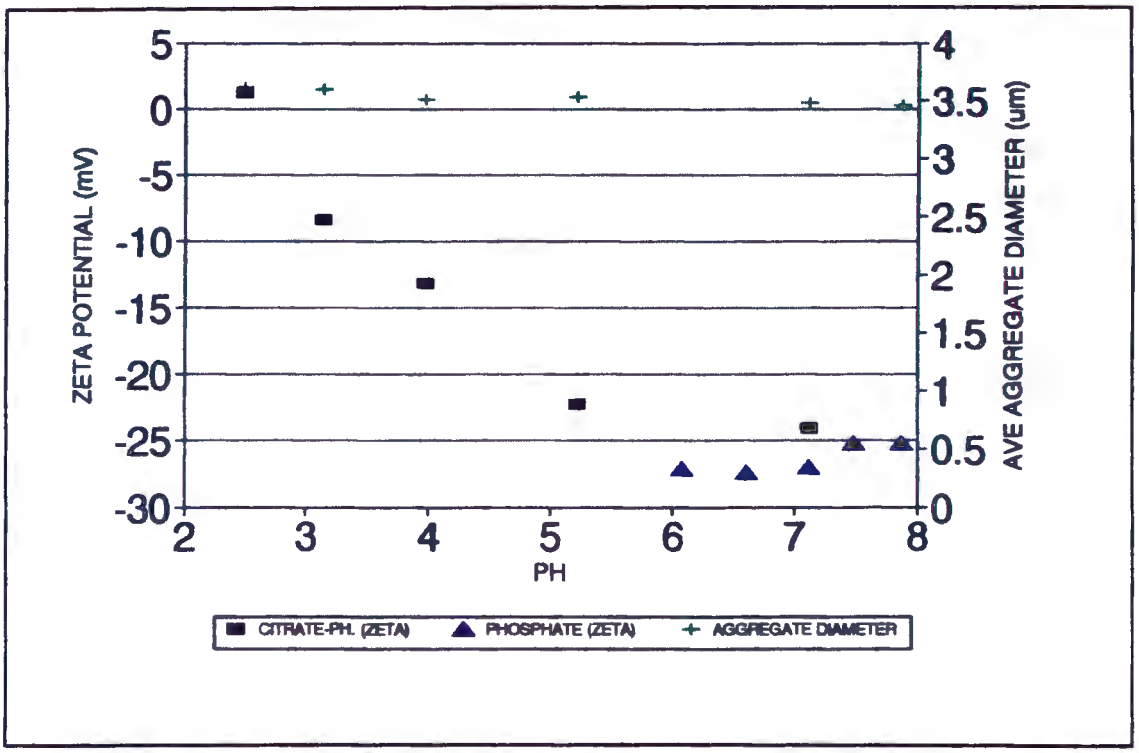

Figure 37 The zeta potential and diameter of *Corynebacterium glutamicum* aggregates suspended in 0.05 M citrate phosphate and 0.05 M phosphate buffer as a function of pH.

Table 22 The effect of the addition of EDTA and Ca^{2+} ions on the reaggregation of disrupted *Corynebacterium glutamicum* aggregates.

EXPERIMENT	PARTICLE DIAMETER μm
Control	3.61
Immediately after flowloop	1.99
1 hour in shake flask after flowloop	1.99
1 day in shake flask after flowloop	3.6
1 hour in shake flask after flowloop and EDTA addition	1.99
1 hour in shake flask after flowloop and EDTA + subsequent $CaCl_2$ addition	1.99
1 hour in shake flask after flowloop and $CaCl_2$ addition	2

5.7 CONCLUSIONS

Based on the findings in this chapter the following conclusions can be drawn:

5.7.1 Biomass formation in batch culture of *Corynebacterium glutamicum* and *Brevibacterium flavum* can be modelled by the logistic equation. The viability, rate of metabolism, metabolic pathway, lysis and morphology results for the *Corynebacterium glutamicum* batch experiment were reproducible. Microscopic observation showed that both types of bacteria form aggregates. The *Corynebacterium glutamicum* batch experiment showed that there were significant morphological changes as a function of physiological status. Early exponential phase cells were more clumped than late exponential phase cells.

5.7.2 The mass transfer potential of the Chemap stirred tank reactor exceeded the maximum oxygen requirements of batch culture *Corynebacterium glutamicum* and *Brevibacterium flavum* at the following conditions: initial glucose concentration 20g/l, impeller tip speed 4.71, air flowrate 10.3 l/min (2.9 vvm) for *Corynebacterium glutamicum* and initial glucose concentration 70 g/l, impeller tip speed 3.35 m/s, air flowrate 9.5 l/min (2.7 vvm) for *Brevibacterium flavum*. These operating conditions were therefore set as the lower limit in the continuous experiments to prevent mass transfer limitation. The following factors affected the mass transfer potential of the bioreactors: viscosity, salinity, addition of antifoam, agitation and aeration conditions.

5.7.3 A comparison of the *Corynebacterium glutamicum* batch experiments performed at mild and stressed conditions showed that there were no significant differences in the viability, integrity, rates of growth and rates of metabolism. There were, however, differences in the specific plate counts (cells/g biomass) which were directly attributed to the breakup of agglomerates at stressed conditions.

5.7.4 Hydrodynamic stress had no effect on the lysis, viability, rate of growth, rate of metabolism, and spectra of amino acids produced in the *Corynebacterium*

glutamicum (ATCC 13032) and *Brevibacterium flavum* (NRRL 11475) in continuous culture stress experiments. Glutamic acid and lysine were the principle amino acids produced by *Corynebacterium glutamicum* and *Brevibacterium flavum* respectively. The most extreme hydrodynamic conditions investigated corresponded to average energy dissipation rates of 76 m^2/s^3 for *Corynebacterium glutamicum* at a dilution rate of 0.1 hr^{-1} and 47.5 m^2/s^3 for *Corynebacterium glutamicum* at a dilution rate of 0.36 hr^{-1} and *Brevibacterium flavum* at a dilution rate of 0.105 hr^{-1}. This result was contrary to the work of Toma *et al.* (1991). In a geometrically similar stirred tank reactor, Toma *et al.* (1991) reported the sucrose uptake rate, oxygen utilisation rate and specific growth rate of *Brevibacterium flavum* (22LD) to decrease at hydrodynamic conditions corresponding to an average energy dissipation rate in excess of 10 m^2/s^3. This difference was attributed to the different strains of *Brevibacterium flavum* used in the experiments.

5.7.5 The breakup of cell aggregates was observed with increasing agitation and aeration in the continuous experiments. The extent of aggregate breakup was dependent on the intensity of the hydrodynamic conditions as well as the species of bacteria. *Corynebacterium glutamicum* were more susceptible to aggregate breakup than *Brevibacterium flavum*. Hydrodynamic stress appeared to mediate a loss in the ability of *Corynebacterium glutamicum* to divide on solid media. *Brevibacterium flavum* cells did not display this phenomenon.

5.7.6 It was shown that aggregation of *Corynebacterium glutamicum* was not a result of the electrostatic interaction of a chelating agent with the negatively charged cells. Hydrophobic interaction of neutral particles was also discounted as a mechanism of inter-cell adhesion as the degree of cell aggregation was independent of the charge of the cells. It was postulated that cells produce a growth-associated biomolecular adhesive which is responsible for the formation of aggregates.

6. THE KINETICS AND MECHANISM OF AGGREGATE BREAKUP

6.1 INTRODUCTION

The continuous and batch *Corynebacterium glutamicum* growth experiments showed that the turbulent forces associated with high levels of agitation and aeration in a stirred tank reactor exerted forces on cell aggregates and resulted in their breakup. Literature findings have indicated that the inhibition of microbial growth in stirred tank reactors may be due to the separate or combined effects of the interaction of cells with similarly sized turbulent eddies in the impeller discharge zone and with breaking air bubbles at the air medium interface (Section 2.6). In this section, the kinetics and predominant mechanism of breakup of *Corynebacterium glutamicum* resulting from in the absence of bubbles has been investigated in a stirred tank reactor and a capillary flow loop system. A model is presented to describe the rate of aggregate breakup in bubble free systems. The applicability of the model to other microbial systems has been sought.

6.2 MODEL DEVELOPMENT

It is generally postulated that eddies larger than the microbial particle will entrain it. Where the density of the particle and surrounding media are similar (as found for microbial systems), there will be little relative motion. Eddies much smaller than the particle have insufficient energy to cause significant breakup. Eddies whose size approaches the particle diameter impart the maximum hydrodynamic force (van Suijdam and Metz, 1981). Studies on particle breakage in turbulent flow suggest that the ratio of the particle size to the Kolmogorov microscale of turbulence (d/λ) is a key parameter in determining the mechanism of breakage (Parker *et al.*, 1972, Matsuo and Unno, 1981; Moreira *et al.*, 1995). These studies were performed on activated sludge, clay and animal cell aggregates respectively. The size of the smallest energy-containing eddies λ (Kolmogorov microscale of turbulence) is

given by:

$$\lambda = \left(\frac{\nu^3}{e}\right)^{\frac{1}{4}} \quad (88)$$

where ν is the kinematic viscosity and e is the energy dissipation rate of turbulence per unit mass. Following the approach of Matsuo and Unno (1981), where d/λ is less than 9, breakage is caused by eddies in the viscous dissipation subrange (Section 2.6.1). Shear stresses due to fluctuating velocities on opposite sides of the aggregate predominate. When the aggregate size, d, is greater than 9λ, breakage is commonly due to the interaction of aggregates with eddies in the inertial convection subrange and the resultant dynamic pressure fluctuations on the aggregate surface (Matsuo and Unno, 1981).

The turbulence in stirred tanks is highly inhomogeneous with maximum fluid velocities occurring in the impeller zone. The reported ratio of the mean energy dissipation rate in the impeller zone to the overall mean energy dissipation rate for standard stirred tank reactors vary from 13 (Wu and Patterson, 1989) through 15.6 (Okomoto *et al*, 1981) to 20 (Cutter, 1966). Wu and Patterson (1989) measured a ratio of maximum and mean energy dissipation rates of 23.5 at a distance of 2 blade widths from the blade tip. Measurement of the local energy dissipation rate in the Chemap stirred tank reactor system used in these experiments gave a ratio of maximum and average energy dissipation rate of 25 (Table 10 in Section 4.2.1). It is therefore reasonable to assume that, in the absence of bubbles, the breakup of particles occurs mainly in the impeller zone, characterised by high energy dissipation rates.

Typical values of the Kolmogorov microscale in the impeller zone of a 5 liter Chemap (Table 9 in Section 4.2.1) and 100 m^3 stirred tank (Einsele, 1978) are 5 μm and 16 μm respectively. Hence for bacteria, unicellular yeasts and *Corynebacterium glutamicum* aggregates (< 10 μm), stresses due to shear forces are significant. For isotropic homogenous turbulence, the viscous force, $F_{VISCOUS}$, acting on a particle of size d where d is less than 9λ, is given by (Matsuo and Unno, 1981):

$$F_{VISCOUS} = 2\mu \left(\frac{2}{15}\right)^{\frac{1}{2}} \left(\frac{e}{\nu}\right)^{\frac{1}{2}} d^2 \quad (89)$$

where μ is the viscosity of the suspension.

The frequency with which a particle of size d would encounter an eddy of size d in the viscous dissipation subrange is given by the frequency of the eddy formation (Levich, 1962),

$$f(d) = \frac{1}{\sqrt{15}} \left(\frac{e}{\nu}\right)^{\frac{1}{2}} \quad (90)$$

Parker *et al.* (1972) assumed that the rate of disruption of protein aggregates in a turbulent flow field was equal to the product of the number concentration of the aggregates, the frequency of disruption of the aggregates by the instantaneous turbulent stresses and the number of primary particles eroded per disruption.

$$R_D = no\ conc.\ aggregates \times \frac{freq\ of\ disruption}{of\ aggregates} \times \frac{no\ 1°particles}{eroded\ per\ disruption} \quad (91)$$

The breakup of *Corynebacterium glutamicum* aggregates in a bioreactor in the absence of a gaseous phase can be modelled by applying the theory developed by Parker *et al.* (1972), Brown and Glatz (1987) and Ayazi Shamlou *et al.* (1990). A comparison of the maximum aggregate diameter (7 μm) and the capillary Kolmogorov eddy microscale (1.6 μm) for the most extreme conditions generated in the flowloop at a flow rate 4.9×10^{-6} m^3/s (Table 11 in Section 4.2.2), shows that the maximum ratio of d/λ in this study is 4.4 *i.e.* d/λ does not exceed 9. Hence viscous forces are expected to predominate.

The number concentration of spherical and uniform aggregates, n_F, can be assumed to be proportional to C_V/d_F^3 where C_V is the volume concentration of aggregates and d_F is the aggregate diameter. The number of primary particles eroded per disruption, n_p, is assumed proportional to the total number of particles in the outside layer of the aggregate, $(d_F/d_p)^2$. The size of the primary particles, d_p, may be assumed to be constant and the size of the aggregates equated to the maximum aggregate size, $(d_F)_{MAX}$. The maximum aggregate size can be determined from a force balance between the instantaneous turbulent forces and the mechanical strength of the aggregate. For the viscous dissipation subrange (Matsuo and Unno, 1981):

$$\sigma_{AGGREGATE}\,(d_F)_{MAX} \propto 2\mu \sqrt{\frac{2}{15}}\,(\frac{e}{\nu})^{\frac{1}{2}}\,(d_F)_{MAX}^{\,2} \tag{92}$$

where $\sigma_{AGGREGATE}$ is the specific aggregate strength in N/m. Therefore

$$(d_F)_{MAX} \propto \frac{\sigma_{AGGREGATE}}{\mu}\,(e/\nu)^{-\frac{1}{2}} \tag{93}$$

Hence, based on Equation 91, the rate of disruption of aggregates of bacteria is given by,

$$R_D \propto \frac{C_V}{d_F^{\,3}} \times \frac{1}{\sqrt{15}}\,(\frac{e}{\nu})^{\frac{1}{2}} \times (\frac{D_F}{d_p})^{2} \tag{94}$$

Substituting $(d_F)_{MAX}$ for d_F from Equation 93 gives,

$$R_D = \frac{dC_V}{dN} = B_3\,\frac{\mu}{\sigma_{AGGREGATE}\,d_p^{\,2}}\,(\frac{e}{\nu})\,C_V \tag{95}$$

Equation 95 indicates that the rate of aggregate disruption by eddies in the viscous dissipation subrange will have a first order dependency on the rate of energy dissipation.

If inertial forces predominate, the rate of aggregate disruption will also have a first order dependency with respect to the rate of energy dissipation. The frequency with which a particle of size d would encounter an eddy of size d, which falls in the inertial convection subrange is given by (Levich, 1962),

$$f(d) = 1.57\,e^{\frac{1}{3}}\,d^{-\frac{2}{3}} \tag{96}$$

According to Matsuo and Unno, the inertial force acting on a particle is,

$$F_{INERTIAL} = \rho\,\overline{u}^2(d)\,d^2 \tag{97}$$

where $u(d)$ is the difference in velocity between two points a distance d apart and is given by:

The size of the aggregate d_F can be equated to the maximum aggregate size $(d_F)_{MAX}$. A force

$$\bar{u}(d) = 1.57\, e^{\frac{1}{3}}\, d^{\frac{1}{3}} \tag{98}$$

balance between the mechanical strength of the aggregate and the inertial force gives the following relation for the maximum aggregate diameter:

$$(d_F)_{MAX} \propto \left(\frac{\sigma_{AGGREGATE}}{\rho\ 1.57^2}\ e^{-\frac{2}{3}}\right)^{\frac{3}{5}} \tag{99}$$

Based on Equations 91, 96 and 99, the rate of aggregate disruption by eddies in the inertial convection subrange is therefore given by,

$$R_D = \frac{dC_V}{dN} = B_4\ \frac{\mu}{\sigma_{AGGREGATE}\ d_p^2}\ \left(\frac{e}{\nu}\right)\ C_V \tag{100}$$

To model the interaction of viscous forces with microorganisms and subsequent cell death, it may be assumed that the rate of cell disruption is proportional to the frequency of the force event, the fraction of undisrupted cells and the ratio between the disruptive force and the strength of the cells.

$$R_D = \textit{fraction of intact cells} \times \textit{frequency of the force event} \times \frac{\textit{disruptive force}}{\textit{strength of the cells}} \tag{101}$$

$$R_D = C_V \times \frac{1}{\sqrt{15}}\ \left(\frac{e}{\nu}\right)^{\frac{1}{2}} \times \frac{2\mu \sqrt{\frac{2}{15}}\ \left(\frac{e}{\nu}\right)^{\frac{1}{2}}\ d_C^2}{\sigma_{CELL}\ d_C} \tag{102}$$

where C_V is the volume concentration of intact cells, σ_{CELL} is the specific cell strength and d_C is the cell diameter. Hence a similar relationship to Equation 95 is obtained:

$$\frac{dC_V}{dN} = B_5\ \frac{\mu}{\sigma_{CELL}\ d_C^2}\ \left(\frac{e}{\nu}\right)\ C_V \tag{103}$$

The strength of the cells is a function of cell size (d_C), cell envelope thickness (δ) and composition (x). For mammalian cells, the cell membrane thickness and composition are the effective cell envelope parameters. For bacteria, the cell wall thickness and composition are the controlling envelope parameters. The probability of cell death increases with time as the total duration of the hostile events increases. It has been reported that fatigue effects may exist *i.e.* the cell wall or membrane strength may decrease with exposure time due to gradual weakening of its structure. Based on experimental findings, Al-Rubeai *et al.* (1995) postulated that sublytic levels of hydrodynamic stress initially invoked repair mechanisms in hybridoma cells, but ultimately caused the induction of apoptosis ("active cell suicide"). The result is cytoskeletal collapse and a sudden decrease in the strength of the cells. Exposure to forces to which the cell was previously resistant, now results in its complete destruction. It was also postulated that, at extreme conditions of hydrodynamic stress, cells died suddenly from the passive process of necrosis. Let it be assumed that the specific cell strength is not constant, but a function of time and hydrodynamic conditions:

$$\sigma_{CELL} = f(d_C,\delta,\chi)\ (eN)^{-y} \tag{104}$$

where y is the fatigue exponent and N is the number of passes through the region of extreme hydrodynamic stress. The rate of cell death is therefore given by:

$$\frac{dC_V}{dN} = B_5 \frac{\mu}{f(d_C,\delta,\chi)\ d_C^2} (eN)^y \left(\frac{e}{\nu}\right) C_V \tag{105}$$

Based on the development of Equation 100, the rate of cell death due to the interaction of microorganisms with inertial forces can be described by:

$$\frac{dC_V}{dN} = B_6 \frac{\mu}{f(d_C,\delta,\chi)\ d_C^2} (eN)^y \left(\frac{e}{\nu}\right) C_V \tag{106}$$

6.3 KINETICS AND MECHANISM OF THE BREAKUP OF *CORYNEBACTERIUM GLUTAMICUM* AGGREGATES

6.3.1 Experimental procedure

On cultivation of *Corynebacterium glutamicum* in continuous culture under different levels of agitation and aeration, it has been shown that the metabolism, viability and integrity of the microorganisms were insensitive to hydrodynamic forces in the stirred tank (Section 5.5). However morphological changes were observed in the form of variation in the aggregation of the bacteria. To further understand the effect of hydrodynamic forces on aggregation, studies were performed in which *Corynebacterium glutamicum* was grown continuously at a dilution rate of 0.36 hr^{-1} under mild agitation conditions (impeller tip speed of 1.68 m/s and a U_{sg} of 0.005 m/s). The resultant culture was subjected to more extreme conditions in the 7.3 liter stirred tank reactors and in the capillary flowloop system. Experiments in the 7.3 liter stirred tank reactor and capillary flow system were carried out in the absence of a gaseous phase. The stirred tank reactor was agitated at impeller speeds of 3.35, 4.6 and 6.7 m/s for periods of up to 150 minutes. The capillary flow loop system was operated at flow rates of 3.93×10^{-6} and 4.93×10^{-6} m^3/s for 120 minutes. Samples were taken at regular time intervals and analysed in terms of dry biomass, specific plate counts, particle size analysis by laser light scattering and photographic observation.

6.3.2 Verification of metabolic response in flowloop

To verify that the metabolism of the microorganisms was not inhibited at the more extreme forces in the flowloop system, samples in the flowloop were analysed in terms of biomass concentration, specific plate counts, oxygen utilisation rate and protein concentration. Samples were analysed at the start of the experiment (zero sample) and after 120 minutes exposure to flow in the capillary system (experiment: 120 min sample) and after 120 minutes in the control flask (control: 120 min sample). The results are presented in Table 23. These show that the hydrodynamic stress in the flowloop system has no effect on the growth, metabolism and integrity of the microorganisms.

Table 23 The response of *Corynebacterium glutamicum* to hydrodynamic forces in the flowloop system (CV is the coefficient of variance).

	SAMPLE	DRY MASS MEAN (CV/MEAN%) g/l	SPECIFIC OXYGEN UTILISATION RATE MEAN (CV/MEAN%) mg/g/hr	SPECIFIC PROTEIN mg/g	SPECIFIC PLATE COUNT 1×10^8 colonies/g
FLOWLOOP $Q=3.93X10^{-6}$ m^3/s	zero control:120 min experiment:120 min	1.98 (7%) 2.16 (0%) 2.02 (7%)	161 (7%) 161 (0%) 173 (3%)	6.7 (10%) 5.9 (3%) 7.0 (3%)	4.7 (9%) 6.3 (7%) 7.6 (2%)
FLOWLOOP $Q=4.93X10^{-6}$ m^3/s	zero control:120 min experiment:120 min	1.78 (6%) 1.87 (9%) 2.07 (3%)	101 (6%) 90 (9%) 85 (4%)	7.5 (19%) 6.7 (13%) 6.5 (6%)	4.3 (15%) 4.15 (4%) 10.3 (13%)

6.3.3 Mechanism of aggregate breakup

Micrographs of *Corynebacterium glutamicum* aggregates agitated in the 7.3 liter Chemap stirred tank reactor at an impeller tip speed of 4.6 m/s in the absence of a gaseous phase are shown as a function of time in Figure 38. Particle size analysis of the aggregates as a function of time is shown in Figure 39. The average particle diameter and relative number of aggregates as a function of time are given in Table 24. The average aggregate diameter and the average number of primary cells per aggregate decreased with increasing number of circulations through the reactor. Figures 38A and 38B show that during the initial 30 minutes of exposure to flow in the reactor, irregular corners are eroded off the main aggregate forming a smoother aggregate. The size distribution B in Figure 39 shows two peaks: one corresponding to the smooth large aggregate, the other to the single cells that have been eroded off. After 60 minutes in the reactor, intermediate sized aggregates (diameters 1.31 to 1.75 μm corresponding to aggregates consisting of 3 to 7 primary cells) appear in the size distribution C in Figure 39, which is shifting towards a monomodal distribution. These aggregates are proposed to originate from the reaggregation of primary particles as the change in size distribution is accompanied by a decrease in the total number of particles (Table 24). Further exposure to turbulent forces resulted in a steady increase in the fraction

of primary particles due to surface erosion as seen in size distribution D (corresponding in Figure 39. Figures 38C and 38D, show an increase in the number of primary particles and a decrease in the maximum aggregate size with time. In Figure 38C, the intermediate sized material may be seen.

Table 24 Summary of the particle size analysis of *Corynebacterium glutamicum* aggregates in the stirred tank reactor at an impeller speed of 4.6 m/s.

TIME OF EXPOSURE min	AVERAGE PARTICLE DIAMETER μm	INCREASE IN NUMBER OF AGGREGATES RELATIVE TO ZERO SAMPLE %
0	2.75	0
30	1.93	260
60	2.08	136
140	1.99	168

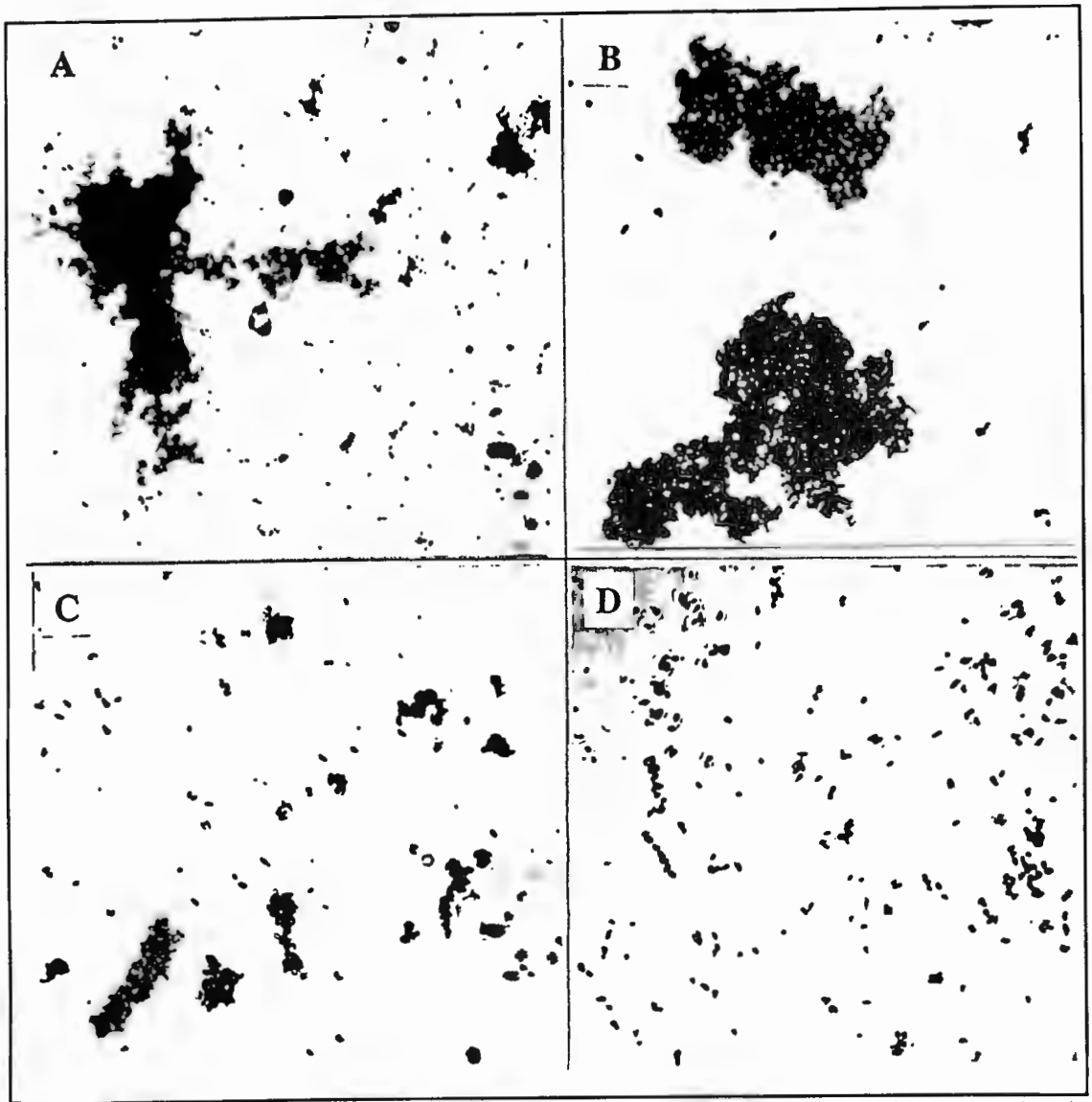

Figure 38 Microscopic photographs of aggregate breakup as a function of the total exposure time in the 7.3 L reactor (v_{imp} 4.6 m/s, no sparging): 1 mm = 1 μm
(A) zero; (B) 30 min; (C) 60 min; (D) 140 min.

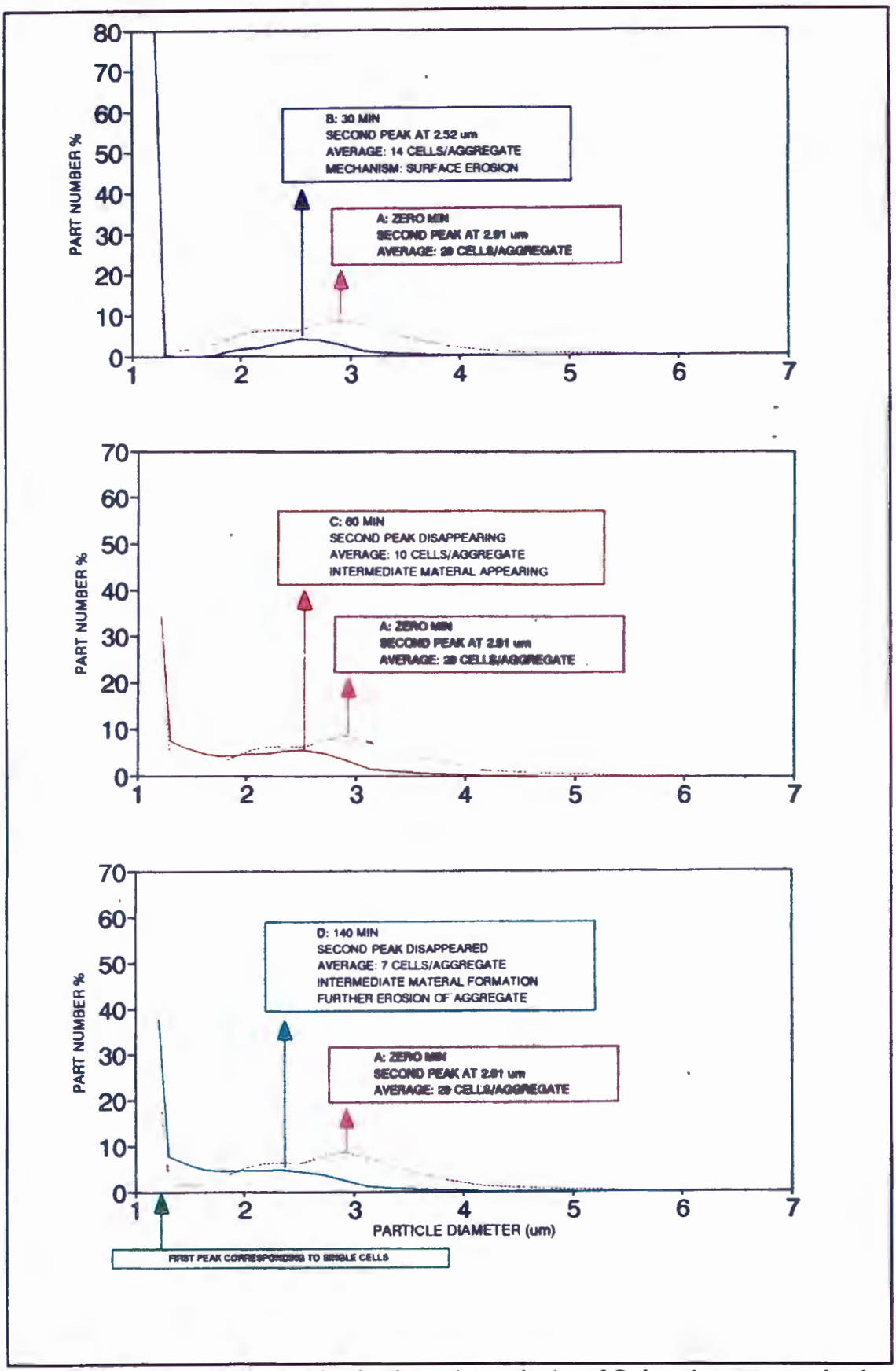

Figure 39 Particle size distribution showing the erosion mechanism of *C.glutamicum* aggregate breakup in a 7.3 liter stirred tank reactor (v_{imp} 4.6 m/s, U_{sg} 0 m/s).

6.3.4 Effect of time of exposure to hydrodynamic forces

The breakup of agglomerates is expected to occur in the impeller zone of the stirred tank reactor and in the capillary section of the flow loop system. The extent of aggregate breakup will therefore be a function of the number of circulations through these "trauma" regions. To investigate this, the erosion of the aggregates is shown as a function of the number of circulations in Figures 40, 41, 42 and 43. Figures 40-42 represent the data collected from the stirred tank reactor at a working volume of 7.3 liters and a maximum energy dissipation rate of 229, 595 and 1830 m^2/s^3 respectively. Figure 43 shows data generated in the flow loop system at a maximum energy dissipation rate of 144810 m^2/s^3.

Aggregate breakup increased with increasing number of circulations. The probability of an aggregate interacting with a similarly sized eddy for a sufficient length of time for erosion to occur increases with increasing number of circulations through the "trauma" zone. The shift in particle size distribution from bimodal to monomodal with increasing number of circulations is apparent in Figure 41, 42 and 43 as the shape of the cumulative particle size curve changes from concave to convex. The shift is due to the formation of intermediate aggregates (diameters 1.31 μm to 1.74 μm). The milder the conditions in the tank, the greater the number of circulations required for the formation of the intermediate sized aggregates. In the flowloop the maximum energy dissipation rate was 2 to 3 orders of magnitude greater than in the stirred tank reactor. The number of circulations required to achieve the same degree of aggregate breakup was 2 to 3 orders of magnitude less.

The rate of change of the particle size distribution decreased with time. It is apparent (Figures 41 and 42) that a point may be reached where the rate of aggregate breakup equals the rate at which reaggregation occurs or that the size of the aggregates reach the point at which similarly sized eddies do not contain sufficient energy for further erosion of the aggregates to occur. Under these conditions, no further change in particle size distribution with increasing number of circulations is seen.

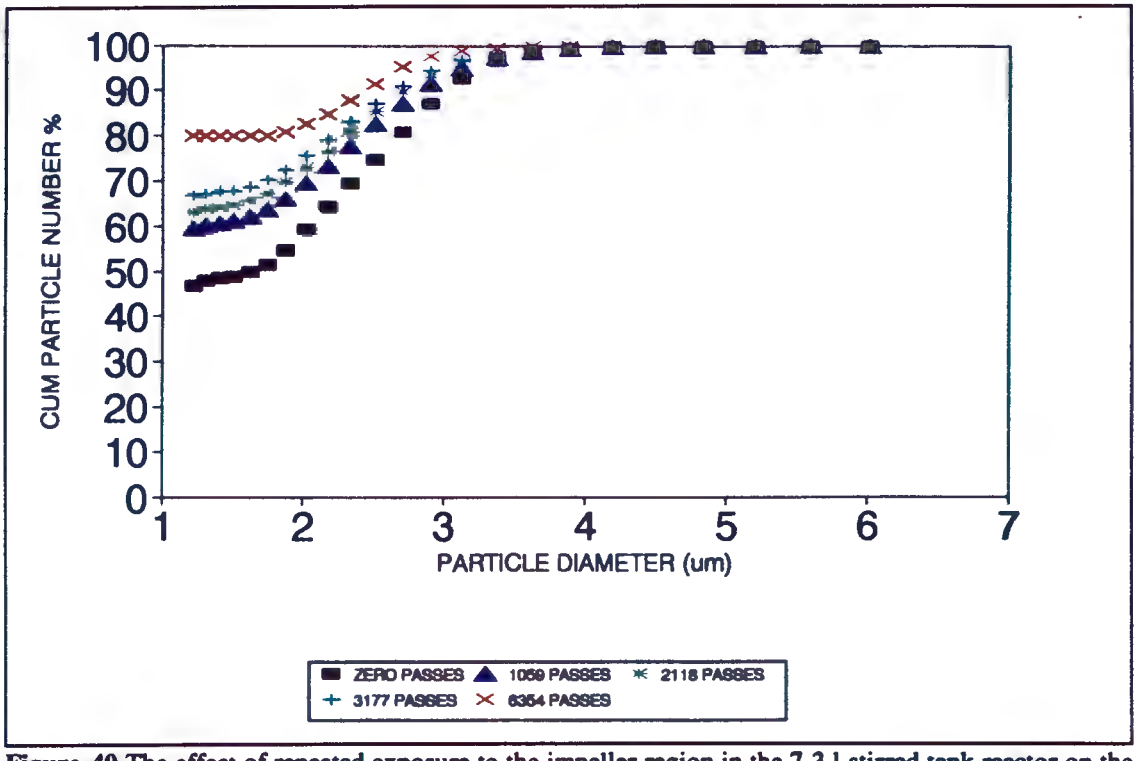

Figure 40 The effect of repeated exposure to the impeller region in the 7.3 l stirred tank reactor on the extent of aggregate breakup:
ϵ_{MAX} 229 m^2/s^3 (v_{imp} 3.35 m/s, U_{sg} 0 m/s).

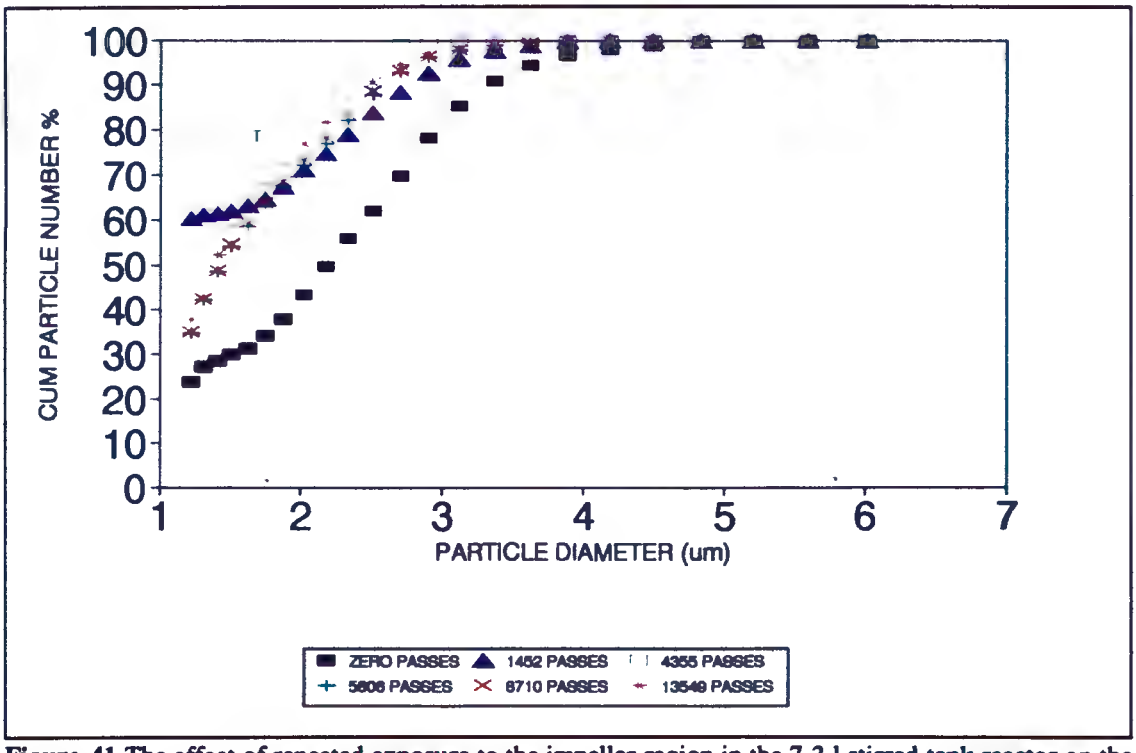

Figure 41 The effect of repeated exposure to the impeller region in the 7.3 l stirred tank reactor on the extent of aggregate breakup:
ϵ_{MAX} 595 m^2/s^3 (v_{imp} 4.6 m/s, U_{sg} 0 m/s).

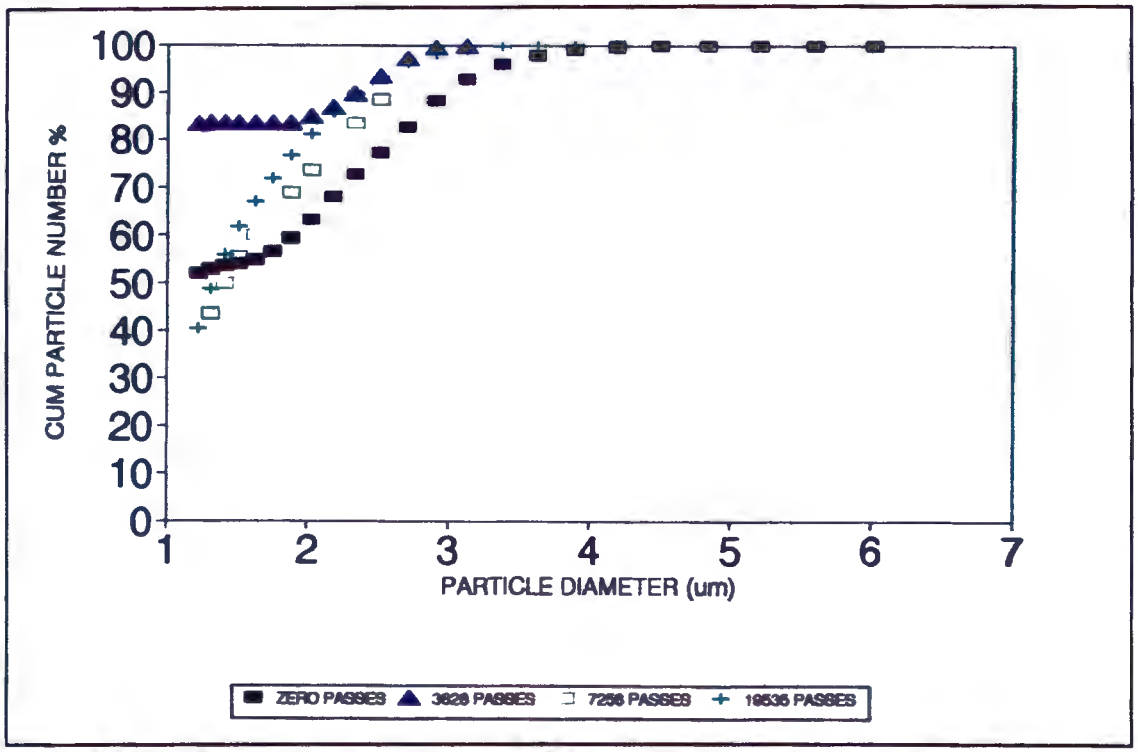

Figure 42 The effect of repeated exposure to the impeller region in the 7.3 l stirred tank reactor on the extent of aggregate breakup:
e_{MAX} 1830 m^2/s^3 (v_{imp} 6.7 m/s, U_{sg} 0 m/s).

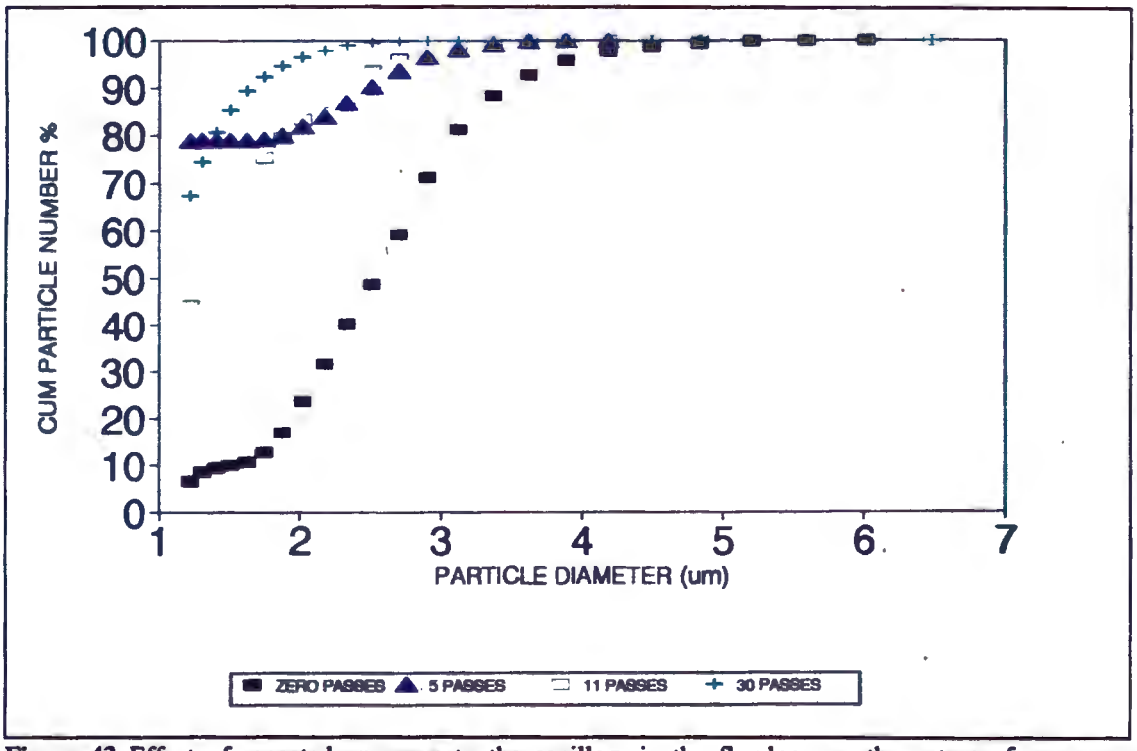

Figure 43 Effect of repeated exposure to the capillary in the flowloop on the extent of aggregate breakup:
e_{MAX} 144810 m^2/s^3 (Q = 4.93X10^{-6} m^3/s).

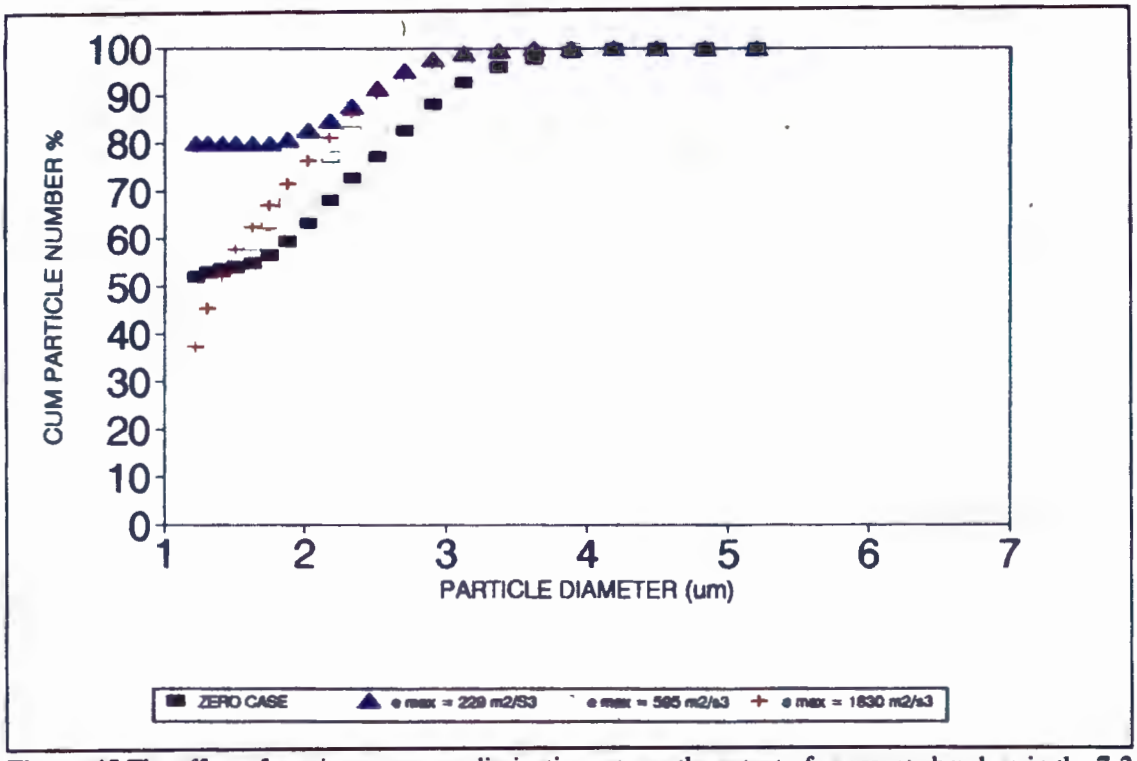

Figure 45 The effect of maximum energy dissipation rate on the extent of aggregate breakup in the 7.3 l stirred tank reactor in the absence of a gaseous phase after 6334 passes.

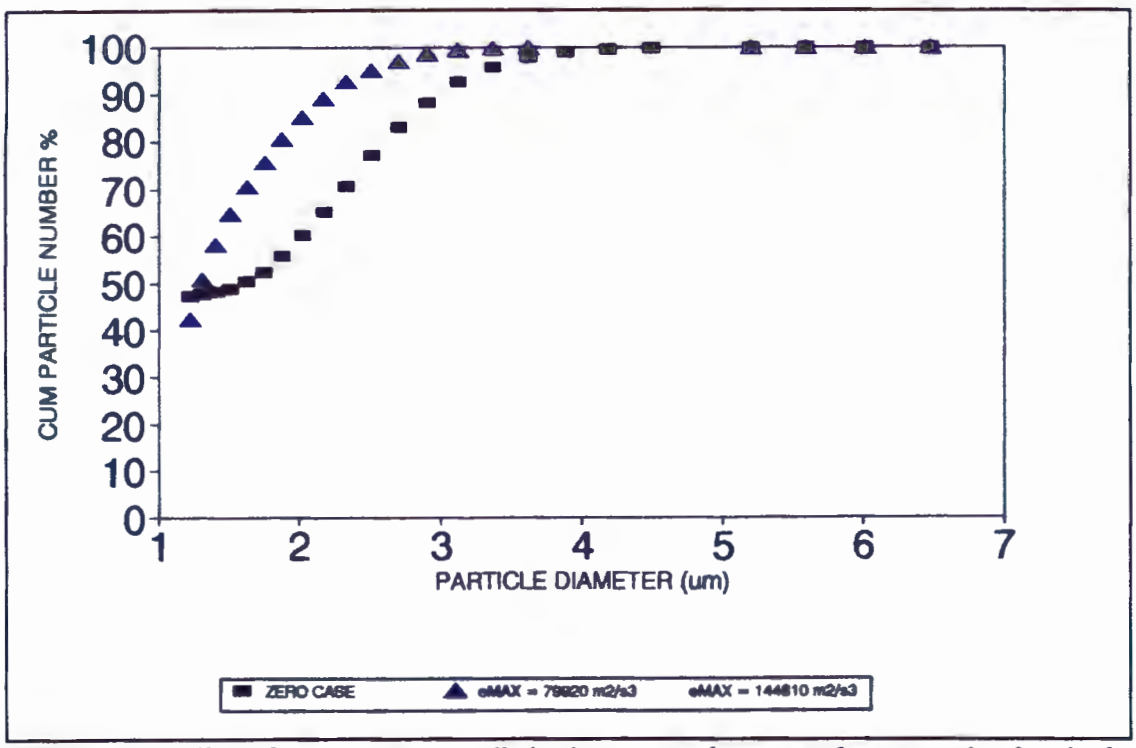

Figure 46 The effect of maximum energy dissipation rate on the extent of aggregate breakup in the flowloop after 11 passes.

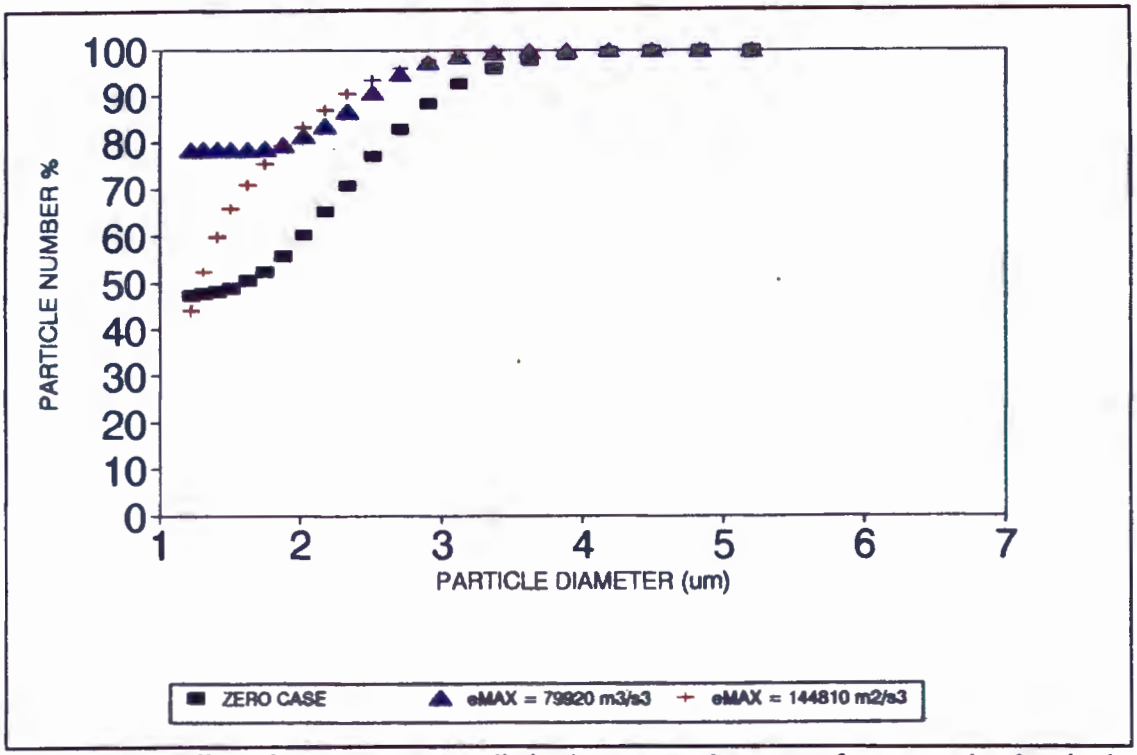

Figure 47 The effect of maximum energy dissipation rate on the extent of aggregate breakup in the flowloop after 25 passes.

6.4 MODELLING OF CELL-TURBULENT EDDY INTERACTIONS IN MICROBIAL SYSTEMS

6.4.1 Breakup of *Corynebacterium glutamicum* aggregates

In order to correlate the biological data with hydrodynamic variables, it was necessary to choose a suitable biological response parameter. The rate at which the number of primary particles changes is determined by the difference between the rate at which large particles are eroded and the rate at which primary particles reaggregate. The rates at which the mean and maximum particle diameters decrease are also a function of surface erosion and reaggregation. The experimental studies on the mechanism of aggregate breakup showed that initially primary cells were chipped off the large aggregates. The concentration of primary cells (less than 1.22 μm) increased until a point was reached where reaggregation of the

primary material occurred to form intermediate sized aggregates (1.31 to 1.75 μm). The point of reaggregation was dependent on the concentration of primary cells and therefore on the extent of erosion.

Hence the point at which the intermediate-sized aggregates form has been used as the independent biological parameter. Assuming a first order response and relating the point of formation of intermediate material to an "extent of disruption":

$$\frac{\partial C_V}{\partial N} = B_3 \frac{\mu}{\sigma_{AGGREGATE}\, d_p^{\,2}} \left(\frac{e}{\nu}\right) C_V \qquad (107)$$

$$CONSTANT_{INTERMEDIATE} = B_7 \frac{\mu}{\sigma_{AGGREGATE}\, d_p^{\,2}} \frac{e}{\nu} N \qquad (108)$$

$$\ln N = -\ln e + \ln A_8 \qquad (109)$$

The energy dissipation rates and corresponding number of passes at which the intermediate-sized aggregates occurred in the flowloop and bubble free stirred tank reactor experiments are correlated in Figure 48. The local energy dissipation rates in the impeller zone and capillary wall region have been used in these calculations as they represent the critical hydrodynamic force to which the cells are subjected. There are two data points for each turbulent energy dissipation rate. The point of appearance of intermediate sized material lies between these two limits. Figure 48 shows that the exponent of the energy dissipation rate in Equation 108 is 1.1, hence the model agrees reasonably well with the experimental data. The predominant mechanism of aggregate breakup is through the action of viscous forces as the ratio between the initial maximum particle diameter ($\pm$ 7μm) and the impeller zone Kolmogorov microscale (varying from 15μm to 1.6μm used in the various flow systems) lay in the range 0.47 to 4.4 *i.e.* it was less than 9.

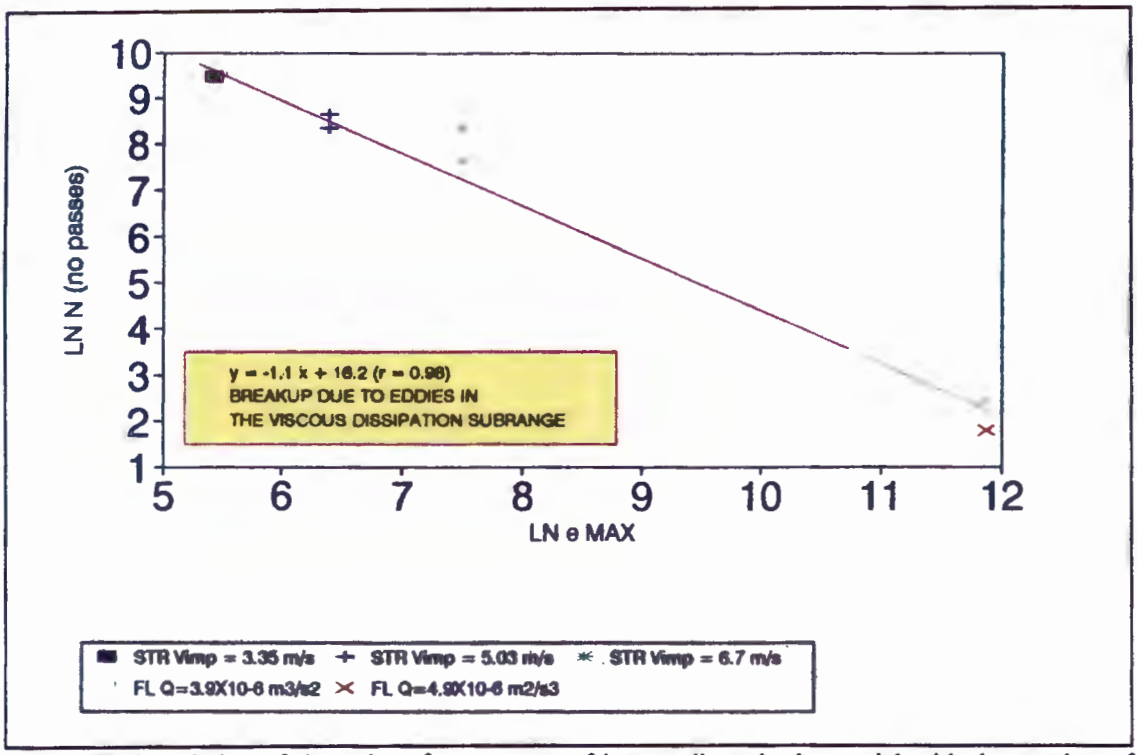

Figure 48 Correlation of the point of appearance of intermediate sized material with the number of passes and maximum energy dissipation rate (constant = B, e N).
STR = stirred tank reactor
FL = flowloop

6.4.2 Hybridoma cell death

To further validate the model of cell turbulent eddy interaction, its application to animal cell systems was sought. The TB/C3 hybridoma cell death data of Zhang *et al.* (1993) determined from a flowloop system and the TB/C3 hybridoma cell death data of Zhang *et al.* (1995) determined in a bubble free stirred tank reactor were analysed.

The flowloop system consisted of a pump, an agitated holding flask and a capillary test section connected into the loop with wide-bore silicone tubing. Capillaries with a diameter of 1.1 mm and L/D ratios of 9.1 and 18.2, and a diameter of 0.51 mm with a L/D ratio of 19.6 were used. Flow rates were adjusted between 1.4×10^{-6} and 4.4×10^{-6} m^3/s so that the Reynold's number was always greater than 3500. The stirred tank reactor had a working volume of 2 liters and was fitted with a standard Rushton turbine impeller with a diameter of 0.0575 m. Care was taken to eliminate the free gas-liquid interface in the experiments.

The model was applied to the data obtained at an impeller speed of 6.02 m/s.

The model developed to describe aggregate breakup by cell-eddy interaction in the viscous dissipation subrange (Equation 95), was modified to account for cell death of unicellular cells (Equation 103). Following the incorporation of an expression for cell strength where fatigue may occur (Equation 104), Equation 110 was developed.

$$\frac{dC_V}{dN} = B_5 \frac{\mu}{f(d_C,\delta,\chi)\, d_C^2} (eN)^y \left(\frac{e}{\nu}\right) C_V \qquad (110)$$

This may be simplified and linearised to give Equation 111:

$$\ln \left(\frac{C_V}{C_{VO}}\right) = B_9 (eN)^{y+1} \qquad (111)$$

where C_{VO} is the initial volume concentration of intact cells and the constant B_9 is a function of the cell suspension viscosity and density and the specific cell membrane strength. The cell death data of hybridoma culture was analysed in a similar manner to the disruption of the aggregates as seen in Figure 49.

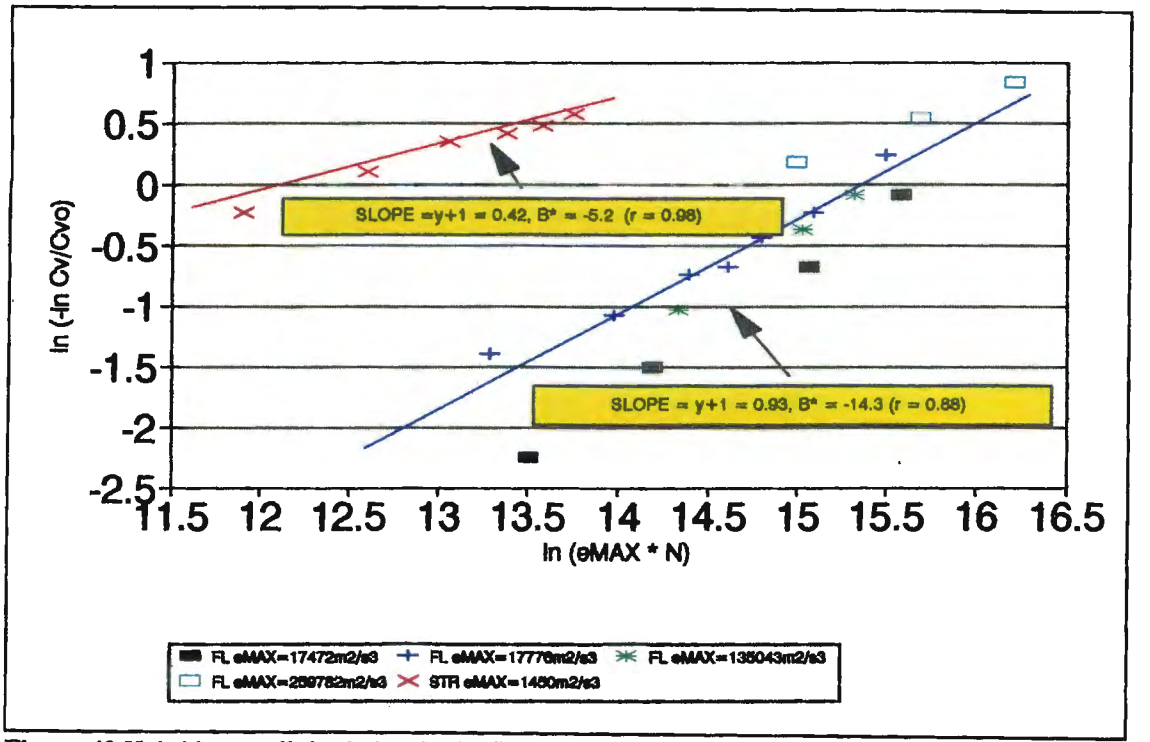

Figure 49 Hybridoma cell death data in the flowloop (FL), (Zhang *et al.*, 1993), and in the 2 l stirred tank reactor (STR), (Zhang *et al.*, 1995): $\ln (C_V/C_{VO}) = B_9 (eN)^{y+1}$.

The hybridoma cell diameter was approximately 12μm, hence the ratio of d/λ was of the order of 2.4 to 8.9. The assumption of viscous forces predominating was therefore valid. The calculated slope of 0.93 for the flowloop data shown in Figure 49 indicated that the fatigue effects, quantified by the exponent y of -0.07, are negligible in the interaction of turbulent eddies with hybridoma cells. The negative value of the fatigue coefficient indicates that there is a marginal increase in the cell membrane strength with increased exposure time due to the preferential destruction of the more susceptible cells. The hybridoma cell death data in the stirred tank reactor gave a slope of 0.42 (fatigue coefficient of -0.58), which indicated a significant increase in the cell membrane strength with exposure time. Since cell membrane strength is a function of cell culture age, it is likely that the cell population used in the flowloop experiments was more homogenous *ie.* all cells had similar cell membrane strengths. A comparison of the intercepts for the two sets of data showed that intercept for the stirred tank reactor data was approximately -5.2 compared to -14.3 for the flowloop system data. Since the intercept is a function of the specific cell wall strength, viscosity and density (Equation 110) it is likely that the animal cells used in the two experiments were not identical in terms of culture age or growth conditions. Suspension viscosity increases with cell concentration. Al-Rubeai *et al.* (1995) have shown that older TB/C3 hybridomas were more susceptible to disruption.

6.4.3 Death of plant cell aggregates

The applicability of the model of cell-turbulent eddy interaction in the range of conditions where inertial forces are expected to dominate was investigated. Inertial forces dominate when the ratio of the cell diameter to the Kolmogorov microscale is greater than 9. For bacteria and yeast this is only likely to be true for flow in cell disruption devices such as high pressure homogenisers. Inertial forces may dominate in plant cell bioreactors as plant cell aggregates are larger than bacteria, yeast and animal cells.

Kieran *et al.* (1995) studied the susceptibility of *Morinda citrifolia* to flow conditions. In the experiments the susceptibility of cell suspension cultures of *Morinda citrifolia* were investigated by subjecting the cells to turbulent capillary flow. The apparatus was similar to that used by Zhang *et al.* (1993). The capillary tube had an internal diameter of 1.35 mm.

Tube lengths of 0.1, 0.5 and 1 m were used. Late exponential phase *Morinda citrifolia* plant cells grown in a stirred tank reactor were cylindrical in shape (± 100 μm long) and formed chains consisting of 4 cells. Flow in the capillary resulted in a reduction in the average viable chain length. The ratio of the plant cell diameter (100 μm) to the minimum Kolmogorov microscale varied from 40 to 50. Inertial forces would therefore be expected to predominate in the interaction of the eddies with the plant cell aggregates. The application of the model of cell-turbulent eddy interaction (Equation 112) to predict the plant cell death data of Kieran *et al.* (1995) was investigated.

$$\frac{dC_V}{dN} = B_6 \frac{\mu}{f(d_{ch},\delta,\chi)\ d_{ch}^2} (eN)^y \left(\frac{e}{\nu}\right) C_V \qquad (112)$$

where d_{ch} is the average chain length. Equation 112 was linearised (Equation 113) and the data correlated in Figure 50.

$$\ln\left(\frac{C_V}{C_{V0}}\right) = B_8 (eN)^{y+1} \qquad (113)$$

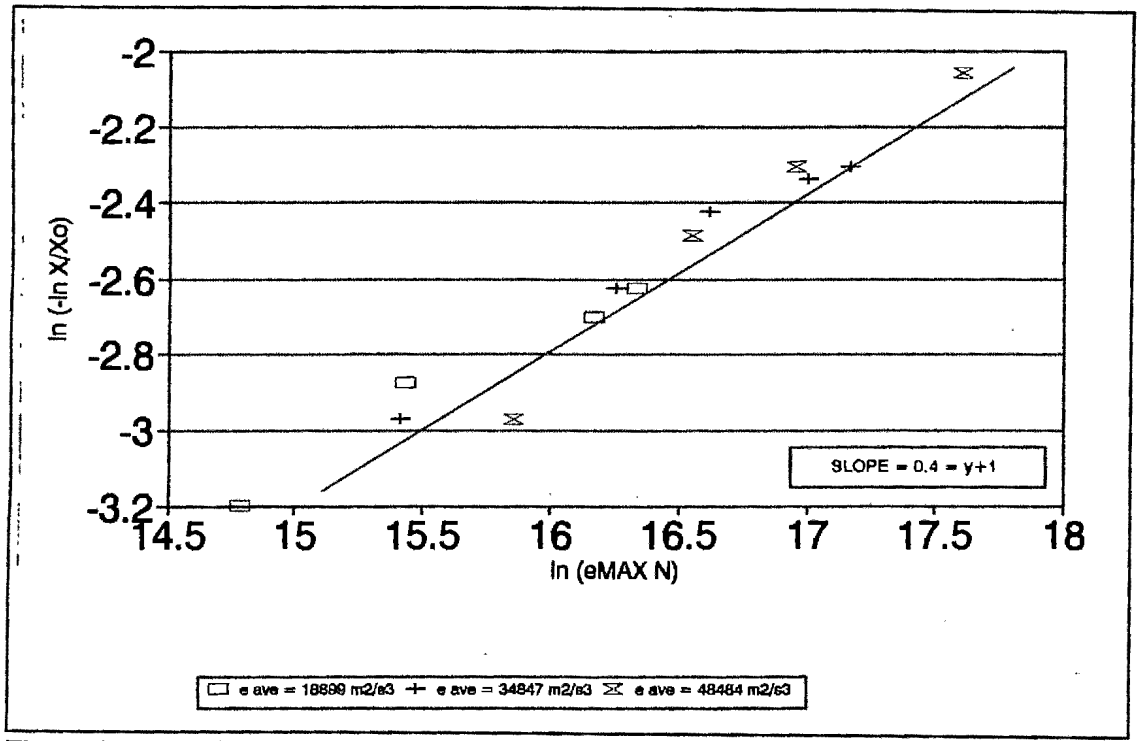

Figure 50 Correlation of the plant cell death data in a flowloop (Kieran *et al.* 1995) with the number of passes and the maximum energy dissipation rate ($\ln C_V/C_{V0} = B_8 (eN)^{y+1}$).

A slope of 0.4 was obtained when the plant cell death data was correlated with the number of passes through the capillary tube and the maximum energy dissipation rate. Assuming the cell turbulent eddy model to be valid, the slope of 0.4 indicates that the fatigue exponent in Equation 113 has a value of -0.6. This would imply that the strength of the cells increased with cumulative stress due to the preferential destruction of the more susceptible cells.

6.5 CONCLUSIONS

Based on the findings in this chapter the following conclusions may be drawn:

6.5.1 The mechanism and kinetics of the breakup of *Corynebacterium glutamicum* aggregates was investigated by exposing cells grown in continuous culture to hydrodynamic forces in various flow systems in the absence of a gaseous phase. The extent of aggregate breakup was a function of the magnitude of the turbulent forces as well as the total duration of the force event. With repeating of the load, the probability of an aggregate interacting with a similar sized eddy for a sufficiently long period of time to cause disaggregation increased. The aggregate breakup experiments showed that initially primary cells were chipped off the large aggregates. The concentration of primary cells increased until a point was reached where reaggregation of the primary material occurred to form intermediate sized aggregates. Erosion of cells off the large aggregates continued to occur after the reggregation point.

6.5.2 Models were presented to describe the rate of aggregate breakup or cell disruption caused by fluid-particle interactions in the absence of a gaseous phase. Both dominance of viscous and inertial forces were considered. It was assumed that viscous forces predominated in the interaction of the bacterial aggregates and the hybridoma cells with turbulent eddies as the diameters of the microbial particles were less than 9λ. Inertial forces predominated in the interaction of *Morinda citrifolia* plant cell aggregates with turbulent eddies as the diameter of the cells was greater than 9λ. The

respective appropriate model equations are given in Equation 114, 115 and 116.

$$\frac{dC_V}{dN} = B_3 \frac{\mu}{\sigma_{AGGREGATE}\, d_p^2} \left(\frac{e}{\nu}\right)^{1.0} C_V \qquad (114)$$

$$\frac{dC_V}{dN} = B_5 \frac{\mu}{\sigma_{CELL}\, d_C^2} \left(\frac{e}{\nu}\right)^{1.0} C_V \qquad (115)$$

$$\frac{dC_V}{dN} = C_2 \frac{\mu}{\sigma_{CELL}\, d_C^2} \left(\frac{e}{\nu}\right)^{1.0} C_V \qquad (116)$$

6.5.3 The experimental data illustrated a first order dependence of the extent of *Corynebacterium glutamicum* aggregate breakup with respect to the maximum energy dissipation rate in the impeller zone of the bubble free reactor and in the wall region of the flow loop capillary, thus verifying the validity of the model of microbial aggregate-turbulent eddy interaction.

6.5.4 In the model of microbial cell death model, it was assumed that the specific cell strength was a function of the cell size, cell envelope thickness and cell envelope composition. It was also postulated that the strength of the cell envelope may decrease with hydrodynamic stress exposure time due to fatigue *i.e.*

$$\sigma_{CELL} = f(d_C, \delta, \chi)\ (eN)^{-y} \qquad (117)$$

The rate of cell death by viscous forces was therefore given by:

$$\frac{dC_V}{dN} = B_5 \frac{\mu}{f(d_C, \delta, \chi)\, d_C^2} (eN)^y \left(\frac{e}{\nu}\right)^{1.0} C_V \qquad (118)$$

The rate of cell death by inertial forces was given by:

$$\frac{dC_V}{dN} = B_6 \frac{\mu}{f(d_C, \delta, \chi)\, d_C^2} (eN)^y \left(\frac{e}{\nu}\right)^{1.0} C_V \qquad (119)$$

6.5.5 The hybridoma cells in the flowloop (Zhang *et al.*, 1993) and stirred tank reactor (Zhang *et al.*, 1995) and plant cell aggregates in a flowloop (Kieran *et al.*, 1995) did not weaken after 300 passes for the flowloop experiments and 16000 passes for the stirred tank reactor experiments as the value of the exponent y in Equation 117, included to describe fatigue, was negative. Al-Rubeai *et al.* (1995) postulated that fatigue effects were significant for hybridoma cultures in a stirred tank reactor. Al-Rubeai *et al.* (1995) however only observed the weakening of the cell membranes after 8.1×10^5 circulations through the impeller zone at sublytic levels of hydrodynamic stress. The difference in the time frame of the experiments may account for the apparent discrepancy in the results for the hybridoma cells.

6.5.6 The results showed that the cell envelope strength of the hybridoma cells in the stirred tank reactor (Zhang *et al.*, 1995) and the *Morinda Citrifolia* plant cell aggregates in the flowloop (Kieran *et al.*, 1995) increased with the total exposure time as the fatigue exponent had a negative value. This may have been due to the preferential destruction of the more susceptible cells. The effect was less significant for the hybridomas in the flowloop (Zhang *et al.*, 1993). It may be possible that the cell population was more homogenous *ie* the cell population had a more even distribution of cell membrane strengths. The cells were also exposed to fewer circulations in the flowloop but at a greater maximum energy dissipation rate.

6.5.7 A comparison of the intercepts for the two sets of hybridoma data obtained in the flowloop and stirred tank reactors showed that the intercept for the stirred tank reactor data was approximately -5.2 compared to -14.3 for the flowloop system data. Since the intercept is a function of the specific cell wall strength, viscosity and density (Equation 110), it is likely that the animal cells used in the two experiments were not identical in terms of culture age or growth conditions. Suspension viscosity increases with cell concentration. Al-Rubeai *et al.* (1995) have shown that older TB/C3 hybridomas were more susceptible to disruption.

7. THE CONTRIBUTION OF COLLAPSING BUBBLES TO AGGREGATE BREAKUP

7.1 INTRODUCTION

Literature findings regarding the causes of hydrodynamic trauma in bioreactors were divided into two groups. The first group attributes metabolic inhibition to the interaction of cells with turbulent eddies of a similar size in regions of high shear stress found near the impeller (Kunas and Papoutsakis, 1990; Smith and Lilly, 1990, Toma *et al.*, 1991, Vanags *et al.*, 1990). The interaction of cells with collapsing air bubbles at the free surface fall in the second category. The surfaces of cells and bubbles are hydrophobic, hence cells tend to adhere to a bubble as it rises to the air liquid interface (Zhang *et al.*, 1992). Boulton-Stone and Blake (1993) numerically modelled the flow resulting on bubble collapse and suggested that the maximum energy dissipation rates, occurring beneath a collapsing bubble just before jet formation, contribute to cell disruption. The smaller the bubbles and the greater the number of bubbles the more energy is dissipated, and therefore the more severe the viability loss or cell disruption (Handa-Corrigan *et al.*, 1989). Protective additives such as Pluronic-F68 coat the bubble and cell surfaces preventing their direct interaction. Antifoam increases the degree of cell damage by increasing the hydrophobicity of cells and bubbles and thereby their interaction (Zhang *et al.*, 1992).

A model of the cell-turbulent eddy interaction has been developed to effectively predict the extent of *Corynebacterium glutamicum* aggregate breakup in a stirred tank reactor and flowloop system in the absence of a gaseous phase. The model was applied to other bubble free microbial systems to describe the cell death of hybridomas and plant cell aggregates. Examples of process situations where the gaseous phase is absent and where the model would be valid would be pump circuits, separation devices and disruption equipment.

In growing systems, the relative contribution of collapsing air bubbles to the total

hydrodynamic force experienced by the microorganisms needs to be considered. In this section the effect of collapsing air bubbles on the breakup of *Corynebacterium glutamicum* breakup in a sparged stirred tank and airlift reactor has been investigated.

7.2 DISRUPTION OF BACTERIAL AGGREGATES IN A STIRRED TANK REACTOR: THE EFFECT OF BUBBLES

The forces associated with turbulent eddies in the impeller discharge zone have been compared with those of collapsing air bubbles at the air liquid interface. The breakup of *Corynebacterium glutamicum* aggregates has been used as a model system. It has been shown previously in Chapter 5 that hydrodynamic stress, due to turbulent eddies in the impeller zone and collapsing air bubbles at the air medium interface, has no effect on the lysis, viability, rate of growth and rate of metabolism of *Corynebacterium glutamicum*.

7.2.1 Experimental procedure

Continuous cultures of *Corynebacterium glutamicum* grown at a dilution rate of 0.36 hr^{-1} at mild agitation conditions (impeller speed 1.68 m/s and U_{sg} of 0.005 m/s) were subjected to flow conditions in a bubble free and sparged stirred tank reactor. In the bubble free 7.3 liter stirred tank reactor, the cells were agitated at 1.68, 4.6 and 6.7 m/s in the absence of an air liquid interface. Special care was taken to completely fill the reactor so that no air was entrained during mixing. The 5 liter sparged stirred tank reactor was agitated at impeller speeds of 1.68, 4.6 and 6.7 m/s and sparged with N_2 at a superficial gas velocity of 0.005 m/s. N_2 was used to simulate the O_2 limiting environment of the bubble free system. Cell samples were analysed in terms of particle size analysis by laser light diffraction, dry mass and specific plate counts.

7.2.2 Results

The cumulative particle size distribution following agitation in the presence and absence of gas sparging are shown in Figure 51. Calculation of the maximum energy dissipation rates in the sparged (Michel and Miller, 1962) and bubble free systems yielded a similar impeller turbulence component at the same agitation rates (Table 25). Aggregate breakup in the sparged system was, however, more severe than in the bubble free system at the same agitation speed. Aggregate breakup after 4186 passes at an impeller speed of 3.35 m/s and a superficial gas velocity of 0.005 m/s ($188 < e_{MAX\ (IMP)} < 260$) exceeded that at 6.7 m/s in the absence of aeration ($e_{MAX\ (IMP)} = 1830\ m^2/s^3$). The maximum energy dissipation rate in the impeller zone was approximated as 25 times the average energy dissipation rate (Table 10, Section 4.2.1) in the stirred tank reactor. The bubble component of the total energy dissipation rate is therefore significant in effecting the breakage of aggregates of *Corynebacterium glutamicum.*

Boulton-Stone and Blake (1993) calculated the peak energy dissipation rates occurring during the collapse of a bubble. They showed that the peak energy dissipation rate increased exponentially with decreasing bubble size (Figure 52). The breakup of the aggregates is more extreme in the sparged system at 3.35 m/s (as shown in Figure 51) than in the bubble free reactor at 6.7 m/s as the cells are subjected to significant forces in the impeller zone ($188\ m^2/s^3 < e_{MAX\ (IMP)} < 260\ m^2/s^3$) and in the vicinity of breaking air bubbles at the air medium interface ($e_{MAX\ (BUB)} = 10^7\ m^2/s^3$ for a 0.5 mm bubble). The frequency with which a cell encounters turbulent forces in the impeller zone is determined by the circulation frequency. The frequency with which a cell encounters the forces associated with collapsing air bubbles is determined by the bubble frequency, the probability of cell bubble attachment and the circulation frequency. Rigorous modelling of the effect of bubble collapse on aggregate breakup requires knowledge of the bubble size distribution.

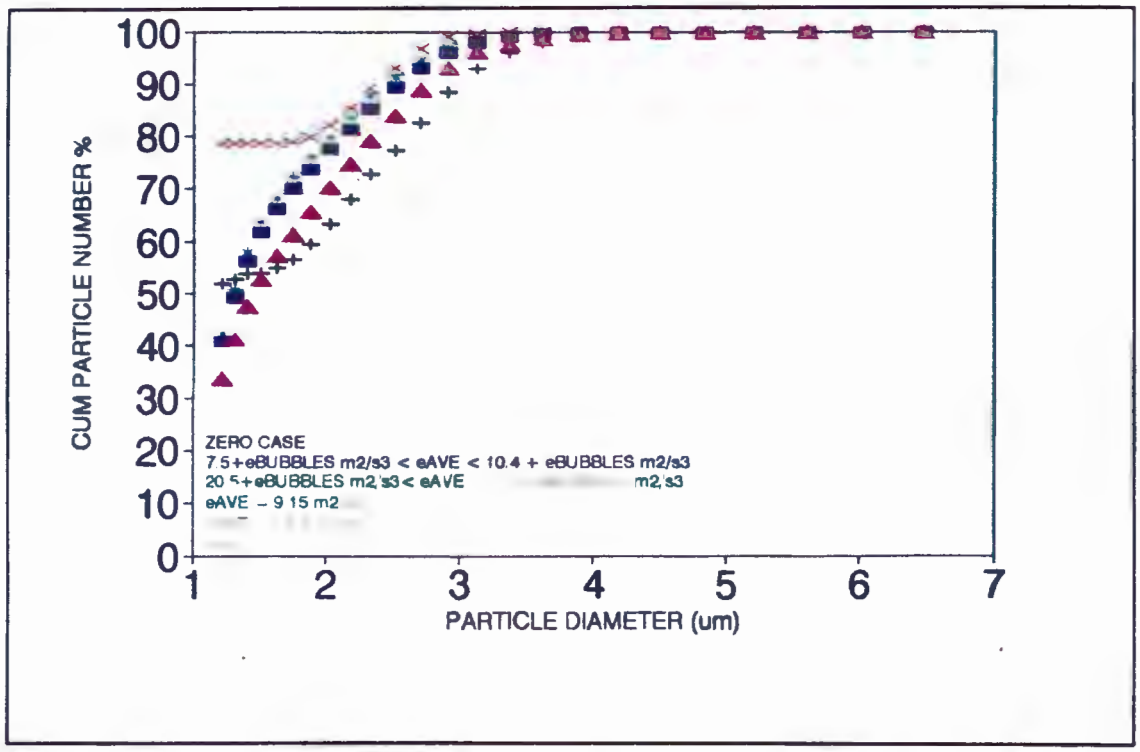

Figure 51 The effect of gas sparging on the extent of *C. glutamicum* aggregate breakup in the stirred tank reactor agitated at impeller tip speeds in the range 1.68 to 6.7 m/s for 4186 passes through the impeller discharge zone.

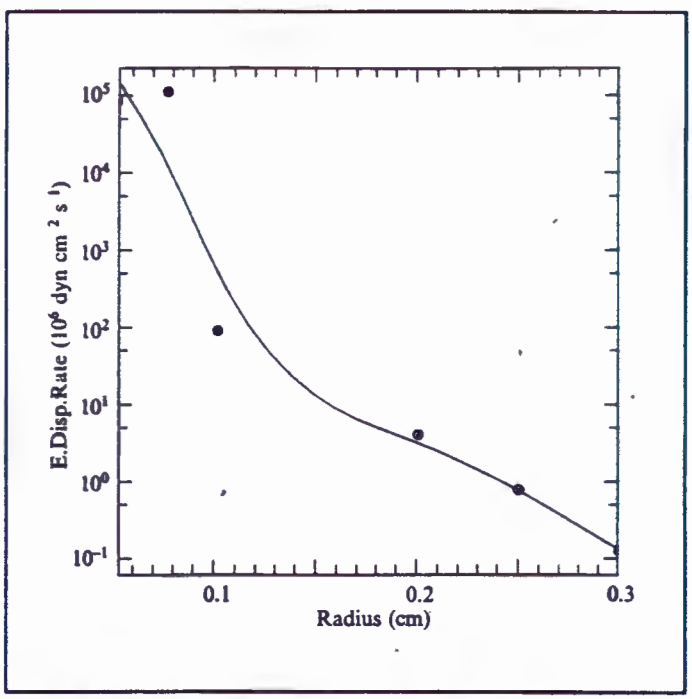

Figure 52 Maximum energy dissipation rate produced during the bubble bursting process, plotted against bubble radius (Boulton-Stone and Blake, 1993)

Table 25 Maximum energy dissipation rates encountered in the stirred tank reactor in the vicinity of the impeller zone and collapsing air bubbles at the air medium interface, bubble sizes, frequency of exposure to forces in the impeller zone, and frequency of bubble collapse.

HYDRODYNAMIC CONDITIONS			$e_{MAX,imp}$ m^2/s^3	$e_{MAX,bubble}$ m^2/s^3	SAUTER MEAN BUBBLE DIAMETER mm	CIRCULATION FREQUENCY circulations per s	BUBBLE FREQUENCY bubbles per s
STIRRED TANK REACTOR							
REACTOR VOLUME l	IMPELLER SPEED m/s	U_{sg} m/s					
5	3.35	0.005	188-260	10^7	0.5	1.5	$2\text{-}3.1\times10^6$
5	4.6	0.005	513-690	4×10^7	0.37	2	$6.1\text{-}7.7\times10^6$
7.3	3.35	0	239			1.2	
7.3	4.6	0	595			1.6	
7.3	6.7	0	1830			2.3	
AIRLIFT REACTOR							
REACTOR VOLUME	U_{gr}						
1	0.2			500	1.77	0.2	6.8×10^4

7.3 AIRLIFT REACTOR

Corynebacterium glutamicum grown in continuous culture at a dilution rate of 0.36 hr^{-1} were also subjected to flow conditions in an airlift reactor (described in Section 3.5.3) operated at a riser superficial N_2 velocity of 0.2 m/s. The particle size analysis of aggregates exposed to 1071 circulations through the airlift reactor are compared to those for the sparged stirred tank reactor, at an impeller speed of 3.35 m/s and a superficial N_2 velocity of 0.005 m/s, after 1336 passes through the impeller zone in Figure 53. The results showed that the total particle count had increased by 15 % for the stirred tank reactor compared to 7.5 % for the airlift reactor, indicating surface erosion in both cases. In the airlift reactor, the forces associated with collapsing air bubbles at the air medium interface are solely responsible for the breakup of aggregates. An average energy dissipation rate of 0.668 m^2/s^3 in the airlift reactor was calculated compared to an average energy dissipation rate in the range 7.5 to 10.42 m^2/s^3 for the 5 liter stirred tank reactor at an impeller speed of 3.35 m/s and superficial gas velocity of 0.005 m/s. The maximum energy dissipation rate produced during the collapse of a 1.7 mm diameter bubble (Sauter mean diameter) found in the airlift reactor was estimated as 500 m^2/s^3 from the analysis of Boulton-Stone and Blake (1993). In the stirred tank reactor, the mean Sauter mean bubble diameter was approximately 0.5 mm. From Figure 52 this corresponds to a maximum energy dissipation rate of 10^7 m^2/s^3. The frequency of the bubbles in the airlift reactor and stirred tank reactor was calculated to be 6.8×10^4 s^{-1} and $2\text{-}3.1\times10^6$ s^{-1} respectively. In the stirred tank reactor both the turbulent eddies in the impeller zone and the collapsing air bubbles at the air liquid interface contribute to the total hydrodynamic force experienced by the cells. It is consistent that the extent of aggregate breakup is more extreme in the stirred tank reactor as was observed in Figure 53. The significance of the effect of breakage of the large bubbles in the airlift reactor is questioned.

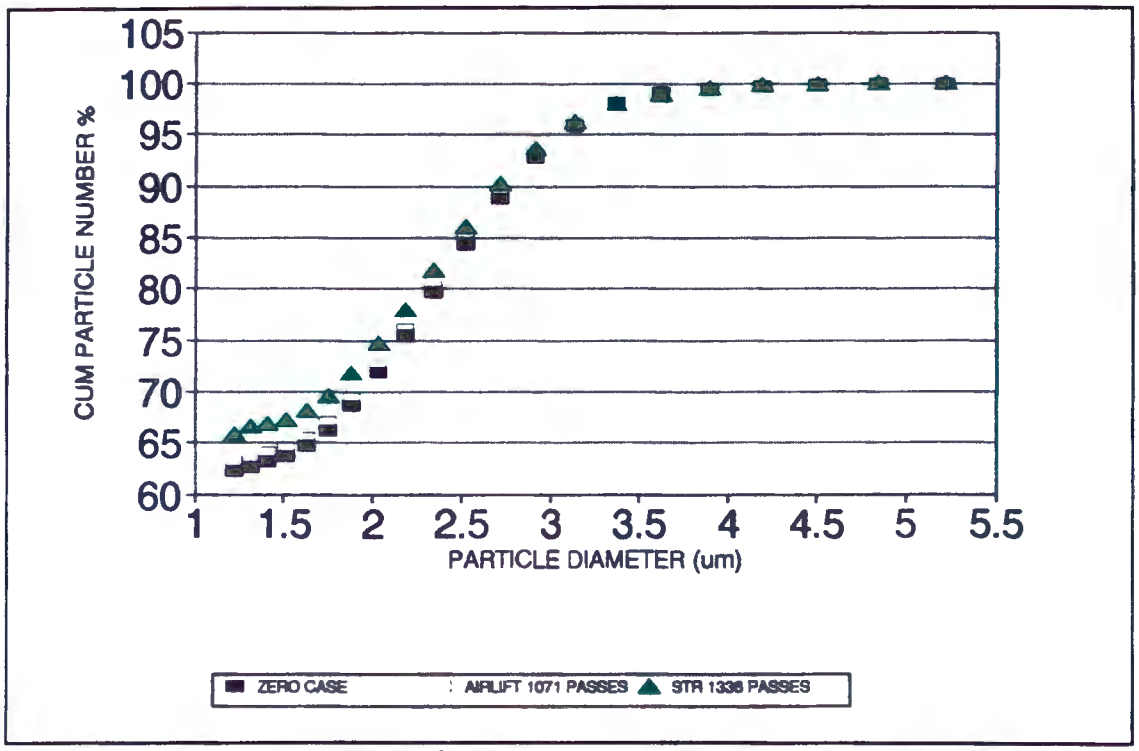

Figure 53 Comparison of the extent of aggregate breakup in the sparged stirred tank reactor (impeller speed 3.35 m/s and U_{sg} 0.005 m/s) after 1071 passes and in the airlift (U_{gr} 0.2 m/s) after 1336 passes.

7.4 CONCLUSIONS

Based on the discussions in this chapter the following conclusions may be drawn:

7.4.1 It has been shown that bubble collapse contributes to the breakup of *Corynebacterium glutamicum* aggregates in stirred tank bioreactors. Both the interaction of cells with turbulent eddies in the impeller zone and with collapsing air bubbles at the air medium interface therefore contribute to the total force acting on cell surfaces. In growing systems, where there is a gas phase present, it is therefore important that the contribution of both is taken into account in determining the effects of hydrodynamic stress.

7.4.2 The magnitude of the maximum energy dissipation rate associated with collapsing air bubbles is inversely proportional to the diameter of the bubbles. The smallest

bubbles exert the greatest forces on cell surfaces. Under standard conditions in the stirred tank reactor, the maximum energy dissipation rate associated with bubble collapse is 5 orders of magnitude greater than the maximum energy dissipation rate in the impeller zone.

7.4.3 The frequency with which a cell encounters the forces associated with collapsing air bubbles is determined by the bubble frequency, the probability of cell bubble attachment and the circulation frequency. The greater the frequency of cell bubble interactions, the greater the rate of aggregate breakup.

7.4.4 It is recommended that rigorous studies on the contribution of collapsing air bubbles to the effect of hydrodynamic stress in bioreactors be addressed in future work. In order to incorporate the contribution of collapsing air bubbles in the disruption model, it is necessary to take into account the degree of bubble cell attachment (dependent on the concentration of surface active agents as Pluronic F-68 and antifoam), the frequency of bubble collapse (dependent on bubble frequency), the frequency with which a cell attaches to bubbles (determined by the circulation time), and the ratio of the disruptive force (dependent on the bubble size) to the strength of the aggregate or cells. Since the bubble size is such a critical parameter in the quantification of the disruptive force and the bubble frequency, it is important to have an accurate method of determining the bubble size distribution at the air liquid interface.

8. CONCLUSIONS

Hydrodynamic forces associated with agitation and aeration exert forces on microbial surfaces. Hydrodynamic characterisation of stirred tank reactors has shown that maximum fluid velocities and hydrodynamic forces occur in the region of the impeller and in the vicinity of collapsing air bubbles. The negative biological response to these forces may manifest itself as a change in the morphology of cells and cell aggregates, decreased growth, substrate utilisation, oxygen utilisation and metabolite production rates, changes in the metabolic pathway of cells, loss of viability and, in the extreme case, cell rupture. Increasing levels of hydrodynamic stress are required to effect changes in the cell shape, metabolic rate, viability, cell death and cell rupture respectively. The sensitivity of cell types is dictated by the biological and physical properties of the cells. Reactor design and operating conditions for stress sensitive microorganisms therefore requires a compromise between the mass transfer requirements and the stress sensitivity of the biological system. The development of a model to predict the biological response of stress sensitive microorganisms as a function of measurable hydrodynamic parameters is desirable.

Based on the literature, it was postulated that *Brevibacterium flavum* and *Corynebacterium glutamicum* may be sensitive to hydrodynamic stress. It was hypothesised that hydrodynamic trauma of microbial cells was due to the interaction of the cells with fluid turbulent eddies in local regions of stress and with collapsing air bubbles at the air medium interface in bioreactors. Based on a fundamental model for the interaction of cells with hydrodynamic stress, it was postulated that the biological response of the bacteria could be correlated with hydrodynamic parameters *eg* impeller speed, bubble size, Reynold's number, circulation time, exposure time, local energy dissipation rates, Kolmogorov microscale *etc.* The formulated hypotheses were investigated using *Brevibacterium flavum* and *Corynebacterium glutamicum*. Findings were then applied to plant and animal cell data available from the literature. Based on the above, the following conclusions can be drawn.

8.1 The turbulence in the Chemap stirred tank reactor was highly inhomogeneous with local energy dissipation rates in the impeller zone being 25 times greater than the overall average values. Since the turbulence in the impeller region was isotropic, the Kolmogorov theory of turbulence can be used to describe the motion of the small scale eddies. In the flowloop system the turbulent velocities were greatest in the wall region. The energy dissipation rates in the flowloop system (e_{AVE} = 9650 m^2/s^3) were 2 orders of magnitude greater than in the Chemap stirred tank reactor. The effects of hydrodynamic stress would therefore be more severe in the flowloop system. The average energy dissipation rate in a typical 100 m^3 industrial scale bioreactor of 1 m^2/s^3 (Einsele, 1978) is lower than values obtained in a 5 liter laboratory scale bioreactor (e_{AVE} = 70 m^2/s^3). The stress sensitivity of microorganisms would therefore become less of a design constraint on scale up.

8.2 The studies showed that hydrodynamic stress, in the absence of mass transfer limitation, had no effect on the lysis, viability, rate of growth, rate of metabolism and spectra of amino acids produced by *Corynebacterium glutamicum* and *Brevibacterium flavum* in a stirred tank reactor at conditions corresponding to average energy dissipation rates of 76 and 47.5 m^2/s^3 respectively. The *Corynebacterium glutamicum* results were confirmed at extreme average energy dissipation rates of 9650 m^2/s^3 using a flowloop system. Contrary to these results, Toma *et al.* (1991) reported that the growth of a different strain of *Brevibacterium flavum* was inhibited at milder conditions (average energy dissipation rate of 10 m^2/s^3).

8.3 The breakup of cell aggregates was observed with increasing agitation and aeration conditions. The extent of aggregate breakup was dependent on the intensity of the hydrodynamic conditions as well as the species of bacteria. *Corynebacterium glutamicum* were more susceptible to aggregate breakup than *Brevibacterium flavum*. Hydrodynamic stress mediated a loss in the ability of *Corynebacterium glutamicum* to divide on solid media. The viability of the cells on the solid growth media did not vary with hydrodynamic conditions. *Brevibacterium flavum* cells did not display this phenomenon.

8.4 It was shown that aggregation of *Corynebacterium glutamicum* was not a result of the electrostatic interaction of a chelating agent with the negatively charged cells. Hydrophobic interaction of neutral cells was also discounted as a mechanism of inter-cell adhesion as the degree of cell aggregation was independent of the charge of the cells. It was postulated that cells produce a growth associated biomolecular adhesive which is responsible for the formation of aggregates.

8.5 Using the breakup of *Corynebacterium glutamicum* aggregates as a model system, the mechanism and kinetics of aggregate breakup in the absence of collapsing air bubbles was investigated. It was shown that the extent of breakup was both a function of the magnitude of the hydrodynamic forces as well as the total duration of the force event. Primary cells were eroded from the surface of large aggregates. As the concentration of the primary cells increased, a point was reached where the reaggregation of the primary material occurred to form intermediate sized aggregates. Erosion of the large aggregates continued after the reaggregation point.

8.6 Based on the fundamental studies of Parker *et al.* (1972), Brown and Glatz (1987) and Ayazi Shamlou *et al.* (1990), it was assumed that the breakup of microbial aggregates in bioreactors in the absence of a gaseous phase was proportional to the product of the number concentration of aggregates, the frequency of disruption of aggregates by the turbulent eddies and the number of primary cells eroded per disruption. The rate of microbial cell death was assumed proportional to the frequency of the force event, the fraction of undisrupted cells and the ratio between the disruptive force and the strength of the cells. It was assumed that microbial particles adsorbed the most energy from similarly sized eddies. Based on equating the root mean square velocity difference for eddies in the viscous dissipation and inertial convection subrange, it was shown that viscous forces predominated when the microbial particles had diameters of less than 9λ. Inertial forces predominated when the particle diameter was greater than 9λ. Models were developed to describe the rate of breakup of bacterial aggregates due to viscous and inertial forces (Equation 120 and Equation 121). Equation 122 and 123 describe the rate of microbial cell death due to the interaction of cells with eddies in the viscous

dissipation and inertial convection subrange respectively.

$$\frac{dC_V}{dN} = B_3 \frac{\mu}{\sigma_{AGGREGATE}\, d_p^{\,2}} \left(\frac{e}{\nu}\right)^{1.0} C_V \qquad (120)$$

$$\frac{dC_V}{dN} = B_4 \frac{\mu}{\sigma_{AGGREGATE}\, d_p^{\,2}} \left(\frac{e}{\nu}\right)^{1.0} C_V \qquad (121)$$

$$\frac{dC_V}{dN} = B_5 \frac{\mu}{\sigma_{CELL}\, d_C^{\,2}} \left(\frac{e}{\nu}\right)^{1.0} C_V \qquad (122)$$

$$\frac{dC_V}{dN} = B_6 \frac{\mu}{\sigma_{CELL}\, d_C^{\,2}} \left(\frac{e}{\nu}\right)^{1.0} C_V \qquad (123)$$

The models adequately described the breakup of *Corynebacterium glutamicum* aggregates, hybridoma cell death and *Morinda citrifolia* plant cell death. Viscous forces predominated in the breakup of *Corynebacterium glutamicum* aggregates and in the death of hybridoma cells. *Morinda citrifolia* plant cells were killed due to their interaction with eddies in the inertial convection subrange.

8.7 The experimental data illustrated a first order dependence of the extent of breakup of aggregates of *Corynebacterium glutamicum* with respect to the maximum energy dissipation rate in the impeller zone of the bubble free reactor and in the wall region of the flow capillary. This is in agreement with the proposed model.

8.8 In the microbial cell death model it was assumed that the specific cell strength was a function of the cell size, cell envelope thickness and cell envelope composition. Furthermore it was assumed that the strength of the cell envelope may decrease with hydrodynamic stress exposure time owing to a fatigue effect *i.e.*

$$\sigma_{CELL} = f(d_C,\delta,\chi)\ (eN)^{-y} \qquad (124)$$

The rate of cell death by viscous forces was therefore given by:

$$\frac{dC_V}{dN} = B_5 \frac{\mu}{f(d_C,\delta,\chi)\ d_C^2} (eN)^y \left(\frac{e}{\nu}\right)^{1.0} C_V \qquad (125)$$

The rate of cell death by inertial forces was given by:

$$\frac{dC_V}{dN} = B_6 \frac{\mu}{f(d_C,\delta,\chi)\ d_C^2} (eN)^y \left(\frac{e}{\nu}\right)^{1.0} C_V \qquad (126)$$

8.10 After a few exposures of hybridoma cells to extreme energy dissipation rates in a turbulent flowloop system (Zhang *et al.*, 1993), fatigue effects were shown to be negligible as the rate of cell death was proportional to $e_{MAX}^{1.0}$. However after many exposures at milder energy dissipation rates in a stirred tank (Zhang *et al.*, 1995), the energy dissipation rate exponent was shown to be less than 1. This indicated a significant increase in the cell membrane strength of the population with exposure time due to the preferential breakage of weaker cells. Complete understanding of fatigue requires a synchronised population and an increase in the number of exposures to hydrodynamic stress. Al-Rubeai *et al.* (1995) observed the fatigue of hybridomas after a considerably longer exposure time to forces in a stirred tank reactor.

8.10 The data of *Morinda citrifolia* plant cell death obtained in a turbulent capillary flow system (Kieran *et al.*, 1995) showed that the exponent of the energy dissipation rate in Equation 126 was 0.4. The strength of the plant cells therefore increased with cumulative stress due to the preferential destruction of the more susceptible cells.

8.11 Exposure of microbial cells to flow conditions in the sparged stirred tank showed

that the interaction of microbial cells with turbulent eddies in the viscous dissipation subrange in the impeller discharge zone, as well as with collapsing air bubbles at the air medium interface in a stirred tank reactor contributed to the total force acting on the cells. Comparison of breakage in a sparged stirred tank reactor and airlift reactor confirmed that small bubbles at higher frequencies were more detrimental to microbial cells.

Examples of process situations where the cell model of the interaction between cells or aggregates and turbulent eddies is applicable include pumping circuits, separation devices and disruption equipment. In aerated growing systems, a modified hydrodynamic stress model is required to take into account both the interaction of cells with turbulent eddies in the impeller discharge zone and with collapsing air bubbles at the air medium interface. In order to incorporate the contribution of collapsing air bubbles into the disruption model, it is necessary to take into account the degree of bubble cell attachment (dependent on the concentration of surface active agents such as Pluronic F-68 and antifoam), the frequency of bubble collapse (dependent on bubble frequency), the frequency with which a cell attaches to bubbles (determined by the circulation time), and the ratio of the disruptive force (dependent on the bubble size) to the strength of the aggregate or cells. It is recommended that rigorous studies be carried out to determine the effect of bubble size, bubble frequency, surface active agents and circulation time on the extent of aggregate breakup or cell death. An accurate method of determining the bubble size distribution at the air medium interface is required.

9. REFERENCES

Abu-Reesh, I., Kargi, F., (1989), "Biological responses of hybridoma cells to defined hydrodynamic stress", *Journal of Biotechnology*, **9**, 167-178.

Al-Rubeai, M., Oh, S.K.W., Musaheb, R., Emery, A.N., (1990), "Modified cellular metabolism in hybridomas subjected to hydrodynamic and other stresses", *Biotechnology Letters*, **12**, 323-328.

Al-Rubeai, M., Singh, R.P., Emery, A.N., Zhang, Z., (1995a), "Cell cycle and cell size dependence of susceptibility to hydrodynamic forces", *Biotechnology and Bioengineering*, **46**, 88-92.

Al-Rubeai, M., Singh, R.P., Goldman, M.H., Emery, A.N., (1995b), "Death mechanisms of animal cells in conditions of intensive agitation", *Biotechnology and Bioengineering*, **45**, 463-472.

Ando, J.T., Kamiya, A., Korenaga, R., Ohtsuka, A., (1991), "Effect of extracellular ATP level on the flow induced calcium response in cultured endothelial cells", *Biochemical Biophysics Res. Communications*, **179**, 1192-1199.

Atkinson, B., Mavituna, F., (1983), In "*Biochemical Engineering and Biotechnology Handbook*", Macmillan, New York.

Augenstein, D.C., Sinskey, A.J., Wang, D.I.C., (1971), "Effect of shear on the death of two strains of mammalian tissue cells", *Biotechnology and Bioengineering*, **12**, 409-418.

Ayazi Shamlou, P.M., Jones, A.G., Djamarani, K., (1990), "Hydrodynamics of secondary nucleation in suspension crystallization", *Chemical Engineering Science*, **45**, 1405-1416.

Ayazi Shamlou, P., Siddiqi, S.F., Titchener-Hooker, N.J., (1995), "A physical model of high-pressure disruption of baker's yeast cells", *Chemical Engineering Science*, **50**, 1383-1391.

Ayazi Shamlou, P., Titchener-Hooker, N., (1993), In "*Processing of Solid-Liquid Suspensions*", Ed., Ayazi Shamlou, Academic Press, New York, 1-191.

Bailey, J.E., Ollis, D.F., (1986), In "*Biochemical Engineering Fundamentals*", Eds., K. Verma amd C.C Martin, McGraw-Hill, Singapore, 228-280.

Barthole, J.P., Maisonneuve, J., Gence, J.N., David, R., Mathieu, J., Villermaux, J., (1983), "Measurement of mass transfer rates, velocity and concentration fluctuations in an industrial stirred tank", *Chemical Engineering Fundamentals*, **1**, 17-26.

Batchelor, G.K., In "*The Theory of Homogenous Turbulence*", Cambridge University Press, Cambridge.

Bates, R.L., Fondy, P.L., Corpstein, R.R., (1963), "An examination of some geometric parameters of impeller power", *Industrial Engineering Chemical Process Design and Development*, **2**, 310-314.

Bates, R.L., Fondy, P.L., Fenic, J.G., (1966), In "*Mixing: Theory and Practice 1*", Eds., V.W Uhl and J.B Gray, Academic Press, New York and London.

Bello, R., Robinson, C.W., Moo-Young, M., 1984, "Liquid circulation and mixing characteristics of airlift contactors", *Canadian Journal of Chemical Engineering*, **62**, 573-577.

Bhavaraju, S.M., Russel, T.W.F., Blanch, H.W., (1978), *AIChE Journal*, **24**, 454.

Blanch, H.W., Bhavaraju, S.M., (1976), "Non-newtonian fermentation broths: rheology and mass transfer", *Biotechnology and Bioengineering*, **18**, 745-790.

Born, C., Zhang, Z., Al-Rubeai, M., Thomas,C.R., (1992), "Estimation of disruption of animal cells by laminar shear stress", *Biotechnology and Bioengineering*, **40**, 1004-1010.

Boulton-Stone, J.M., Blake, J.R., (1993), "Gas bubbles at the free surface", *Journal of Fluid Mechanics*, **254**, 437-466.

Bronnenmeier, R., Märkl, H., (1982), "Hydrodynamic stress capacity of microorganisms", *Biotechnology and Bioengineering*, **26**, 553-578.

Brown, D.L., Glatz, C.E., (1987), "Aggregate breakage in protein precipitation", *Chemical Engineering Science*, **42**, 1831-1839.

Bryant, R.S., Sadeghzadeh, S., (1979), *Proc. 4th Eur. Conf. on Mixing*, University of York, York, England, BHRA Fluid Eng., Cranfield, England, 325.

Büschelberger, H.G., Loncin, M., (1989), "Wissenschaftliche Forscungsarbeit", *Chem.-Ing.-Tech.*, **61**, 420-421.

Calabrese, R.V., Stoots, C.M., (1989), "Flow in the impeller region of a stirred tank", *Chemical Engineering Progress*, **85**, 43-50.

Calderbank, P.H., (1958), "Physical rate processes in industrial fermentation. II. Mass transfer coefficients in gas liquid contacting with and without mechanical agitation", *Trans. Inst. Chem. Eng.*, **36**, 443.

Chalmers, J.J., Bavarian, F., (1991), "Microscopic visualisation of insect cell-bubble interactions. II: the bubble film and bubble rupture", *Biotechnology Progress* **7**, 151-158.

Chandrasekhar, K. and Calderbank, P.H., (1981), "Further observations on the scale-up of aerated mixing vessels", *Chemical Engineering Science*, **36**, 819-823.

Chen, K.Y., Hajduk, J.C., Johnson, J.W., (1988), "Laser-doppler anemometry in a baffled mixing tank", *Chemical Engineering Communication*, **72**, 141-157.

Cherry, R.S., Papoutsakis, E.T., (1986), "Hydrodynamic effects on cells in agitated tissue culture reactors", *Bioprocess Engineering*, **1**, 29-41.

Chiampo, F., Marotto, R., (1995), "Flow regimes in gas-liquid reactors stirred with dual Rushton turbines", *The 1995 IChem Research Event/First European Conference*, 689-691.

Chisti, M.Y., Moo-Young, M., (1987), "Airlift reactors: characteristics, applications and design considerations", *Chemical Engineering Communications*, **60**, 195-242.

Chisti, M.Y., Moo-Young, M., (1988), "Prediction of liquid circulation velocity in airlift reactors with biological media", *Journal of Chemical Technology and Biotechnology*, **42**, 211-219.

Chisti, M.Y., Moo-Young, M., (1993), "Improve the performance of airlift reactors", *Chemical Engineering Progress*, **89**, 38-45.

Cooper, R.G., Wolf, D., (1968), "Velocity profiles and pumping capacities for turbine type impellers", *Canadian Journal of Chemical Engineering*, **46**, 94-100.

Costes, J., Couderc, J.P., (1988), "Study by laser Doppler anemometry of the turbulent flow induced by a Rushton turbine in a stirred tank: influence of the size of the units-I.mean flow and turbulence", *Chemical Engineering Science*, **43**, 2751-2764.

Cutter, L.A., (1966), "Flow and turbulence in a stirred tank", *AIChE Journal*, **12**, 35-45.

Dabee, S., Harrison, S., (1996), In "*Maximising O_2 Transfer and Minimising Shear Damage in the Microbial Production of GLA by Mucor Rouxii*", Master of Science, Chemical Engineering, University of Cape Town.

Dahlback, B., Hermansson, M., Kjelleberg, S., Norkans, B., (1981), "The hydrophobicity of bacteria-an important factor in their initial adhesion at the air water interface", *Arch. Microbiology*, **128**, 267-270.

Deindoerfer, F.H., Gaden, E.L., (1955), "Effect of liquid physical properties on O_2 transfer in penicillin fermentation", *Applied Microbiology*, **3**, 253-257.

Doelle, H.W., Ewings, K.N., Hollywood, N.W., (1983), *Advanced Biochemical Engineering*, **23**, 1

Drblohlav, J., Fort, I., Maca, K., Placek, J., (1978), "Studies on mixing. IL. Turbulent characteristics of discharge flow from a turbine impeller", *Coll Czech Chem Commun*, **43**, 3148-3162.

Dunlop, E.H., Namdev, P.K., Rosenberg, M.Z., (1994), "Effect of fluid shear forces on plant cell suspensions", *Chemical Engineering Science,* **49**, 2263-2276.

Durst, F., Melling, A., Whitelaw, J,H., (1976), In *Principles and Practice of Laser Doppler Anemometry*, Academic Press, New York.

Dussop, G., Gros, J.B., (1982), "Energy consumption and interfacial mass transfer in an airlift fermenter", *Chemical Engineering Journal*, **25**, 151-162.

Edwards, N., Beeton, S., Bull, A.T., Merchuk, J.C., (1989), "A novel device for the assessment of shear effects on suspended microbial cultures", *Applied Microbial Technology*, **30**, 190-195.

Einsele, A., (1978), "Scaling up bioreactors", *Process Biochemistry*, 13-14.

Falke, L., Edwards, K.L., Misler, S., Pickard, B.G., (1986), "A mechanotransductive ion channel in patches from cultured tobacco cell plasmalemma", *Plant Physiology*, **80**, 9.

Fazekas de St. Groth, S., (1983),"Automated production of monoclonal antibodies in a cytostat", *Journal of Immunological Methods*, **57**, 121-136.

Fowler, J.D., Robinson, C.R., (1991), "Metabolic behaviour of immobilized aggregates of *Escherichia coli* under conditions of varying mechanical stress", *Applied and Environmental Microbiology*, 93-101.

Garcia-Briones, M.A., Chalmers, J.J., (1994), "Flow parameters associated with hydrodynamic injury", *Biotechnology and Bioengineering*, **44**, 1089-1098.

Gardner, A.R., Galner, J.L., Kirwan, D.J., (1990), "Effects of stirring and sparging on cultured hybridoma cells", *Biotechnology and Bioengineering*, **35**, 940-947.

Glasgow, B.A., (1989), "Effects of the physiochemical environment on floc properties", *Chemical Engineering Progress*, **85**, 51-62.

Gray, P.P., Dunnill, P., Lilly, M.D., (1972), In "*Fermentation Technology Today*", Ed, G. Terui, Society for Fermentation Technology, Japan, 347-351.

Gunkel, A.A., Weber, M.E., (1975), "Flow phenomena in stirred tanks", *AIChE Journal*, **21**, 931-949.

Gusek, T.W., Johnson, R.D., Tyn, M.T., Kinsells, J.E., (1991), "Effect of agitational shear on growth and protease production by *Thermomonospora fusca*", *Biotechnology and Bioengineering*, **37**, 371-374.

Gustin, M.C., Martinac, B., Saimi, Y., Culbertson, M.R., Kung, C., (1986),"Ion channels in yeast", *Science*, **233**, 1195-1197.

Handa-Corrigan, A., Emery, A.N., Spier, R.E., (1989), "Effect of gas-liquid interfaces on the growth of suspended mammalian cell: mechanisms of cell damage by bubbles", *Enzyme Microbial Technology*, **11**, 230-235.

Hicks, R.W., Gates L.E., (1976), "How to select turbine agitators for dispersing gas into liquids", *Chemical Engineering*, 141-148.

Hinze, J.O., (1955), "Fundamentals of the hydrodynamic mechanism of splitting up in dispersion processes", *AIChE Journal*, **1**, 289-295.

Holmes, D.B., Voncken, R.M., Dekker, J.A., (1964), "Fluid flow in turbine-stirred, baffled tanks-I", *Chemical Engineering Science*, **19**, 201-208.

Hooker, B.S., Lee, J.M., An, G.A., (1989), "Response of plant tissue culture to a high shear environment", *Enzyme Microbial Technology*, **11**, 484-490.

Joshi, J.B., Pandit, A.B., Sharma, M.M., (1982), "Mechanically agitated gas-liquid reactors", *Chemical Engineering Science*, **37**, 813-844.

Kargi, F., Moo-Young, M., (1985), In "*Comprehensive Biotechnology*", Ed, Moo-Young, M., Vol 2, Pergamon, Oxford.

Kawase, Y., Moo-Young, M., (1990), "Mathematical models for the design of bioreactors: applications of Kolmogoroff's theory of isotropic turbulence", *Chemical Engineering Journal*, **43**, 19-41.

Kieran, P.M., O'Donnel, H.J., Malone, D.M., MacLoughlin, P.F., (1995), "Fluid shear effects on suspension cultures of *Morinda citrifolia*", *Biotechnology and Bioengineering*, **45**, 415-425.

Kiss, R.D., Stephanopoulos, G. (1991), "Metabolic activity control of the L-lysine fermentation by restrained growth fed-batch strategies", *Biotechnology Progress*, **7**, 501-509.

Kjelleberg, S., (1985), In "*Bacterial adhesion: mechanisms and physiological significance*", Eds D.C Savage and M. Fletcher, Plenum, New York, 163-194.

Kolmogorov, A.N., (1941), "The local structure of turbulence in incompressible viscous fluid for very large Reynold's numbers", *C.R.Acad. Scie.*, URSS, **30**, 301.

Komasawa, I., Kuboi, R., Otake, T., (1974), "Fluid and particle motion in turbulent dispersion", *Chemical Engineering Science*, **29**, 641-650.

Kunas, K.Y., Papoutsakis, E.T., (1990), "Damage mechanisms of suspended animal cells in agitated bioreactors with and without bubble entrainment", *Biotechnology and Bioengineering*, **36**, 476-483.

Laufer, J., 1954, "The structure of turbulence in fully developed pipe flow", *National Advisory Committee for Aeronautics Report 1174*, 1-18.

Laufhutte, H.D., Mersmann, A.B., (1985), "Dissipation of power in stirred vessels", *5th European Conference on Mixing*, Wurzburg, Germany, 331-340.

Leckie, F., Scraggs, A.H., Cliffe, K.R., (1991), "Effect of impeller design and speed on large-scale cultivation of suspension cultures of *Caranthus roseus*", *Enzyme Microbial Technology*, **13**, 801-809.

Lee, G.M., Huard, T.K., Kaminski, M.S., Palsson, B.O., "Effect of mechanical agitation on hybridoma cell growth", *Biotechnology Letters*, **10**, 625-628.

Lee, G.M., Savinell, J.M., Palsson, B.O., (1989), "Serum can act as a shear protecting agent in agitated hybridoma cell cultures", *Hybridoma*, **8**, 639-645.

Levich, V.G., 1962, In *Physiochemical Hydrodynamics*, Prentice-Hall Inc, New York.

Lintilhac, P.M., Vasecky, T.B., (1984), "Stress induced alignment of division plane in plant tissues grown in vitro", *Nature*, **307**, 363-364.

Lloyd, C.W., (1982), In "*The Cytoskeleton in Plant Growth and Development*", Academic Press, New York.

Logan, B.E., Wilkinson, D.B., (1991), "Fractal dimensions and porosities of *Zoogloea ramigera* and *Saccharomyces cerevisiae* aggregates", *Biotechnology and Bioengineering*, **38**, 389-396.

Loiseau, B., Midoux, N., Charpentier, J., (1977), "Some hydrodynamics and power input data in mechanically agitated gas-liquid contactors", *AIChE Journal*, **23**, 931-935.

Lowry, O.H., Rosebrough, N.J., Farr, N.J., Randall, R.J., (1951), "Protein measurement with Folin reagent", *Journal of Biological Chemistry*, **193**, 265-275.

Majumdar, A.S., Huang, M., Wolf, D., Weber, M.E., Douglas, W.J.M., (1970), "Turbulence parameters in a stirred tank", *Canadian Journal of Chemical Engineering*, **48**, 475-483.

Märkl, H., Bronnenmeier, R., (1985), In "*Biotechnology*", Vol 2, Eds., H.J Rehm, New York, 369-393.

Matsuo, T., Unno, H., (1981), "Forces acting on floc and strength of floc", *Journal of Environmental Engineering Divisions*, **107**, 527-545.

Meneveau, C., Sreenivasan, K.R., (1991), "The multifractal nature of turbulent energy dissipation", *Journal of Fluid Mechanics*, **224**, 429-484.

Mersmann, A., Schneider, G., Voit, H., Wenzig, E., (1990), "Selection and design of aerobic bioreactors", *Chemical Engineering Technology*, **13**, 357-370.

McQueen, A.,Meilhoc, E., Bailey, J.E., (1987), "Flow effects on the viability and lysis of suspended mammalian cells", *Biotechnology Letters*, **9**, 831-836.

Michaels, J.D., Nowak, J.E., Mallik, A.K., Koczo, K., Wasan, D.T., Papoutsakis, E.T., (1995), "Analysis of cell-to-bubble attachment in sparged bioreactors in the presence of cell protecting additives", *Biotechnology and Bioengineering*, **47**, 407-419.

Michel, B.J., Miller, S.A., (1962), "Power requirements of gas liquid agitated systems", *AIChE Journal,* **13**, 262-266.

Midler, M., Finn, R.K., (1966), "A model system for evaluating shear in the design of stirred fermenters", *Biotechnology and Bioengineering*, 8, 71-84.

Mitard, A., Riba, J.P., "Morphology and growth of *Aspergillus niger* ATCC 26036 cultivated at several shear rates", *Biotechnology and Bioengineering*, **32**, 835-840.

Moreira, J.L., Cruz, P.E., Santana, P.C., (1995), "Formation and disruption of animal cell aggregates in stirred vessels: mechanisms and kinetic studies", *Chemical Engineering Science*, **50**, 2747-2764.

Moreira, J.L., Alves, P.M., Aunins, J.G., Carrondo, M.J.T., (1995b), "Hydrodynamic effects on BHK cells grown as suspended natural aggregates", *Biotechnology and Bioengineering*, **46**, 351-360.

Mukutaka, S., Kataoka, H., Takahashi, J., (1981), "Circulation time and degree of fluid exchange between the upper and lower circulation regions in a stirred vessel with a dual impeller", *Journal of Fermentation Technology*, **59**, 303-307.

Nakatani, Y., Fujioka, M., Higashino, K., (1972), "Enzymatic determination of L-lysine in biological materials", *Analytical Biochemistry*, **49**, 225-231.

Neseratnam, S.T., Wase, D.A.J., Blakebrough, N., (1982), "The susceptibility to ultrasonic disentigration of *Klebsiella pneumonia* NCTC 418", *European Journal of Applied Microbiology and Biotechnology*, **15**, 56-58.

Nienow, A.W., Miles, D., (1971), "Impeller power numbers in closed vessels", *Ind. Eng. Chem. Process Des. Develop.*, **10**, 41-43.

Nollert, M.U., Diamond, S.L., McIntre, L.V., (1991), "Hydrodynamic shear stress and mass transport modulation of endothelial cell metabolism", *Biotechnology and Bioengineering*, **38**, 588-602.

O'Connel,F.P., Mack, D.E., (1950), "Simple turbines in fully baffled tanks", *Chemical Engineering Progress*, **46**, 358-362.

O'Connor, C.T., Randall, E.W., Goodall, C.M., (1990), "Measurement of the effects of physical variables on bubble size", *International Journal of Mineral Processing*, **28**, 139-149.

Oh, S.K.W., Nienow, A.W., Al-Rubeai, M., Emery, A.N., (1989), "The effects of agitation intensity with and without continuous sparging on the growth and antibody production of hybridoma cells", *Journal of Biotechnology*, **12**, 45-62.

Okamoto, Y., Nishikawa, M., Hashimoto, K., (1981), "Energy dissipation rate distribution in mixing vessels and its effects on liquid-liquid dispersion and solid-liquid mass transfer", *International Chemical Engineering*, **21**, 88-94.

Özbas, T., Kutsal, T., (1991), "Effects of agitation and aeration rates on riboflavin fermentation by *Ashbya gossypii*", *Biotechnology and Applied Biochemistry*, **13**, 97-105.

Parker, D.S., Asce, A.M., Kaufman, W.J., Asce, M., Jenkins, D., (1972), "Floc breakup in turbulent flocculation processes", *Journal of Sanitary Engineering Division*, 79-99.

Peterson, J.F., McIntire, L.V., Papoutsakis, E.T., (1990), "Shear sensitivity of hybridoma cells in batch, fed-batch, and continuous cultures", *Biotechnology Progress*, **6**, 114-120.

Pickard, B.G., (1984), "Voltage transients elicited by sudden step-up of auxin", *Plant Cell Environment*, **7**, 171-178.

Placek, J., Tavlarides, L.L., (1985), "Turbulent flow in stirred tanks. Part I: Turbulent flow in the turbine impeller region", *AIChE Journal*, **31**, 1113-1120.

Poncelet, D., Neufeld, R.J., (1989), " Shear breakage of nylon membrane microcapsules in a turbine reactor, *Biotechnology and Bioengineering*, **33**, 95-103.

Prokop, A., Bajpai, R.K., (1992), "The sensitivity of biocatalysts to hydrodynamic shear stress", *Advances in Applied Biochemistry*, **37**, 165-233.

Ramirez, O.T., Mutharasan, R., (1990), "The role of the plasma membrane fluidity on the shear sensitivity of hybridomas grown under hydrodynamic stress", *Biotechnology and Bioengineering*, **36**, 911-920.

Ranz, W.E., (1958), "Electrolytic methods of measuring water velocities", *AIChE Journal*, **4**, 338-342.

Rao, M.A., Brodkey, R.S., (1972), "Continuous flow stirred tank turbulence parameters in the impeller stream", *Chemical Engineering Science*, **27**, 137-156.

Ranada, V.V., Joshi, J.B., (1990), "Flow generated by a disc turbine: Part I Experimental", *Trans IChemE*, **68**, 19-33.

Reuß, M., (1988), "Influence of mechanical stress on the growth of *Rhizopus nigricans* in stirred bioreactors", *Chemical Engineering Technology*, **11**, 176-187.

Robinson, C.W., Wilke, C.R., (1973), "Oxygen absorption in stirred tanks: a correlation for ionic strength effects", *Biotechnology and Bioengineering*, **15**, 755-782.

Ruklisha, M.P., Vanags, J.J., Rikmanis, M.A., Toma, M.K., Viesturs, U.E., (1989), "Biochemical reactions of *Brevibacterium flavum* depending on medium stirring intensity and flow structure", *Acta Biotechnology*, **9**, 565-575.

Rushton, J.H., Costich, E.W., Everett, H.J., (1950), "Power characteristics of mixing impellers", *Chemical Engineering Progress*, **46**, 467-476.

Sato, M., Ishii, K., Horie, Y., Kawimano, M., Yamamoto, K., (1967), "Turbulent flow in a stirred vessel", *Kagaku Kogaku*, **34**, 104-111.

Smith, C.G., Greenfield, P.F., Randerson, D.H., (1987), "A technique for determining the shear sensitivity of mammalian cells in suspension culture", *Biotechnology Techniques*, **1**, 39-44.

Smith, J.J., Lilly, M.D., Fox, R.I., (1990), "The effect of agitation on the morphology and penicillin production of *Penicillin chrysogenum*", *Biotechnology and Bioengineering*, **35**, 1011-1023.

Smith, T.J., Reilly, C.D., (1992), "Predictions of the flow in fermenters and the implications for scale-up", *2nd International Conference on Bioreactor Fluid Dynamics*, Ed., R. King, 431-439.

Solomons, G.L., Perkin, M.D., (1958), "The measurement and mechanism of O_2 transfer in submerged culture", *Journal of Applied Chemistry*, **8**, 251-259.

Stent, G.S., Calendar, R., (1978), In "*Molecular Genetics: An Introductory Narrative*", W.H. Freeman and Co, San Fransisco, 76.

Stockbridge, L.L., French, A.S., (1988), "Stretch activated cation channels in human fibroplasts", *Biophysics Journal*, **54**, 187-190.

Stoots, R.V., and Calabrese, C.M., (1989), "Flow in the impeller region of a stirred tank", *Chemical Engineering Progress*, 43-50.

Tan, W.S., Chen, Y.L., Dai, G.C., (1993), "Growth and damage of continuous suspension cultured hybridoma cells in an agitated bioreactor with and without bubble entrainment or sparging", *3rd International Conference on Bioreactor and Bioprocess Fluid Dynamics*, Cambridge,153-159.

Toma, M.K., Ruklisha, M.P., J.J., Zeltina, M.O., Leite, M.P., Galinina, N.I., Viesturs, U.E., Tengerdy, R.P., (1991), "Inhibition of microbial growth and metabolism by excess turbulence", *Biotechnology and Bioengineering*, **38**, 552-556.

Tramper, J., Williams, J.B., Joustra, D., Vlak, J.M., (1986), "Shear sensitivity of insect cells in suspension", *Enzyme Microbial Technology*, **8**, 33-36.

Trinh, K., Garcia-Briones, M., Hink, F., Chalmers, J.J., (1994), "Quantification of damage to suspended insect cells as a result of bubble rupture", *Biotechnology and Bioengineering*, **43**, 37-45.

Tsouris, C., Tavlarides, L.L., (1994), "Breakage and coalescence for drops in turbulent dispersions", *AIChE Journal*, **40**, 395-406.

Ujcovo, E., Fencl, Z., Musilkova, M., Seichert, L., (1980), "Dependence of release of nucleotides from fungi on fermenter turbine speed", *Biotechnology and Bioengineering*, **22**, 237-241.

Vanags,J.J., Rikmanis, M.A., Ushkans, U.E., Viesturs, U.E., (1990), "Stirring characteristics in bioreactors", *AIChE Journal*, **36**, 1361-1369.

Van der Molen, K., Van Maanen, H.R.E., (1978), "Laser Doppler measurements of the turbulent flow in stirred vessels", *Chemical Engineering Science*, **33**, 1161-1168.

Van 't Riet, K., Smith, J.M., (1975), "The trailing vortex system produced by Rushton turbine agitators", *Chemical Engineering Science*, **30**, 1093-1105.

Van't Riet, K., (1979), "Review of measurement methods and results in nonviscous gas-liquid mass transfer in stirred vessels", *Industrial Engineering Chemistry Process Design and Development*, **18**, 357-364.

van Suijdam, J.C., Metz, B., (1981), "Influence of engineering variables upon the morphology of filamentous molds", *Biotechnology and Bioengineering*, **23**, 111-148.

Vrana, D., Votruba, J., Placek, J., (1982), "Age related changes in the physiology state of budding yeast cells", *Experimental Cell Research*, **138**, 57-62.

Wase, J.D.A., Patel, Y.R., (1985), "Variations in the volumes of microbial cells with change in the agitation rates of chemostat cultures", *Journal of General Microbiology*, **131**, 725-736.

Watt, F.M., (1986), *Trends in Biochemical Science*, **11**, 482.

Wu, H., Patterson, G.K., (1989), "Laser-doppler measurements of turbulent flow parameters in a stirred tank", *Chemical Engineering Science*, **44**, 2207-2221.

Yianneskis, M., Popiolek, Z., Whitelaw, J.H., (1987), "An experimental study of the steady and unsteady flow characteristics of stirred reactors", *Journal of Fluid Mechanics* **175**, 537-555.

Yung, C.N., Wong, C.W., Chang, C.L., (1979), "Gas holdup and aerated power consumption in mechanically stirred tanks", *The Canadian Journal of Chemical Engineering*, **57**, 672-676.

Zhang, Z., Al-Rubeai, M., Thomas, C.R., (1992a), "Mechanical properties of hybridoma cells in batch culture", *Biotechnology Letters*, **14**, 11-16.

Zhang, Z., Al-Rubeai, M., Thomas, C.R., (1992b), "The effect of Pluronic-F68 on the mechnical properties of mammalian cells", *Enzyme Microbial Technology*, **14**, 980-983.

Zhang, Z., Al-Rubeai, M., Thomas, C.R., (1993), "Estimation of disruption of animal cells by turbulent capillary flow", *Biotechnology and Bioengineering*, **42**, 987-993.

Zhang, Z., Al-Rubeai, M., Thomas, C.R., (1995), "Preliminary modelling of animal cell disruption in a closed stirred tank", *The 1995 Research Event/First European Conference*, 1088-1090.

Zhang, S., Handa-Corrigan, A., Spier, R.E., (1992c), "Foaming and media surfactant effects on the cultivation of animal cells in stirred and sparged bioreactors", *Journal of Biotechnology*, **25**, 289-306.

Zhang, Z., Ferenczi, M.A., Thomas, C.R., (1992d), "A micromanipulation technique with a theoretical cell model for determining mechanical properties of single mammalian cells, *Chemical Engineering Science*, **47**, 1347-1354.

Zhang, Z., Thomas, C.R., (1996), "Using eddy number distribution in turbulent flows to describe direct cell-eddy interactions", *Fluid Particle Interactions IV*, Engineering Foundation, Davos, Switzerland.

APPENDIX A

A.1 BIOCHEMICAL ANALYTICAL PROCEDURES

A.1.1 Plate counts

Cell samples were diluted in sterile water containing g/l peptone so that plates contained between 10 and 300 colonies. In the plate count procedure, 0.1 ml of diluted cell sample was spread on the agar plates with a sterile glass rod. The colonies were counted after 2 days incubation in a 30 °C oven.

A.1.2 Dry weight

Empty 1.5 ml micro-centrifuge tubes were dried at 80 °C, cooled in a dessicator and pre-weighed to 4 decimal places. 1.5ml aliquots of cell sample were pipetted into the pre-weighed centrifuge tubes. The tubes were centrifuged and the supernatant poured off. The cell residue was washed twice with distilled water. The tubes were dried for 72 hrs in a 80 °C oven. Using forceps, the dried tubes were transferred to a dessicator and the dry mass determined to four decimal places. The difference between the weight of the empty tube and the sample tube, divided by 1.5ml gave the dry weight per unit volume. Dry weights were performed in triplicate. The error associated with the method was less than 5%.

A.1.3 Turbidity

Samples were placed in plastic cuvettes and the absorbance at 660nm determined against water. Where necessary samples were diluted so that the read absorbance was less than 1.4. The correlation of turbidity versus dry biomass yielded a linear relationship with a correlation coefficient of (Figure A1). The error of the method was less than 4%.

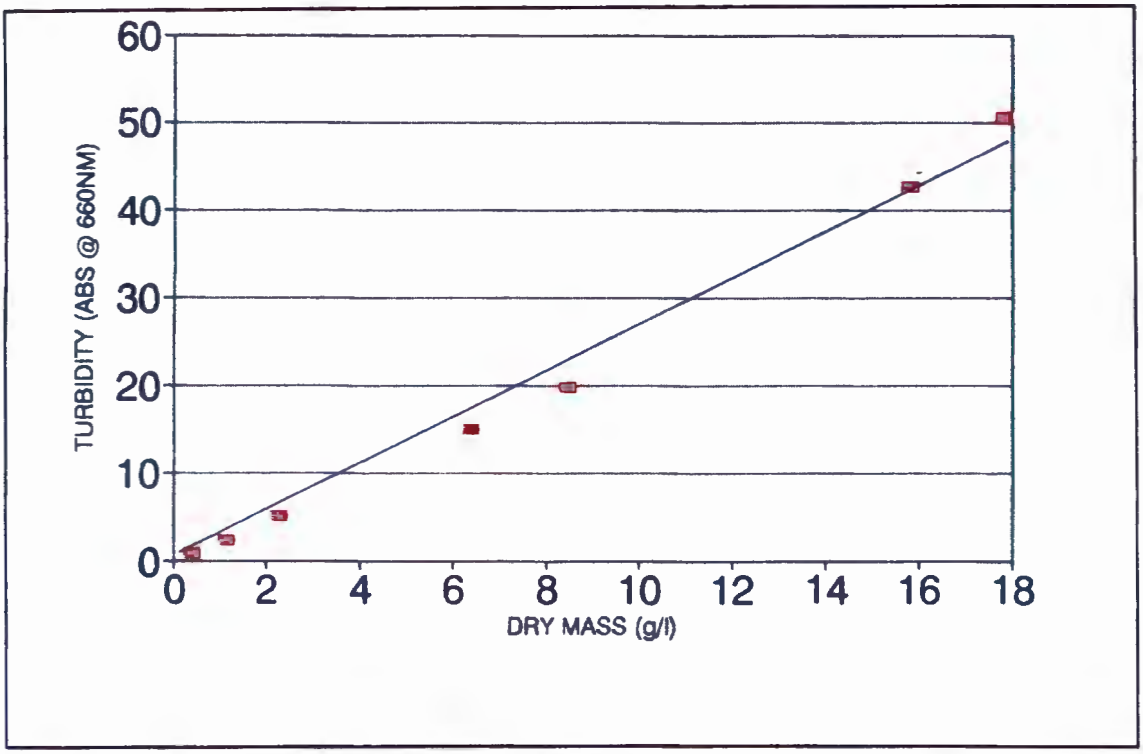

Figure A1 Turbidity versus dry biomass concentration.

A.1.4 Glucose

The glucose concentration was measured colorimetrically following its stoichiometric reaction to gluconate and H_2O_2 in the presence of glucose oxidase. The equlibrium of this reaction was maintained towards gluconate by constant removal of H2O2 by reaction with ABTS to form a coloured complex as shown by the reaction sequence:

$$glucose + O_2 + H_2O \xrightarrow{glucoseoxidase} gluconate + H_2O_2$$

$$H_2O_2 + ABTS \xrightarrow{peroxidase} colouredcomplex + H_2O$$

The coloured complex was quantified spectrophotometrically at 610 nm and is directly proprtional to the glucose concentration. ABTS is di-ammonium 2,2-azino-bis(3-ethylbenzothiazoline-6-sulphonate). Cell samples were centrifuged and the supernatant analysed using the a Boehringer Mannheim kit, catalogue number 124 036. In the assay procedure, 0.06 ml of diluted sample (0 to 0.5 g glucose/l) was mixed in a test tube with 3

ml of reagent solution and incubated at 20-25 °C. After 25-50 minutes, the absorbance was read at 610 nm against a reagent blank. The calibration curve showing the linear range of the assay is presented in Figure A2 (correlation coefficient 0.99). The method error was less than 4%.

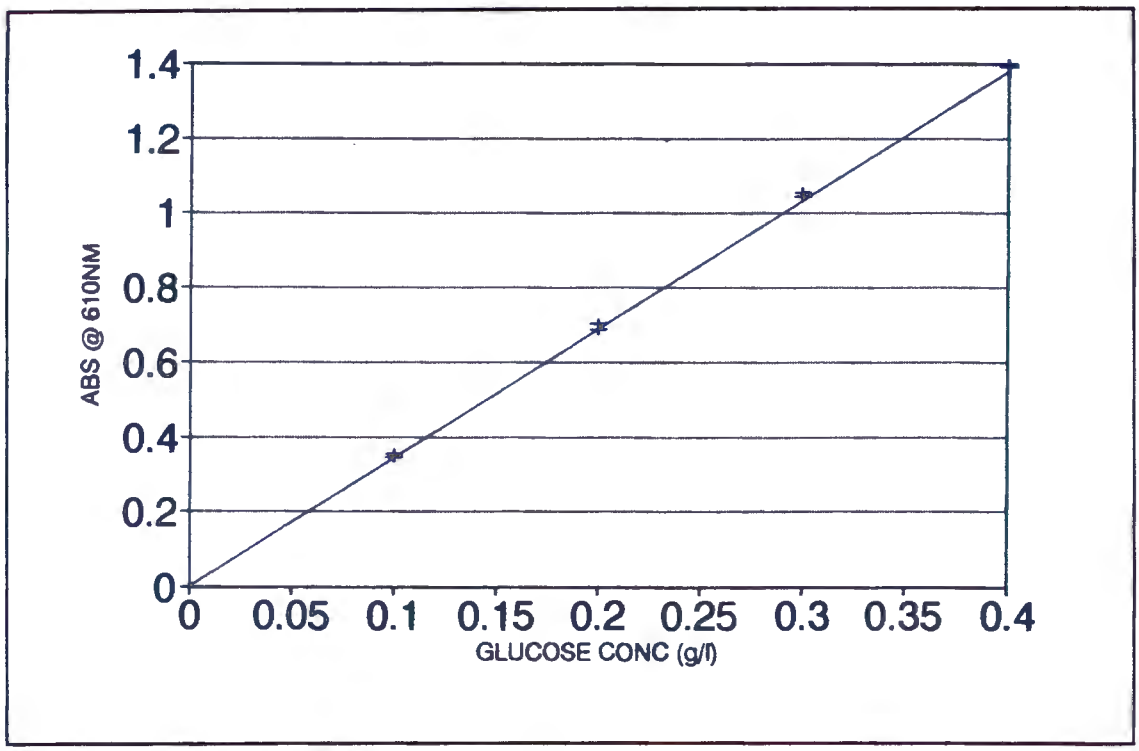

Figure A2 Glucose assay standard curve.

A.1.5 Oxygen utilisation rate

The oxygen utilisation rate measurement apparatus consisted of a Yellow Springs oxygen probe (model S739) fitted into the custom-made side port of a 125ml conical flask. The neck of the flask was closed with a tightly fitting rubber stopper housing a thermometer and a sparging tube. The flask contained a stirrer bar and was positioned on a magnetic stirrer.

The flask was filled with sterile medium consisting of (per liter): 5g glucose, 0.8g NaCl, 0.2g KI, 2.254g Na_2HPO_4 and 0.2g KH_2PO_4. The glucose was autoclaved separately from the other ingredients and the two components mixed after cooling. The medium was preheated in a 30 °C waterbath. The amount of medium used depended on the dilution ratio required *eg.* for a dilution ratio of 5, 100 ml of medium and 25 ml of sample were used.

The oxygen probe was zeroed by placing it in a saturated sodium sulphite solution. The probe was then calibrated by fitting it in the medium-containing flask saturated with oxygen at 30 °C. The bacterial sample was added after turning the stirrer speed down to 250 rpm and shutting off the air. The flask was then immediately stoppered. The entrapment of air bubbles was avoided by letting a small amount of solution leak out from the stopper.

The data recording system monitored the decrease in dissolved oxygen concentration with time. The data was regressed linearly to obtain the oxygen utilisation rate. A typical oxygen utilisation rate curve is presented in Figure A3. The error associated with the technique was less than 10%.

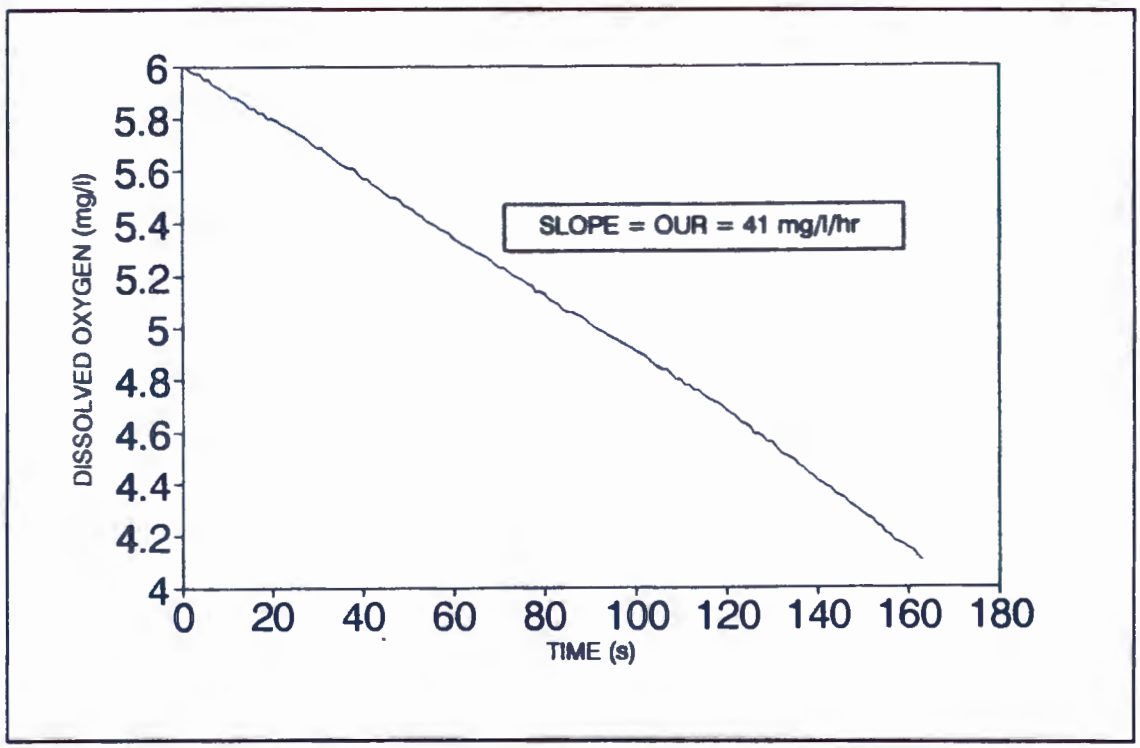

Figure A3 Oxygen utilisation rate data for *Corynebacterium glutamicum*.

A.1.6 Lysine

L-lysine was measured by a variation of an enzymatic assay (Nakatani *et al.*, 1972; Kiss and Stephanopoulos, 1991) using saccharopine dehydrogenase. The enzymatic assay is based on

the following reaction catalysed by saccharopine dehydrogenase:

L-lysine + α-ketoglutarate + NADH + H^+ $\rightleftarrows$ saccharopine + NAD^+ + H_2O

The reaction favours the formation of saccharopine ($K_{eq} \approx 10^{15}$). L-lysine is quantitated by following the decrease in the absorbance at 340nm due to NADH consumption. The assay protocol is as follows:

Reagent A: Prepare 0.25 M phosphate buffer (pH 6.8).
Reagent B: Dissolve 0.996 g $NaHCO_3$ in 100 ml distilled water.
Reagent C: Dissolve 25 g B NADH in 5 ml reagent B.
Reagent D: Dissolve 0.1 g α-ketoglutaric acid in 5 ml distilled water.
Reagent E: Dissolve 25 units saccharopine dehydrogenase in 1 ml distilled water.

2.5 ml reagent A, 0.1 ml reagent C, 0.1 ml reagent D and 0.1 ml of L-lysine standard (0 to 0.5 g/l) or 0.1 ml diluted sample supernatant were mixed in a test tube. The contents were transferred to a 4 ml cuvette and the absorbance at 340 nm (A_0) measured against phosphate buffer. After the addition of 0.02 ml reagent D to each cuvette, the solutions were incubated for 35 minutes at room temperature. The absorbance at 340 nm were measured (A_{35}). The difference between A_0 and A_{35} was linearly proportional to the lysine.HCl concentration in the range 0.05 to 0.5 g/l (correlation coefficient of 0.99) as shown in Figure A4.

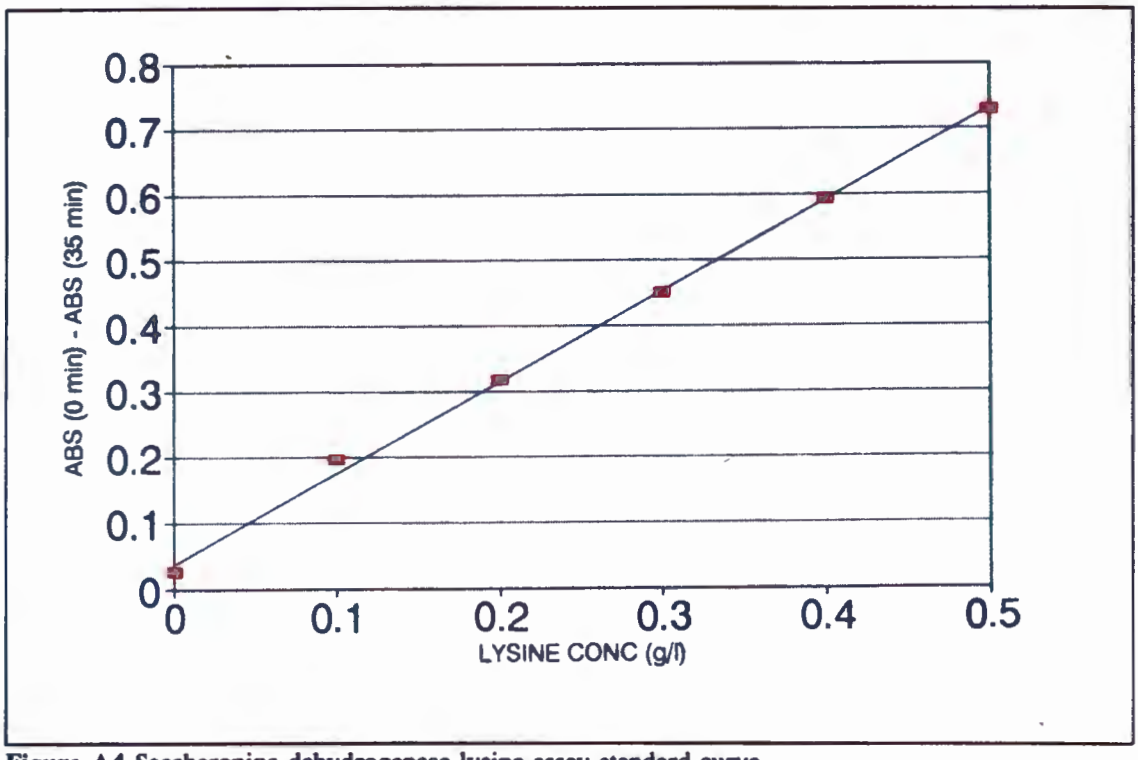

Figure A4 Saccharopine-dehydrogenase lysine assay standard curve.

A.1.7 HPLC amino acid analysis

Ion exchange chromotography with post column ninhydrin derivatization and visible colorometric detection is used in the Beckman System 6300 Series amino acid analyser. A cation exchange column was used. This has an insoluble matrix with positive charged groups covalently bonded to the outside of the matrix. Positive charged particles (acidic) pass more quickly than negative charged particles which are attracted to the matrix. Acidic amino acids therefore elute first, followed by neutral and basic amino acids. The separation of particles is also affected by molecular size, buffer pH, buffer ionic strength and temperature.

All amino acids differ in size (molecular weight), shape (side chains), charge (positive or negative) and chemical reactivity (hydrophilic or hydrophobic etc.).

In the preparation of the samples, 50 μl of AEC (aminoethylcysteine) was added to 1ml of supernatant sample. AEC is an internal standard that allows for dilution during sample preparation. The mixture was deproteinased with the addition of 100 μl 15% aqueous

sulfosalicyclic acid dihydrate and centrifuged for 5 min at 13000 rpm. 800 μl of the supernatant was filtered to remove all particles greater than 0.22 μm. The pH was adjusted to pH 2-2.2. The samples were stored in the fridge. For each sample set a standard sample, containing known standards of known concentration, was prepared.

In the HPLC run, 100 μl of prepared sample was loaded onto the coil and the analysis initiated. The run lasted 180 minutes. During the first 20 minutes a temperature of 38°C was maintained after which the temperature was increased to and held at 65°C.

Table A1 Elution procedure for amino acids in HPLC run.

TIME	BUFFER	PH
0-45 min	A	2.8
45-103 min	D	3.2
103-116 min	E	3.5
116-170 min	F	3.8

After the amino acids eluted, they reacted with ninhydrin to form a colour complex (purple) which was read by a colorimeter at 570 nm. Iminoacids (proline and hydroxyproline) reacted to form a yellow complex which was measured at 440 nm.

The results from the amino acid analyser are given as peak heights as a function of elution time. Each amino acid has a characteristic elution time. To calculate the unknown concentrations of amino acids in the sample, the peak height of the sample was compared with that of the known standard peak height as well as the peak height of AEC and the concentration calculated accordingly. The error associated with the method was less than 5%.

$$conc(unknown) = \frac{conc(standard)}{height(standard)} \times height(unknown) \times \frac{heightAEC(standard)}{heightAEC(unknown)}$$

A.1.8 Protein

A.1.8.1 Bio-rad protein assay

Protein analysis was carried out using the Bio-rad protein assay (Catalogue number 500-0006) for very dilute protein concentrations. The method is based on the differential colour change of an acidic solution of Coomassie Brilliant Blue G-250 when binding to protein occurs. The absorbance maximum shifts from 465 nm to 595 nm. In the assay procedure, 0.2 ml of dye reagent concentrate was added to 0.8 ml of diluted supernatant sample (0 to 0.025 g protein/l) in a 1.5ml cuvette. The cuvette was gently inverted several times. The absorbance was read at 595 nm against a reagent blank after 5 minutes. Measurements remained stable for 1 hour. A typical standard curve showing the linear range of the Bio-rad protein assay is presented in Figure A5. The straight line had a correlation coefficient of 0.98.

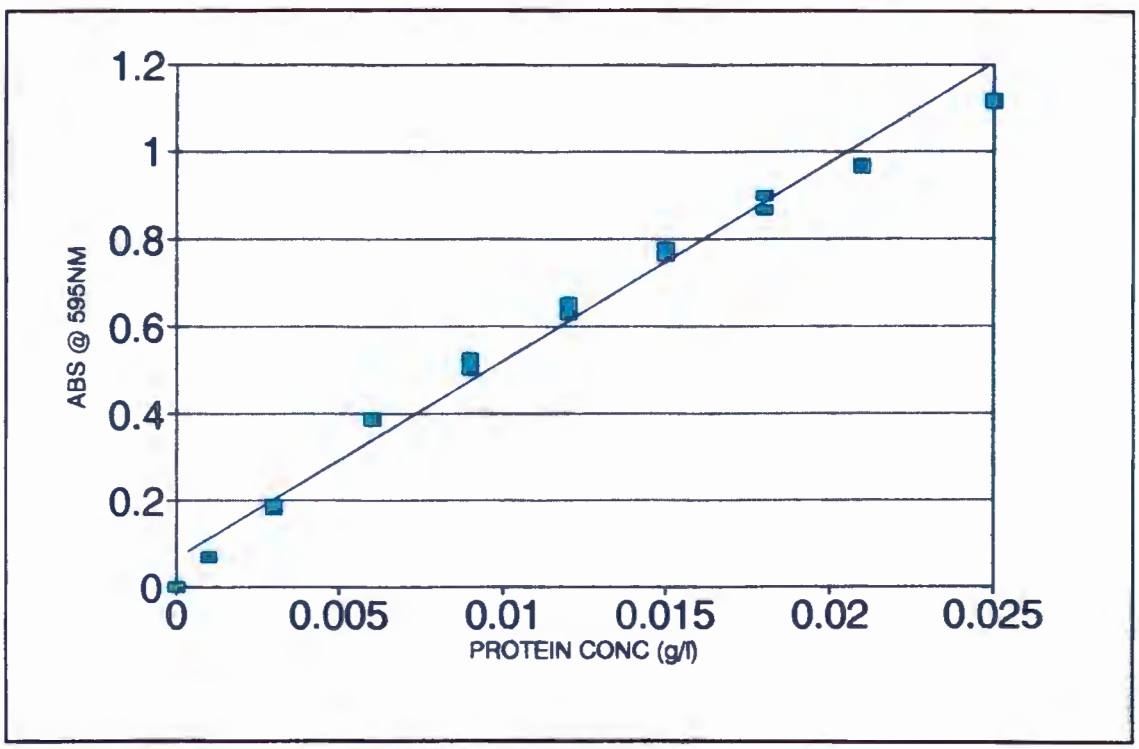

Figure A5 Bio-rad protein assay standard curve.

A.1.8.2 Lowry protein assay

The Lowry protein assay (Lowry *et al.*, 1951) was used to analyse sample supernatants where protein concentrations were greater than 0.05 g/l. The assay is based on the Folin

phenol reagent of Folin and Ciocalteu, which contains the active constituent, phosphomolybdic-tungstic mixed acid. Proteins, complexed with cupric ions, reduce the mixed acid to yield one or more of several reduced species which have a characteristic blue colour. The concentration of these reduced species can be measured spectrophotometrically. Prior complexing of the protein with cupric ions by chelation facilitates the reduction reaction. Since the Folin-Ciocalteu reagent is unstable alkaline environment required to favour reduction, rapid mixing of the copper protein solution with the reagent is essential.

Reagent A: dissolve 1 g $CuSO_4.5H_2O$ in 100 ml distilled water.
Reagent B: Dissolve 100 g Na_2CO_3 in 1 liter 0.5 N NaOH.
Reagent C: Dissolve 2g potassium tartrate in 100 ml distilled water.
Reagent D: Dissolve 0.3 g bovine serum albumin in 1 liter distilled water.
Reagent E: Mix 5 ml 2N Folin phenol reagent with 50 ml distilled water.
Reagent F: Mix 15 ml reagant A, 0.75 ml reagent B and 0.75 ml reagent C.

1ml of a range of protein standards (0 to 0.3 g/l) and 1ml of the diluted sample supernatant were pipetted into separate test tubes. To each test tube 1 ml of reagent F was added. Following incubation of the mixture at room temperature for 15 minutes, 3 ml of reagent E were rapidly added to each tube. The tubes were mixed immediately after the addition of reagent E and incubated in the dark at room temperature for 45 minutes. The absorbance at 660nm was measured after incubation. The colour remained constant for 50 minutes after incubation. Figure A6 illustrates the linear range of the Lowry protein assay (correlation coefficient 0.99).

A.1.9 Malvern particle sizer

Particle size analysis by laser light diffraction of bacterial samples was carried out in a Malvern 3600Ec particle sizer fitted with a 63 mm lens. The particle size distribution and relative increase in the total particle count of samples were determined. The principle of operation of the particle sizer was based on conventional Fourier optics. A beam of light from a low power Helium-Neon laser was scattered by particles in its path. The scattered

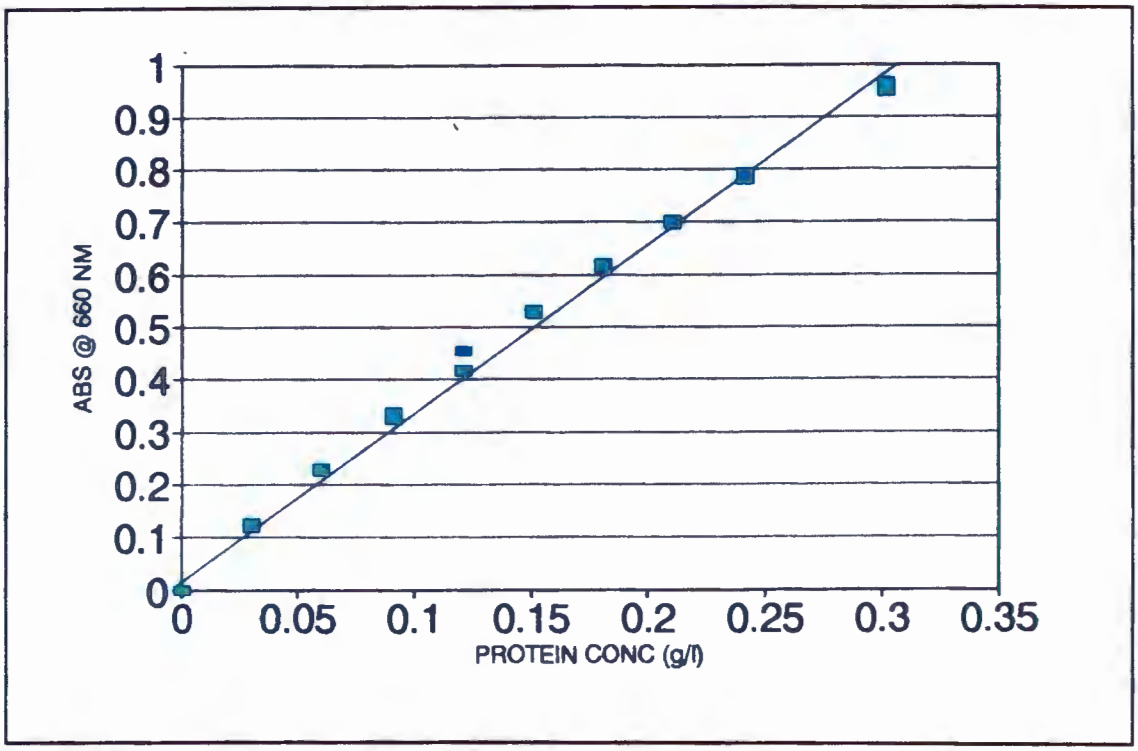

Figure A6 Lowry protein assay standard curve.

light was incident on a Fourier transform lens which formed a diffraction pattern of the scattered light on a detector. The scattering angle was related to the particle diameter. Large particles had peak energies at low angles of scatter and *vice versa*.

Phosphate buffered saline (PBS) was used as background medium for particle size analysis. The medium contained (per liter): 0.8g NaCl, 0.2g KI, 2.254g Na_2HPO_4 and 0.2g KH_2PO_4. The saline was passed through a 0.22 μm filter.

Before measurements were taken, the laser beam was aligned by manipulation of the x and y alignment screws. Samples were analysed using the magnetically stirred stationary cell. The particle size analyser was zeroed with PBS at ambient temperature. 5000 measuring sweeps were chosen to ensure significant results. Using a pipette, a few drops of bacterial sample were added to the PBS in the agitated sample cell so that the concentration was between 0.2 and 0.3 vol %. The particle size distribution was measured. Experiments showed that the morphology remained stable for 15 minutes after sampling (Figure A7). Special care was therefore taken to analyse the bacteria immediately after sampling. Repeated analysis of

samples showed that the method was 100% reproducibile.

To verify the total particle count using laser light diffraction, results were compared with those obtained using a microscopic counting chamber. Cell aggregates were broken up by subjecting bacteria grown in a shake flask to ultrasonic cavitation in a water bath for 3 minutes. The total particle count using laser light scattering increased by 534% compared to 634 ± 185% using the counting chamber. These results agreed reasonably well.

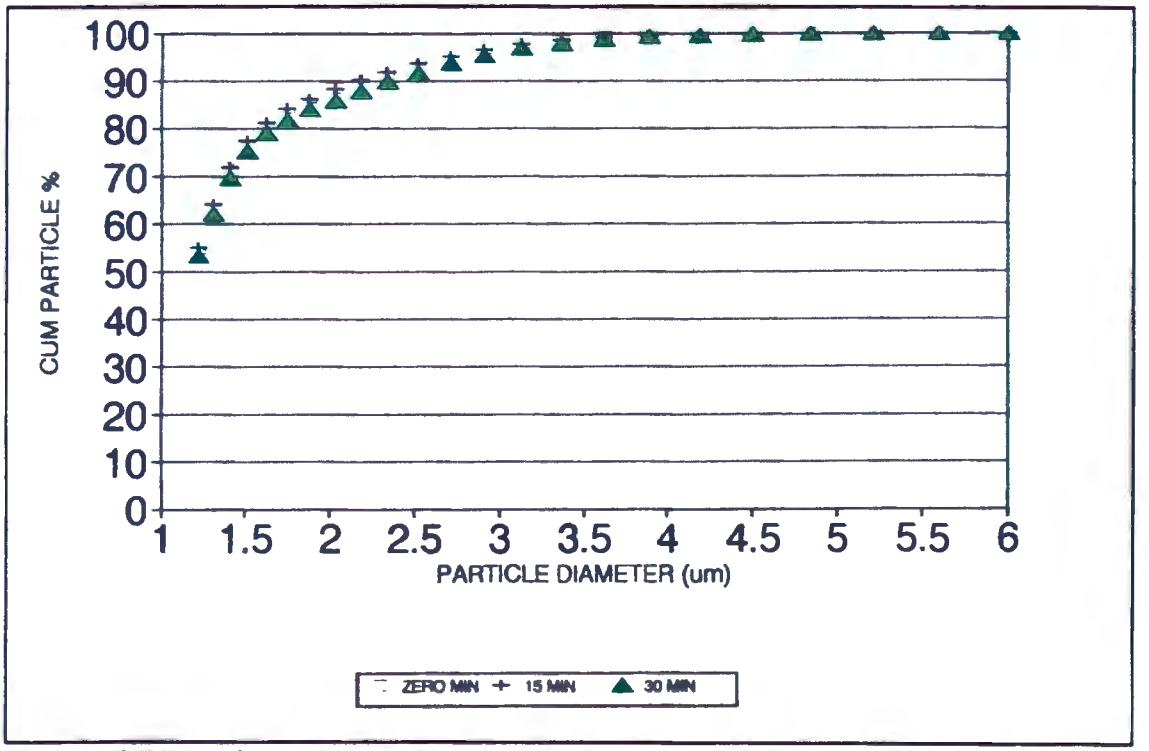

Figure A7 Effect of sampling standing time on the particle size distribution of *Corynebacterium glutamicum* aggregates.

A.1.10 Zeta potential

Cells were diluted 0.05 M phosphate and citrate-phosphate buffers made up to specified pH's in the range pH 3 to 8.

For the preparation of the 0.05 M phosphate buffer, 1.78g Na_2HPO_4 and 1.38g NaH_2PO_4 were each dissolved in 200ml distilled water. The buffers in the pH range between 6 and 8 contained x ml Na_2HPO_4 solution, (50-x) ml NaH_2PO_4 and 50ml distilled water (Table A2).

Table A2 Preparation of phosphate buffers

pH	x
6	6.15
6.5	15.75
7	30.5
7.5	42
8	47.35

For the preparation of the citrate-phosphate buffer, 4.2g of citrate and 3.56g Na_2HPO_4 were each dissolved in 200ml distilled water. The buffers contained x ml citric acid, (50-x) ml Na_2HPO_4 and 50ml distilled water (Table A3).

Table A3 Preparation of citrate-phosphate buffers.

pH	x
3	39.8
4	30.7
5	24.3
6	17.9
7	6.5

APPENDIX B

B.1 STERILISATION PROCEDURE

The cultivation unit consists of a 7.3 liter Chemap stirred tank reactor fitted with Rushton turbine impellers. The reactor was fitted with sterilizable pH and oxygen probes. The pH was controlled using a pH controller and a peristaltic dosing pump. The air supply to the vessel was passed through a pressure regulating unit, an oil filter, a rotameter and a sterile carbon filter before entering the reactor. The exhaust gasses passes through a sterile carbon filter and a condensor cooled with tap water. The bioreactor rested on a senstive load cell. For continuous culture, sterile reactor feed was pumped in at a constant flowrate. Cells were harvested at the same flow rate. During the sterilisation procedure the following protocol was followed.

The fermenter was cleaned, dried and assembled. Opposite nuts on the four vertical bars were tightened first. The glucose solution was poured into the fermenter. The pH probe was calibrated prior to being fitted in the fermenter. The oxygen probe was placed in a port. The exhaust filter was fitted into the central lid port. All empty ports were sealed.

The inlet air filter and the acid, base, salt, inoculum, feed and harvesting units were sterilized separately in an autoclave at 1 bar for 20 minutes.

The boiler was switched on. When the pressure gauge read 3 bar, the red steam tap was opened. The stirrer was turned up to 600 rpm. During this procedure the cold water green tap was shut and the temperature controller was switched off. The stainless steel protection cage was placed around the fermenter. As soon as steam started escaping from the exhaust filter, the filter was closed. As the pressure built up inside the vessel, as indicated by the pressure gauge, the pH probe was pressurised using a bicycle pump. In the sterilization process, the fermenter must remain at 1 bar (121 °C) for 20 minutes. After this time period, the red steam tap was turned off and the green cold water tap opened. Once the pressure had

dropped to 0.5 bar, the exhaust filter was opened to prevent the formation of a vaccum inside the vessel. The condenser tap was opened.

To place the air inlet filter, acid, base, salt, inculum, feed and harvesting needles into the ports, the following procedure was followed. The air inlet filter was positioned first. The plug in the port was unscrewed and pulled out. Using fire resistent welding gloves, the port "cup" was filled to a third of its volume with 96% ethanol and lit. The sterile needle was flamed, carefully pierced through the flamed septa and rapidly screwed into position. The air filter was connected to the air line and the air switched on. The other needles were then similarly positioned.

APPENDIX C

C.1 CALCULATION OF THE MEAN ENERGY DISSIPATION RATES IN THE STIRRED TANK REACTOR

Rushton turbine impeller geometry

diameter:0.08 m

width: 0.02 m

length: 0.02 m

impeller spacing: 0.12 m

impeller clearance off bottom: 0.04 m

C.1.1 7.3 liter bubble free stirred tank reactor

Sample calculation for an impeller speed of 800 rpm

The mean power input was calculated from the power number correlation:

$$P_o = N_p \rho n^3 D^5 \qquad \text{(C1)}$$

The power number was estimated from a correlation developed for 6-bladed Rushton turbines with a w/D ratio of 0.2 by Bates *et al.* (1966) shown in Figure 9 in Chapter 2. For an impeller diameter of 0.08 m and an impeller speed of 3.35 m/s, the Reynolds number is 29 440. According to Figure 9, the corresponding power number is 5.

Bates et al. (1963) showed that the clearance beneath the impeller affects the power number. The power number evaluated above was for an impeller clearance of 1. If the impeller clearance is 0.5 as is the case for the impeller in the Chemap reactor, the power number would decrease to 0.45 (Bates *et al.*, 1963).

The dependent effect of blade width and blade number on the agitated power drawn was investigated by O'Connel and Mack (1950) who showed that:

$$\frac{(N_p)_1}{(N_p)_2} = \frac{19.4\ (\frac{w_1}{D_1})^{1.15}}{23.7\ (\frac{w_2}{D_2})^{1.09}} \qquad \text{(C2)}$$

where N_{p2} is the power number for the reference 6 bladed impeller, N_{p1} is the power number for the 4 bladed impeller, and w is the blade width. According to this correlation the power number for a 4 bladed impeller in the Chemap reactor is 4.3.

Using a value of power number of 4.3, the power drawn in the Chemap reactor fitted with a single impeller according to Equation C1 is 33.4 W. The effect of 2 impellers on the agitated power drawn was estimated from the correlation developed by Bates *et al.* (1963) in Figure 10. For an impeller spacing of 1.5 as was used in the Chemap stirred tank reactor, the agitated power drawn is double that for a single impeller. The agitated power drawn in the 7.3 liter Chemap reactor is therefore 66.8 W. This corresponds to an average energy dissipation rate of 9.15 m^2/s^3 (Equation 33).

C.1.2 Sparged 5 liter Chemap reactor

Sample calculation for an impeller speed of 800 rpm and an aeration rate of 9.5 l/min

The agitated power drawn in a single impeller Chemap stirred tank reactor was calculated to be 33.4 W as shown by the calculations in the previous section. For the 2 impeller ungassed system it was shown that the power drawn was double that for the single impeller system. The introduction of air into the stirred tank reduces the medium viscosity and therefore the power drawn by the impeller. For 2 impeller gassed systems it has been shown that the lower impeller draws less power than the upper impeller as the gas flow through the lower impeller is higher (Chiampo and Marotto, 1995). Since all the gas passes through the lower impeller the power drawn by the lower impeller can be estimated by gassed power correlations.

Michel and Miller (1962) correlated the gassed power drawn by a single impeller:

$$P_g = A_7 \left[\frac{P_o^2 N D^3}{Q^{0.56}}\right]^{0.45} \quad \text{(C3)}$$

where A_7 is a function of impeller geometry. For the Chemap impeller the value of A_7 is 0.829 (Yung *et al.*, 1979). For the lower impeller system the ungassed power drawn is 33.4 W and the gassed power drawn is therefore 18.7 W.

The gassed power drawn by the upper impeller is always greater than that drawn by the lower impeller and always less than the ungassed power of the upper impeller.

$$(P_g/P_o)_1 < (P_g/P_o)_2 < 1 \quad \text{(C4)}$$

Therefore the gassed power drawn by the upper impeller is less than 33.4 W and greater than 18.7 W. The total power drawn can be obtained from the sum of the power drawn by the lower impeller and the power drawn from the upper impeller. The total power is therefore in the range 37.4 W to 52.1. This corresponds to an average energy dissipation rate of between 7.5 and 10.42 m^2/s^3.

C.2 CALCULATION OF ENERGY DISSIPATION RATES IN TURBULENT CAPILLARY FLOW.

In the capillary tube, a laminar sublayer exists immediately adjacent to the inner wall. The thickness of the sublayer (Equation C10) is approximately the 3 d_p, where d_p is the bacterial particle diameter. A negligible fraction of the cells will penetrate this sublayer when passing through the capillary. However, significant energy dissipation occurs in this region. This needs to be subtracted from the total energy dissipation to calculate the energy dissipation in the turbulent core.

The pressure drop in the developing turbulent flow at the entrance of a capillary tube can be estimated by flat plate theory. The mean apparent friction factor is given by (Zhang *et al*, 1993) is given by:

$$\bar{f}_{app} = \frac{0.296}{[Re(L/D)]^{0.2}} \tag{C5}$$

where Re is the pipe Reynold's number and L/D is the length to diameter ratio. The pressure drop is given by:

$$\Delta P = \frac{1}{2} \bar{f}_{app} \rho (\frac{L}{D}) \overline{U}^2_{MAX} \tag{C6}$$

where ρ is the fluid density and U_{MAX} is the maximum fluid velocity in the capillary. The total energy dissipation in the tube, E_T, can be estimated as:

$$E_T = \Delta P \frac{\pi}{4} D^2 \overline{U}_{AVE} \tag{C7}$$

where U_{AVE} is the mean flow velocity. The energy dissipated in the laminar sublayer can be calculated from the fluid viscosity μ, the wall shear rate γ and the volume of the laminar sublayer V_L:

$$E_L = \mu \gamma^2 V_L \tag{C8}$$

The wall shear rate is given by the wall shear stress τ_0 divided by the fluid viscosity μ:

$$\gamma = \frac{\tau_0}{\mu} \tag{C9}$$

The thickness of the laminar sublayer δ can be estimated as:

$$\delta = \frac{5\nu}{(\frac{\tau_0}{\rho})^{0.5}} \tag{C10}$$

The volume of the laminar sublayer is therefore,

$$V_L = \frac{\pi}{4} [D^2 - (D-2\delta)^2] L \tag{C11}$$

The energy dissipated in the turbulent core can be calculated by subtracting the energy dissipated in the laminar sublayer (E_L) from the total energy dissipation in the capillary tube (E_T). The corresponding energy dissipation rate, e_{AVE}, is determined by dividing the energy

dissipation by the product of the turbulent core volume and the fluid density.

The maximum energy dissipation rate (e_w) was calculated according to Laufer (1954):

$$e_w = \frac{460\ u^{*3}}{D} \tag{C12}$$

where u^* (friction velocity) is equal to:

$$u^* = \sqrt{\frac{\tau_0}{\rho}} \tag{C13}$$

and τ_0 is the wall shear stress.

The numerical results of the average and maximum energy dissipation rate calculations for a 0.8 mm diameter capillary, 0.14 m long at two different flow rates are presented in Table C1.

Table C1 Energy dissipation rates in turbulent capillary flow.

Q m^3/s	R_e	f_{app}	δ μm	ΔP $kg/m/s^2$	τ_o $kg/m/s^2$	e_{AVE} m^2/s^3	u^* m/s	e_w m^2/s^3
3.9×10^{-6}	6260	0.018	9.7	1.5×10^5	268	5030	0.52	79920
4.9×10^{-6}	7850	0.018	7.4	2.2×10^5	399	9650	0.63	144810